

2021

Dynamics and evolution of efflux pump-mediated antibiotic resistance

<https://hdl.handle.net/2144/41885>

Boston University

BOSTON UNIVERSITY
COLLEGE OF ENGINEERING

Dissertation

**DYNAMICS AND EVOLUTION OF
EFFLUX PUMP-MEDIATED ANTIBIOTIC RESISTANCE**

by

ARIEL MARIE LANGEVIN

B.S., Clarkson University, 2015
M.S., Boston University, 2019

Submitted in partial fulfillment of the
requirements for the degree of
Doctor of Philosophy

2021

© 2021 by
ARIEL M. LANGEVIN
All rights reserved except for chapters 2 and
3, which are respectively:
© 2017 American Society for Microbiology
© 2018 Springer Nature

Approved by

First Reader

Mary Dunlop, Ph.D.
Associate Professor of Biomedical Engineering

Second Reader

Ahmad S. Khalil, Ph.D.
Associate Professor of Biomedical Engineering

Third Reader

Allyson E. Sgro, Ph.D.
Assistant Professor of Biomedical Engineering

Fourth Reader

James E. Galagan, Ph.D.
Associate Professor of Biomedical Engineering
Associate Professor of Microbiology

Fifth Reader

Aimee Shen, Ph.D.
Associate Professor of Molecular Biology & Microbiology
Tufts University

ACKNOWLEDGMENTS

I would like to firstly acknowledge my amazing advisor, Dr. Mary Dunlop, who has been a pillar of patience, understanding, and guidance through my rather unconventional graduate journey. She has taught me invaluable lessons in experimental design, story crafting, mentorship, and leadership. I would also like to express my gratitude for the rest of my incredible committee, Dr. Mo Khalil, Dr. Allyson Sgro, Dr. Aimee Shen, and Dr. James Galagan for their guidance and input. This work would not be what it is without them.

I would like to thank all the phenomenal colleagues who I had the opportunity to meet and work with during my graduate studies. In particular, Dr. Imane El Meouche, Dr. Xi Wen, and Yik Siu, for their optimism and lessons at the bench; Dr. Brandon Wong, Dr. Chris Mancuso, and Zack Heins, for their help troubleshooting the eVOLVER; as well as Dr. Nick Rossi, Dr. Tiebin Wang, Dr. Nadia Sampaio, Dr. Jean-Baptiste Lugagne, Dr. Tim Tomko, Dr. Jonghyeon Shin, Dr. Razan Alnahhas, Michael Sheets, Nathan Tague, and Caroline Blassick for their insights and camaraderie.

I would also like to thank my wonderful family for their unrelenting support during my education and beyond. I am sincerely grateful to my mother, Mary Beth Langevin, for fostering my love for nature and science, to my father, Joseph Langevin, for fostering my love for technology, and to my aunt, Mary E. Langevin, for inspiring me to achieve my wildest career ambitions. Last but not least, I would like to thank my incredible husband and partner, Dr. Bob Van Hove; thank you for supporting me, encouraging me, and helping me grow into the scientist I am today.

**DYNAMICS AND EVOLUTION OF
EFFLUX PUMP-MEDIATED ANTIBIOTIC RESISTANCE**

ARIEL MARIE LANGEVIN

Boston University College of Engineering, 2021

Major Professor: Mary Dunlop, Ph.D., Associate Professor of Biomedical Engineering

ABSTRACT

Antibiotic resistance is a worldwide health threat, as bacteria continue to evade antibiotic treatment. In order to survive, bacteria utilize a number of resistance mechanisms, including efflux pumps, which efficiently export antibiotics outside of the cell to reduce intracellular damage. While such mechanisms are well known, there remains a significant gap in knowledge regarding how different environmental dynamics, such as the rate of antibiotic introduction or the diversity within a microbial community, play a role in resistance. In this work, we used the AcrAB-TolC efflux pump as a case study to explore how such complex dynamics promote antibiotic resistance and its evolution. First, through a combined effort using experiments and mathematical modeling, we discovered that the rate of antibiotic introduction impacts the fraction of resistant bacteria in a population. We then explored the impact of mixed populations on survival following antibiotic treatment. In mixed microcolonies, we found that resistant cells can harm their susceptible neighbors by exporting antibiotics to increase the local concentrations of these drugs. Next, we aimed to understand how these environmental effects may impact longer-term survival of an antibiotic treatment, focusing on the evolution of resistance over ~72 hours. Through a series of adaptive evolution experiments, we identified that near-MIC treatments were the

most likely to promote antibiotic resistance, regardless of whether the strains contained the AcrAB-TolC pump at wild type or overexpressed levels, or whether the strains lacked the pump altogether. In studying antibiotic introduction rates on evolution, we found that slower introduction rates facilitated the evolution of high levels of resistance with a minimal fitness cost. Meanwhile, mixed populations demonstrated limited evolvability after rapid antibiotic introductions. This work provides important insights into the impacts of environmental factors, such as the rate of antibiotic introduction and the homogeneity of populations, on the promotion and evolution of antibiotic resistance. These lessons may help inform future policies on antibiotic use and mitigate the continued pattern of resistance evolution.

PREFACE

After a two-week vacation in 1928, Alexander Fleming returned to his lab at St. Mary's Hospital in London to continue his research on the influenza virus from the 1918 pandemic. There Fleming found an old plate of *Staphylococcus* had been contaminated with mold. Under closer inspection, he observed that the growth of the contaminated mold had produced a zone of inhibition, in which the bacterial colonies were smaller and were lysing. The mold was penicillin-producing *Penicillium rubens*. By 1941, Howard Florey and Ernst Boris Chain from the Radcliffe Infirmary had scaled-up the research of penicillin for mass production.

Yet, in 1940, Ernst Boris Chain and Edward Abraham already reported an *Escherichia coli* strain that inactivated penicillin. After the clinical trials in 1942, four clinical strains of *Staphylococcus aureus* demonstrated resistance to penicillin. By 1970, over 80% of all *S. aureus* strains collected from communities and hospitals were penicillin-resistant. As of 2019, nearly 3 million cases of antibiotic-resistant infections are reported every year in the United States alone.

TABLE OF CONTENTS

ACKNOWLEDGMENTS	iv
ABSTRACT.....	v
PREFACE.....	vii
TABLE OF CONTENTS.....	viii
LIST OF TABLES.....	xi
LIST OF FIGURES	xii
1. INTRODUCTION	1
1.1. Antibiotic Resistance	1
1.1.1. Mechanisms of Antibiotic Resistance.....	1
1.1.2. Early Efforts to Combat Rising Levels of Antibiotic Resistance	5
1.1.3. The Continued Threat of Antibiotic Resistance.....	6
1.1.4. Driving Factors of Antibiotic Resistance and its Evolution	7
1.1.5. Gap in Knowledge of Complex Environments.....	10
1.2. Efflux Pumps and Antibiotic Resistance	11
1.2.1. AcrAB-TolC Efflux Pumps	11
1.2.2. Regulation of AcrAB-TolC Efflux Pumps	14
1.2.3. Importance of AcrAB-TolC Efflux Pumps in Complex Environments.....	16
1.3. Summary	17
2. STRESS INTRODUCTION RATE ALTERS BENEFIT OF AcrAB-TolC EFFLUX PUMPS	19
2.1. Disclosure & Copyright Statement.....	19
2.2. Abstract.....	19
2.3. Introduction.....	20

2.4. Results.....	22
2.5. Discussion	34
2.6. Contributions Statement.....	36
2.7. Methods.....	36
3. ANTIBIOTIC EXPORT BY EFFLUX PUMPS AFFECTS GROWTH OF NEIGHBORING BACTERIA.....	43
3.1. Disclosure & Copyright Statement	43
3.2. Abstract	43
3.3. Introduction.....	44
3.4. Results.....	46
3.5. Discussion	56
3.6. Contributions Statement.....	57
3.7. Methods.....	57
4. MAPPING THE ROLE OF AcrAB-TolC EFFLUX PUMPS IN THE EVOLUTION OF ANTIBIOTIC RESISTANCE REVEALS NEAR-MIC TREATMENTS FACILITATE RESISTANCE ACQUISITION	62
4.1. Abstract	62
4.2. Introduction.....	63
4.3. Results.....	66
4.4. Discussion	76
4.5. Contributions Statement.....	78
4.6. Methods.....	78
5. ANTIBIOTIC INTRODUCTION RATE AND MIXED POPULATIONS INFLUENCE THE EMERGENCE OF ANTIBIOTIC RESISTANCE.....	84
5.1. Abstract	84
5.2. Introduction.....	85

5.3. Results.....	87
5.3.1. Short-term fluctuations can promote fitness from antibiotic exposure.....	87
5.3.2. Slow introduction of stress promotes growth and resistance.....	97
5.3.3. Co-cultures impact how populations survive environmental fluctuations....	100
5.3.4. Correlations between fitness and resistance for evolution studies.....	102
5.4. Discussion	104
5.5. Contributions Statement.....	107
5.6. Methods.....	107
6. CONCLUSION.....	114
6.1. Future Directions and Outlook.....	117
Appendix A: Supplementary Information for Chapter 2	120
Appendix B: Supplementary Information for Chapter 3	129
Appendix C: Supplementary Information for Chapter 4	133
Appendix D: Supplementary Information for Chapter 5	142
Appendix E: Predicting Single Cell Fate with a c-di-GMP Biosensor.....	153
E.1. Introduction	153
E.2. Results	155
E.3. Discussion.....	160
E.4. Contributions Statement	160
E.5. Methods	161
BIBLIOGRAPHY	163
CURRICULUM VITAE.....	194

LIST OF TABLES

Table 1-1. Mechanisms of Antibiotic Resistance.	2
Table 1-2. Substrates of AcrAB-TolC Efflux Pumps in <i>E. coli</i>	12
Table 4-1. Summary of whole genome sequencing results.	75
Table A-1. Goodness-of-fit between model and experimental data.	120
Table A-2. Primers used for the construct of plasmids.....	121
Table A-3. Model parameters.	122
Table A-4. Statistics for model parameter selection data.	123
Table B-1. Model parameters.	129
Table C-1. <i>p</i> values for differences in growth rates for each strain.	133
Table C-2. Primers for <i>acrR</i> knockout.....	133
Table C-3. <i>p</i> values of toxicity curves with and without Tween20.	134
Table C-4. <i>p</i> values for differences in inhibition zone diameters for each strain.	134
Table D-1. Inhibition zones for parent strains prior to treatment.	142
Table D-2. <i>p</i> values from two-sample t-test for growth rate difference.	142
Table D-3. Pearson correlation coefficients and their <i>p</i> values.	143

LIST OF FIGURES

Figure 1-1. Schematic of an AcrAB-TolC efflux pump.	13
Figure 1-2. Native regulation of the <i>acrAB</i> operon.	16
Figure 2-1. Benefits and costs of AcrAB-TolC efflux pumps.	24
Figure 2-2. Schematic of methodology and data collection.	26
Figure 2-3. Rate of chloramphenicol addition affects survival.....	29
Figure 2-4. Model predictions and experiments measuring benefit of pumps.	31
Figure 2-5. Benefit ratios for lower initial inoculum size.....	32
Figure 2-6. Benefit and cost trade-offs of AcrAB-TolC efflux pumps in pinene.....	33
Figure 3-1. Neighbors with pumps impact cell growth.	47
Figure 3-2. Δ <i>acrB</i> cells with and without <i>acrAB</i> complementation show neighbor- dependent differences in growth.....	50
Figure 3-3. Relative abundance of Δ <i>acrB</i> cells decreases when they have AcrAB-GFP neighbors.....	51
Figure 3-4. Model predicts cell growth rate differences under antibiotic conditions.	53
Figure 3-5. Impact of neighborhood on focal cell growth rate.	54
Figure 3-6. <i>E. coli</i> and <i>S. typhimurium</i> co-culture.....	55
Figure 4-1. Evolution experiment schematic.	67
Figure 4-2. Temporal landscapes based on treatment concentration of chloramphenicol.....	68
Figure 4-3. Resistance and Fitness Evolution Trajectories.....	71
Figure 4-4. Number of Biological Replicates with Highly Resistant Sub-populations through Time.....	73
Figure 5-1. Experimental conditions and growth of wild type <i>E. coli</i> in the eVOLVER.	88
Figure 5-2. Experimental and data analysis workflows quantifying the emergence of resistance and tolerance for wild type <i>E. coli</i>	90

Figure 5-3. Impact of antibiotic introduction rate and strain background on the emergence of resistance and tolerance for <i>acrAB</i> ⁺ and Δ <i>acrB</i> cultures.	94
Figure 5-4. Impact of antibiotic introduction rate on the emergence of resistance and tolerance for Δ <i>acrB</i> cultures exposed to different concentrations of chloramphenicol.	98
Figure 5-5. Impact of slow, long-term antibiotic introduction rate on populational fitness and resistance.	100
Figure 5-6. Impact of antibiotic introduction rate on a co-cultured population.....	101
Figure 5-7. Correlations between final growth rates of cultures, initial growth rates, and number of dilution events.	103
Figure A-1. Data fitting to extract model parameters.	124
Figure A-2. Benefit and cost trade-offs of AcrAB-TolC efflux pumps in pinene.	125
Figure A-3. Competitive growth in pinene.	126
Figure A-4. Rate of pinene addition affects survival.	127
Figure A-5. Susceptible cells more readily recover from short-term pulses of antibiotics at sub-inhibitory concentrations.....	128
Figure B-1. Full data sets for figures including outliers and number of cells (n).....	130
Figure B-2. Toxicity curves and data fitting for model parameters.....	131
Figure B-3. Fold change in cell length over time for all individual cells.	132
Figure C-1. Growth rates for each biological replicate and chloramphenicol treatment concentration.....	135
Figure C-2. Toxicity curves for each parent strain.	136
Figure C-3. Inhibition zone diameters for each biological replicate and chloramphenicol treatment concentration.....	137
Figure C-4. Colony forming units (CFU) per mL counts for each treatment concentration.	138
Figure C-5. Linear map between the natural log of the MIC and inhibition zone areas.	139
Figure C-6. Resistance and fitness of WT cells exposed to ciprofloxacin for 168 h.....	140

Figure C-7. Toxicity curves in the presence of Tween20.	141
Figure D-1. Wild type control without antibiotics and the emergence of resistance and tolerance.	144
Figure D-2. <i>acrAB</i> ⁺ resistance relative to WT and Δ <i>acrB</i>	145
Figure D-3. Normalized inhibition zones for example isolates.	146
Figure D-4. Mutation frequencies at the end of the experiment.	147
Figure D-5. All co-cultured experiments and the emergence of resistance and tolerance.	148
Figure D-6. All wild type experiments and the emergence of resistance and tolerance.	149
Figure D-7. All <i>acrAB</i> ⁺ experiments and the emergence of resistance and tolerance. ..	150
Figure D-8. All Δ <i>acrB</i> experiments and the emergence of resistance and tolerance at MIC _{wt} (1 μ g/mL).	151
Figure D-9. All Δ <i>acrB</i> experiments and the emergence of resistance and tolerance at MIC _{Δ<i>acrB</i>} (0.5 μ g/mL).	152
Figure E-1. Schematic of the regulation pathway of c-di-GMP and measuring c-di-GMP with the biosensor.	155
Figure E-2. Regulation of intracellular c-di-GMP concentrations shifts populations c-di-GMP and cell morphology.	156
Figure E-3. Lower c-di-GMP levels reduces cell size.	157
Figure E-4. Higher c-di-GMP levels are associated with increased survival.	158
Figure E-5. Single cell oscillation of c-di-GMP from a single mother.	159

1. INTRODUCTION

1.1. Antibiotic Resistance

Antibiotic resistance remains a global health crisis as the number of resistant infections continues to rise (1–3). Each year in the United States, there are over 2.8 million cases of antibiotic-resistant infections resulting in over 35,000 deaths (4). While antibiotics are still essential for both medicine and science, over-prescription has led to high levels of resistant infections in the clinic (2, 5). While this over-prescription was an early contributor to the spread of resistance, the anthropological use of antibiotics for sterilization has only aggravated the problem (5–7). Such applications include agriculture, veterinary care, industrial and household cleaning processes, and wastewater treatment (5, 8). Together these applications have resulted in the rapid spread of antibiotic resistant microbes not only through person-to-person transmission, but also in our soil, water, and food (2, 5, 9–11). The ability for microbes to so quickly acquire resistance requires a deeper dive into how antibiotic resistance mechanisms allow microbes to survive antibiotic treatment (2).

1.1.1. Mechanisms of Antibiotic Resistance

The first step in understanding why antibiotics fail is understanding how they fail (12). Mechanisms by which microbes become resistant include altering drug targets, producing enzymes for antibiotic degradation or modification, tuning gene expression, reducing cell membrane permeability, and increasing active efflux (5, 13, 14) (Table 1-1). For example, in order to protect itself against an antibiotic treatment with a β -lactam, a bacterium can actively alter gene expression to increase the target to antibiotic ratio (15). However, it is also important to note that microbes do not need to rely solely on one

resistance mechanism to survive and that microbes simultaneously use multiple strategies to increase their chance of survival (1). For example, in the presence of a β -lactam, a cell may achieve resistance by reducing membrane permeability, increasing efflux, and modifying the target protein, in addition to degrading the antibiotic with β -lactamases (13). Most of the time, bacteria using multiple mechanisms are resistant to a larger range of antibiotics; however, in some cases, mutants which evolved resistance mechanisms to combat one antibiotic simultaneously become more sensitive to other antibiotics (16).

Mechanism of Resistance	Example Antibiotics	Antibiotic Targets
<i>Antibiotic efflux</i>	Amphenicol (e.g. chloramphenicol) Tetracyclines (e.g. doxycycline) Bacitracin (e.g. bacitracin) Nitrofurans (e.g. nitrofurantoin)	50S Ribosome 30S Ribosome Cell wall DNA
<i>Reduced permeability</i>	Rifamycins (e.g. rifampicin) Glycopeptides (e.g. vancomycin) Macrolides (e.g. azithromycin) Aminoglycosides (e.g. gentamicin)	mRNA Transcription Cell wall 50S Ribosome 30S Ribosome
<i>Expression changes</i>	β -lactams (e.g. ampicillin) Sulfonamides (e.g. sulfamethoxazole) Fusidanes (e.g. fusidic acid) Isoniazid (e.g. isoniazid)	Cell wall Nucleic Acid synthesis 50S Ribosome Cell wall
<i>Antibiotic modification or degradation</i>	Quinolones (e.g. ciprofloxacin) Nitroimidazoles (e.g. metronidazole) Fosfomycin (e.g. fosfomycin) Lipopeptide (e.g. daptomycin)	DNA gyrase DNA Cell wall Cell membrane
<i>Target modification or protection</i>	Polymyxin (e.g. colistin) Mupirocin (e.g. mupirocin) Oxazolidinone (e.g. linezolid) Trimethoprim (e.g. trimethoprim)	Cell membrane RNA synthetase 50S Ribosome Nucleic Acid synthesis

Table 1-1. Mechanisms of Antibiotic Resistance.

The key mechanisms of antibiotic resistance are shown here, along with examples of antibiotic classes, antibiotics, and the targets of the associated antibiotics (5, 13, 14).

Different mechanisms of antibiotic resistance can be achieved by both permanent and transient changes to the cells' physiology (17, 18). One method by which cells can permanently acquire antibiotic resistance mechanisms is through the uptake of antibiotic resistance genes via horizontal gene transfer (HGT) (19–21). This transfer is facilitated through conjugation of plasmids, transduction by bacteriophages, or natural transformation of extracellular DNA (22, 23). HGT allows for microbes to be shared through a larger and more diverse genetic pool and can provide resistance faster than spontaneous mutations (21, 22). Yet, the prevalence of HGT in clinics remains unknown as HGT likely fluctuate depending on environmental conditions (22, 24).

Resistant genotypes are also often inherited through vertical gene transfer, in which a fixed genetic mutation is passed down to an offspring (14). One type of mutation that contribute to increased resistance are single point mutations; these include missense point mutations, which may alter protein function by using an alternative amino acid, and as well as insertions, deletions, and nonsense mutations, which may disrupt protein function more severely through frameshifts (13). Such point mutations often affect gene expression, protein binding, or protein inactivation (20). Additionally, mobile genetic elements, such as insertion sequences or transposons from the host's own chromosome, rapidly integrate into target genes (5, 23, 25) to disrupt local stress response regulators (26). These mobile genetic elements can also cause larger chromosomal rearrangements (27) and can provide an intermediate pathway to gene duplication (28, 29), which can lead to increased copy numbers of antibiotic resistance genes (23, 30, 31).

Nevertheless, bacteria do not survive antibiotic treatment exclusively through

permanent changes, but can also survive through transient measures; therefore, it is important to make the distinction between permanent antibiotic resistance and transient antibiotic tolerance. Bacteria exhibiting the aforementioned permanent genetic changes, such as a gene encoding for a resistance factor from Table 1-1, are considered resistant (32). Populations of resistant bacteria are capable of growing and surviving at concentrations of antibiotics that susceptible cells cannot (32). Thus, since a higher antibiotic concentration is required to kill the resistant population, the minimum inhibitory concentration (MIC) for resistant cells is higher than the MIC for susceptible cells (32–34). Yet, there are cases where bacterial populations do not encode for a resistance factor, similarly to susceptible cells, but are able to survive much higher antibiotic concentrations, similarly to resistant cells (32, 35). Such bacteria are defined as tolerant and enable a subpopulation to survive at higher antibiotic concentrations through dormancy or persistence (32). For example, one subset of tolerant cells — persister cells — present a resistant phenotype to survive conditions with a susceptible genotype that should otherwise lead to cell death (32). This tolerance can emerge either spontaneously or as a result of a trigger, such as starvation, cell density, or chemical stressors (32, 36). For example, diversity in a general stress response activator, MarA in *E. coli*, improves single-cell survival against carbenicillin; yet, the single cells that survive do not retain resistance (37). Thus, bacteria can leverage transient changes to their physiology to improve a bacterial population's survival (5, 14). Today, it is well understood that bacteria have the innate and robust ability to both evolve permanent and employ transient antibiotic resistance mechanisms.

1.1.2. Early Efforts to Combat Rising Levels of Antibiotic Resistance

Many of these mechanisms were first identified in early antibiotic resistance surveillance studies (38). In 1994, the World Health Organization revealed a surveillance study which found antibiotic resistance to be wide-spread across 22 countries (39). Since then, surveillance efforts have aimed to study the spread of antibiotic resistance (40–43). Such surveillance efforts identified the over-prescription and over-medication of antibiotics (8, 44–46), as well as the downstream environmental impact of antibiotics use for non-medical applications (47–49). These studies have played a key role in identifying how antibiotic applications increased levels of antibiotic resistant microbes in our soil, food, and waterways (2, 5, 9–11).

Though these studies have helped policy makers and physicians reduce superfluous antibiotic use, the resistance in microbes continues to outpace the discovery of novel treatments (6, 7, 12). In an effort to combat the lack of usable antibiotics, policy makers created the 10 x '20 initiative in 2010 with the goal to discover at least 10 novel antibiotics by 2020 (50). During this past decade, numerous novel antibiotics have been identified and subsequently approved by the U.S. Food and Drug Administration (FDA); however, clinical and laboratory studies have already reported resistant microbes for a significant portion of these novel antibiotics (51–56). Additional efforts have also begun to explore antimicrobial peptides or antibiotics linked to antimicrobial peptides in the hope that these more complex chemicals will curtail the ability of bacteria to resist treatment (57). However, resistance to antimicrobial peptides has also already been reported (12, 58). Combinatorial treatments with multiple drugs have also been explored for their potential

to preserve legacy antibiotics (59, 60). That said, combinatorial therapeutics need to be carefully assessed to ensure that the effect of the drug combination is indeed additive, and not antagonistic (61–63). Misused combinatorial treatments could be another threat to promoting antibiotic resistance, especially Liu *et al.* found that bacteria could still evolve resistance to such treatments within days (64).

1.1.3. The Continued Threat of Antibiotic Resistance

One novel antibiotic produced by the 10 x '20 initiative is eravacycline (previously known as TP-434), which belongs to the tetracycline antibiotic class (65). While it was found to have a broad range of antimicrobial activity, treatment failure of *Enterococcus faecalis* in clinics has already been noted; these microbes evolved resistance by mutating the target and upregulating antibiotic efflux (51). In a similar fashion, the discovery of omadacycline also of the tetracycline family, touted the potential against multidrug resistant bacteria, such as MRSA (66, 67); unfortunately, due to gene expression regulation, resistance of *S. aureus* isolates from Chinese clinics were found only two years after its clinical trials (52). Such a pattern has been omnipresent, as even the novel antibiotic, daptomycin (68), from 2004 had resistance reported within a few years (69). Today, every class of antibiotics can be negated by at least one resistance mechanism (13); *Pseudomonas aeruginosa* alone has developed a resistance mechanism against every class of its intended antimicrobials (1). As such, we stand in a more ominous position as the discovery of resistance to novel antibiotics outpaces the discovery of novel antibiotics (7). One hope is for us to understand how and why resistance is emerging before these novel antibiotics are used in clinics.

Since the 1990s, antibiotic resistance studies in the clinic have focused on uncovering what and how resistance mechanisms evolve (19, 70, 71). Such studies have also led to observations of cross-resistant phenotypes in clinical isolates from treatment with a single antibiotic (72). Additionally, these studies have found resistance after sub-inhibitory antibiotic exposure (73). Further, they have helped identify certain combinations of antibiotics, microbes, and treatments that promote the emergence of multidrug antibiotic resistance (74). On the other hand, these studies are often dealing with lethal consequences of already evolved antibiotic resistance in real time and not in a predictive fashion (75). In addition to this, studying the evolution of antibiotic resistance in the clinics remains restrictive and time-consuming; as a consequence, there have been an uptick in laboratory evolution studies of antibiotic resistance (19).

1.1.4. Driving Factors of Antibiotic Resistance and its Evolution

Prior to the last decade, many of the laboratory studies focused on understanding why antibiotic resistance lingered and how the quantity of resistant cells in bacterial populations could be reduced (76, 77). Unfortunately, simply reducing the presence of resistant population members is not a robust solution to combat pathogenic bacteria; this solution is only viable if resistance phenotypes are costly to the microbe, which is not always the case (78, 79). While strategies for reducing resistance in a population aligns with policies to avoid antibiotic use (77), there remain many cases where antibiotic treatment is appropriate and essential (80). As such, researchers have turned their efforts to exploring other contributing factors to antibiotic resistance that were not previously studied: microbial population variations, such as variations in diversity and density, and

fluctuations in inhibitory antibiotic concentration (78, 81–83). The goal of these studies was to identify which combinations of environmental factors and antibiotic treatments could eliminate resistant cells in a population (78). This ability to reverse antibiotic resistance during treatment requires extensive forethought and planning to properly eradicate resistant sub-populations (84, 85). As a result, new efforts have begun to investigate the stability of resistance in bacterial populations (78).

Resistant and susceptible cells can stably co-exist in a population at sub-inhibitory antibiotics concentrations; this has been observed in waterways and in soil (86). The effect of low antibiotic concentrations on the emergence of antibiotic resistance has only recently become studied more in depth. While bacterial evolution at sub-inhibitory concentrations are less often studied, Wistrand-Yuen *et al.* found that bacteria grown in sub-inhibitory concentrations were still able to achieve high-levels of resistance through unique evolutionary pathways (87). The divergence of evolutionary trajectories at different concentrations suggests that elements of bacteria's evolutionary landscapes remain unexplored. In a recent publication, Russ *et al.* found that the emergence of escape mutations was more likely under certain antibiotic concentrations (88). Additional studies have also reported problematic levels of antibiotic resistance after sub-inhibitory antibiotic exposures (89–91). Thus, antibiotic concentrations may influence the emergence of antibiotic resistance.

The activity of bacterial communities, such as in cells in a biofilm, also influences the presence of resistant phenotypes (92–96). Further, bacterial population dynamics, including diversity, density, and spatial organization, impact antibiotic resistance

independent of biofilms (97). For example, one study identified how population diversity hindered the effectiveness of antibiotic cycling — a treatment strategy where an infection is targeted with one antibiotic then another in a cyclic manner (98). Even changes in experimental parameters alone can cause large fluctuations in population diversity (99). These studies indicate that the impact of population dynamics on antibiotic resistance could be more complicated than previously thought (64, 92).

Evolution studies have also been key in unveiling important factors in the emergence of antibiotic resistance (19). The Lenski experiments uncovered the power of experimental evolution to study the long-term effect on bacterial populations in a predictive fashion (100, 101). Previously, evolution using serial dilutions was the traditional set up; today, more researchers have begun using bioreactors to study long-term dynamics, either with turbidostats or chemostats (97, 102–104). Toprak *et al.* developed a turbidostat-derivative — the morbidostat — to direct bacteria to evolve by only providing nutrients along with higher antibiotic concentrations (102, 103, 105). This method pushes the evolved MIC to astronomically high levels. Likewise, the MEGApate experiment was key at understanding how and what genotypes can lead to this high level survival (106). While the morbidostat experiments revealed the extent of the evolutionary pathway of the bacteria, it is unlikely that such a treatment would be possible for patients due to antibiotic toxicity (107). On the other hand, scientists have often explored the evolution of antibiotic resistance at antibiotic concentrations that fall between inhibitory for bacteria and non-toxic for patients (13, 64, 108). Such evolution studies have elucidated how bacteria might respond to stressful static environments, changing environments (e.g. drug switching or

rising antibiotic concentration), and realistically complex environments (e.g. mouse models) (97).

Predictive modeling has also improved the understanding of antibiotic resistance, beyond current laboratory studies (109, 110). One model by Marrec and Bitbol identified how the timing of environmental switching could have dramatic consequences on the emergence of antibiotic resistance (111). Another model by Chevereau *et al.* identified how heterogeneity in resistance could accelerate or delay the evolution of antibiotic resistance (112). Yet, novel factors in the evolution of resistance still need to be better understood to produce improved models (110). Luckily, these factors are now being elucidated in laboratory and clinical studies (113). One such study found that different bacterial populations evolved convergent, resistant phenotypes (114). In the future, predictive modeling can give us a glimpse into the consequences of different environments on the evolution of antibiotic resistance (110).

1.1.5. Gap in Knowledge of Complex Environments

Despite the attributes that these predictive models provide, there still remains a lack of understanding of antibiotic resistance in complex and dynamic environments (111, 115–117). Such conditions need to be explored experimentally before including them in models (110). Furthermore, despite the incredible attributions from these cumulative works, the overarching conclusions are difficult to interpret due to variations in experimental parameters, such as conditions, species, antibiotics, and temporal changes to antibiotic concentrations (118, 119). Another example of this comes from a recent study by Hallinen *et al.*, who demonstrated how a combination of factors could lead to both population

survival or extinction after identical treatments (120). The emergence of antibiotic resistance is dependent not only on genotypes and phenotypes, but also on the type of antibiotics, antibiotic concentrations, and population composition; thus, there remains a need to more systematically explore how these complex environmental dynamics — including fluctuations in antibiotic doses and diversity within microbial populations — may promote antibiotic resistant populations and their emergence (118, 121).

1.2. Efflux Pumps and Antibiotic Resistance

One mechanism capable of providing high levels of resistance to many different drugs are efflux pumps (122–125). Efflux pumps are an energy-dependent mechanism for the active export of a substrate from a cell (126). This mechanism is ubiquitous across both prokaryotic and eukaryotic cells (127); for example, even cancer cells to express efflux pumps that actively export anti-cancer drugs (128). This ability for cells to maintain low intracellular concentrations of toxic substrates improves survival rates (44, 125). As such, many different classes of efflux pumps have evolved to export out heavy metals, bile salts, antimicrobial lipids, and antibiotics (129–132).

1.2.1. AcrAB-TolC Efflux Pumps

The AcrAB-TolC efflux pump was first identified in *E. coli* as providing resistance to acriflavin through a mutation in *acrB* in 1978 (133). It is now known to export a plethora of substrates from *E. coli* cells, from antibiotics to biofuel precursors (Table 1-2) (134). AcrAB-TolC efflux pumps are found in gram-negative bacteria, including *Salmonella enterica* and *Yersinia pestis* (135, 136). Many homologs of AcrAB-TolC can also be found widely throughout other gram-negative bacteria, including MexAB-OprM from

Substrate Type	Substrate	Fold change in MIC ^a	References
<i>Antibiotics</i>	Ampicillin	2-4	(134, 219, 258)
	Chloramphenicol	2-8	(134, 189, 219)
	Ciprofloxacin	4	(134, 258, 352)
	Cloxacillin	256	(145, 353)
	Erythromycin	16-64	(134, 145, 258, 353)
	Enoxacin	4	(145)
	Florfenicol	8	(134)
	Fusidic Acid	128	(134, 353)
	Minocycline	4-8	(145, 352)
	Nalidixic Acid	2-8	(134, 219)
	Norfloxacin	1-4	(134, 145, 353)
	Novobiocin	32-256	(134, 145, 258, 353)
	Puromycin	32-64	(134, 219)
	Rifampicin	1-2.5	(134, 145, 219)
	Tetracycline	2-10	(134, 219, 258, 353)
<i>Antiseptics</i>	Acridavine	32-64	(134, 145)
	Proflavin	8	(134)
<i>Dyes</i>	Carbonyl Cyanide Chlorophenylhydrazone (CCCP)	2	(134)
	Crystal Violet	8-32	(134, 145, 353)
	Ethidium Bromide	128-256	(134, 145)
	Plumagin	4	(134)
	Rhodamine 6G	256-512	(134, 145)
<i>Detergents</i>	Benzalkonium Chloride	32-64	(134, 145)
	Dequalinium	128	(134, 145)
	Sodium Dodecyl Sulfate (SDS)	128	(134, 353)
<i>Terpenes</i>	α -Pinene	4	(189)
<i>Salts</i>	Tetraphenylphosphonium	256	(134)
	Tetraphenylarsonium	512	(134)
<i>Acids</i>	Deoxycholate	2	(134)
<i>Antifungals</i>	Clotrimazole	2	(134)
<i>Anti-cancer drugs</i>	Methotrexate	8	(134)

Table 1-2. Substrates of AcrAB-TolC Efflux Pumps in *E. coli*.

^a The fold change in the MIC of each substrate for strains with and without the AcrAB-TolC efflux pump.

Pseudomonas aeruginosa and MacAB-TolC from *Actinobacillus* (14, 125).

The AcrAB-TolC complex is comprised of three different proteins: TolC, the outer-membrane channel protein (137), AcrA, the periplasmic linker protein (138), and AcrB, the inner membrane protein (139). AcrB is the functional unit of the efflux pump, which uses the proton motive force to actively expel substrates from the cell (Figure 1-1) (139–141). In order to assemble the AcrAB-TolC efflux pump, an AcrAB subcomplex first forms containing a 6:3 ratio AcrA to AcrB proteins (142). It is hypothesized that the AcrAB subcomplex then walks along the inner membrane until it encounters a TolC trimer and then forms AcrAB-TolC (142, 143). In this configuration, AcrB can recruit and expel substrates in a single direction (144) through conformational changes (140–142). Additionally, AcrB has multiple channels through which it recruits substrates (145, 146).

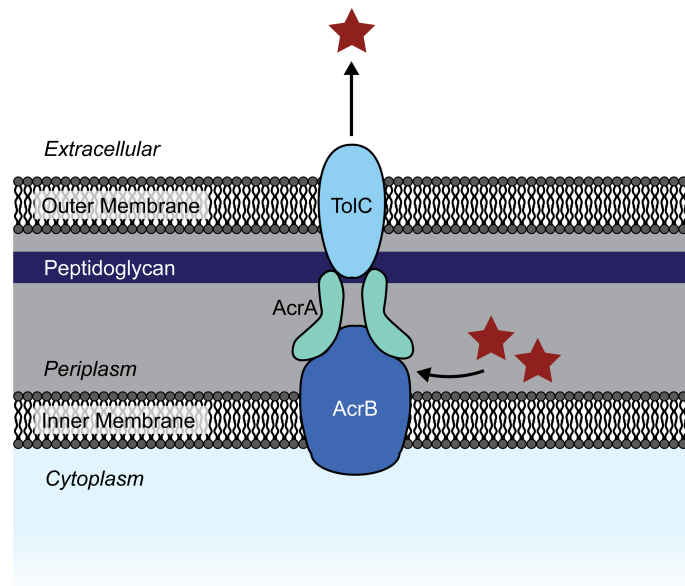


Figure 1-1. Schematic of an AcrAB-TolC efflux pump.

The AcrAB-TolC efflux pump consist of the functional pump unit, AcrB, the periplasmic linker protein, AcrA, and the outer membrane channel, TolC. Substrates can be exported through AcrAB-TolC by either entering AcrB channels located in the cytoplasm or the (141, 143).

The different channels could explain how AcrAB-TolC can export such a broad spectrum of substrates (145, 147); for example, ethidium bromide prefers one channel, while erythromycin prefers another channel (142).

The outer membrane channel, TolC, is also important as a porin (148), a cell-surface receptor (149), and a component of numerous other efflux pumps in *E. coli*, including AcrEF-TolC, MdtEF-TolC, EmrAB-TolC, EmrKY-TolC, MdtABC-TolC, and MacrAB-TolC (150–155). However, TolC primarily provides resistance through the AcrAB-TolC complex as only these TolC-related genes have been found to be upregulated in clinical isolates (156). Additionally, due to its role in numerous and critical cellular functions, including cell division, metabolite regulation, and growth, TolC exists in excess relative to AcrA and AcrB (157, 158). Gene expression of *tolC* also follows the same upregulation and downregulation under different stressors (159, 160) as it has a upstream DNA binding regions to the *acrAB* operon (161). Thus, *acrAB* expression governs the quantity of AcrAB-TolC efflux pumps and the levels of antibiotic resistance.

1.2.2. Regulation of AcrAB-TolC Efflux Pumps

Both *tolC* and the *acrAB* operon are upregulated via a ‘marbox’ or a binding site for transcriptional stress response activators, MarA, SoxS, and Rob (161, 162). The marbox is located upstream of *acrA*’s promoter in the coding region of *acrR* (163). The different stress response activators SoxS, Rob, and MarA are upregulated by different stress response signals and turn on a suite of over 60 downstream genes, including efflux pumps, porins, and enzymes (164–166). SoxS is upregulated in the presence of oxidative stress by the active form of its local regulator SoxR (167). Rob is post-translationally activated in

the presence of osmotic stress, such as bile salts, fatty acids, and antimicrobial peptides (168, 169). MarA is regulated by the positive-negative feedback loop of the *marRAB* operon (165, 170, 171). The activator, MarA, is upregulated when its repressor, MarR, binds to the stressor, such as salicylate, and becomes inactive (172, 173). The marbox allows robust upregulation of *acrAB* under the presence of a wide variety of stressors (165) (Figure 1-2).

Meanwhile, the *acrAB* operon is primarily downregulated by the operon's local repressor, AcrR (163, 174). AcrR binds upstream of *acrA* on the coding region of *acrR* (174, 175) (Figure 1-2). Deletion of *acrR* leads to a 1.5- to 6-fold increase in *acrAB* gene expression compared to wild type (157, 159, 175). Studies have found that *acrR* knockout strains display increased swimming motility, biofilm formation, and virulence (175–177). The AcrR homodimer can also be post-translationally regulated by certain substrates of the AcrAB-TolC efflux pump, such as ethidium bromide, proflavine, and rhodamine 6G (178, 179). The *acrAB* operon can also be repressed by overexpression of AcrS (formerly EnvR), which is the local repressor for another multidrug efflux pump, AcrEF-TolC (180). Additionally, it is hypothesized that both MprA (formerly EmrR), which is the transcriptional regulator of the *emrAB* operon for EmrAB efflux pump (181), and phosphorylated PhoP, which is a transcriptional regulator responsible for the stress response of magnesium starvation (182), can repress *acrAB* expression due to consensus in their binding sites with the promoter region of *acrA* (182, 183). The quantity of AcrAB-TolC efflux pumps is carefully tuned by its local and global regulators under a variety of stresses and different conditions.

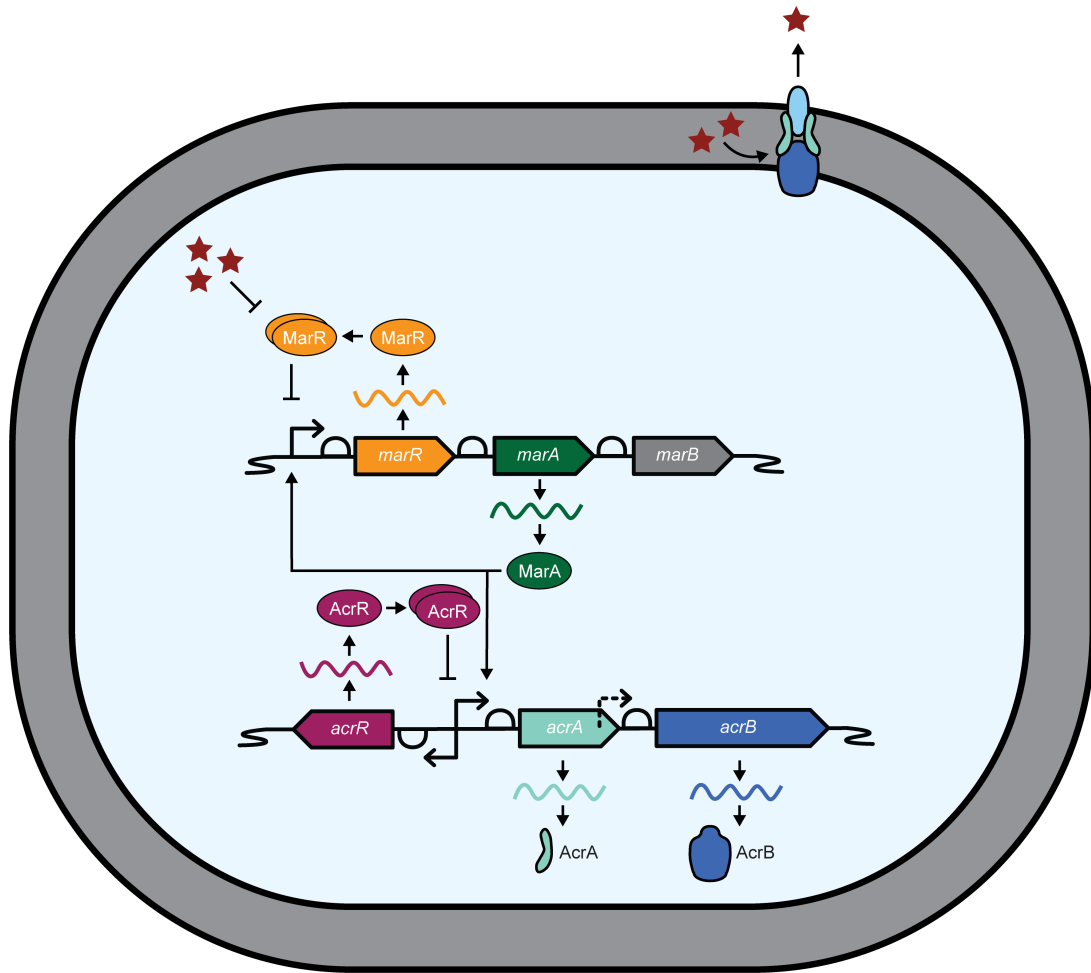


Figure 1-2. Native regulation of the *acrAB* operon.

The global stress response *mar* operon and the local repressor *acrR* are the main pathways to upregulate *acrAB* in response to aromatic stress compounds, such as chloramphenicol.

1.2.3. Importance of AcrAB-TolC Efflux Pumps in Complex Environments

Increased levels of multidrug resistance are often attributed to the AcrAB-TolC efflux pump system (156, 184–186). While this correlation between efflux pumps and resistance is well understood, the role of efflux pumps in more realistic and dynamic conditions remains relatively unknown due to these experimental parameters being less often studied (187). For example, the concentration of an antibiotic at the site of a bacterial

infection will slowly increase over time opposed to a sudden treatment (188); yet, most in vivo studies hold the antibiotic concentration constant (189). Additionally, in industrial biosynthesis, cells may be engineered to produce a toxic compound, causing the intracellular toxicity to slowly rise (190). Recent findings have also identified how the expression of efflux pumps, such as AcrAB-TolC, can affect mutation rates (191, 192). Here, we use the AcrAB-TolC efflux pumps to explore how antibiotic resistance genes impact survival and evolution in different environmental conditions.

1.3. Summary

The objective of this work was to gain insight into how complex dynamics, such as fluctuations in antibiotic concentration and differences in population diversity, affect antibiotic resistance and its evolution using the AcrAB-TolC efflux pumps as a case study. In **Chapter 2**, we explored how different rates of antibiotic introduction impact population diversity and increase resistant phenotypes. We found that faster rates of antibiotic introduction could reduce the benefit of having an antibiotic resistance gene and, thus, improve treatments. In **Chapter 3**, we studied heterogenous microcolonies treated with antibiotics. We observed that, within these microcolonies, cells containing efflux pumps could have a detrimental effect on their neighboring cells. In doing so, we identified how both antibiotic introduction rates and mixed populations impact the short-term emergence of antibiotic resistance.

To further understand how these two factors could impact long-term antibiotic resistance and its evolution, we turned to adaptive evolution experiments. In **Chapter 4**, we investigated how antibiotic concentrations and genotypic backgrounds may promote

survival of antibiotic treatments. High levels of resistance were more likely to evolve under near-MIC treatments, regardless of the starting genotype. Yet, depending on the presence of efflux pumps, different genetic backgrounds followed distinct genetic pathways to reach this phenotypic convergence. Next, in **Chapter 5**, we explored how complex dynamics — variations in antibiotic introduction rate and population diversity — could further promote the emergence of antibiotic resistance. We identified that slow introduction of antibiotic resistance could provide high levels of antibiotic resistance, while reducing fitness burdens. Meanwhile, we found that co-cultured populations were significantly less likely to evolve antibiotic resistance under fast changing stress introductions opposed to slow changing stress introduction rates.

This work provides insight into the complex and confounding factors that contribute to the evolution of antibiotic resistance, and what lessons may help us mitigate this continued pattern of evolution of antibiotic resistance.

2. STRESS INTRODUCTION RATE ALTERS BENEFIT OF

AcrAB-TolC EFFLUX PUMPS

2.1. Disclosure & Copyright Statement

This chapter is a modified version of “Stress Introduction Rate Alters Benefit of AcrAB-TolC Efflux Pumps” by Ariel M. Langevin and Mary J. Dunlop, 2017. Journal of Bacteriology, 200 (1) e00525-17. ©2017 by American Society for Microbiology. The publisher allows authors to retain the right to reuse full article in dissertations.

2.2. Abstract

Stress tolerance studies are typically conducted in an all-or-none fashion. However, in realistic settings—such as in clinical or metabolic engineering applications—cells may encounter stresses at different rates. As such, how cells tolerate stress may depend on its rate of appearance. To address this, we study how the rate of introduction affects bacterial stress tolerance by focusing on a key mechanism for stress response. Efflux pumps, such as AcrAB-TolC from *E. coli*, are membrane transporters well known for their ability to export a wide variety of substrates, including antibiotics, signaling molecules, and biofuels. Although efflux pumps improve stress tolerance, pump overexpression can result in a substantial cost to the cells by altering membrane fluidity and slowing growth. We hypothesized that the ideal pump expression level would involve a rate-dependent trade-off between the benefit of pumps and the cost of their expression. To test this, we evaluated the benefit of the AcrAB-TolC pump under different rates of stress introduction, including a step, fast ramp, and slow ramp. Using two chemically diverse stresses, the antibiotic chloramphenicol and the bio-jet fuel precursor pinene, we assessed the benefit provided by

the pumps. A mathematical model describing these effects predicted the benefit as a function of the rate of stress introduction. Our findings demonstrate that as the rate of introduction is lowered, stress response mechanisms provide a disproportionate benefit to pump-containing strains, allowing cells to survive beyond the original inhibitory concentrations.

2.3. Introduction

In realistic conditions, the environments bacteria are exposed to are seldom as constant as those in the laboratory. For example, in clinical applications, antibiotic concentrations at the site of the infection will depend on *in vivo* drug absorption and elimination (193). In metabolic engineering, the synthesis of a product such as a biofuel can depend heavily on the cell cycle or stage of the production process, and thus changes dramatically with time (194). Studying how bacteria respond to dynamic, stressful environments is key to both understanding drug resistance, as well as harnessing their power for metabolic engineering applications. Although recent literature has begun to explore the effect of fluctuating environments on bacterial fitness, the focus has primarily remained on step changes, such as switching suddenly from a non-stressful to a stressful environment (195–199). Other studies have focused on the long-term effects of changing environments, including the impact of spatial gradients on mutations and the response of a general stress response pathway to environmental change (106, 200, 201). In contrast, here we study how varying the rate at which stress is applied over short, key periods of time affects fitness.

To survive in stressful environments, cells utilize numerous stress response

mechanisms. Examples include efflux pumps, inactivating enzymes, and outer membrane protein channels (79, 202, 203). However, despite the substantial benefit these mechanisms can provide, they can also be costly and thus place an extraneous burden on the cell (109, 204). As such, expression of stress response genes may introduce negative fitness effects. Understanding how cells balance these cost-benefit trade-offs will provide insight into how cells respond and cope with stressful environments.

As a case study, we focused on a well-known multidrug resistance pump, AcrAB-TolC from *E. coli*. Multidrug resistance pumps have been studied extensively for their ability to export a wide variety of compounds, including antibiotics, biofuel intermediates, signaling molecules, dyes, and detergents (140, 205). The pumps maintain low intracellular concentrations of stressors through active efflux via the proton motive force (206–208). These membrane transporters are found across prokaryotic and eukaryotic species (209). In eukaryotic cells, efflux pumps present a significant hurdle as they provide resistance to anticancer drugs (210). In prokaryotic cells, efflux pumps increase the antibiotic dose required for treatment of infections and also play a role in quorum sensing and biofilm formation (140, 211). Along with their clinical relevance, efflux pumps offer potential as a metabolic engineering tool. For instance, efflux pumps are able to improve fitness and solvent tolerance of cells with engineered biofuel production pathways (212–215). Thus, efflux pumps are a significant stress tolerance mechanism that operate on a diverse range of substrates.

In this work, we investigated how the trade-off between the benefit of the pumps and the cost of pump expression depends on the rate of stress introduction. By analogy,

consider a bilge pump on a boat. If water leaks slowly into the boat, the pump can keep up and the boat will stay afloat. However, if the same volume of water appears rapidly, the boat may sink. We asked whether stress tolerance has a similar rate-dependent effect. To study this, we evaluated the benefit of the AcrAB-TolC pump under time-varying stress environments. We assess the performance of cells with and without pumps when the stressors were presented in different forms—as a step, a fast ramp, or a slow ramp. Our overall goal was to quantitatively determine the trade-off between stress tolerance and growth advantage for cells with pumps. To achieve this, we co-cultured cells with and without AcrAB-TolC efflux pumps. The relative fraction of cells with and without the pumps changed with time and depended on the rate of stress introduction. We validated our results using two structurally distinct pump substrates, the antibiotic chloramphenicol and the bio-jet fuel precursor pinene. We developed and experimentally validated a mathematical model that captures the system behavior. Using this model to evaluate the cost-benefit landscape of pump expression, we found that slower rates of stress introduction exaggerate the benefit of the pumps. This work demonstrates that the rate at which stress is applied can have a dramatic impact on bacterial fitness.

2.4. Results

We began by quantifying the benefit and cost of expressing efflux pumps in an environment with a constant, unchanging level of stress. We initially used chloramphenicol as a stressor because it is often considered for treatment of bacterial infections (216, 217). It is a bacteriostatic agent that works by inhibiting protein synthesis (218). Chloramphenicol is a known substrate of the AcrAB-TolC pumps; the pump conveys a

five-fold increase in the minimum inhibitory concentration (219). To measure the benefit of pumps, we initially grew cells with and without *acrB* in different levels of constant chloramphenicol. Since the AcrB protein is the active pumping unit and produces efflux driven by the proton motive force, deleting *acrB* renders the entire AcrAB-TolC efflux pump non-functional (206). We conducted experiments in wild type *E. coli* and in the same strain with an *acrB* deletion, and confirmed that the efflux pump provides protection against chloramphenicol (Figure 2-1A). We were able to recover chloramphenicol tolerance by complementing Δ *acrB* cells with a plasmid containing an IPTG-inducible version of the *acrAB* operon, *acrAB-sfgfp*. Even without induction, the basal expression was sufficient to restore wild type levels of chloramphenicol tolerance. Therefore, the AcrAB-TolC efflux pumps provide a benefit under constant chloramphenicol conditions.

Next, we asked whether there was a cost associated with expressing these pumps. Although it is known that overexpression of membrane proteins can be costly to cells (220–222), the mechanisms behind the fitness cost of efflux pumps are not entirely clear (222). One potential mechanism is due to a change in intracellular pH that impacts cellular metabolic pathways (223). When inducing the *acrAB-sfgfp* strain with IPTG, we found that at high induction levels there was a severe growth cost, indicative of the harmful effects of overexpression (Figure 2-1B). As a result, we conducted subsequent experiments without IPTG induction to balance the chloramphenicol-tolerance benefit against the cost of the pumps.

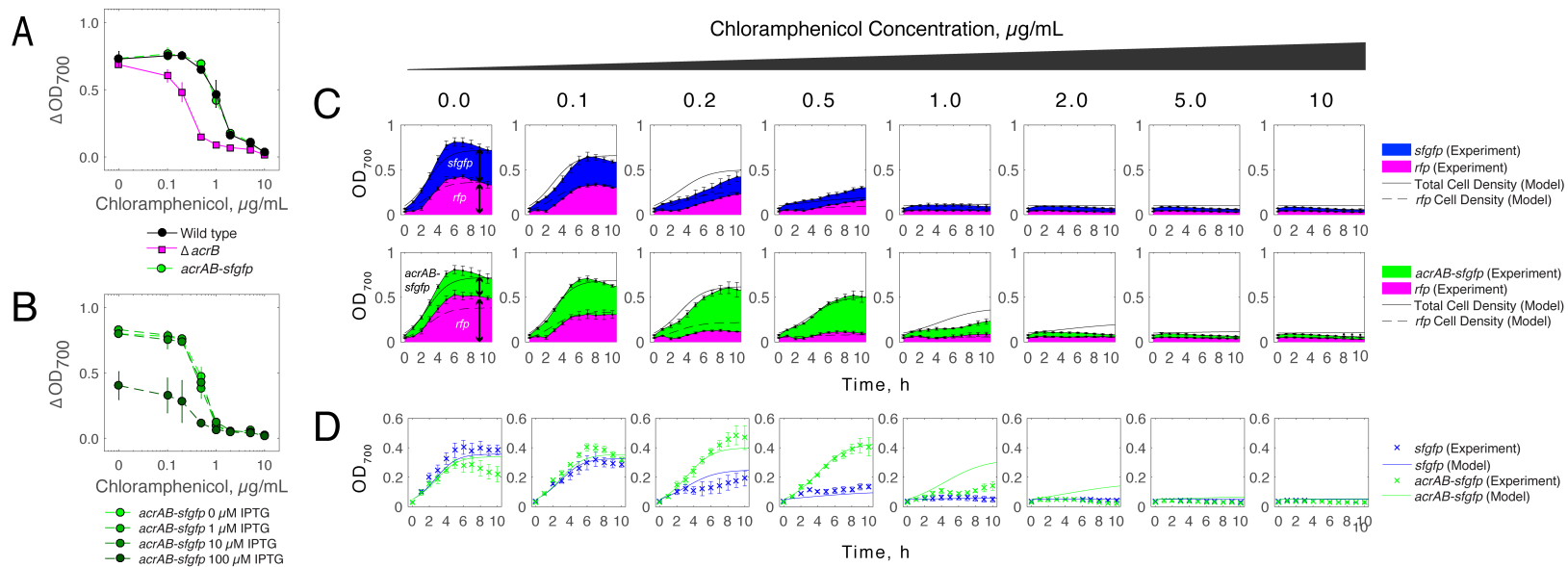


Figure 2-1. Benefits and costs of AcrAB-TolC efflux pumps.

(A) Cell density as a function of chloramphenicol concentration. Wild type is *E. coli* BW25113, the knockout strain is *E. coli* BW25113 ΔacrB , and acrAB-sfgfp is *E. coli* BW25113 ΔacrB transformed with the plasmid pBbA5k- acrAB-sfgfp , which contains an IPTG-inducible promoter controlling a transcriptional fusion of the acrAB efflux pump operon and super folder green fluorescent protein gene, sfgfp . ΔOD_{700} is the difference in optical density at 700nm between the initial sample at $t = 0$ h and after $t = 24$ h. **(B)** Induction of acrAB-sfgfp reduces cell growth. Error bars in (A-B) show standard deviations of $n = 3$ biological replicates. **(C)** Growth of two competing strains under different chloramphenicol doses. The full dose of chloramphenicol is added at the beginning of the experiment, $t = 0$ h. The plots depict the total cell density of the co-culture, and the stacked shaded areas under the curve quantify the fraction of the culture containing either a rfp or sfgfp plasmid (Figure 2-2). As a control, top row shows competition between two strains lacking efflux pumps, sfgfp and rfp . The bottom row shows competition between a strain with the efflux pump, acrAB-sfgfp , and one without the efflux pump, rfp . Dots show experimental data with error bars corresponding to standard deviations of $n = 3$ biological replicates. Lines are the computational model predictions for the total population (solid line) and the rfp strain (dashed line). **(D)** Data extracted from the multispecies competition experiments shown in (C) comparing strains with and without pumps. Biomass of acrAB-sfgfp (green) compared with biomass of sfgfp (blue) after $t = 8$ h. Data points show mean and standard deviations of $n = 3$ biological replicates; solid lines show mathematical model predictions.

To determine whether the benefit and cost of efflux pumps change in dynamic stress environments, we competed strains with and without pumps against each other and recorded the relative population sizes over time under different antibiotic treatment conditions. In clinical settings, bacteria that contain efflux pumps are able to outcompete those without and are found at a higher frequency in clinical isolates (224), motivating our use of a competition assay. This assay can identify subtle differences in growth among strains because more fit strains become overrepresented in the population (198, 213).

We began by competing strains with and without efflux pumps in a constant environment where we added antibiotics at $t = 0$ h. First, we conducted a control experiment with two $\Delta acrB$ strains, one harboring a plasmid encoding super-folder green fluorescent protein (*sfgfp*) and a second with a plasmid encoding red fluorescent protein (*rfp*) (Figure 2-1C). We first measured the optical density of the co-cultured competing strains (Figure 2-2A). The fluorescent reporters allowed us to quantify the fraction of each cell present in the co-culture over time using flow cytometry (Figure 2-2B). Consequently, we were able to quantify the relative proportions of the two competing strains by using the fraction of sorted cells containing *rfp* or *sfgfp* to estimate the fraction of the total population harboring each plasmid (Figure 2-2C-D). We recorded cumulative cell density and the proportion of the two competing strains in the co-culture as a function of time.

As expected, the *sfgfp* and *rfp* strains performed similarly under all levels of antibiotics since the only difference between the strains was the color of fluorescent reporter. Next, we competed a $\Delta acrB$ strain complemented with *acrAB-sfgfp*, against the same strain with *rfp* alone. We found that in the absence of antibiotics, the strain without

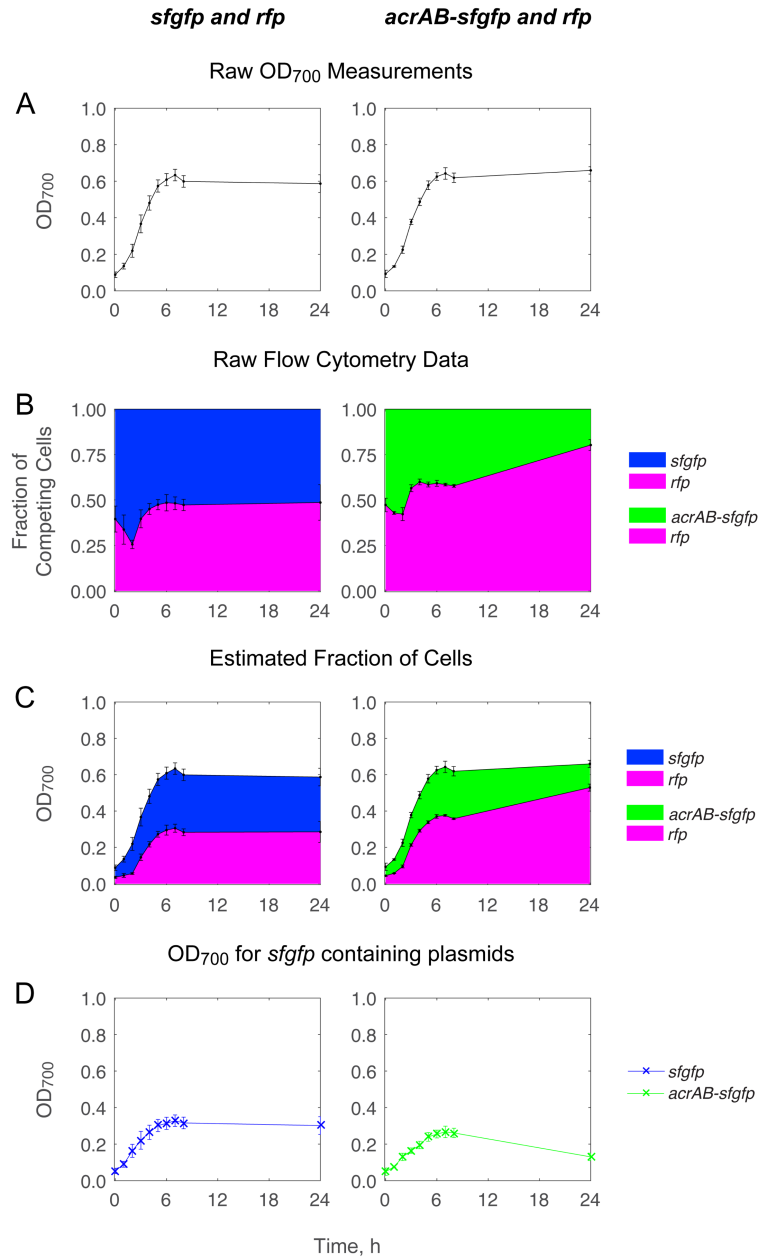


Figure 2-2. Schematic of methodology and data collection.

(A) Multispecies growth curves depicting the raw optical density readings at 700nm for the co-cultured samples. The error bars are the standard deviations of the optical density for $n = 3$ biological replicates. (B) Flow cytometry data is collected for a subset of the samples. Error bars are standard deviations of $n = 3$ biological replicates. (C) The fraction of biomass attributed to each strain in the co-culture is approximated by multiplying the optical density by the fraction of these strain. (D) OD₇₀₀ for the *sfgfp*-containing strains extracted from the co-culture data sets. (C-D) Data points and their error bars are based upon the standard deviations for the raw optical density and sorted flow cytometry data.

pumps outperformed the strain with pumps (Figure 2-1C). Because efflux pumps are costly and unnecessary in conditions without antibiotics, the strain with no pumps was able to dominate. In contrast, under conditions with low doses of chloramphenicol, the efflux pump containing strain dominated. Beyond a certain concentration of antibiotic neither strain was able to survive. These results are consistent with our earlier findings that the benefit of the pumps exists only for certain antibiotic doses (Figure 2-1A).

In order to explore the effects of antibiotic addition and the benefit of pumps, we developed a mathematical model using a system of coupled ordinary differential equations to describe the competition between the species. The model is based on the Van Impe *et al.* bacterial growth model, which builds upon the Monod equation for growth kinetics (225–227). The state variables describe the population size for each of the species, and the substrate consumed by both species. The growth rate of each population depends upon the available substrate and also the concentration of the antibiotic in the environment. The model parameters were estimated by minimizing the sum of squared residuals and using the growth and toxicity curves for the single species experimental data (Figure A-1). The multispecies growth was then fit using the parameters determined from the toxicity curves and single species data. The model shows good agreement with the trends in our experimental findings, both in the overall growth of the two species as well as the approximate proportion of each species in the culture.

To visualize the relative effect of efflux pumps, we plotted the data from *sfgfp* alongside *acrAB-sfgfp* (Figure 2-1D). These data are extracted from the co-culture experiments shown in Figure 2-1C where *sfgfp* is competed against *rfp* (top) and *acrAB-*

sfgfp is competed against *rfp* (bottom). This comparison allows us to directly highlight the growth differences across environments and strains without and with efflux pumps. The model captures these trade-offs, demonstrating its predictive power in estimating where strains outcompete each other in competitive growth conditions.

Next, we asked how differences in the rate of antibiotic addition affected the cost and benefit trade-offs for efflux pump expression. We tested dynamic environments where antibiotics were applied at different rates during the exponential growth phase. We kept the cumulative amount of antibiotic added constant, but varied the ramp rate (Figure 2-3A-C). We first considered a step increase in antibiotics at $t = 3$ h (Figure 2-3A, D). Under these conditions the cells grew rapidly prior to addition of antibiotics, with *sfgfp* outperforming *acrAB-sfgfp* prior to $t = 3$ h, making it difficult for *acrAB-sfgfp* to recover after antibiotic was added, even in conditions where the pumps offer an advantage.

When we decreased the rate of chloramphenicol addition, the *acrAB-sfgfp* strain was able to outperform the *sfgfp* strain under a broader range of chloramphenicol concentrations. First, we spaced the addition of chloramphenicol out over the range from $t = 2$ to 4 h (Figure 2-3B, E). As predicted by the mathematical model, at intermediate chloramphenicol concentrations we observed a modest benefit to the pumps. For the slowest antibiotic addition rate, we added chloramphenicol from $t = 0.5$ to 5.5 h (Figure 2-3C, F). In this case, we found a more dramatic increase in the benefit of the pumps. In particular, we observed a substantial benefit in fitness for efflux pump containing strains that exists well above their minimum inhibitory concentration of 1 $\mu\text{g/mL}$ (Figure 2-1A-B). This finding emphasizes the importance of the rate at which stresses are introduced.

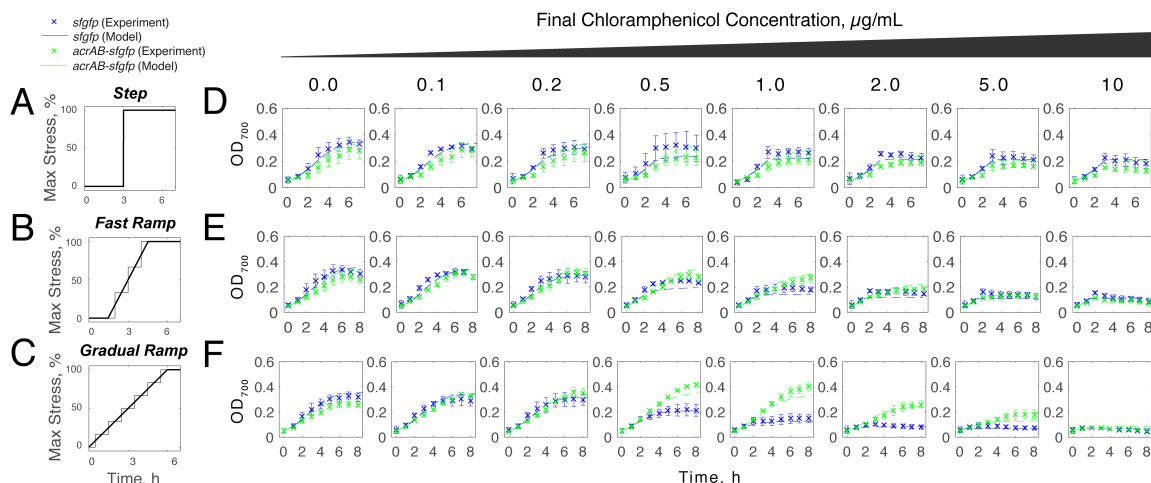


Figure 2-3. Rate of chloramphenicol addition affects survival.

(A-C) Three different rates of chloramphenicol introduction: (A) step introduction, (B) fast ramp, and (C) gradual ramp. The thick solid line shows the values used in the mathematical model; thin solid line shows experimental treatment used to approximate the constant introduction rate. The total amounts of chloramphenicol added in (A-C) are equal. (D-F) Competitive growth under different rates of chloramphenicol addition. The growth of *acrAB-sfgfp* (green) compared against growth of *sfgfp* in the competition experiments (dots) and model predictions (solid lines) for different chloramphenicol introduction rates as shown in (A-C), respectively. As in Figure 2-1D, these data have been extracted from competition experiment data. Note that dead cells can still cloud the solution; therefore, non-zero optical densities do not necessarily imply that cells are alive. Data points show mean and standard deviations of $n = 3$ biological replicates.

Building on the success of our model predictions, we next used the model to quantify the benefits and costs of efflux pump expression as a function of the total amount of antibiotic added and the rate at which it is introduced. In order to quantify the growth advantage provided by the efflux pumps, we calculated the ‘benefit ratio’ provided by the pumps, which we defined as the ratio of the biomass of *acrAB-sfgfp* to biomass of *sfgfp* after 8 hours (228). As a result, a benefit ratio greater than one means that strains with efflux pumps are able to outcompete cells without, while a value less than one means that pump expression hinders growth. Using our model, we calculated the benefit ratio across

a range of chloramphenicol introduction rates and total antibiotic amounts (Figure 2-4A). At very low concentrations of chloramphenicol, pumps are unnecessary and there is a cost to their expression so the benefit ratio is below one, regardless of the rate of introduction. At very high concentrations, neither strain can grow so the benefit ratio is approximately one for all introduction rates. Meanwhile, at intermediate chloramphenicol concentrations, we observed dramatic rate dependent differences between the strains. When the stress appears slowly, the strains with the pumps are at a significant advantage. In fact, this phenomenon can result in conditions where bacteria are able to survive antibiotic doses well beyond those they can tolerate with rapid drug introduction. This benefit is likely due to the ability of bacteria to maintain low intracellular levels of antibiotics using efflux pumps when undergoing slow antibiotic introduction. Therefore, the rate at which an antibiotic or stressor is added will have a critical impact on bacterial survival.

To verify the model predictions, we calculated the benefit ratio from the experimentally measured data from Figure 2-3D-F by evaluating the ratio of *acrAB-sfgfp* to *sfgfp* biomass under the same antibiotic treatment profiles. When the rate of introduction is a quick step introduction, cells with efflux pumps have a negligible benefit (Figure 2-4B); as the introduction rate is slowed, the benefit of the pumps slightly increases at intermediate chloramphenicol concentrations (Figure 2-4C) and slowing the rate further provides even greater benefit (Figure 2-4D). We note that the model was fit to raw data from toxicity curves and growth curves performed without antibiotics (Figure 2-2). Without further fitting, the model is able to predict trends in the benefit of the efflux pumps given different rates of stress introduction. Statistical analysis suggests that the model

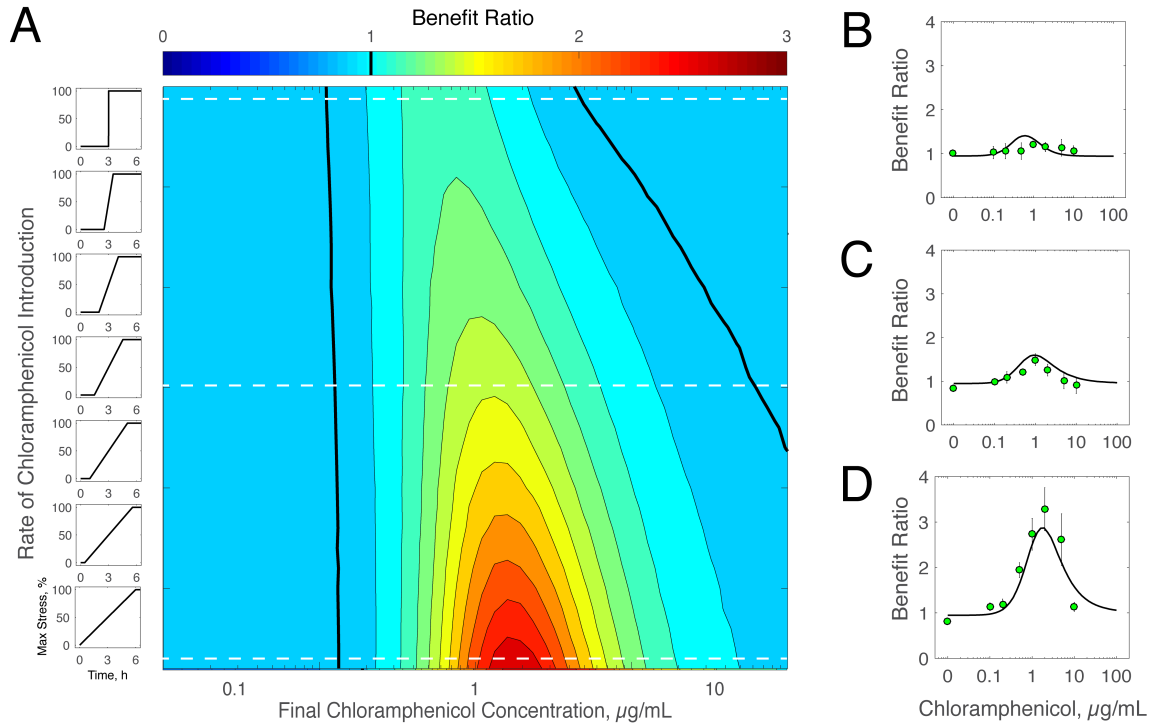


Figure 2-4. Model predictions and experiments measuring benefit of pumps.

(A) Contour plot of the benefit ratio of the efflux pumps. Model predictions for biomass, N , of an *acrB*-containing strain in relation to an Δ *acrB* control strain after $t = 8$ h are used to predict the benefit ratio landscape. Plot shows results for different maximum levels of chloramphenicol (x-axis) and different rates of chloramphenicol addition (y-axis). **(B-D)** Experimental results (dots) showing benefit of efflux pumps compared to model predictions (solid line). Data is ratio of biomass of *acrAB-sfgfp* strain to *sfgfp* after $t = 8$ h. Rate of antibiotic introduction is shown in Figure 2-3A-C, respectively, and denoted on the contour plot in (A) with white dashed lines. Error bars show standard deviation for $n = 3$ biological replicates.

agrees well with the data, with Pearson's correlation coefficients close to 1 (Table A-1).

Additionally, we performed experiments where the initial biomass was an order of magnitude lower than in the original conditions (Figure 2-5). The data show good qualitative agreement with the model predictions, where slow antibiotic introduction results in a greater benefit of pumps. These results indicating that our findings are not specific to one set of initial conditions.

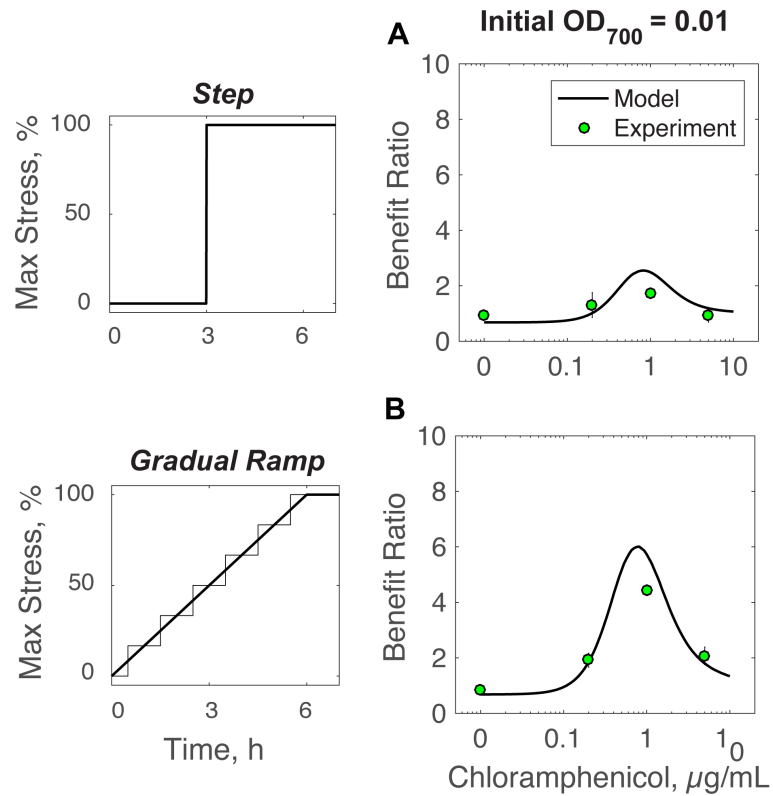


Figure 2-5. Benefit ratios for lower initial inoculum size.

(A-B) Experimental results (dots) showing benefit of efflux pumps compared to model predictions (solid line). Data is ratio of biomass of *acrAB-sfgfp* to *sfgfp* after $t = 24$ h. These co-cultures were tested under a gradual ramp (A) and step at $t = 3$ h (B) over 6 hours. Error bars show standard deviations for $n = 3$ biological replicates.

We next asked whether our findings on the rate-dependent benefit of efflux pumps would generalize to other stressors. To do this, we conducted experiments with a structurally and functionally dissimilar efflux pump substrate. Pinene is a bio-jet fuel precursor that can be synthesized by *E. coli*; however, pinene is also toxic to the cells (229). The AcrAB-TolC efflux pump is known to increase tolerance to pinene and other solvents (213, 230). We first measured the benefit of the pumps and, as expected, observed an increase in pinene tolerance in strains with the efflux pump (Figure 2-6A). We next measured the cost of pump expression in the presence of pinene using the IPTG-inducible

acrAB-sfgfp strain (Figure 2-6B). As *acrAB-sfgfp* is induced, there is an impact on cell growth. However, low levels of induction do convey a slight benefit compared to basal levels (Figure A-2), therefore we conducted the subsequent experiments using 5 μ M IPTG, as this induction level best mirrors wild type in the presence of pinene (Figure 2-6A). The cost-benefit characteristics of pinene closely mirror the trade-offs that we observed for

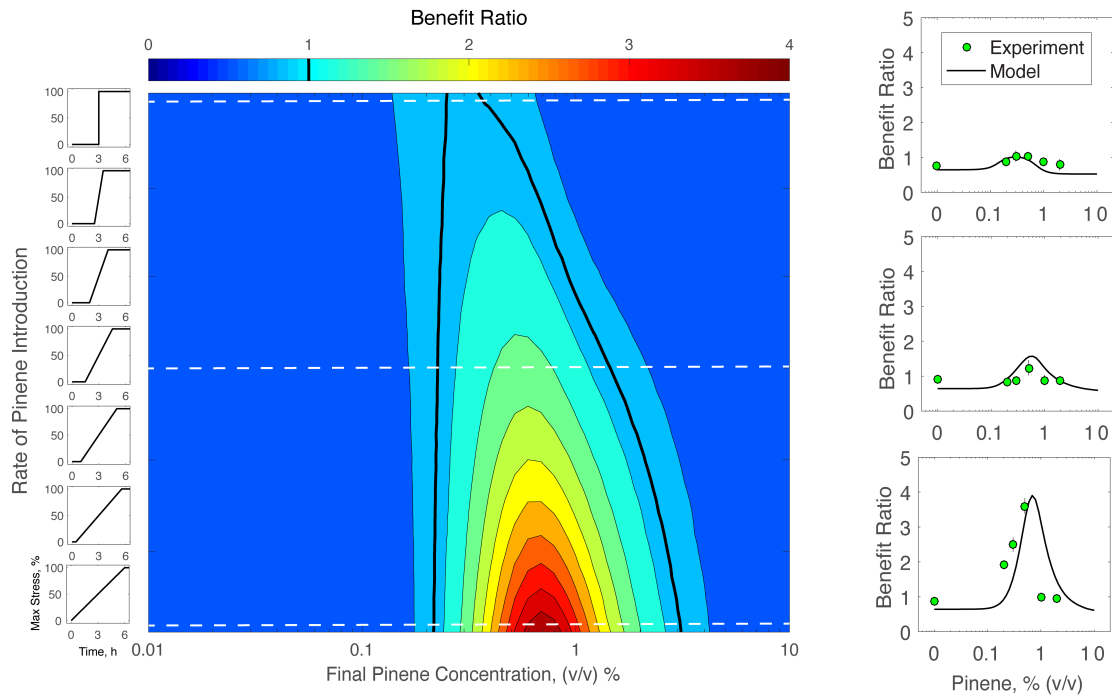


Figure 2-6. Benefit and cost trade-offs of AcrAB-TolC efflux pumps in pinene.

(A) Cell density as a function of pinene concentration. Wild type is *E. coli* BW25113, the knockout strain is *E. coli* BW25113 Δ *acrB*, and rescue strain is *acrAB-sfgfp*. Δ OD₇₀₀ is the difference in optical density between the initial sample at $t = 0$ h and after $t = 8$ h. (B) Induction of *acrAB-sfgfp* reduces cell growth in the presence of pinene. Error bars in (A-B) show standard error of $n = 3$ biological replicates. (C) Contour plot of the benefit ratio of the efflux pumps. Model predictions for biomass of an *acrB*-containing strain in relation to an Δ *acrB* strain after $t = 8$ h. Plot shows results for different maximum levels of pinene (x-axis) and different rates of pinene addition (y-axis). (D-F) Experimental results (dots) showing benefit of efflux pumps compared to model predictions (solid line). Data is ratio of biomass of *acrAB-sfgfp* to *sfgfp* after $t = 8$ h. The rate of pinene introduction is shown in Figure 2-3A-C, respectively, and denoted by white dashed lines on the contour plot in (C). Error bars show standard deviation for $n = 3$ biological replicates.

chloramphenicol in a constant environment.

To accurately capture the effect of pinene we modified our mathematical model to include a term that allows for cell lysis. Chloramphenicol is bacteriostatic so optical density measurements remain roughly constant after the cells have died (231). In contrast, we observed decreases in optical density following pinene treatment (Figure A-3). To accommodate the bactericidal effect of pinene, we adjusted our model to include a term describing this effect. We simulated the trade-off landscape for different rates of pinene addition (Figure 2-6C) and observed a general trend where, as with chloramphenicol, the benefit ratio is high at intermediate levels of pinene stress when the rate of introduction is low. However, the peak for pinene is taller, as the efflux pumps convey an even larger benefit.

We next used the model to select pinene rates that show low, moderate, and high benefit ratios and conducted competition experiments under these conditions (Figure A-4). Extracting these data, the experimental and computational results demonstrate that there is a dramatic benefit conveyed for slow introduction rates (Figure 2-6D-F). We observed that cells with pumps can survive significantly higher levels of pinene when it is added slowly than they can when it is added all at once.

2.5. Discussion

In this study, we focused on the rate-dependent nature of the benefit of efflux pumps, which is significant given the role pumps play across diverse fields. Our work here extends to both understanding antibiotic tolerance and potential applications in biosynthetic processes. By studying two unique substrates of the AcrAB-TolC pump, we

were able to validate that under slow introduction of stress, pumps provide a disproportionate benefit that is not unique to the individual substrate. Understanding complex strategies bacteria employ to tolerate stress can provide insight into development of therapeutic techniques and can enable us to exploit these effects in biochemical engineering. By determining conditions where efflux pump containing strains lack a competitive edge, we can identify domains where antibiotic tolerance is reduced. For metabolic engineering applications, this optimization can help characterize and improve yields of biosynthetic compounds such as biofuels (232, 233).

In realistic conditions, cells are rarely exposed to environments as constant as in laboratory experiments. Since the environment can have a large impact on how bacteria respond to stress, it is important to study the behavior of cells in time-varying conditions. These ideas have been explored previously in the context of extended exposure to stress and through temporal and spatial gradients. In spatially-distinct environments, studies have demonstrated that prolonged exposure to a stressful spatial barrier can be overcome by cells adapting to the stress through tolerance, then resistant mutants (106). Similarly, graded increases in antibiotic concentrations across several days can lead to mutations (201). Thus, even a subtle benefit in fitness on a short-term scale, can result in mutants in daughter cells in stressful environments. Additionally, on a shorter time scale, stress response pathways have been shown to depend on the rate of environmental change. For example, *Bacillus subtilis* turns on stress-specific or general stress response pathways depending on the rate at which stress is applied (234). By studying time-varying stress, we can better understand how stress response mechanisms operate under realistic

environments.

In this work, we have demonstrated that the benefit of efflux pumps depends heavily on the rate of stress introduction. We found that strains exposed to slower stress introduction rates were able to tolerate cumulative concentrations well beyond what they could survive if the stress appeared suddenly. We also confirmed this through mathematical modeling; fits to data where the stressor was added all at once allowed us to accurately predict the benefit that pumps confer under different stress introduction rates. We found that efflux pumps provide a disproportionate benefit when the rate of stress introduction is slow.

2.6. Contributions Statement

The authors of this work were Ariel M. Langevin (A.M.L.) and Mary J. Dunlop (M.J.D.). A.M.L. conducted the experiments, analyzed the data, and performed the modeling, M.J.D. supervised the research. Both authors wrote the manuscript.

2.7. Methods

2.7.1. Strains and Plasmids

We used *E. coli* strains BW25113 and BW25113 $\Delta acrB$. The wild type strain BW25113 is the parent strain for the Keio collection (235). BW25113 $\Delta acrB$ was derived from Keio collection strain JW0451 (BW25113 $\Delta acrB::kan$), where we removed the kanamycin resistance marker following the pCP20 protocol from (236).

We used the plasmids pBbA5k-rfp, pBbA5k-sfgfp, and pBbA5k-acrAB-sfgfp in experiments. The plasmid pBbA5k-rfp is from the BglBricks library (237, 238). The

pBbA5k vector contains a medium-copy number (p15A) origin of replication, a P_{lacUV5} promoter, and a kanamycin resistance marker. pBbA5k-sfgfp was constructed using the pBbA5k vector and *sfgfp* from pBbSFk-sfgfp (239). Plasmid pBbA5k-acrAB-sfgfp is a transcriptional fusion of *acrAB* and *sfgfp*. We constructed it using the pBbA5k-acrAB plasmid (213) and *sfgfp*, retaining the ribosome binding site of *sfgfp* from pBbSFk-sfgfp (239) in the cloning process. For all constructs, we used the Gibson assembly method and verified results by sequencing (240). Primers for all constructs are listed in Table A-2. Plasmids were transformed into *E. coli* BW25113 $\Delta acrB$ and isolated on Luria Broth (LB) plates with kanamycin (30 $\mu\text{g/mL}$).

2.7.2. Bacterial Growth Conditions

For all experiments, overnight cultures were inoculated from a single colony in 5 mL LB with 30 $\mu\text{g/mL}$ kanamycin, where necessary. Overnight cultures were then grown at 37°C with 200 rpm orbital shaking. Following this, precultures were prepared by diluting the overnight culture 1:50 in LB with 30 $\mu\text{g/mL}$ kanamycin, where necessary. The precultures were grown at 37°C with 200 rpm orbital shaking for 2 hours and then diluted back to an optical density at 700nm (OD_{700}) of approximately 0.2. We used OD_{700} to minimize overlapping of the RFP emission spectrum (241, 242). These 800 μL cultures were then aliquoted into 24-well plates and chloramphenicol, pinene, or IPTG was added, as described below.

For toxicity curves of the individual species and single species growth parameters, 800 μL of these cultures were aliquoted into 24-well plates and chloramphenicol, IPTG, or pinene was added, as described below.

For the competition experiments, co-cultures were created by mixing 400 μ L each of the two competing strains, *acrAB-sfgfp* and *rfp* or *sfgfp* and *rfp*, after individually diluting the strains back to OD₇₀₀ 0.2 as described above. As a result, there was a total of 800 μ L per well in a 24-well plate with the final OD₇₀₀ of 0.2.

2.7.3. Toxicity Experiments

To determine the toxicity of chloramphenicol, we added a final concentration of 0, 0.1, 0.2, 0.5, 1, 2, 5, or 10 μ g/mL to each culture. To evaluate the benefit of pump expression, P_{lacUV5} was induced with 0, 1, 10, or 100 μ M of IPTG. The samples were sealed with evaporation-limiting membranes (Thermo Scientific AB-0580) and grown in 24-well plates at 37°C with 200 rpm orbital shaking. OD₇₀₀ readings were taken using a BioTek Synergy H1m plate reader before incubation (t = 0 h) and after antibiotic exposure (t = 24 h). All experiments were performed in triplicate using biological replicates.

Mirroring to the chloramphenicol toxicity experiments, pinene (α -pinene, Sigma Aldrich P45680) was added to each culture to a final concentration of 0, 0.1, 0.2, 0.5, 1, or 2 (v/v) %. To evaluate the benefit of pump expression, P_{lacUV5} was induced with 0, 1, 5, 10, 50, or 100 μ M of IPTG. OD₇₀₀ readings were taken before incubation (t = 0 h) and after the end of exponential growth phase (t = 8 h).

2.7.4. Competition Experiments

Co-cultures were created by mixing 400 μ L each of the two competing strains, *acrAB-sfgfp* and *rfp* or *sfgfp* and *rfp*, for a total of 800 μ L per well in a 24-well plate. Cultures were treated with increasing concentrations of substrates as shown in Figure 2-

3A-C. The OD₇₀₀ was measured at intervals, every hour for chloramphenicol and every other hour for pinene, through exponential growth phase. In addition, after the OD₇₀₀ readings, 15 µL samples from each culture were diluted 1:10 in phosphate buffered saline (PBS) and measured using a Guava easyCyte HT Sampling Flow Cytometer. Excitation and emission values were 485 and 510 nm for *sfGFP* (sfGFP) and 555 and 584 nm for *rfp* (RFP) fluorescent channels (243, 244).

Flow cytometry data was collected as FCS 3.0 files and was analyzed with custom Matlab scripts. To avoid crosstalk between the red and green channels, control experiments using single-color strains were performed to identify a threshold for classifying a cell as containing sfGFP or RFP during post-processing. The same thresholds were applied for all experiments.

2.7.5. Mathematical Model

To fit the growth of single strains under different environmental conditions, we used a single species model for predicting biomass N (Eq. 1) and substrate availability S (Eq. 2) based on the Van Impe *et al.* model of cell growth (212, 227, 245). This model incorporates environmental conditions, such as a substrate limiting term based on the physiological environment. For the version presented here, we include a term describing the effect of a stressor, E (225).

2.7.5.a. Single species model

$$\frac{dN}{dt} = \alpha \mu_{max} \left(\frac{S}{K_s + S} \right) \left(\frac{1}{1 + \frac{E^n}{R}} \right) N(t) \quad \text{Eq. 1}$$

$$\frac{dS}{dt} = -\frac{1}{\gamma} \mu_{max} \left(\frac{S}{K_S + S} \right) N(t) \quad \text{Eq. 2}$$

The maximum growth rate is μ_{max} , the growth yield provided by the substrate is γ , and the half-saturation constant is K_S . α is a normalizing term that converts the biomass from cell concentration to optical density. The parameters for these models were selected using a least-squares regression minimizing the sum of the residuals for the best fits to the growth curves and the toxicity curves. The coefficients from the models were fit simultaneously. The values for μ_{max} , γ , and K_S were selected based upon the growth curves of individual strains (Figure A-1A-B). Parameter values are listed in Table A-3. Additionally, we added a stressor term to adjust the growth based on the effect of a given stressor concentration E at time t , where

$$E_{step} = \begin{cases} 0 & t < 3 \\ 1 & t \geq 3 \end{cases} \quad \text{Eq. 3}$$

$$E_{fast\ ramp} = \begin{cases} 0 & t < 1.5 \\ \left(\frac{t - 1.5}{3} \right) & 1.5 \leq t < 4.5 \\ 1 & t \geq 4.5 \end{cases} \quad \text{Eq. 4}$$

$$E_{slow\ ramp} = \begin{cases} 0 & t < 0 \\ t/6 & 0 \leq t < 6 \\ 1 & t \geq 6 \end{cases} \quad \text{Eq. 5}$$

The Hill coefficient n and tuning parameter R were fit to the species' toxicity curve (Figure A-1C):

$$V_i(t) = \frac{1}{1 + \frac{E_i^n}{R_i}} \quad \text{Eq. 6}$$

The single species model was extended to a multispecies model based upon (226), which models the growth of two species N_1 (Eq. 3) and N_2 (Eq. 4), as well as the substrate availability S (Eq. 5). We used two different multispecies models, one for bacteriostatic stressors such as chloramphenicol, which stop cells from growing, and one for bactericidal stressors such as pinene, which cause cell lysis (246).

2.7.5.b. Multispecies bacteriostatic model

$$\frac{dN_1}{dt} = 2\alpha\mu_{max,1} \left(\frac{S}{K_S + S} \right) V_1(t)N_1(t) \quad \text{Eq. 7}$$

$$\frac{dN_2}{dt} = 2\alpha\mu_{max,2} \left(\frac{S}{K_S + S} \right) V_2(t)N_2(t) \quad \text{Eq. 8}$$

$$\frac{dS}{dt} = -\frac{1}{\gamma} \left(\frac{S}{K_S + S} \right) (\mu_{max,1}N_1(t) + \mu_{max,2}N_2(t)) \quad \text{Eq. 9}$$

For the multispecies bacteriostatic model, the growth yield provided by the substrate γ , and the half-saturation constant K_S , were fit using the growth curves of a co-culture of the two strains with equal initial biomasses. The maximum growth rates for each individual species ($\mu_{max,1}$ and $\mu_{max,2}$) were derived from the individual growth curves and the coefficients for the antibiotic terms (R_1 , R_2 , n_1 and n_2) were fit to individual species' toxicity curves. Additional information on the accuracy of model fits to the growth and toxicity curve data can be found in Table A-4.

2.7.5.c. Multispecies bactericidal model

$$\begin{aligned} \frac{dN_1}{dt} = & 2\alpha\mu_{max,1} \left(\frac{S}{K_S + S} \right) \left(1 - \frac{1}{1 + (c_1E)^{n_1}} \right)^2 N_1(t) \\ & - b_1 \left(\frac{1}{1 + (c_1E)^{n_1}} \right)^2 N_1(t) \end{aligned} \quad \text{Eq. 10}$$

$$\begin{aligned} \frac{dN_2}{dt} = & 2\alpha\mu_{max,2} \left(\frac{S}{K_S + S} \right) \left(1 - \frac{1}{1 + (c_2 E)^{n_2}} \right)^2 N_2(t) \\ & - b_2 \left(\frac{1}{1 + (c_2 E)^{n_2}} \right)^2 N_2(t) \end{aligned} \quad \text{Eq. 11}$$

$$\frac{dS}{dt} = -\frac{1}{\gamma} \mu_{max,1} \mu_{max,2} \left(\frac{S}{K_S + S} \right) N_1(t) N_2(t) \quad \text{Eq. 12}$$

The parameters of the bactericidal multispecies model were fit as described above. We calculated the sum of squared residuals to estimate the relative precision of the model, along with the maximum and average error for the model sets. In addition, we evaluated the goodness-of-fit by calculating the Pearson's correlation coefficient (247).

3. ANTIBIOTIC EXPORT BY EFFLUX PUMPS AFFECTS GROWTH OF NEIGHBORING BACTERIA

3.1. Disclosure & Copyright Statement

This chapter is a modified version of “Antibiotic Export by Efflux Pumps Affects Growth of Neighboring Bacteria” by Xi Wen, [Ariel M. Langevin](#), and Mary J. Dunlop, 2018. Scientific Reports, 8 15120. ©2018 by Springer Nature. The publisher allows unrestricted use or reproduction provided proper citations of the original work.

3.2. Abstract

Cell-cell interactions play an important role in bacterial antibiotic resistance. Here, we asked whether neighbor proximity is sufficient to generate single-cell variation in antibiotic resistance due to local differences in antibiotic concentrations. To test this, we focused on multidrug efflux pumps because recent studies have revealed that expression of pumps is heterogeneous across populations. Efflux pumps can export antibiotics, leading to elevated resistance relative to cells with low or no pump expression. In this study, we co-cultured cells with and without AcrAB-TolC pump expression and used single-cell time-lapse microscopy to quantify growth rate as a function of a cell’s neighbors. In inhibitory concentrations of chloramphenicol, we found that cells lacking functional efflux pumps ($\Delta acrB$) grow more slowly when they are surrounded by cells with AcrAB-TolC pumps than when surrounded by $\Delta acrB$ cells. To help explain our experimental results, we developed an agent-based mathematical model, which demonstrates the impact of neighbors based on efflux efficiency. Our findings hold true for co-cultures of *E. coli* with and without pump expression and also in co-cultures of *E. coli* and *Salmonella*

typhumirium. These results show how drug export and local microenvironments play a key role in defining single-cell level antibiotic resistance.

3.3. Introduction

Despite intensive study, antibiotic resistance remains an essential problem, in part due to the myriad of mechanisms by which cells can evade drug treatment. Classical tests, such as measurements of the minimum inhibitory concentration (MIC), are important for quantifying drug resistance, but can obscure single-cell level differences in resistance (17). This is a significant problem because cell-to-cell differences in antibiotic resistance can establish concentration gradients, which can accelerate the resistance acquisition process (248, 249). In addition, sub-populations of antibiotic resistant or tolerant cells can decrease treatment efficacy (37, 201).

Individual cells can exhibit phenotypic differences in drug resistance even in the absence of community-level effects. For example, persister cells use dormancy or slow growth to evade antibiotic treatment (17). Single-cell level resistance can also affect group growth. For instance, *Streptococcus pneumoniae* cells with chloramphenicol acetyltransferase can deactivate chloramphenicol, resulting in a decrease in both the intracellular and environmental chloramphenicol concentrations (250). Bacteria also transiently express resistance-conferring genes such as drug export pumps or those that modify membrane permeability, resulting in cell-to-cell difference in susceptibility (37, 239).

Antibiotic efficacy can also be dependent on community-level phenomena. For example, the inoculum effect describes the cell density dependence of the MIC, where

more dense cultures are less susceptible to antibiotics resulting in increases in the MIC (251, 252). Cell density plays an essential role in influencing group behaviors, such as quorum sensing and biofilm formation, which in turn can dramatically increase the antibiotic resistance of the population (253, 254). Furthermore, certain cells within a community may exhibit altruistic behavior, such as those that release resistance proteins upon death to enable other cells to survive (253, 255). These examples highlight the importance of cellular interactions and collective behavior in antibiotic resistance.

Bacterial efflux pumps are an important source of multidrug resistance (219, 256). These pumps export antibiotics from the cell, increasing their antibiotic resistance. Their expression can be taxing, reducing growth and imposing a fitness cost (189, 257); therefore, their expression is often regulated to limit the burden. The primary multidrug resistance efflux pump in *E. coli* is AcrAB-TolC. This pump is composed of three proteins that span the inner and outer cell membrane: a periplasmic linker protein AcrA, the inner membrane efflux transporter AcrB, and the outer membrane channel TolC (206). Knocking out *acrB*, the pump protein responsible for substrate recognition and export via the proton motive force, leads to a significant increase in antibiotic susceptibility (156, 219). For instance, the MIC of *E. coli* Δ *acrB* to chloramphenicol is an eighth of that of wild type cells (134). Complementing Δ *acrB* with the *acrAB* operon is sufficient to restore drug resistance (189). Efflux pumps have been recognized to play a major role in clinical isolates in the emergence of resistant strains of *E. coli*, *S. enterica*, and other pathogens, and thus have been identified as clinical targets (258, 259).

Recent studies have shown that AcrAB-TolC expression is heterogeneous across

populations (260, 261), suggesting that differential pump expression exists even within isogenic populations. Since the cost and benefit of expressing pumps can both be significant, these cell-to-cell differences may have important implications for bacterial populations. Here, we asked how efflux pump export of antibiotics affects the growth of neighboring cells and, ultimately, the composition of the population.

To accomplish this, we focused on differential expression of *acrAB*. We monitored single-cell growth rates using time-lapse microscopy, and analyzed growth of cells as a function of whether their neighbors have AcrAB-TolC efflux pumps. We found that individual bacteria that are surrounded by AcrAB-expressing neighbor cells will tend to grow more slowly than when the same cells are surrounded by Δ *acrB* neighbors under antibiotic exposure. By developing a mathematical model, we were able to characterize this effect and predict the cell growth in the presence of a different antibiotic. Furthermore, we tested co-cultures of *E. coli* and *S. enterica* serovar Typhimurium (hereafter referred to as *S. typhimurium*) and observed the same neighbor dependence, which has implications for the broader relevance of our findings since these results likely extend to mixed-species communities. This work contributes additional evidence for the critical role of single-cell level effects in antibiotic resistance.

3.4. Results

To examine the effect of drug efflux on neighboring cells, we designed an experiment where Δ *acrB* cells were surrounded either wild type cells containing functional AcrAB-TolC pumps or by identical Δ *acrB* cells (Figure 3-1A). We hypothesized that Δ *acrB* cells which had wild type neighbors would experience a higher local concentration

of antibiotics due to drug efflux in their immediate vicinity, leading to a reduced growth rate relative to cells with neighbors lacking pumps. To test this, we conducted experiments with *E. coli* growing on agarose pads and measured single cell growth rates under different levels of antibiotic exposure.

To visualize the two cell types, we labeled the $\Delta acrB$ cells with red fluorescent protein (denoted $\Delta acrB$ -RFP) and wild type cells with green fluorescent protein (WT-

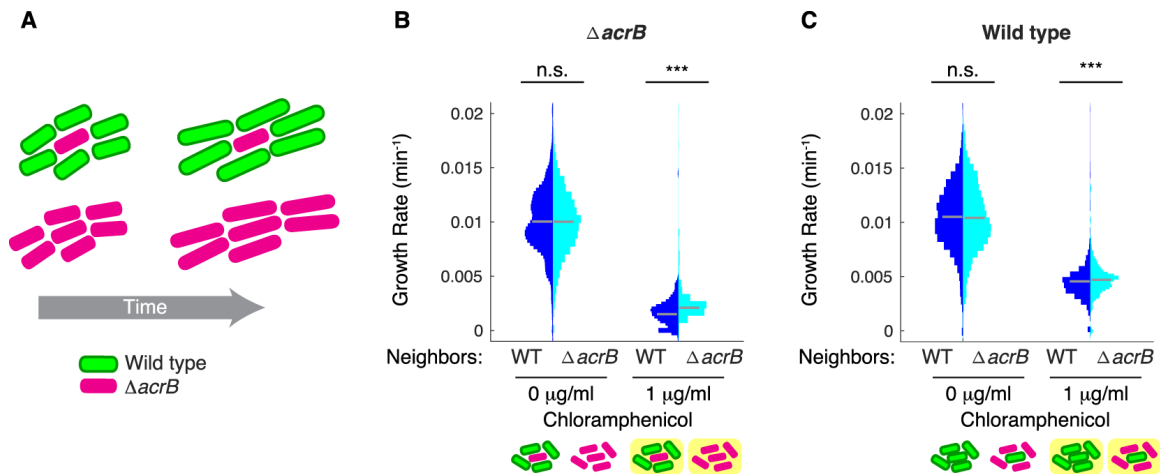


Figure 3-1. Neighbors with pumps impact cell growth.

(A) Schematic showing when $\Delta acrB$ cells are surrounded by cells with AcrAB-TolC pumps they grow more slowly than when surrounded by other $\Delta acrB$ cells. (B) Growth rates of wild type cells expressing *gfp* (WT-GFP) and $\Delta acrB$ cells expressing *rfp* ($\Delta acrB$ -RFP). Cells were mixed in ratios of 5:1 and 1:5 and the growth rate of $\Delta acrB$ -RFP cells was then quantified for the two different ratios. (C) Growth rates of wild type cells, given WT-GFP or $\Delta acrB$ -RFP neighbors. For (B, C) statistical significance was calculated using the Kolmogorov-Smirnov test, where *** p < 0.001, n.s.: not significant. Gray bars show mean growth rate. Distribution mean, standard deviation, and p-values are listed in Table S1 from reference (337). Plot axis limits were set to show >97% of cells; however full data set including outliers and n values (number of cells) for each are shown in Figure B-1. Schematics under (B, C) show the type of neighbors surrounding the cell in the middle whose growth rate is calculated. Background color indicates presence of antibiotics.

GFP).¹ Chloramphenicol is a broad-spectrum antibiotic which diffuses through the bacterial cell membrane and reversibly binds to the ribosome to inhibit protein synthesis. We quantified the growth rates of $\Delta acrB$ -RFP cells surrounded by either WT-GFP or $\Delta acrB$ -RFP neighbors. To do this, we mixed $\Delta acrB$ -RFP with WT-GFP cells in ratios of 1:5 and 5:1 to bias the community structure.

Growth rates for cells were similar for both ratios for conditions with no chloramphenicol. However, under chloramphenicol treatment just below the MIC (1 μ g/ml, Figure B-2), we found that the growth rate of $\Delta acrB$ cells with WT-GFP neighbors was lower than those with $\Delta acrB$ -RFP neighbors (Figure 3-1B), indicating that the influence of drug efflux by neighboring cells is important in local growth inhibition. When we compared the growth of WT-GFP cells with WT-GFP or $\Delta acrB$ -RFP neighbors, we observed more modest differences in growth rates under chloramphenicol treatment. This is likely because cells with pumps are able to maintain low intracellular antibiotic concentrations regardless of their neighbors (Figure 3-1C).

Building upon these results, we next conducted a series of experiments where we used $\Delta acrB$ as the strain background for both types of cells in the co-culture, allowing us to isolate the effect of efflux pumps independent of endogenous regulation. We tested microbial communities with $\Delta acrB$ -RFP cells and a $\Delta acrB$ strain overexpressing *acrAB*, which we labeled with green fluorescent protein (denoted AcrAB-GFP). We then monitored the growth of the $\Delta acrB$ -RFP cells surrounded by either AcrAB-GFP or $\Delta acrB$ -

¹ For consistency, these appear as defined in the original manuscript; however, please note that the names and definitions of each strain differ from Chapter 2, 4, and 5.

RFP neighbors. As before, we found that $\Delta acrB$ -RFP cells grow more slowly when they are in the vicinity of AcrAB-GFP neighbors than when they are surrounded by $\Delta acrB$ -RFP neighbors (Figure 3-2A). Differences in the growth rate are apparent in measurements of cell length over time. As a negative control, we also measured $\Delta acrB$ -RFP cells mixed with $\Delta acrB$ -GFP cells and found no differences in growth rate (Figure 3-2B).

To confirm our findings across measurements of hundreds of individual cells, we quantified the growth rates of single cells with $\Delta acrB$ -RFP or AcrAB-GFP neighbors. We found statistically significant differences in the growth rates in conditions where antibiotics were applied (Figure 3-2C). In addition, we observed a shift in the mean growth rate in the opposite direction without antibiotic treatment, indicative of the cost of efflux pump expression. Under sub-MIC levels of chloramphenicol (0.2 $\mu\text{g/ml}$), the neighbor effect was more apparent than chloramphenicol concentrations near the MIC (1 $\mu\text{g/ml}$). This is likely because at the higher antibiotic concentration growth of both $\Delta acrB$ -RFP and AcrAB-GFP cells is impacted by chloramphenicol treatment. As expected, control experiments with $\Delta acrB$ -RFP and $\Delta acrB$ -GFP cells showed no statistical difference in growth rates, regardless of the antibiotic concentration (Figure 3-2D). These results indicate that the AcrAB-TolC efflux pump plays a role in attenuating growth of neighboring cells in conditions where antibiotics are present.

Since competition will change the composition of cells in mixed species communities, we next extended our analysis to ask what the implications were for co-cultures. To do this, we compared the biomass of the $\Delta acrB$ -RFP cells at the start of the co-culture experiment to the end. More specifically, we quantified the relative abundance

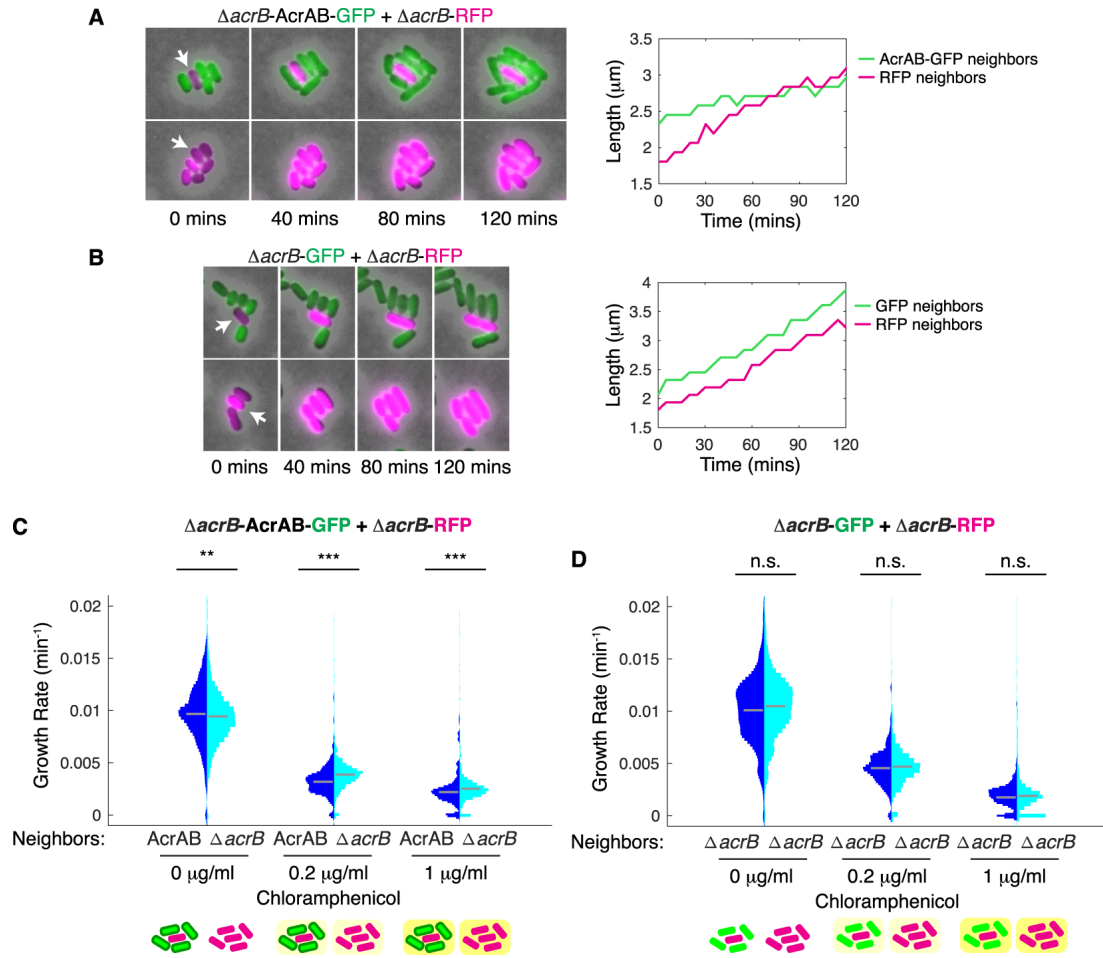


Figure 3-2. $\Delta acrB$ cells with and without *acrAB* complementation show neighbor-dependent differences in growth.

(A) $\Delta acrB$ -RFP and AcrAB-GFP cells were mixed in ratios of 1:5 and 5:1 and grown on agarose pads with 0.2 $\mu g/ml$ chloramphenicol. Left panel is representative series of time-lapse images showing growth of a $\Delta acrB$ -RFP cell surrounded by AcrAB-GFP neighbors. Right panel shows the cell length over time for the cell indicated with an arrow in the left panel. (B) $\Delta acrB$ -RFP and $\Delta acrB$ -GFP cells for conditions as described in (A). Length data for all cells for conditions from (A, B) are shown in Figure B-3. (C) Growth rates of $\Delta acrB$ -RFP cells with either AcrAB-GFP or $\Delta acrB$ -RFP neighbors quantified at different chloramphenicol concentrations. (D) Growth rates of $\Delta acrB$ -RFP cells with either $\Delta acrB$ -GFP or $\Delta acrB$ -RFP neighbors. Statistical significance was calculated using the Kolmogorov-Smirnov test. *** $p < 0.001$; ** $p < 0.01$; n.s.: not significant. Gray bars show mean growth rate. Distribution mean, standard deviation, and p-values are listed in Table S1 from reference (337). Full data set including outliers and n values are shown in Figure B-1. Schematics under (C, D) show the type of neighbors surrounding the cell in the middle whose growth rate is calculated. Background color indicates antibiotic concentration.

of the $\Delta acrB$ -RFP cells by comparing what fraction of the biomass they made up at the end divided by the fraction at the start. Thus, if there is no change in the composition of the co-culture then the relative abundance will be one; values below one correspond to AcrAB-GFP cells outcompeting the $\Delta acrB$ -RFP cells. When no antibiotic was applied we found that $\Delta acrB$ -RFP and AcrAB-GFP cells grew similarly and the relative abundances of the two strains were maintained near one (Figure 3-3A). However, under chloramphenicol treatment the relative abundance of the $\Delta acrB$ -RFP cells decreased when they were surrounded by AcrAB-GFP cells, but not when they were in close proximity with other $\Delta acrB$ -RFP cells. We note that under these conditions there are still AcrAB-GFP cells, but since they are mixed in a ratio of 5:1, the AcrAB-GFP cells are comparatively rare. Control

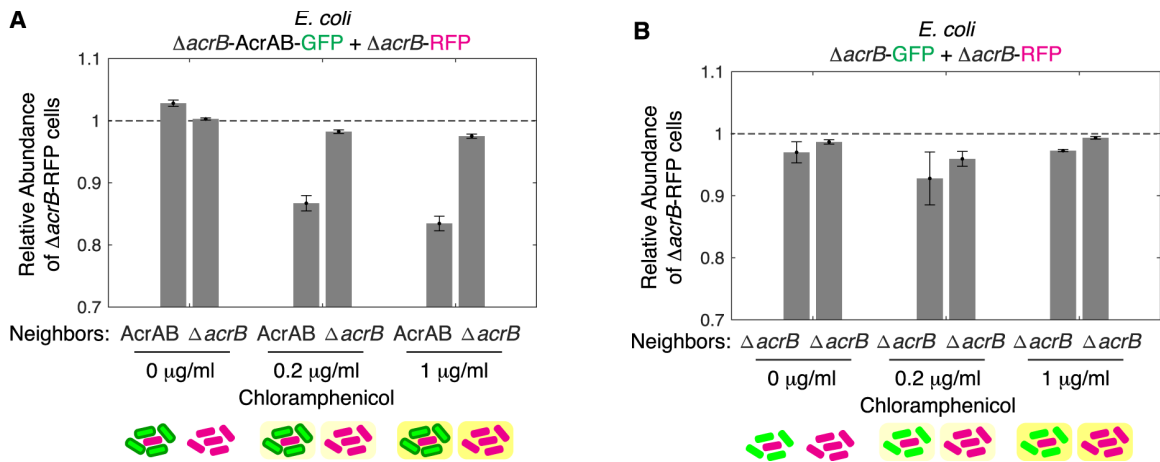


Figure 3-3. Relative abundance of $\Delta acrB$ cells decreases when they have AcrAB-GFP neighbors.

(A) Relative abundance was calculated using the data set in Figure 3-2C, where we define relative abundance as the fraction of the biomass $\Delta acrB$ -RFP cells make up at the end, divided by their fraction at the start. (B) Relative abundance calculated using the data set in Figure 3-2D. Dashed line at one indicates value if there is no change in the abundance of $\Delta acrB$ -RFP cells over time. Error bars show standard deviation between replicates. Schematics under plots show the type of neighbors surrounding the cell in the middle whose growth rate is calculated. Background color indicates antibiotic concentration.

experiments with $\Delta acrB$ -RFP and $\Delta acrB$ -GFP co-cultures had relative abundance values near one regardless of the chloramphenicol concentration (Figure 3-3B). Overall, these results indicate that proximity related inhibition from drug efflux can lead to rapid changes in the community composition.

To understand the impact of antibiotic export on neighboring cells, we developed a mathematical model to describe cell growth. The agent-based model applies a fixed spatial architecture to describe cell proximity. Within each cell, we used a system of ordinary differential equations to model changes in the intracellular antibiotic concentration due to drug efflux (Figure 3-4A). Model parameters were estimated from measurements of cell density in the presence of antibiotics (Figure B-2). We found that cell growth and the intracellular antibiotic concentration are strongly influenced by the type of neighbors in the simulation (Figure 3-4B). We next simulated a range of chloramphenicol concentrations and found that the growth rate decreased significantly for cells with higher efflux compared to cells with $\Delta acrB$ neighbors (Figure 3-4C), in good agreement with the experimental results (Figure 3-1B).

A key finding of the model is that the efflux rate is proportional to the neighbor effect. In other words, if the AcrAB-TolC pump exports a specific antibiotic well, then the neighbor effect will be more apparent than if the pump does not export it well. To test this, we conducted additional modeling and experiments with ciprofloxacin, which is a substrate of the AcrAB-TolC pump, but has a smaller fold reduction of the MIC than chloramphenicol for $\Delta acrB$ cells (Figure B-2B). Using parameter fits from experimental data, we lowered the efflux rate of wild type cells to model the lower efflux efficiency for

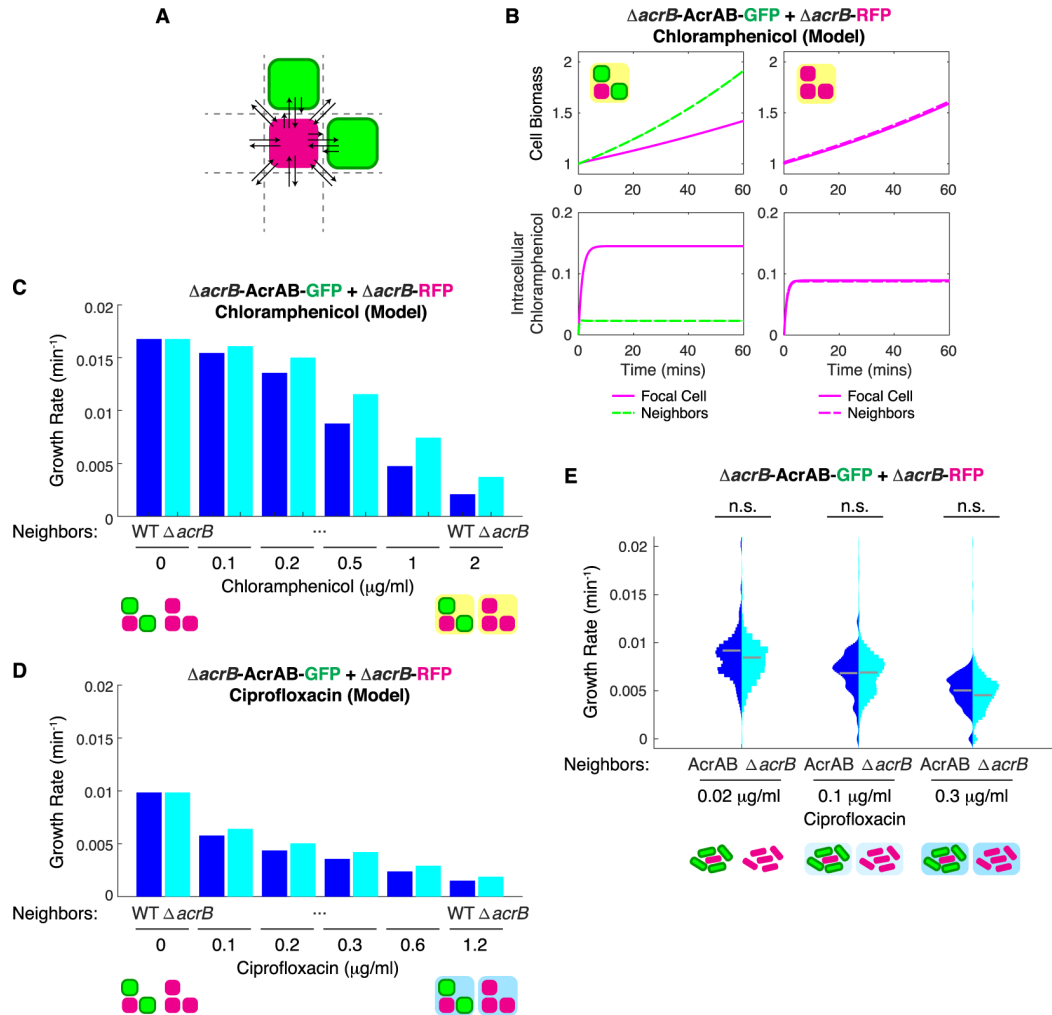


Figure 3-4. Model predicts cell growth rate differences under antibiotic conditions.

(A) Schematic depicting the spatial relationship between the focal cell in the center, its neighbors, and the environment. (B) Biomass and intracellular chloramphenicol concentration of $\Delta acrB$ cells with wild type neighbors or $\Delta acrB$ neighbors simulated in an environment with 0.1 $\mu\text{g/mL}$ of chloramphenicol. (C) Cell growth of $\Delta acrB$ cells with different chloramphenicol concentrations given wild type or $\Delta acrB$ neighbors. Growth rate is calculated as the average change in biomass divided by the time simulated. Model parameters and initial conditions are listed in Table B-1. (D) Cell growth under ciprofloxacin treatment for the same cell configurations as in (C). (E) $\Delta acrB$ -RFP and AcrAB-GFP cells were mixed in different ratios (1:5 or 5:1) and grown on agarose pads with ciprofloxacin. Statistical significance was calculated using the Kolmogorov-Smirnov test, where n.s.: not significant. Gray bars show mean growth rate. Distribution mean, standard deviation, and p-values are listed in Table S1 from reference (337). Full data set including outliers and n values for each are shown in Figure B-1. Schematics under (C–E) show the type of neighbors surrounding the cell in the middle whose growth rate is calculated. Background color indicates presences of antibiotics.

ciprofloxacin. The simulated results show a decrease in the impact of neighbors on the focal cell's growth rate (Figure 3-4D). We confirmed this experimentally with ciprofloxacin, observing modest, but not statistically significant differences between the different neighboring cells (Figure 3-4E). In an extension to the model, we explored how the neighborhood affected the focal cell's growth rate. We observed that the overall number of neighbors was an important determining factor of the focal cell's growth rate and the exact spatial arrangement of the neighbors played only a minor role (Figure 3-5).

In microbial communities bacterial cross-species interactions are common. Therefore, we tested whether the neighbor effect was limited to our single-species co-

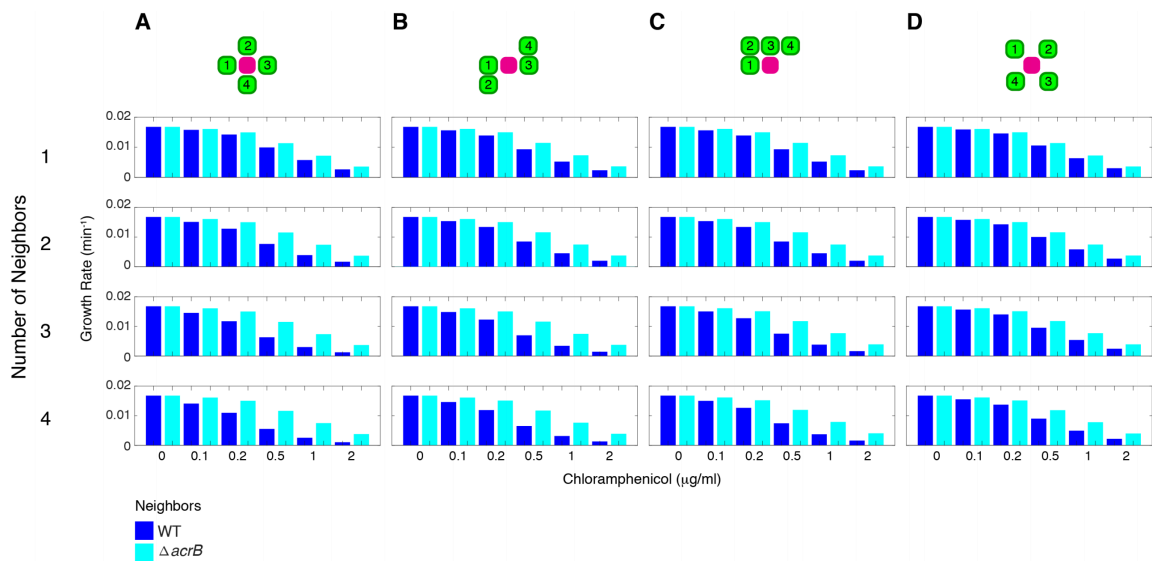


Figure 3-5. Impact of neighborhood on focal cell growth rate.

(A-D) Each row represents a different number of neighbors and each column represents different neighborhood layouts. When the number of neighbors is one (first row) only the cell labeled “1” in the schematic is included in the simulation. For two neighbors, cells “1” and “2” are included, and so on. The neighborhoods evaluated are (A) spread out, but close to the focal cell, (B) neighbors are closer to each other, (C) neighbors are clustered around focal cell, and (D) spread out, but further from focal cell. The model was evaluated for $\Delta acrB$ -RFP cells with $\Delta acrB$ -AcrAB-GFP (blue) and $\Delta acrB$ -RFP (cyan) neighbors exposed to different concentrations of chloramphenicol.

cultures with *E. coli* or if it extended to cross-species interactions. *E. coli* (e.g. ETEC or STEC) and *S. typhimurium* are both foodborne pathogens and their co-existence can lead to mixed biofilm formation and a higher resistance against sanitization (262). We investigated the growth of *S. typhimurium* co-cultured with *E. coli* WT-GFP or $\Delta acrB$ -RFP under conditions with and without chloramphenicol. Consistent with our results from the single-species co-cultures, we observed that *S. typhimurium* grows more slowly with *E. coli* WT-GFP neighbors than *E. coli* $\Delta acrB$ -RFP neighbors (Figure 3-6). These results indicate that the neighbor effect generalizes to cross-species interactions.

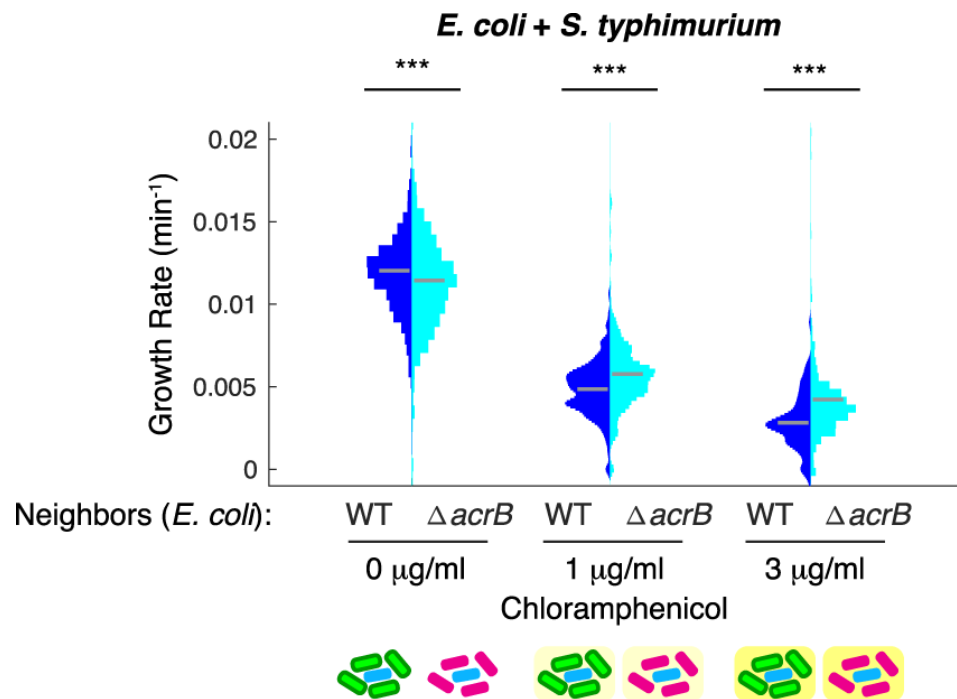


Figure 3-6. *E. coli* and *S. typhimurium* co-culture.

S. typhimurium cells were mixed with either WT-GFP or $\Delta acrB$ -RFP *E. coli*. Statistical significance was calculated using the Kolmogorov-Smirnov test. *** $p < 0.001$. Gray bars show mean growth rate. Distribution mean, standard deviation, and p-values are listed in Table S1 from reference (337). Full data set including outliers and n values for each are shown in Figure B-1. Schematic under plot shows the type of neighbors surrounding the cell in the middle whose growth rate is calculated. Background color indicates antibiotic concentration.

3.5. Discussion

Single cell level effects are important for bacterial growth and survival under antibiotic treatment. Here we focused on differences in antibiotic efflux as a mechanism for generating cell-to-cell differences in antibiotic survival. This work is motivated by recent studies showing that efflux pump expression is variable across cells within a bacterial population (260, 261). Using detailed quantitative measurements of single cell growth rates, we asked how differences in drug efflux affect the growth of neighboring cells. We found that $\Delta acrB$ cells have a lower growth rate when surrounded by cells with the AcrAB-TolC pump than when surrounded by like $\Delta acrB$ cells. This effect leads to a rapid shift in the community composition towards more resistant cells that occurs within a small number of generations. Further, the effect extends to *E. coli* and *S. typhimurium* co-cultures, suggesting that these findings are likely to be broadly relevant for mixed-species communities and stress tolerance mechanisms that work by exporting antibiotics or other compounds into the immediate vicinity.

Efflux pump expression can be burdensome to cells and there is a tradeoff between the benefit of pumps and their cost (189). Under the conditions we tested here, the cost of pumps was modest and conditions with no antibiotics produced only minor differences in growth rates between $\Delta acrB$ -RFP and AcrAB-GFP cells; however, we note that as experiment durations are extended this burden will become more apparent. These cost and benefit tradeoffs will likely depend on the environment, as cells balance the burden of pump expression, the impact of their neighbors, and the local antibiotic concentration to maximize growth.

In the future, it will be interesting to study the interaction between drug efflux and other antibiotic resistance mechanisms that function at the single-cell level. Also, efflux pump expression is stochastic and can change over time in individual cells (260, 261), suggesting the potential for experiments that quantify how these dynamics affects growth of neighboring bacteria. The implications for the eventual evolution of permanent genetic changes that lead to antibiotic resistance are also an interesting area for future research. Single cell level effects and how bacteria interact, including their proximity, can have a profound impact on whether antibiotics are effective.

3.6. Contributions Statement

The authors of this work were Xi Wen (X.W.), Ariel M. Langevin (A.M.L.), and Mary J. Dunlop (M.J.D.). X.W. conducted the experiments and analyzed the data, A.M.L. performed the modeling, M.J.D. supervised the research. All authors wrote the manuscript.

3.7. Methods

3.7.1. Strains and plasmids

We used BW25113 as the wild type strain of *E. coli*. BW25113 $\Delta acrB$ was derived from the Keio collection strain JW0451 (BW25113 $\Delta acrB::kan^R$) (235), and we removed the kanamycin resistance marker using the pCP20 plasmid (236). For the *Salmonella* co-culture experiments, we used the model strain *S. typhimurium* LT2 (263).

Plasmids were constructed using the Gibson assembly method (240). To distinguish the strains, we used fluorescent reporters encoded on plasmids. For RFP, we used the plasmid pBbA5k-rfp (238), for GFP we used pBbA5k-sfgfp (189), and for AcrAB-GFP we used pBbA5k-acrAB-sfgfp (189), where *acrAB* and *sfgfp* are transcriptionally fused. All

plasmids described above have an IPTG-inducible P_{lacUV5} promoter controlling gene expression, a medium copy p15A origin of replication, and kanamycin resistance marker. The plasmids were transformed into either the *E. coli* wild type strain (pBbA5k-sfgfp to make WT-GFP), *E. coli* $\Delta acrB$ strain (pBbA5k-rfp for $\Delta acrB$ -RFP; pBbA5k-acrAB-sfgfp for AcrAB-GFP; pBbA5k-sfgfp for $\Delta acrB$ -GFP), or *S. typhimurium* strain (pBbA5k-rfp).

3.7.2. Growth conditions

E. coli and *S. typhimurium* were cultured in Luria Broth (LB) medium. For all experiments, overnight cultures were inoculated from a single colony in LB with 30 μ g/ml kanamycin for plasmid maintenance. Overnight cultures were then grown at 37 °C with orbital shaking at 200 rpm. Before experiments, cultures were refreshed 1:50 in LB with kanamycin and grown at 37 °C with orbital shaking. After 5 h, we added 100 μ M IPTG and then incubated an additional 2 h to induce fluorescent protein or AcrAB expression. For *S. typhimurium*, 100 μ M IPTG was added after cultures were refreshed for 0.5 h and cells were grown for an additional 2 h induction. Co-cultures were mixed in ratios of 1:5 and 5:1 each for $\Delta acrB$ -RFP and WT-GFP or $\Delta acrB$ -RFP and AcrAB-GFP experiments (and control with $\Delta acrB$ -RFP and $\Delta acrB$ -GFP).

3.7.3. Time-lapse microscopy

For imaging experiments, the co-cultures were placed on an agarose pad with 100 μ M IPTG and with either 0, 0.2, 1 μ g/ml chloramphenicol or 0.02, 0.1, 0.3 μ g/ml ciprofloxacin for *E. coli* co-cultures, or 0, 1, 3 μ g/ml chloramphenicol for the *E. coli* and *S. typhimurium* co-culture. We imaged at least three positions per pad,

resulting in measurements of hundreds of single cells for each position (for n values for each case see Figure B-1). 1.5% low melting agarose pads were made using M9 minimal medium containing 0.2% glycerol, 0.01% casamino acids, 0.15 $\mu\text{g/ml}$ biotin, and 1.5 μM thiamine. Cells were diluted and mixed at ratios as indicated above and placed on pads containing 100 μM IPTG and chloramphenicol or ciprofloxacin. Images were taken using a Nikon Ti-E microscope with 100x objective lens for 130 mins at 5 min intervals. The temperature of the microscope chamber was held at 32°C for the duration of the experiment.

3.7.4. Data Analysis

Images were analyzed in Matlab. We used the automated image processing package SuperSegger30 to measure cell growth rates and identify neighboring cells. An individual cell's lineage starts just after its mother has divided, forming it and a sister cell, and it ends when the cell divides into two daughter cells. Growth rate is defined as the natural log of the ratio of the length of the cell at the end of the lineage to its length at the start of the lineage, divided by the length of the lineage in minutes. Thus, the growth rate is the exponential rate constant (264). Custom Matlab scripts were used to analyze growth data and neighbor effects. Statistical analysis of growth rates was performed in Matlab.

3.7.5. Toxicity experiments

To determine the antibiotic toxicity of the strains, we added a final concentration of 0, 0.1, 0.2, 0.5, 1, 2, 5, or 10 $\mu\text{g/ml}$ of chloramphenicol or 0, 0.05, 0.1, 0.2, 0.5, 1, 2, or 5 $\mu\text{g/ml}$ of ciprofloxacin to each culture. The samples were sealed with evaporation-

limiting membranes (Thermo Scientific AB-0580) and grown in 96-well plates at 37 °C with orbital shaking at 200 rpm. OD₆₀₀ readings were taken with a BioTek Synergy H1m plate reader every 10 m for 18 h. The toxicity curves represent change in growth for the first 2 h for consistency with the length of the microscopy experiments. All experiments were performed in triplicates with biological replicates.

3.7.6. Mathematical model

To simulate cell growth with different neighbors in the presence of antibiotics, we used an agent-based model with Moore neighborhood architecture to describe the spatial interactions between cells and the environment (265–267). We represent each cell with two ordinary differential equations describing intracellular antibiotic concentration (Eq. 13) and cell biomass (Eq. 14). The model assumes exponential growth, which is valid for the short durations (~2 h) over which modeling and experiments are conducted. The biomass equation has a term for the toxicity of the environment, which is derived from Van Impe *et al.* (189, 227, 268).

$$\begin{aligned} \frac{dC_{in}}{dt} = \frac{1}{6} & \left[\sum_{j=1}^{all\ adjacent\ Neighbors} \left(\frac{1}{2} K_{out,j} + \frac{1}{2} K_{in} \right) C_{in,j} \right. \\ & + \sum_{k=all\ adjacent\ Neighbors+1}^4 K_{in} C_{out} \left. \right] \\ & + \frac{1}{12} \left[\sum_{j=1}^{all\ diagonal\ Neighbors} \left(\frac{1}{2} K_{out,j} + \frac{1}{2} K_{in} \right) C_{in,j} \right. \\ & + \sum_{k=all\ diagonal\ Neighbors+1}^4 K_{in} C_{out} \left. \right] \end{aligned} \quad \text{Eq. 13}$$

$$\frac{dN}{dt} = \mu N \left(\frac{1}{1 + \left(\frac{C_{in}}{K_c} \right)^{h_c}} \right) \quad \text{Eq. 14}$$

The total antibiotic concentration at each time point is assumed to be equal to the antibiotic concentration in the environment and inside cells. We assume instantaneous diffusion within environments separated by a membrane.

$$C_{total} = C_{out} + \sum_{i=1}^{all\ cells} C_{in,i} \quad \text{Eq. 15}$$

Our model focuses on the focal cell and its neighbors. C_{in} is the intracellular antibiotic concentration, and C_{out} is the extracellular concentration. N is biomass of the cell, and μ is the maximum growth rate. K_{in} and K_{out} are antibiotic entry and exit based on the presence of efflux pumps. We assume that if two cells are close together, the efflux from the neighbor will create a small area with a higher relative antibiotic concentration. We model this as the influx into the focal cell where an edge with a neighbor has an influx rate of $\frac{1}{2} K_{out,neighbor} + \frac{1}{2} K_{in}$. The first term represents the effect of the gradient produced by efflux from the neighboring cell with some loss to the environment and the second term represents passive influx that may occur. The second term sets a lower bound so that $\frac{1}{2} K_{out,neighbor} + \frac{1}{2} K_{in} \geq K_{in}$.

For the effect of antibiotics on change in biomass, we fit experimental data to a Hill function. Parameters for the toxicity term, h_c and K_c , were fit to $\Delta acrB$ toxicity curves for chloramphenicol and ciprofloxacin (Figure B-2). For modeling cell growth under ciprofloxacin, we decreased K_{out} by using fits to experimental data. All model fits were conducted by minimizing least-squares error. All model parameters are listed in Table B-1.

4. MAPPING THE ROLE OF AcrAB-TolC EFFLUX PUMPS IN THE EVOLUTION OF ANTIBIOTIC RESISTANCE REVEALS NEAR-MIC TREATMENTS FACILITATE RESISTANCE ACQUISITION

4.1. Abstract

Antibiotic resistance has become a major public health concern as bacteria evolve to evade drugs, leading to recurring infections and a decrease in antibiotic efficacy. Systematic efforts have revealed mechanisms involved in resistance; yet, in many cases, how these specific mechanisms accelerate or slow the evolution of resistance remains unclear. Here, we conducted a systematic study of the impact of the AcrAB-TolC efflux pump on the evolution of antibiotic resistance. We mapped how population growth rate and resistance change over time as a function of both the antibiotic concentration and the parent strain's genetic background. We compared the wild type strain to a strain overexpressing AcrAB-TolC pumps and a strain lacking functional pumps. In all cases, resistance emerged when cultures were treated with chloramphenicol concentrations near the MIC of their respective parent strain. The genetic background of the parent strain also influenced resistance acquisition. The wild type strain evolved resistance within 24 h through mutations in the *acrAB* operon and its associated regulators. Meanwhile, the strain overexpressing AcrAB-TolC evolved resistance more slowly than the wild type strain; this strain achieved resistance in part through point mutations in *acrB* and the *acrAB* promoter. Surprisingly, the strain without functional AcrAB-TolC efflux pumps still gained resistance, which it achieved through upregulation of redundant efflux pumps. Overall, our results suggest that treatment conditions just above the MIC pose the largest risk for the

evolution of resistance and that AcrAB-TolC efflux pumps impact the pathway by which chloramphenicol resistance is achieved.

4.2. Introduction

Despite the new wave of antibiotic discovery (269–273), bacteria continue to acquire resistance shortly after the introduction of new drugs for medicinal and industrial applications (5, 274). This is due in large part to the overuse of antibiotics, which results in pressures that drive resistance (275). With limited novel antibiotics and numerous futile antibiotics, doctors and scientists alike are presented with the challenge of how to best treat infections while keeping the evolution of resistance in check.

Adaptive evolution studies have begun exploring how certain antibiotic pressures influence the evolution of resistance. For instance, studies using a ‘morbidityostat’—a continuous culture device that dynamically adjusts antibiotic concentrations to inhibitory levels—have found numerous targets that can be readily mutated to promote resistance (102, 103, 105) and have also identified how drug switching can limit the evolution of resistance (276). While these studies have provided pivotal insights for this field, the morbidityostat design causes antibiotic concentrations to rise to levels that exceed clinically relevant concentrations due to toxicity for patients (107). In recognition of the drug concentration-dependent nature of evolution, researchers have begun to explore bacterial evolution under treatment conditions with lower antibiotic concentrations as well. Wistrand-Yuen *et al.* found that bacteria grown in sub-inhibitory drug concentrations were still able to achieve high levels of resistance (87, 277, 278). Notably, the study identified that the same antibiotic produced unique evolutionary pathways when cells were treated

with sub-inhibitory concentrations as opposed to inhibitory concentrations (87).

One limitation of current studies within the field is that they can be difficult to compare due to variations in experimental parameters, such as species, antibiotics, or other experimental conditions (118). Given the unique evolutionary pathways at different antibiotic concentrations, systematic mapping of these evolutionary landscapes could provide an improved understanding of which conditions pose the highest risk by allowing direct comparisons between different antibiotic concentrations. For instance, Jahn *et al.* demonstrated that variations in treatment dynamics can significantly alter evolved resistance for some antibiotics, such as tetracycline, but not others, such as amikacin and piperacillin (279). Other evolution experiments that were systematically conducted using a range of concentrations for beta-lactams (88) and erythromycin (280) have highlighted the concentration-dependent adaptability of *E. coli*.

There are many mechanisms by which antibiotic resistance can be achieved, including enzymatic inactivation, alteration of antibiotic binding sites, and increased efflux or reduced influx of antibiotics (281, 282). Efflux pumps are omnipresent in prokaryotic and eukaryotic cells alike, and are an important contributor to multidrug resistance (222). AcrAB-TolC in *E. coli* is a canonical example of a multidrug efflux pump, providing broad-spectrum resistance and raising the MIC of at least nine different classes of antibiotics (283). The pump is composed of three types of proteins: the outer membrane channel protein, TolC; the periplasmic linker protein, AcrA; and the inner membrane protein responsible for substrate recognition and export, AcrB (222). Using the proton motive force, AcrB actively exports antibiotics from the cell (222, 230). The presence of

AcrAB-TolC efflux pumps can increase the MIC by ~2-fold to ~10-fold, depending on the antibiotic (145, 189, 219). Furthermore, genes associated with these multidrug resistant efflux pumps, including their local and global regulators, are common targets for mutation as strains evolve high levels of drug resistance (106, 277, 284–286).

Recent studies have indicated that in addition to providing modest increases in the MIC due to drug export, pumps can also impact mutation rate and evolvability of strains, which may ultimately be more important for the acquisition of high levels of drug resistance. Firstly, mutants overexpressing *acrAB* emerge first and then are able to further evolve facilitate high levels of quinolone resistance (287). Secondly, heterogeneity in efflux pump expression can also predispose subsets of bacterial populations to mutation even prior to antibiotic treatment (191). Deleting genes associated with efflux pumps, such as *tolC*, can also reduce evolvability under antibiotic exposure (288). Further, a recent study in *S. aureus* found that higher NorA pump levels increased evolvability, and that adding a pump inhibitor could prevent resistance evolution (192). These studies provoke the question of how AcrAB-TolC efflux pumps can serve to promote or attenuate the evolution of drug resistance.

Our overall goal in this study was to identify temporal, phenotypic, and genetic patterns in how strains with different AcrAB-TolC genotypes evolve antibiotic resistance under a range of chloramphenicol concentrations. Chloramphenicol is both a well-validated substrate of AcrAB-TolC and can serve as a last resort antibiotic in multi-drug resistant infections, as most clinical isolates are still susceptible to this drug (289, 290). To identify how AcrAB-TolC impacts the evolution of resistance, we used a turbidostat as an

evolutionary platform (291) and measured changes in fitness and resistance. We evolved three strains with different levels of AcrAB-TolC: a wild type strain with the native regulatory network controlling AcrAB-TolC expression (WT); a strain which lacks the local regulator AcrR (AcrAB⁺), which results in a 1.5 to 6-fold increase in expression of the pumps (157, 159, 175); and a strain lacking functional AcrAB-TolC efflux pumps (Δ *acrB*).² We allowed the cultures to grow and evolve for 72 h in continuous culture while continuously recording growth rates. We periodically sampled the cultures and assessed the population's resistance. We then charted the evolutionary landscapes for each strain under different chloramphenicol concentrations to identify which circumstances gave rise to resistance.

4.3. Results

In order to systematically evaluate the evolutionary landscape of efflux pump-mediated antibiotic resistance, we used the eVOLVER, a modular turbidostat capable of growing independent cultures in parallel (291). This platform allowed us to track a culture's fitness by measuring growth rate continuously over multi-day experiments. In addition to this, we collected samples at selected intervals and, with these samples, performed antibiotic disc diffusion assays to assess the population's resistance and spot assays to quantify the presences of high-resistance isolates within the population (Figure 4-1).

² For consistency, these appear as defined in the original pre-print; however, please note that the names and definitions of each strain differ from Chapter 2, 3, and 5.

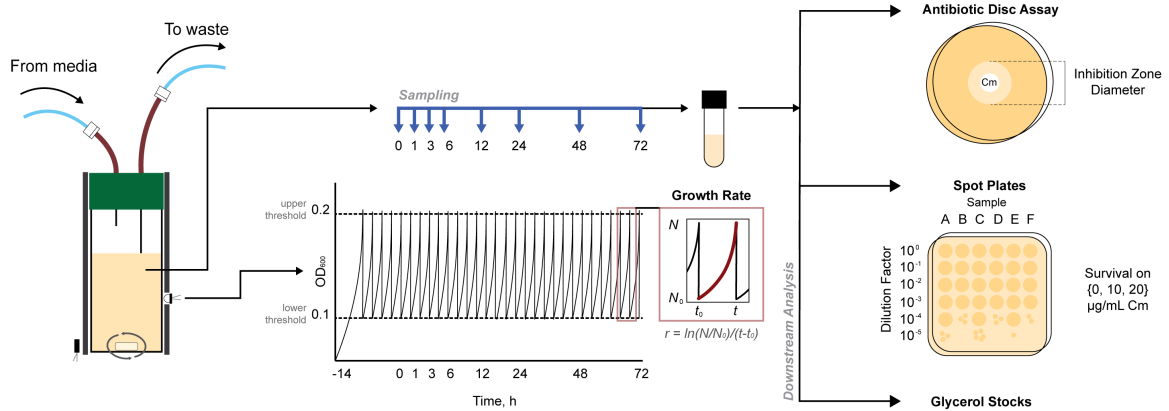


Figure 4-1. Evolution experiment schematic.

We used the eVOLVER, a modular turbidostat, as an evolutionary platform to measure and record absorbance data at 600 nm (OD_{600}). We calculated growth rate after each dilution event and collected samples at defined timepoints ($t = 0, 1, 3, 6, 12, 24, 48, 72$ h). We performed antibiotic disc assays and spot assays for all samples.

We mapped growth rates over time for cultures subjected to a range of chloramphenicol treatment concentrations (Figure 4-2A & Figure C-1). To compare across strains, we defined MIC^0_{parent} as the MIC of the parent strain ($MIC^0_{WT} = 2 \mu\text{g/mL}$, $MIC^0_{AcrAB+} = 2 \mu\text{g/mL}$, $MIC^0_{\Delta acrB} = 0.5 \mu\text{g/mL}$). We found similar values for MIC^0_{WT} and MIC^0_{AcrAB+} (Figure C-2), which may be due to induction of efflux pump expression in the WT strain in the presence of chloramphenicol. Prior studies have shown that the presence of stress can increase pump expression by 4-fold (157, 292), which is comparable to the impact of deleting *acrR* (157, 159, 175). We found that treatment with high concentrations of chloramphenicol repressed bacterial growth for multiple days. We observed this growth inhibition at $\sim 10 \mu\text{g/mL}$ for WT and AcrAB+, and at $\sim 2 \mu\text{g/mL}$ for $\Delta acrB$. These inhibitory concentrations represent treatments of $\sim 5 \times MIC^0_{parent}$ for all three strains. We found that cultures grown in lower chloramphenicol concentrations were able to recover growth. For example, when we treated cultures with $\sim 1\text{-}2 \times MIC^0_{parent}$, we observed a significant

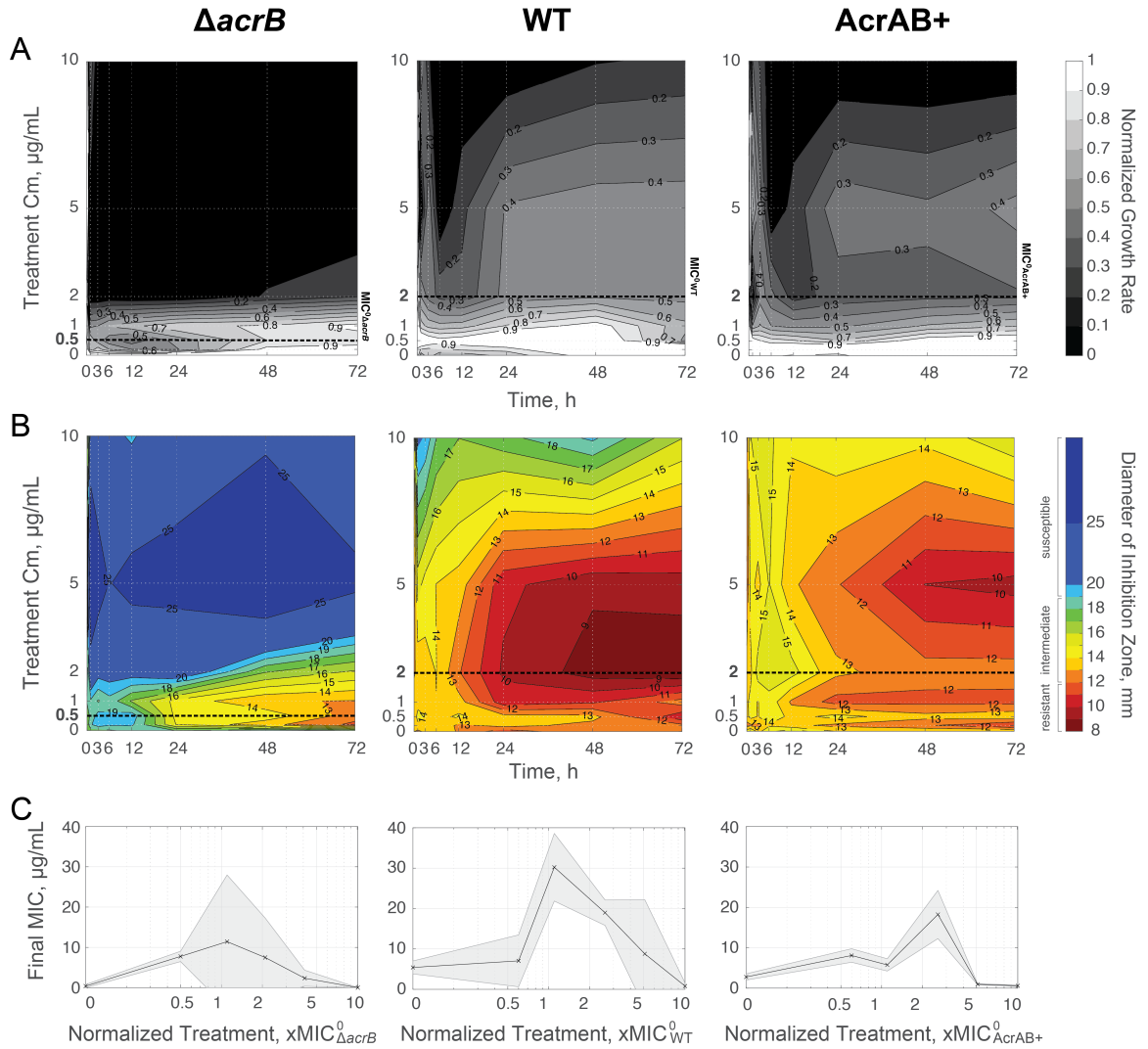


Figure 4-2. Temporal landscapes based on treatment concentration of chloramphenicol.

(A) Average growth rate. Growth rates are normalized to growth of strains at $t = 0$ h; for raw data see Figure C-1. Lighter areas represent growth rates closer to pre-treatment values; darker areas represent reduced growth rates. MIC^0 concentration is denoted with a bold dashed line for each strain (Figure C-2). **(B)** Average resistance. Diameter of inhibition zones were plotted for each time and treatment. Smaller inhibition zones are shown in red and correspond to resistant cells (≤ 12 mm) and larger inhibition zones are shown in blue and represent susceptible cells (≥ 19 mm); intermediate inhibition is shown with color scale from orange to green. $\text{MIC}_{\text{parent}}^0$ is denoted with a bold dashed line. **(C)** Final resistance at 72 h based on treatment concentration normalized to $\text{MIC}_{\text{parent}}^0$. The calculated, absolute final MIC is based on data from Figure C-5. Data points show the mean of three biological replicates. Shaded error bars show standard deviation.

decrease in the growth rate between 0 and 12 h (Table C-1). However, after 12 to 24 h, growth in these populations was partially restored. At lower treatment concentrations ($<1\times \text{MIC}^0_{\text{parent}}$), all cultures were able to grow, though usually at a deficit compared to the 0 $\mu\text{g/mL}$ chloramphenicol condition. For all three strains, there were qualitatively similar growth recovery patterns, with an initial growth repression phase followed by a partially restored growth phase (Figure C-1).

The growth rate results suggested the evolution of drug resistance within the population (102, 279). To quantify this, we used an antibiotic disc assay to map the corresponding resistance levels (Figure 4-2B & Figure C-3). We found distinct increases in resistance levels that corresponded to populations which recovered growth. While there were qualitative similarities for the three strains, the timing and level of resistance achieved was dependent on the strain background. We classified populations as resistant when their inhibition zone diameters were smaller than 12 mm, following established standards for antimicrobial susceptibility testing (293). The WT strain gained resistance under a broad range of chloramphenicol treatment concentrations; this resistance emerged within 24 h when cells were treated with $\sim 1\text{-}2\times \text{MIC}^0_{\text{WT}}$. The AcrAB⁺ strain, where efflux pumps are overexpressed, was able to evolve resistance as well, albeit at a slower rate and at lower levels than WT. AcrAB⁺ achieved resistance within 48 h when treated with $2.5\times \text{MIC}^0_{\text{AcrAB}^+}$, but the range of chloramphenicol concentrations that resulted in resistance was narrower than for the WT strain. The ΔacrB cells achieved resistance more slowly, but for the range of $\sim 1\text{-}2\times \text{MIC}^0_{\Delta\text{acrB}}$ chloramphenicol cultures were still able to reach resistant levels (Figure 4-2B & Figure C-3).

To compare the ultimate evolved resistance levels, we calculated the final, absolute MIC of the populations at 72 h. When we normalized the treatment concentration by MIC^0_{parent} , we found that treatments concentrations $\sim 1-2x MIC^0_{parent}$ evolved the most resistant populations (Figure 4-2C). Selective pressures of subinhibitory antibiotic concentrations have often been considered high-risk for the evolution of resistance (87, 294). Yet, our results indicated that concentrations near or just above MIC^0_{parent} lead to the highest resistance levels in these conditions. In short, all three strains were able to evolve resistance when treated with $\sim 1-2x MIC^0_{parent}$ chloramphenicol, with WT achieving the highest final, absolute MIC of the three strains. WT evolved more rapidly than AcrAB+ or $\Delta acrB$. Moreover, the relative range of chloramphenicol concentrations that supported the evolution of resistance in the AcrAB+ strain was narrower than for WT or $\Delta acrB$ strains.

We next asked how resistance and growth changed through time. We found that in the absence of antibiotics, the trajectories trended largely towards faster growth, with minimal changes to resistance levels (Figure 4-3). With subinhibitory chloramphenicol treatments, we observed that the populations first experienced a slight growth decrease, followed by increased resistance, and then restored growth within 48 h. While these populations did gain resistance, they did not tend to reach very high final MIC values in absolute terms, with inhibition zone diameters just at the border of being defined as resistant. In contrast, with inhibitory chloramphenicol treatment, there was a more dramatic reduction in growth within the first 12 h. Though growth was impacted, the populations tended to walk towards high resistance during this period. As depicted in the schematics, the zig-zag patterns trending towards high resistance may be indicative of the cultures

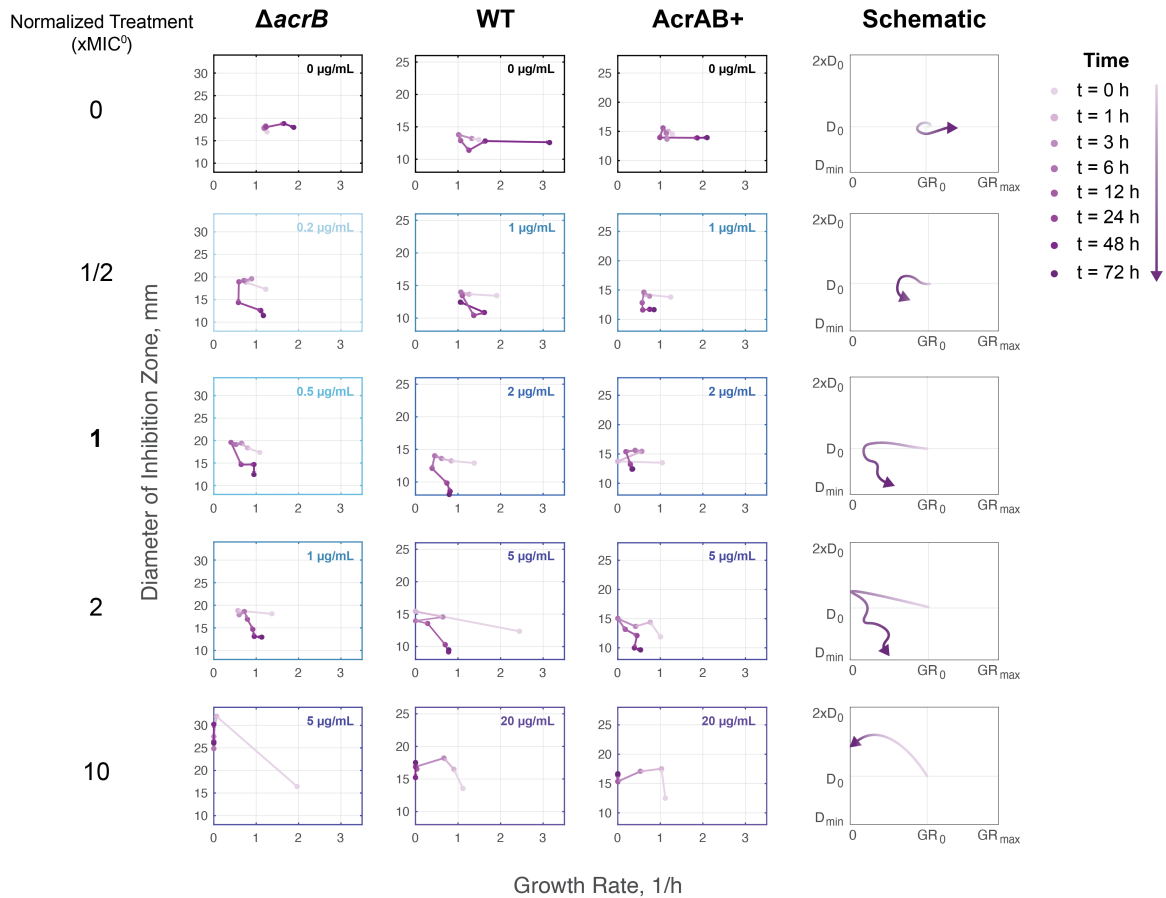


Figure 4-3. Resistance and Fitness Evolution Trajectories.

(A) Average diameter of inhibition zone and average growth rate plotted against each other. Lighter purple markers represent trajectories occurring earlier; darker purple are later timepoints. The longer the distance between markers, the greater the change between time points. Colors of boxes indicate the absolute treatment concentration for the depicted trajectories. (B) Schematics summarize patterns for each treatment concentration ($xMIC^0_{parent}$). Schematic plots show growth rate in terms of initial growth rate (GR_0) and maximum physiological growth rate (GR_{max}). Resistance is shown in terms of relative diameter of inhibition, where D_0 is the diameter of inhibition at $t = 0$ h and D_{min} is the diameter of the antibiotic disc.

acquiring resistant mutations and compensating for the associated fitness costs of these mutations. Finally, at high chloramphenicol concentrations, bacteria first became more susceptible and then stopped growing entirely within 12 h; growth was never restored for these populations. We found that all strains followed similar evolutionary trajectories while

balancing the trade-off between growth and resistance. These findings highlight the importance of using antibiotic concentrations that are sufficiently inhibitory.

While these results tell us about the growth rate and resistance of the overall population, it is difficult to determine if sub-populations of cells within the culture have acquired high levels of resistance from disc assays alone. First, because the disc assays do not quantify resistance associated with individual cells in the culture, they cannot reveal the presence of sub-populations of resistant and susceptible cells. Second, beyond a certain resistance level, cells will grow up to the boundary of the disc; thus, it is not possible to quantify resistance increases beyond this. Determining which conditions can give rise to high levels of resistance is important for revealing particularly dangerous treatment regimes. In addition, sub-populations with increased resistance to one antibiotic can promote cross-resistance to other drugs (294).

To quantify the fraction of resistant cells that emerged during our evolution experiment, we conducted a spot assay, in which we measured the fraction of the population capable of surviving on specific chloramphenicol concentrations. For all three strains, we observed sub-populations that were capable of growing on 10 $\mu\text{g/mL}$ chloramphenicol (Figure 4-4A & Figure C-4). Interestingly, these cells primarily emerged from treatment conditions with lower levels of chloramphenicol, and not from conditions where cells were subjected to 10 $\mu\text{g/mL}$ chloramphenicol. For example, at least 0.1% of the population from each of the three WT replicates that were treated at 2 $\mu\text{g/mL}$ chloramphenicol could survive on 10 $\mu\text{g/mL}$ at the end of the experiment. We did find cases where WT cells treated with 10 $\mu\text{g/mL}$ evolved resistance to 10 $\mu\text{g/mL}$, however this

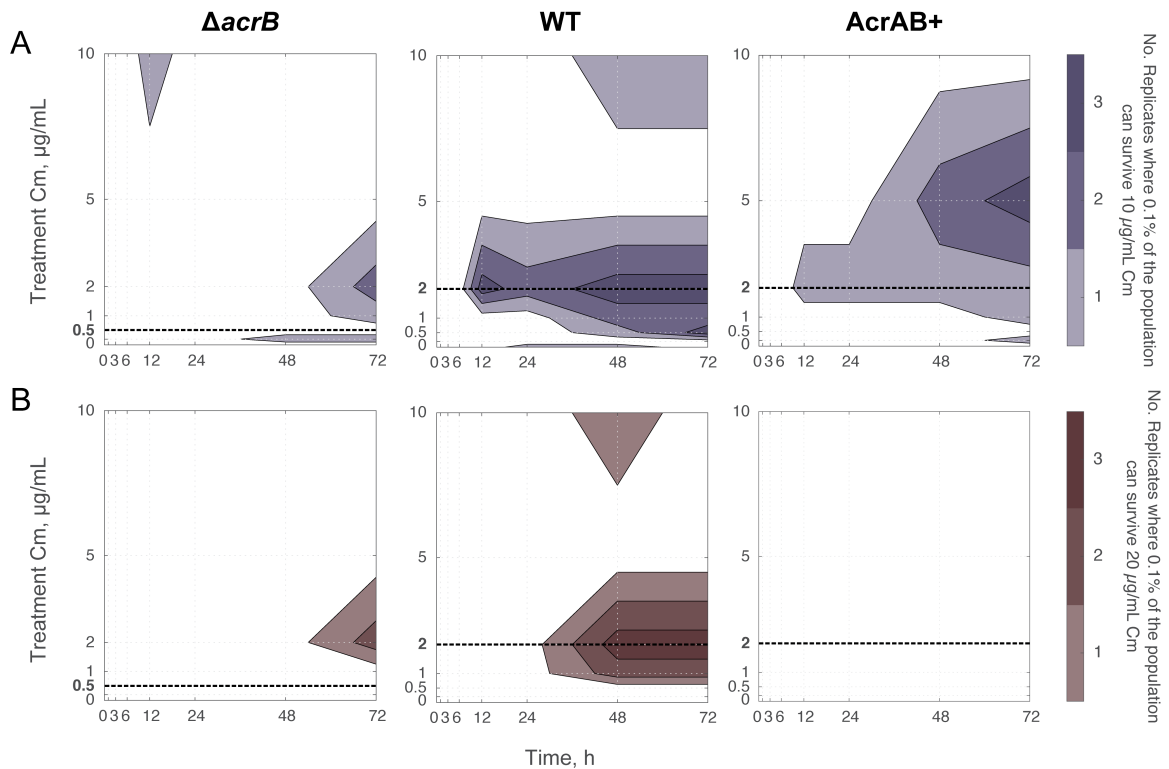


Figure 4-4. Number of Biological Replicates with Highly Resistant Sub-populations through Time.

Number of biological replicates that had a sub-population greater than 0.1% of their total population, which could grow on LB plates containing (A) 10 µg/mL or (B) 20 µg/mL chloramphenicol. Raw data is shown in Figure C-4. Initial populations contained $\sim 10^7$ CFUs. MIC^0_{parent} compared to treatment concentration is denoted with a bold dashed line (Figure C-2).

was less frequent compared to lower treatment concentrations. Thus, cultures were able to evolve resistance to higher levels of chloramphenicol than they were exposed to, a feature that was most pronounced when treatments were just above or at MIC^0_{WT} . These results closely match trends in the population's overall resistance (Figure 4-2B). We also found isolates capable of growing on 20 µg/mL chloramphenicol, albeit with a reduced frequency relative to 10 µg/mL (Figure 4-4B & Figure C-4).

In contrast, the AcrAB+ strain was capable of evolving resistance to 10 µg/mL

when treated with 5 µg/mL chloramphenicol; yet, surprisingly, AcrAB⁺ never produced a sub-population that was able to grow on 20 µg/mL as the WT did. Meanwhile, despite the higher initial susceptibility of $\Delta acrB$ ($MIC^0_{\Delta acrB} < MIC^0_{WT}$ and MIC^0_{AcrAB+}), the $\Delta acrB$ strain consistently produced sub-populations that were able to grow at 20 µg/mL chloramphenicol by 72 h. This sub-population appeared for chloramphenicol concentrations around 2 µg/mL, similar to the WT strain.

A key question remained: which mutations were responsible for the increases in resistance we observed? To address this, we used whole genome sequencing to analyze three biological replicates from the 72 h timepoint for the WT, AcrAB⁺, and $\Delta acrB$ strains (Table 4-1). For the WT strain, each of the sequenced isolates contained a single point mutation in the DNA binding region of *marR*, which can upregulate AcrAB-TolC efflux pumps and expression of other stress response genes (295). Two of these point mutations were missense mutations in *marR* and have been observed in other studies (35, 296–299). Additionally, one isolate had a missense mutation in the periplasmic encoding region of *acrB*. The other two isolates had an IS1 or IS5 insertional sequence interrupting *acrR*, which is known to upregulate *acrAB* (300). One question these results raise is why the AcrAB⁺ strain, where *acrR* is removed, is outperformed by WT strains with mutations in *acrR*. A potential explanation for this is that the ‘marbox’ through which *acrAB* is upregulated sits within *acrR* (163). The AcrAB⁺ strain lacks this marbox (235), while in the sequenced isolates the insertion sequence is located further upstream in *acrR* and the marbox remains intact, providing global stress response regulation while eliminating the impact of the local repressor. Thus, the exact position of the insertion sequence matters.

These sequencing results indicate that strains containing AcrAB-TolC efflux pumps use mutations related to the pumps and their regulation to optimize survival and increase resistance in the presence of chloramphenicol.

When we evolved the AcrAB⁺ strain and performed whole genome sequencing of the most resistant isolates, all isolates had mutations in the noncoding, promoter region of *acrAB* (Table 4-1). These mutations indicate that the AcrAB⁺ strain might require further

Parent Strain			WT			AcrAB ⁺			Δ <i>acrB</i>		
Treatment Concentration			2 μ g/mL Cm			5 μ g/mL Cm			1 μ g/mL Cm		
Region	Mutation	Position	1	2	3	1	2	3	1	2	3
<i>acrR</i>	IS1 + 4bp	481,420			X						
	IS5 + 8bp	481,481	X								
<i>P_{acrRAB}</i>	IS2 + 4bp	481,163						X			
	Δ 1bp	481,174				X					
	T \rightarrow C	481,187					X				
<i>acrB</i>	Q569L	478,154		X				X			
	V139F	479,445					X				
<i>marR</i>	+ 1bp	1,613,590		X							
	T72P	1,613,590	X								
	V84E	1,613,267			X						
<i>acrS</i>	IS5 + 4bp	3,407,126							X	X	
	IS2 + 4bp	3,407,133									X
<i>rpoB</i>	K126Q	4,174,956				X					
<i>fimD</i>	T393N	4,536,090					X				
<i>yhjB</i>	IS4 + 12bp	3,664,650						X			
<i>clpX</i>	IS186 + 2bp	454,251						X			
<i>selA</i>	D441G	3,753,288							X		
<i>rrsG</i>	+58 bp	2,723,638							X		
Isolation [Cm] (μ g/mL)			20	20	20	10	10	10	10	5	5

Table 4-1. Summary of whole genome sequencing results.

Non-clonal mutations for each resistant isolate from eVOLVER experiments. Each isolate from each parent strain is derived from a different biological replicate. In addition to the mutations, the table also lists the treatment concentrations that each isolate evolved at, as well as the concentration of chloramphenicol that the isolate was selected on at t = 72 h. Genetic regions that do not exist in the parent strain are grayed out.

tuning of *acrAB* expression for improved resistance. Further, two of these isolates also had missense mutations in the coding region of *acrB* as well. Of these, the V139F missense mutation is known to produce high levels of multidrug resistance by accelerating export for a number of AcrAB-TolC substrates (105, 279, 301, 302). We observed *acrB* Q569L evolve from two different parent strains, WT and AcrAB+, suggesting it plays a role in chloramphenicol export. Additionally, the evolved AcrAB+ isolates all had other mutations less directly related to the AcrAB-TolC efflux pump and its regulators, such as genes related to transcription (*rpoB*, *yhjB*), fimbriae assembly (*fimD*), or degradation (*clpX*) (Table 4-1).

In contrast, when we evolved the Δ *acrB* strain, we found that all three isolates had an insertion sequence located in *acrS* (Table 4-1). AcrS is the local regulator of the AcrEF-TolC efflux pump, a homolog to AcrAB-TolC (180). This result agrees with findings from Cudkiewicz & Schuldiner, who showed that the Δ *acrB* strain gained high resistance by upregulating redundant efflux pumps in *E. coli*, such as AcrEF-TolC or MdtEF-TolC (105). One of the three isolates also contained a missense mutation in the tRNA for selenocysteine (*selA*) and a short insertion sequence in the 16S rRNA of the 30S subunit (*rrsG*), though whether or how these play a role in chloramphenicol resistance is unclear.

4.4. Discussion

In this work, we identified that treating strains with antibiotic concentrations close to MIC^0_{parent} promotes the evolution of resistance; however, the evolvability and ultimate resistance level achieved differed between WT, AcrAB+, and Δ *acrB* strains. WT populations evolved mutations that conferred high levels of resistance within 24 h after

antibiotic exposure. Maximal resistance was evolved at $\sim 1x$ MIC^0_{WT} , however $0.25-2.5x$ MIC^0_{WT} chloramphenicol treatment concentrations all gave rise to resistance. We observed similar trends WT treated with another antibiotic, ciprofloxacin, as well (Figure C-6). In contrast, AcrAB⁺ evolved resistance, but this was only possible at precise chloramphenicol concentrations at $2.5x$ MIC^0_{AcrAB+} . The evolved AcrAB⁺ populations were less resistant than their WT counterparts, and spot assays determining resistance confirmed this trend. In contrast, the $\Delta acrB$ strain was able to evolve resistance under $1-4x$ $MIC^0_{\Delta acrB}$ chloramphenicol treatments, and ultimately achieved absolute resistance levels comparable to those observed in the WT strain.

Our results identify that antibiotic treatments near MIC^0_{parent} are especially prone to evolving resistance. Reding *et al.* observed this hotspot for adaptability of *E. coli* in the presence of another antibiotic, erythromycin, just below the MIC of their parent strains (280). While doctors measure resistance of bacterial infections, they sometimes prescribe antibiotic treatment prior to obtaining the results of this assay (303) or use a treatment concentration too low to effectively penetrate the infection site (304). This blind treatment could lead to increased levels of resistance (305, 306). These results highlight the presence of regimes that are especially problematic and which should be avoided to limit the evolution of antibiotic resistance.

While we observed that all strains were capable of evolving resistance, sequencing revealed the different pathways that each strain took to achieve this. WT achieved resistance through mutations and insertion sequences in the regulators AcrR and MarR, suggesting that WT cells can fine-tune expression of the AcrAB-TolC pumps to gain

resistance to chloramphenicol. Interestingly, these mutations may produce cross-resistance to other antibiotics as well since these regulators control many genes involved in multi-drug resistance (164, 165). AcrAB⁺ cells utilized mutations in *acrB* and the promoter region controlling its expression to achieve resistance. Δ *acrB* populations achieved resistance by targeting homologous efflux pump systems, such as AcrEF-TolC. Although resistance was slow to emerge in this strain compared to WT or AcrAB⁺, this alternative pathway for achieving resistance ultimately resulted in levels comparable to those achieved by the WT strain. By charting evolutionary landscapes across different antibiotic concentrations, we have gained insight into treatments that impact the emergence of antibiotic resistance and the effect of efflux pumps on this process.

4.5. Contributions Statement

The authors of this work were Ariel M. Langevin (A.M.L.), Imane El Meouche (I.E.M.), and Mary J. Dunlop (M.J.D.). A.M.L. and I.E.M. designed experiments, A.M.L. conducted the experiments and analyzed the data, M.J.D. supervised the research. All authors wrote the manuscript.

4.6. Methods

4.6.1. Strains and Plasmids

We used *E. coli* strains BW25113 (WT), BW25113 Δ *acrB* (Δ *acrB*), and BW25113 Δ *acrR* (AcrAB⁺). The wild type strain BW25113 is the parent strain for the Keio collection (235). BW25113 Δ *acrB* was derived from Keio collection strain JW0451 (BW25113 Δ *acrB::kan^R*) (189). For BW25113 Δ *acrR*, we designed primers with homology regions on *acrR* and amplified the kanamycin resistance marker and FRT sites of pKD13 (235).

Primers are listed in Table C-2. The linear DNA was then treated using a DpnI digest and PCR purification. We electroporated the purified linear DNA into competent BW25113 cells containing the plasmid pSIM6 (307). We removed kanamycin resistance markers from JW0451 and BW25113 $\Delta acrR::kan^R$ following the pCP20 protocol from Reference (308).

4.6.2. Determination of MIC

For all experiments, overnight cultures were inoculated from a single colony in 10 mL LB and grown in a 50 mL Erlenmeyer flask at 37°C with 200 rpm orbital shaking. After overnight growth, the optical density at 600 nm (OD_{600}) was measured, and the initial volume was diluted back to $OD_{600} = 0.1$. To determine the MIC of the parent strains (Figure C-2), we added a final concentration of 0, 0.2, 0.5, 1, 2, 4, 8, or 12 $\mu\text{g/mL}$ of chloramphenicol to each culture; to determine the MIC of the evolved strains (Figure C-5), we added 0, 0.5, 1, 2, 5, 10, 20, or 50 $\mu\text{g/mL}$ to each culture. Chloramphenicol stocks were prepared with 100% ethanol. The samples were sealed with evaporation-limiting membranes (Thermo Scientific AB-0580) and grown in 24-well plates at 37°C with 200 rpm orbital shaking. OD_{600} readings were taken using a BioTek Synergy H1m plate reader before incubation ($t = 0$ h) and after antibiotic exposure ($t = 24$ h). As Tween20 is a detergent and a potential substrate of the AcrAB-TolC efflux pumps, we also conducted the toxicity curve experiments with Tween20 at our working concentration 0.2% (v/v). We found there was no significant change in resistance for any of the strains under the presence of Tween20 (Figure C-7). All experiments were performed in triplicate using biological replicates.

4.6.3. Experimental Conditions in the eVOLVER

In the eVOLVER, cultures were inoculated from a single colony in LB at 37°C. A stir bar mixed the cultures on a medium setting, or approximately 1000 rpm (291). The LB was supplemented with the detergent Tween20 (Sigma Aldrich Cat. # P1379) at 0.2% (v/v) to reduce spurious OD₆₀₀ measurements caused by biofilm growth on the flask. As Tween20 is a detergent and a potential substrate of the AcrAB-TolC efflux pumps, we also conducted the toxicity curve experiments with Tween20 at our working concentration 0.2% (v/v). We found there was no significant change in resistance for any of the strains in the presence of Tween20 (Figure C-7 & Table C-4).

Cells were inoculated in the eVOLVER overnight ($t \approx -16 - -14$ h) prior to the beginning of the experiment ($t = 0$ h) to establish steady-state exponential growth. We set the eVOLVER using an upper OD₆₀₀ bound of 0.2 and a lower bound of 0.1; thus, cultures were grown to a turbidity of 0.2 and then diluted back to 0.1 to maintain the turbidostat at approximately constant cell density. Samples were collected during the experiment at set time points ($t = 0, 1, 3, 6, 12, 24, 48, \text{ and } 72$ h) and used for downstream analysis. All experiments were performed in triplicate using biological replicates.

At $t = 0$ h, we introduced chloramphenicol at a predetermined final treatment concentration ($[Cm] = 0, 0.2, 0.5, 1, 2, 5, 10, \text{ or } 20$ µg/mL). This introduction was implemented by switching the media source from one containing 0 µg/mL chloramphenicol to another containing the final treatment concentration; in addition, we spiked the samples directly with the treatment concentration of chloramphenicol at the same time to avoid a delay due to the time required for media cycling in the turbidostat.

4.6.4. Downstream Assays and Data Collection from eVOLVER Samples

4.6.4.a. Growth Rate Measurements

Growth rate measurements were calculated after each dilution event using:

$$\text{Growth Rate} = \frac{\ln\left(\frac{OD_{600,high}}{OD_{600,low}}\right)}{t_{OD_{600,high}} - t_{OD_{600,low}}} \quad \text{Eq. 16}$$

The growth rate between each dilution was then averaged across sampling time points to compare against disc diffusion assays and spot assays. For example, the growth rate given at $t = 0$ h is the growth rate from $t = -6$ h to $t = 0$ h. To evaluate statistically significant differences in growth rate between two time points, we used the paired- t test; to evaluate statistically significant differences in growth rate between two strains, we used the t test (Table C-1).

4.6.4.b. Antibiotic Disc Diffusion Assay

We aliquoted samples from the eVOLVER, where the OD_{600} from each sample was between 0.1 and 0.2. We used cotton swabs to cover LB agar plates with a layer of the sample (309). An antibiotic disc containing chloramphenicol (30 g) (Thermo Fisher Scientific Cat. # CT0013B) was then placed on the plate. The plate was incubated for 24 h at 37°C. The diameter of the zone of inhibition around each disc was then measured. Diameter of inhibition zones were classified as susceptible, intermediate, or resistant based on Reference (293). Additionally, we calculated the MIC using a linear mapping between MIC and diameter of inhibition zones for our samples (Figure C-5) (310). To evaluate statistically significant differences in diameter of inhibition zones or resistance between two time points, we used the paired- t test; to evaluate statistically significant differences in

resistance between two genotypes, we used the t test (Table C-4).

4.6.4.c. Spot Assay

The samples from the eVOLVER experiment were diluted in PBS to the following dilution series: 1, 10^{-1} , 10^{-2} , 10^{-3} , 10^{-4} , and 10^{-5} . We then plated 2.5 μ L of each dilution on LB agar plates containing 0, 0.5, 1, 2, 5, 10, and 20 μ g/mL chloramphenicol. The plates were then incubated for 24 h at 37°C. To count colonies, we identified the dilution factor with the most countable colonies, and recorded the number of colony forming units (*CFU*) and dilution factor (d). The CFU/mL for each sample was then calculated by:

$$\text{CFU/mL} = \frac{\text{CFU} * d}{V} \quad \text{Eq. 17}$$

where V is the volume plated. We also calculated the proportion of the population able to grow on different concentrations of chloramphenicol by calculating the CFU/mL from LB agar plates containing 0, 0.5, 1, 2, 5, 10, and 20 μ g/mL chloramphenicol.

4.6.5. Whole Genome Sequencing

DNA was extracted from single isolates and parent strains using the QIAGEN DNeasy PowerBiofilm kit. For each strain, we selected three isolates to sequence; each of these isolates originated from a different biological replicate that was evolved under the same experimental conditions (i.e. each isolate comes from a different eVOLVER culture). Samples were sequenced at the Microbial Genome Sequencing Center (MiGS) in Pittsburg, PA, USA, who conducted library preparation and multiplexing using the Illumina Nextera kit series and then sequenced using a NextSeq 550 platform with 150 bp paired-ends and an average coverage of 50 reads. We analyzed reads using *breseq* (311) version 0.35.1.

Reads were aligned to the BW25113 Keio reference genome (Accession: CP009273) in consensus mode. The treatment concentrations and isolation concentrations used to select each isolate are listed in Table 4-1. Whole genome sequencing data for the parent strains and the isolates are available on GenBank (BioProject: PRJNA666010; Accession no.: CP062239 to CP062250).

5. ANTIBIOTIC INTRODUCTION RATE AND MIXED POPULATIONS INFLUENCE THE EMERGENCE OF ANTIBIOTIC RESISTANCE

5.1. Abstract

Antibiotic resistance remains a public health concern as bacteria readily utilize resistance mechanisms, including efflux pumps, to evade antibiotic treatments. Previously, we found that the rate of antibiotic administration could compromise the effectiveness of such multidrug efflux pumps (**Chapter 2**). For instance, the AcrAB-TolC efflux pump exports antibiotics out of the cell, increasing resistance levels. These pumps are more effective when antibiotics are introduced slowly. In this study, we assessed how short-term and long-term differences in antibiotic introduction rates affect the longer-term evolution of drug resistance. We monitored this in different genetic backgrounds: *E. coli* harboring AcrAB-TolC efflux pumps with their native regulatory networks intact, constitutive expression of the efflux pumps, and a strain lacking functional pumps. We compared cultures exposed to a rapid step increase in chloramphenicol to those exposed to a slow short-term ramp increase. We found that efflux pump expression increases tolerance to antibiotics and promotes the emergence of resistance through mutations. In genotypes lacking the native regulation networks, slow rates of antibiotic introduction increase the number of resistant isolates and decrease the number of susceptible cells compared to rapid antibiotic introduction. We also identified how slow and long-term antibiotic introduction rates promote increased fitness over resistant phenotypes relative to step antibiotic introduction rates. Lastly, we found that in co-cultured populations containing strains with and without the pumps, the results were not simply the additive response of the single-

strain evolution experiments. Co-cultured populations exposed to a step increase in chloramphenicol produced few resistant isolates, whereas in populations exposed to a short-term ramp over half of the isolates were resistant. These results highlight the importance of studying the interplay between the rate of antibiotic introduction, population composition, as well as the regulatory networks controlling expression of resistance genes.

5.2. Introduction

Although the antibiotic revolution represents a significant advance in modern medicine, bacteria have historically acquired resistance shortly after the introduction of new antibiotics (5, 274). Moreover, the discovery of novel antibiotics has dwindled, presenting doctors and scientists alike with the challenge of how to best treat infections while keeping the evolution of resistance in check. Overuse of antibiotics results in pressures further driving resistance (275). A potential solution is to focus not solely on finding new drugs, but also on leveraging dosing strategies that minimize the frequency of resistant and tolerant bacteria. Here, we define resistance as a genetically-encoded mechanism that allows bacteria to survive antibiotic treatment and tolerance as a phenotypic response that enables survival.

There are many mechanisms by which antibiotic resistance can be achieved, including enzymatic inactivation, alteration of antibiotic binding sites, and increased efflux or reduced influx of antibiotics (230). Due to their active role in exporting antibiotics, we focused on efflux pumps, specifically the multidrug AcrAB-TolC pump in *E. coli*. The proteins that compose the pump are the outer membrane channel TolC, the periplasmic linker protein AcrA, and the functional unit of the efflux pump AcrB. AcrB uses the proton

motive force to actively export substrates out of the cell (222, 230). Deletion of *acrB* eliminates pump functionality, resulting in a five-fold reduction of minimum inhibitory concentration (MIC) for chloramphenicol (189). Chloramphenicol is often used as a last resort antibiotic in multidrug resistant infections since most clinical isolates are susceptible to this drug (289, 290). Despite the pump-mediated increase in resistance, upregulation of the efflux pumps incurs a growth cost and can increase mutation frequencies (189, 191).

Current antibiotic resistance research primarily explores binary conditions – where a stress is or is not present; however, realistic environments are seldom as well-defined as those in the laboratory (193). Our prior results have demonstrated a relationship between the rate of antibiotic addition and the benefit of efflux pumps on population fitness, where the efflux pumps' ability to convey a population-level fitness benefit is amplified when antibiotics are added slowly (189). We found that cells with constitutive expression of efflux pumps were more represented than those without pumps when a slow dose of antibiotics was applied over the course of several hours (189). Further, recent theoretical results suggest that the emergence of mutations giving rise to antibiotic resistance may also depend on the dynamics of stress (111). These results prompt the question of whether the rate of antibiotic addition can influence levels of resistance and tolerance (312).

Our overall goal in this work was to identify how antibiotic resistance and tolerance emerge based on antibiotic dose dynamics. To achieve this, we used a turbidostat as an evolutionary platform (291). We introduced chloramphenicol at two different rates: a short-term ramp over 6 hours and a step over 1 minute. We allowed the cultures to grow and evolve for 72 hours in continuous culture and then assessed whether resulting colonies

derived from the culture were either nongrowing, susceptible, tolerant, or resistant to antibiotics. We conducted these tests in strains with the native regulatory network controlling AcrAB-TolC expression intact, in strains with constitutive expression of the pumps, and in strains lacking the pumps. We then identified cases where different antibiotic introduction rates and the genetic background of the strain play a role in survival.

5.3. Results

5.3.1. Short-term fluctuations can promote fitness from antibiotic exposure

We tested two antibiotic introduction profiles and measured how they impacted population shifts over the course of 72 hours. We compared a short-term ramp and step introduction of an antibiotic (Figure 5-1A). For these experiments, we used a final concentration of 1 $\mu\text{g/mL}$ chloramphenicol, which is the half maximal inhibitory concentration (IC_{50}) for wild type cells (189). Cultures subjected to both treatment profiles receive the same amount of antibiotic, but the rate at which it was introduced differs between the two.

In order to assess the appearance of tolerance and resistance under these treatments, we grew cells in a modular turbidostat called the eVOLVER (291). The eVOLVER maintains cultures in exponential phase by using serial dilutions to introduce media when the optical density reaches an upper threshold so that the optical density, or turbidity, of the culture stays within a narrow range of values (Figure 5-1B). To investigate whether differences in antibiotic introduction rates of chloramphenicol would impact the growth, we first tested wild type cells that have the AcrAB-TolC pump controlled by its native upstream stress response regulators. Since it is quite rare for advantageous mutations to

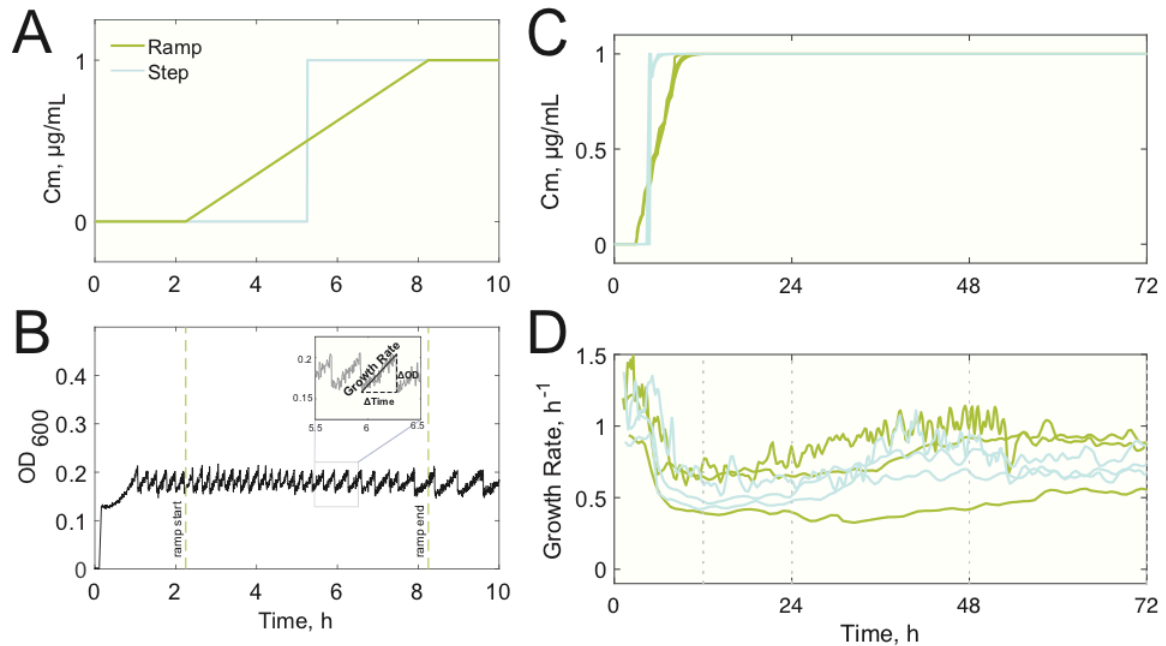


Figure 5-1. Experimental conditions and growth of wild type *E. coli* in the eVOLVER.

(A) Schematic of two antibiotic introduction rates: a short-term ramp increase to the final antibiotic concentration (green) and a step increase (blue). (B) OD₆₀₀ of an individual culture exposed to a short-term ramp increase in chloramphenicol. Cells are grown to an upper bound of OD₆₀₀=0.2 and then diluted back to OD₆₀₀=0.15. Note that the growth rate decreases after antibiotic introduction begins. (Inset) Schematic showing how the growth rate is calculated from raw OD₆₀₀ measurements. (C) Actual concentration of chloramphenicol over time in wild type cultures for a short-term ramp (green) and step (blue). (D) Growth rates for wild type cultures. $n = 3$ biological replicates for each treatment.

appear at a high frequency within hours (313, 314), we allowed the bacteria to grow continuously for 72 hours. Previous evolution experiments identified trimethoprim-resistant isolates in under 50 hours (106). This timing allowed us to assess changes in resistance that emerge from changes in the antibiotic introduction rate. We found that wild type cells exposed to a chloramphenicol step had a period of growth inhibition followed by a modest increase in growth rate approximately 24 hours after treatment (Figure 5-1C-D). The cells exposed to a short-term ramp were similar, though the increase in growth was

more variable across replicates. On average, after 72 hours the final growth rates were near 0.7 h^{-1} for cultures from both the short-term ramp and step treatments. For comparison, we also ran tests with no chloramphenicol addition and observed growth rates of $>1.0 \text{ h}^{-1}$ (Figure D-1A). Therefore, although wild type cells partially recover, their population distributions are still impacted at 72 hours relative to untreated cultures.

To determine resistance and tolerance levels of cells within the cultures, we plated samples from the 72-hour time point (Figure 5-2A). To first confirm viability, we used LB plates; for the antibiotic tests, we plated cells on LB plates with a high concentration of chloramphenicol (Cm) ($25 \text{ }\mu\text{g/mL}$). We were also interested in investigating whether cross-resistance to other antibiotics could emerge without prior exposure. To test this, we also plated cells on LB plates containing high doses of tetracycline (Tet) ($6 \text{ }\mu\text{g/mL}$) and LB plates ciprofloxacin (Cp) ($0.1 \text{ }\mu\text{g/mL}$) (191, 315, 316).

From each of these plates we isolated three colonies and cultured them individually in fresh LB medium. Interestingly, cultures derived from a subset of these colonies did not grow when re-cultured in fresh LB. We categorized these as *nongrowing* in our subsequent analysis (Figure 5-2A). For the colonies that we were able to culture, we used an antibiotic disc assay to further categorize results. In this assay, media containing a single isolate was plated to confluence and a disc containing antibiotics was placed on the plate. Antibiotic from the disc diffuses into the surrounding media. At areas close to the disc, known as the inhibition zone, antibiotic concentrations are high and bacterial growth is inhibited (317). This test could determine changes in resistance of isolates compared to the original parent strain, which is the strain that was not subjected to treatment in the eVOLVER. For

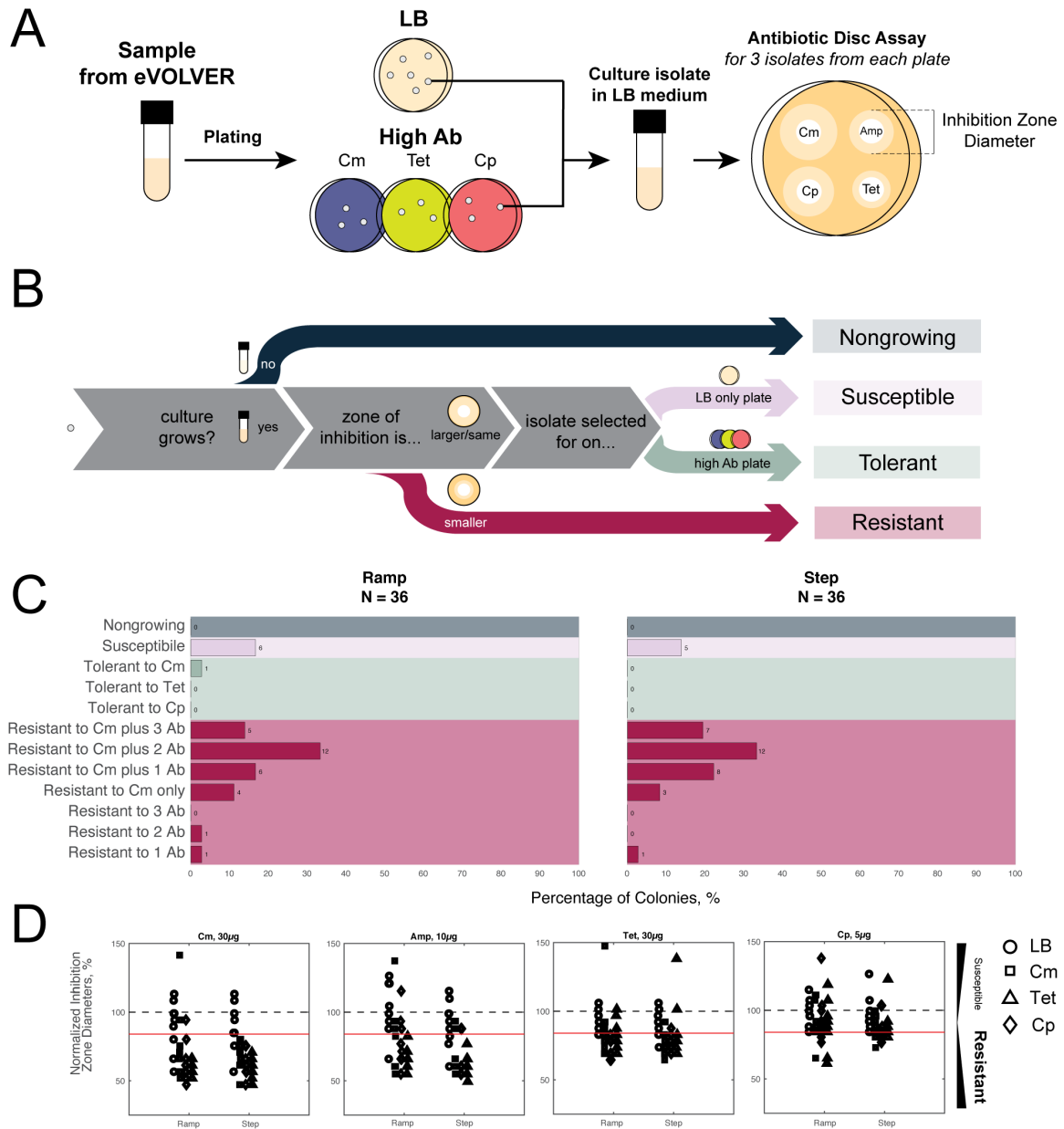


Figure 5-2. Experimental and data analysis workflows quantifying the emergence of resistance and tolerance for wild type *E. coli*.

(A) After 72 hours, cultures were plated on a control LB plate and on three high dose antibiotic plates (25 µg/mL chloramphenicol (Cm), 6 µg/mL tetracycline (Tet), 0.1 µg/mL ciprofloxacin (Cp)). From each of these plates, three colonies were grown to exponential phase, then plated and used to perform an antibiotic susceptibility disc assay to determine changes in resistance relative to the parent strain. (B) Information on each isolate was then used to classifying strains as nongrowing, susceptible, tolerant, or resistant. (C) Fates of all isolated colonies from all plates. Results are classified as: nongrowing (navy),

susceptible (light pink), tolerant (light green), and resistant (burgundy). Ab, antibiotics. N represents the number of isolates from each experiment that were picked. If no colonies were found on a high antibiotic plate then no isolate could be picked. Counts are shown at the end of each bar, listed as a number on the figure. **(D)** Normalized inhibition zone diameters for the four antibiotic disc assays: 30 µg chloramphenicol, 10 µg ampicillin (Amp), 30 µg tetracycline, and 5 µg ciprofloxacin. The inhibition zone diameters were normalized to the parent strain's mean inhibition zone, where no change is denoted by the dashed, black line. The threshold we used to classify colonies as resistant is shown in red. The symbol shape indicates which plate the colony was originally isolated from: LB only (circle), LB+Cm (square), LB+Tet (triangle), LB+Cp (diamond). Each individual replicate for data presented here is shown in Figure D-6.

example, if the inhibition zone diameter is smaller for the isolate than the parent, then the isolate is more resistant than the parent.

We exposed each isolate to four antibiotic susceptibility discs: chloramphenicol, ampicillin, tetracycline, and ciprofloxacin (Figure 5-2A). We selected these antibiotics because of their diverse mechanisms of action, allowing us to test whether the changes in resistance target a specific antibiotic mechanism or are more general. In addition, the AcrAB-TolC efflux pump has a range of efficacies for these antibiotics (Figure D-2). Chloramphenicol is a protein synthesis inhibitor that is actively exported by the AcrAB-TolC efflux pump (218, 219). Ampicillin is a β -lactam that inhibits cell wall synthesis and known to be exported by AcrAB-TolC (222, 318). Tetracycline inhibits protein synthesis and ciprofloxacin inhibits DNA replication (319). We measured the inhibition zone for each isolate and compared it to the inhibition zone for the parent strain (Table D-1).

We classified results into four different categories (Figure 5-2B). (1) *Nongrowing* cells were no longer culturable after the initial plating, as described above, and the isolates did not grow in LB media or on LB plates. (2) *Susceptible* cells grew on LB, but did not grow on any of the high antibiotic plates and had no reduction in inhibition diameter in the

disc assay relative to the parent strain. (3) *Tolerant* cells were able to grow in high concentrations of antibiotics on the plates, but exhibited no reduction in inhibition zone diameter relative to the parent strain. (4) *Resistant* cells had a reduction in inhibition zone diameter compared to the parent strain.

For the wild type strain, we isolated both tolerant and resistant strains, but saw no significant differences between short-term ramp and step antibiotic treatment, indicating that regardless of the introduction rate, wild type cells have a similar response (Figure 5-2C). These results are in contrast to control experiments without antibiotic addition, where instances of resistance were rare and susceptible isolates were prevalent (Figure D-1B). In the antibiotic disc assay we tested for resistance and cross-resistance by normalizing relative to the parent strain's inhibition zone diameter (Figure 5-2D). Thus, isolates with data points falling below 100% are more resistant than the parent strain. Here, we again observed clear differences between the antibiotic treatments and the no antibiotic control, with chloramphenicol-treated samples acquiring resistance, while those without chloramphenicol exposure did not (Figure 5-2D, Figure D-1C). Step and short-term ramp exposures were similar in their effect on the zone of inhibition.

Despite using only chloramphenicol in the eVOLVER continuous culture, we found many examples of cross-resistance, where cells were resistant to ampicillin, tetracycline, or ciprofloxacin as well (Figure 5-2D and Figure D-3, Column 4). These results indicate that the mechanisms involved in resistance extend beyond the impact of a single stressor. From our whole genome sequencing results from **Chapter 4**, we speculate that this observation of cross-resistance may be the consequence of wild type cells readily

evolving through insertion sequences placed in far-reaching stress response regulators, such as *marR* (164–166).

Although results for the wild type strain were similar for both step and short-term ramp treatments, we asked what impact efflux pump expression had on these findings. Mutations in the stress response regulators, *acrR* and *marR*, are observed in both clinical and laboratory settings; notably, these regulators primarily improve resistance by upregulating expression of the AcrAB-TolC efflux pump (106, 285, 320). We expected that the rate of antibiotic introduction would impact survival in an efflux pump-dependent fashion (189) and asked how this would translate to differences in the distributions of nongrowing, susceptible, tolerant, and resistant strains. In these experiments, we compared strains with two genetic backgrounds: an *acrB* deletion mutant with the efflux pump genes expressed on a plasmid (*acrAB*⁺) and a strain without efflux pumps (Δ *acrB*).³ An important distinction between *acrAB*⁺ and wild type is that the native regulation of the *acrAB* operon has been removed in *acrAB*⁺ and the pump genes are constitutively expressed. For our experimental conditions, where *acrAB*⁺ is exposed to chloramphenicol during exponential phase, *acrAB*⁺ and wild type demonstrate the same dose response to increasing concentrations of chloramphenicol (Figure 5-3B); for growth on agar plates the complementation is partial (Table D-1).

To compare fitness after antibiotic treatment for *acrAB*⁺ and Δ *acrB*, we grew cells in continuous culture in the eVOLVER and exposed them to a step and a short-term ramp

³ For consistency, these appear as defined in the original and, in this case, unpublished manuscript; however, please note that the names and definitions of each strain differ from Chapter 2, 3, and 4.

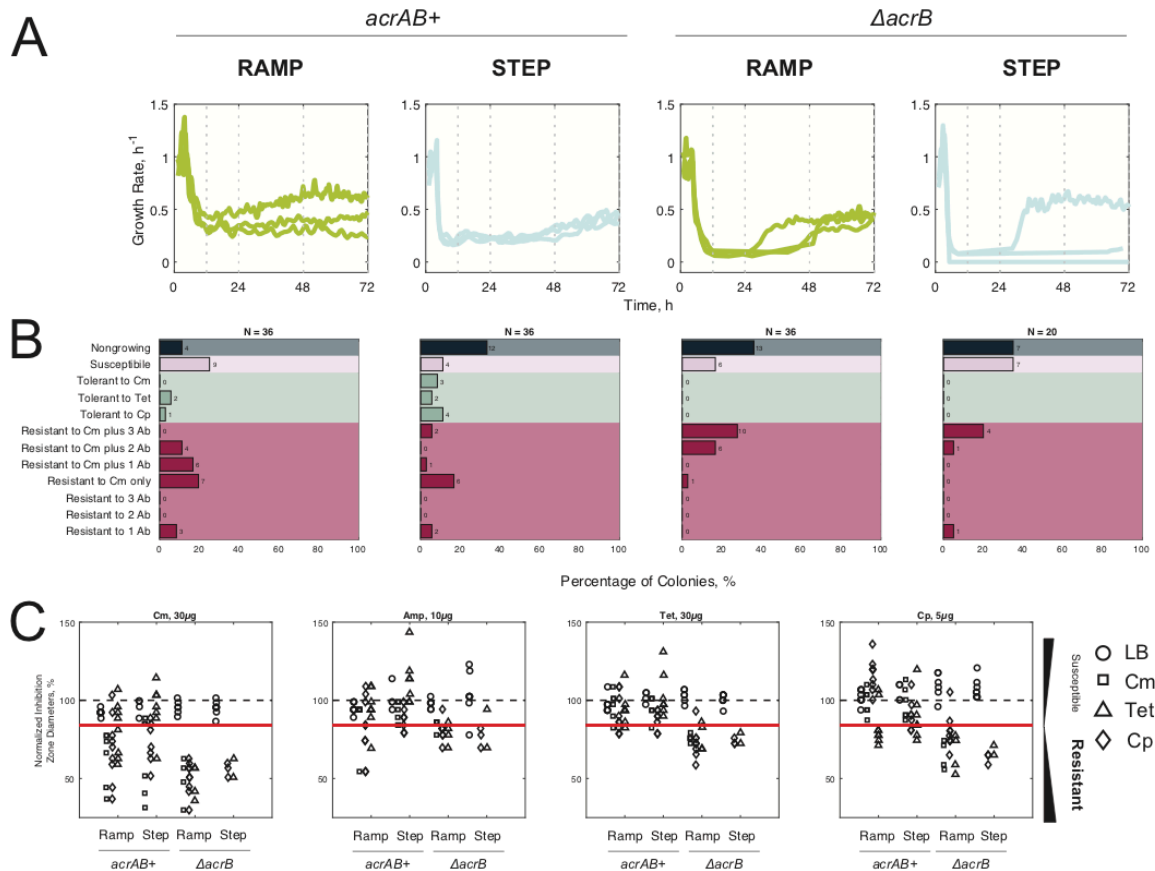


Figure 5-3. Impact of antibiotic introduction rate and strain background on the emergence of resistance and tolerance for *acrAB+* and $\Delta acrB$ cultures.

(A) Growth rates in *acrAB+* and $\Delta acrB$ cultures where the two chloramphenicol introduction rates are a short-term ramp (green) and a step (blue) as shown in Figure 5-1C. $n = 3$ biological replicates for each treatment. (B) Fates of all isolated colonies from all plates. Results were classified as: nongrowing (navy), susceptible (light pink), tolerant (light green), and resistant (burgundy). Ab, antibiotics. N represents the number of isolates, counts shown at end of bar. (C) Normalized inhibition zone diameters for the four antibiotic disc assays. The inhibition zone diameters were normalized to the parent strain's mean inhibition zone (black, --); resistance threshold (red). The symbol shape indicates which plate the colony was originally isolated from: LB only (circle), LB+Cm (square), LB+Tet (triangle), LB+Cp (diamond). Each individual replicate for data presented here is shown in Figure D-7 and Figure D-8.

of chloramphenicol introduction. For both types of treatment, we observed a sharp decrease in growth rate for cells without efflux pumps ($\Delta acrB$), whereas cells with efflux pumps (*acrAB+*) had a more gradual shift to their minimum growth rates (Figure 5-3A). Cells

exposed to a step also had a sharper decrease in growth rate than cells exposed to a short-term ramp. We found that slower introduction of antibiotics led to significantly higher growth rates in the first 24 hours for *acrAB*⁺ cells, but that at 72 hours the cultures with the step treatment had recovered (Table D-2). Growth of Δ *acrB* cells was severely impacted at 24 hours for both treatments, however the samples experiencing short-term ramps were more likely to recover by 72 hours (Figure 5-3A). Thus, the presence of efflux pumps improves growth immediately after antibiotic treatment. In addition, the antibiotic introduction rate also influences growth of the culture many hours after it is applied.

At the 72-hour timepoint, we plated cells on LB and plates containing high antibiotic concentrations and, following the procedures outlined in Figure 5-2A-B, we classified outcomes of the isolates from the different strain backgrounds and chloramphenicol treatment profiles. We found that functional efflux pumps were key to promoting tolerance in contrast this phenotype rarely appeared for Δ *acrB* cells (Figure 5-3B). We also found that cells exposed to short-term ramp treatments were more likely to exhibit resistance than cells exposed to a step (Figure 5-3B). For Δ *acrB* cultures exposed to a step, 70% of the isolates were nongrowing or susceptible. In contrast, *acrAB*⁺ cells exposed to a short-term ramp had ~35% nongrowing and susceptible cells. Δ *acrB* exposed to a short-term ramp and *acrAB*⁺ exposed to a step were intermediate. These results indicate that both the rate of antibiotic introduction, along with the genetic background of the cells influences propensity for survival through tolerance and resistance. For the *acrAB*⁺ cells, there were isolates surviving to 72 hours based only on tolerance, without acquisition of resistance, regardless of the antibiotic introduction rate. For both *acrAB*⁺

and $\Delta acrB$, populations exposed to a short-term ramp had higher incidences of resistant isolates compared to those exposed to a step; this can also be observed by a higher frequency of mutations on 25 $\mu\text{g/mL}$ chloramphenicol plates (Figure D-4, Row 1, Columns 2-3).

We also used the disc diffusion assay to test for changes in resistance relative to the parent strain. $acrAB^+$ cells exhibited a range of resistance to chloramphenicol, with examples spanning no change to greatly increased resistance (Figure 5-3C). Comparing the two introduction rates for $acrAB^+$ cells, results were largely similar in the distribution of resistance for the antibiotics (Figure 5-3C). In contrast, we observed that the $\Delta acrB$ cells were divided into two sub-populations for both of the antibiotic introduction rates. One population remained susceptible to chloramphenicol. We noted that these isolates were all obtained from the LB plate, so although they survived the continuous culture with chloramphenicol, they showed no difference in resistance in the disc diffusion assay in comparison with the parent. Meanwhile, the second population contained isolates that were resistant to chloramphenicol. Interestingly, for $\Delta acrB$ cells alone, we observed that this bimodal distribution exists for tetracycline and ciprofloxacin cross-resistance as well and is most pronounced in the case of the step treatment.

Since the IC_{50} of chloramphenicol for $\Delta acrB$ is lower than the IC_{50} for wild type and $acrAB^+$, we also investigated whether lower chloramphenicol concentrations would result in higher levels of resistance for the $\Delta acrB$ strain. The higher, instantaneous concentration of chloramphenicol introduced as a step led to low recovery of $\Delta acrB$ cells; we became interested in how lower concentrations of chloramphenicol might affect $\Delta acrB$

differently. As expected, growth recovered much more quickly when $\Delta acrB$ was exposed to 0.5 $\mu\text{g/mL}$ instead of 1 $\mu\text{g/mL}$ chloramphenicol (Figure 5-4A). In the case of the step exposure to chloramphenicol, all replicates maintained growth after treatment. At both chloramphenicol concentrations, we still observed more resistant isolates and fewer susceptible and nongrowing cells emerging under short-term ramp treatments, as opposed to step treatments (Figure 5-4B). Further, while we did find more resistant isolates when cultures were exposed to a lower dose of chloramphenicol (Figure 5-4B), the degree of resistance was lower (Figure 5-4C). There were also no colonies isolated on the high dose chloramphenicol plates (Figure D-4, Row 1, Column 4). Finally, the bimodal distribution of resistance among isolates that was observed for $\Delta acrB$ populations at 1 $\mu\text{g/mL}$ chloramphenicol was not observed at lower chloramphenicol concentrations (Figure 5-4C). While the lower concentrations of chloramphenicol did increase the proportions of resistant cells, the magnitude of resistance conveyed did not reach that of wild type nor $acrAB^+$ cells. Interestingly, we found that $\Delta acrB$ cells were only able to reach the same high level of chloramphenicol resistance when exposed to slower changing, but inhibitory conditions – a short-term ramp increase to 1 $\mu\text{g/mL}$ chloramphenicol.

5.3.2. *Slow introduction of stress promotes growth and resistance*

Next, we investigated how even longer variations in antibiotic treatment might impact the antibiotic resistance and fitness of a population. To do this, we exposed cells to a long-term ramp over 72 h to a final antibiotic concentration. We then compared this to conditions with similar antibiotic levels, but different long-term dynamics, including: (1) a step treatment with the same final concentration of chloramphenicol as the long-term ramp,

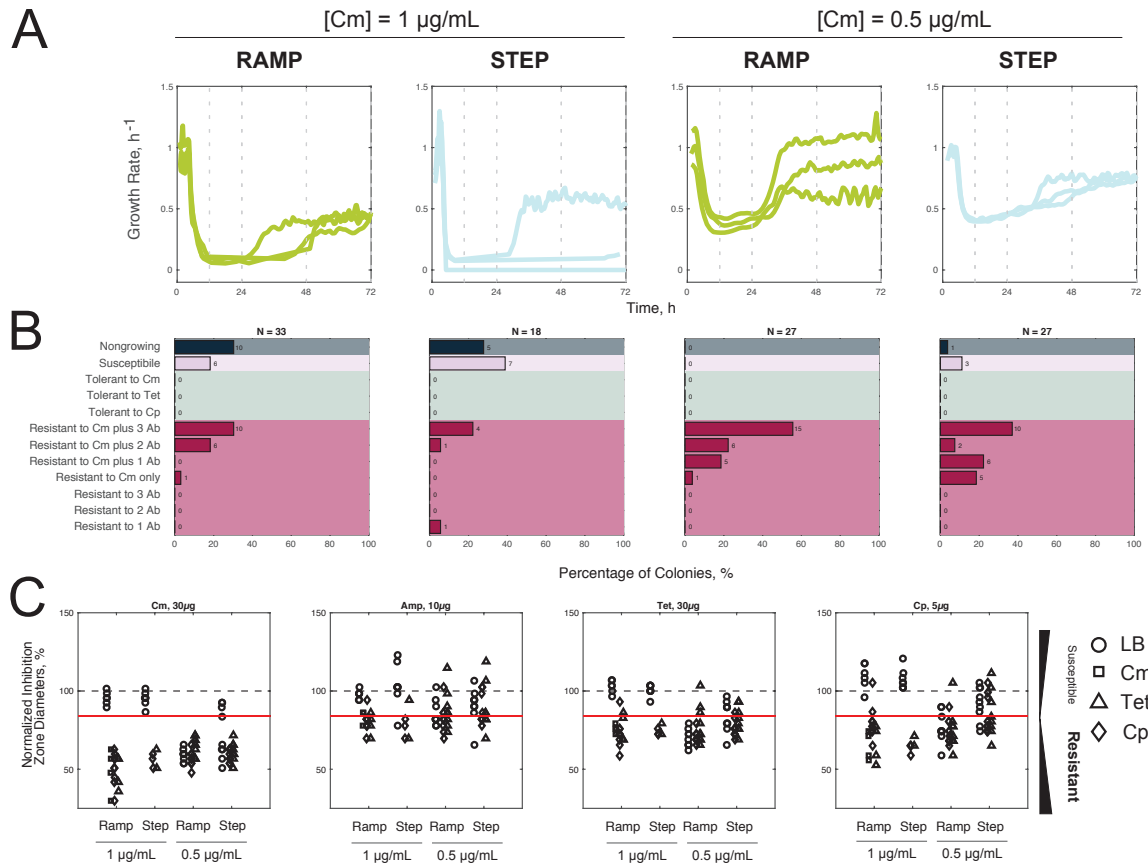


Figure 5-4. Impact of antibiotic introduction rate on the emergence of resistance and tolerance for ΔacrB cultures exposed to different concentrations of chloramphenicol.

(A) Growth rates in ΔacrB cultures where the two chloramphenicol introduction rates are a short-term ramp (green) and a step (blue) with a final concentration of 1 $\mu\text{g/mL}$ or 0.5 $\mu\text{g/mL}$ of chloramphenicol. $n = 3$ biological replicates for each treatment. (B) Fates of all isolated colonies from all plates. Results were classified as: nongrowing (navy), susceptible (light pink), tolerant (light green), and resistant (burgundy). Ab, antibiotics. N represents the number of isolates from each experiment that were picked. If no colonies were found on a high antibiotic plate then no isolate could be picked. Counts are shown at the end of each bar. (C) Normalized inhibition zone diameters for the four antibiotic disc assays. The inhibition zone diameters were normalized to the parent strain's mean inhibition zone (black). The threshold to classify as resistant is shown in red. The symbol shape indicates which plate the colony was originally isolated from: LB only (circle), LB+Cm (square), LB+Tet (triangle), LB+Cp (diamond). Each individual replicate for data presented here is shown in Figure D-8 and Figure D-9.

and (2) a step treatment with an equivalent area under the curve as the ramp experiment, which means that it was treated with the same total amount of antibiotic for the same

amount of time. We first found that wild type cells treated with this long-term ramp to 5 $\mu\text{g/mL}$ chloramphenicol had a distinct fitness advantage when compared to both step treatments (Figure 5-5A, Column 1); however, this fitness advantage did not translate increased levels of resistance (Figure 5-5B, Column 2). We also treated wild type cells with a more inhibitory, long-term ramp reaching a final concentration of 10 $\mu\text{g/mL}$ chloramphenicol. Under these more inhibitory treatments (Figure 5-5A-B), we found that populations treated with the long-term ramp had an even greater fitness benefit compared to populations from both step treatments (Figure 5-5A); yet, again, this did not translate to higher evolved levels of resistance (Figure 5-5B).

In contrast, ΔacrB had both significantly higher fitness and resistance levels when treated with a long-term ramp to 5 $\mu\text{g/mL}$ compared to treatments with a step introduction of antibiotics (Figure 5-5A-B). Interestingly, all long-ramp conditions experienced small fitness costs until they reached a very resistant phenotype at 48 h (Figure 5-5C). Yet, by 72 h, all these populations experienced resistance loss along with increased fitness (Figure 5-5C). This reversion is in stark contrast to the step conditions, whose trajectories first experience significant fitness costs, but are able to start projecting towards resistant phenotypes by 24 h (Figure 5-5C). For the long-term ramp conditions, this could indicate that the evolved resistance was either only transiently present or that the mechanisms were too costly to retain.

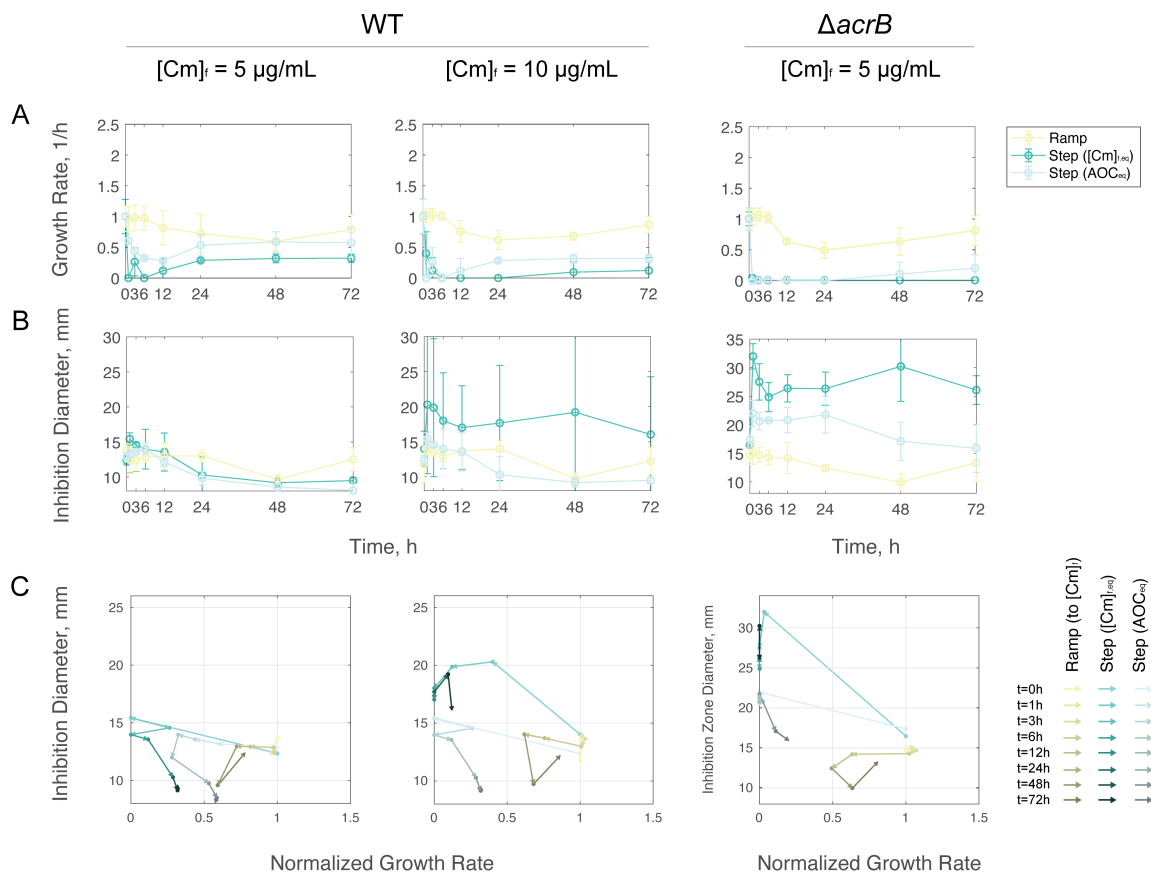


Figure 5-5. Impact of slow, long-term antibiotic introduction rate on populational fitness and resistance.

Cultures were evolved under a 72 h ramp introduction of chloramphenicol, compared to a step introduction of chloramphenicol equivalent to the final $[Cm]$ achieved by the ramp or by the AOC equivalent concentration. Impact of the different dynamics on (A) growth rates and (B) resistance, measured by inhibition zone diameters for the population. Data is shown for $n = 3$ biologically replicated evolution experiments. (C) Fitness-resistance trajectories mapped through time.

5.3.3. Co-cultures impact how populations survive environmental fluctuations

Competition assays can identify subtle differences in growth; when strains are forced to compete for survival, more fit strains become overrepresented in the population (198, 213). We next asked how a 1:1 co-culture of *acrAB*⁺ and ΔacrB cells performed given either a step or short-term ramp of antibiotic introduction (Figure 5-6). We found

that while bacteria exposed to a short-term ramp of chloramphenicol acquired resistance, the three replicates with the step introduction had many fewer resistant isolates (Figure 5-6B). In addition, co-cultures exposed to the short-term ramp were more likely to be resistant not just to chloramphenicol, but also to exhibit cross-resistance to ampicillin and ciprofloxacin (Figure 5-6B). These cells also had an increase in resistance as measured by the disc diffusion assay. In contrast, co-cultures exposed to a step had similar inhibition zone diameters to the parent strain for all tested antibiotics (Figure 5-6C). To assess

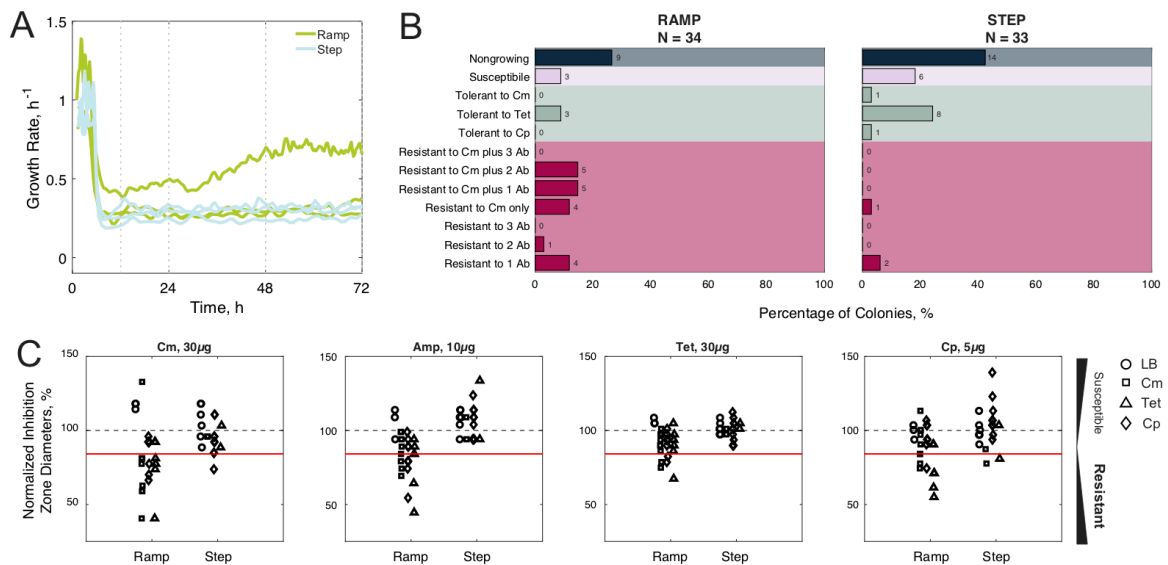


Figure 5-6. Impact of antibiotic introduction rate on a co-cultured population.

(A) The growth rates in co-cultures of 1:1 *acrAB*⁺ and Δ *acrB*. Chloramphenicol introduction rates were a short-term ramp (green) and a step (blue). *n* = 3 biological replicates for each treatment. (B) Fates of all isolated colonies from all plates. Results were classified as: nongrowing (navy), susceptible (light pink), tolerant (light green), and resistant (burgundy). Ab, antibiotics. N represents the number of isolates, counts are shown at the end of bar. (C) Normalized inhibition zone diameters for the four antibiotic disc assays. The inhibition zone diameters were normalized to the parent strain's mean inhibition zone (black, --); resistant threshold (red). The symbol shape indicates which plate the colony was originally isolated from: LB only (circle), LB+Cm (square), LB+Tet (triangle), LB+Cp (diamond). Each individual replicate for data presented here is shown in Figure D-5.

population composition over time, we measured what fraction of the population were *acrAB*⁺ versus Δ *acrB* cells at intermediate time points. We accomplished this by including a gene for green fluorescent protein (*sfgfp*) in our *acrAB*⁺ strain to allow for straightforward identification of *acrAB*⁺ cells via flow cytometry. Despite an initial ratio of 1:1, we found that the majority of cells at the end of the experiments for both the short-term ramp and the step input were *acrAB*⁺ (Figure D-5B). These results were specific to antibiotic treatment, as control experiments without chloramphenicol were not dominated by the *acrAB*⁺ strain (Figure D-5). We also assessed the parent strain of the isolates, and found that resistant isolates emerged from the *acrAB*⁺ strain over 60% of the time (Figure D-5B).

5.3.4. Correlations between fitness and resistance for evolution studies

In the eVOLVER continuous culture experiments, cells are maintained within a small window of optical densities (OD₆₀₀ 0.15 to 0.2) before being diluted; however, the growth rates of cultures within these bounds can vary significantly. Based on qualitative patterns between early spikes in growth rates and higher final growth rates (Figure 5-3A, Figure 5-6A), we asked if there was a relationship between the initial growth rate and the final growth rate. We found a correlation between the maximum initial growth rate and the maximum growth rate after treatment (Figure 5-7A, Table D-3), as well as between the number of dilution events until reaching the maximum post-treatment growth and the maximum post-treatment growth rate itself (Figure 5-7B). Thus, cultures that were growing faster before antibiotic addition continued to grow faster after treatment.

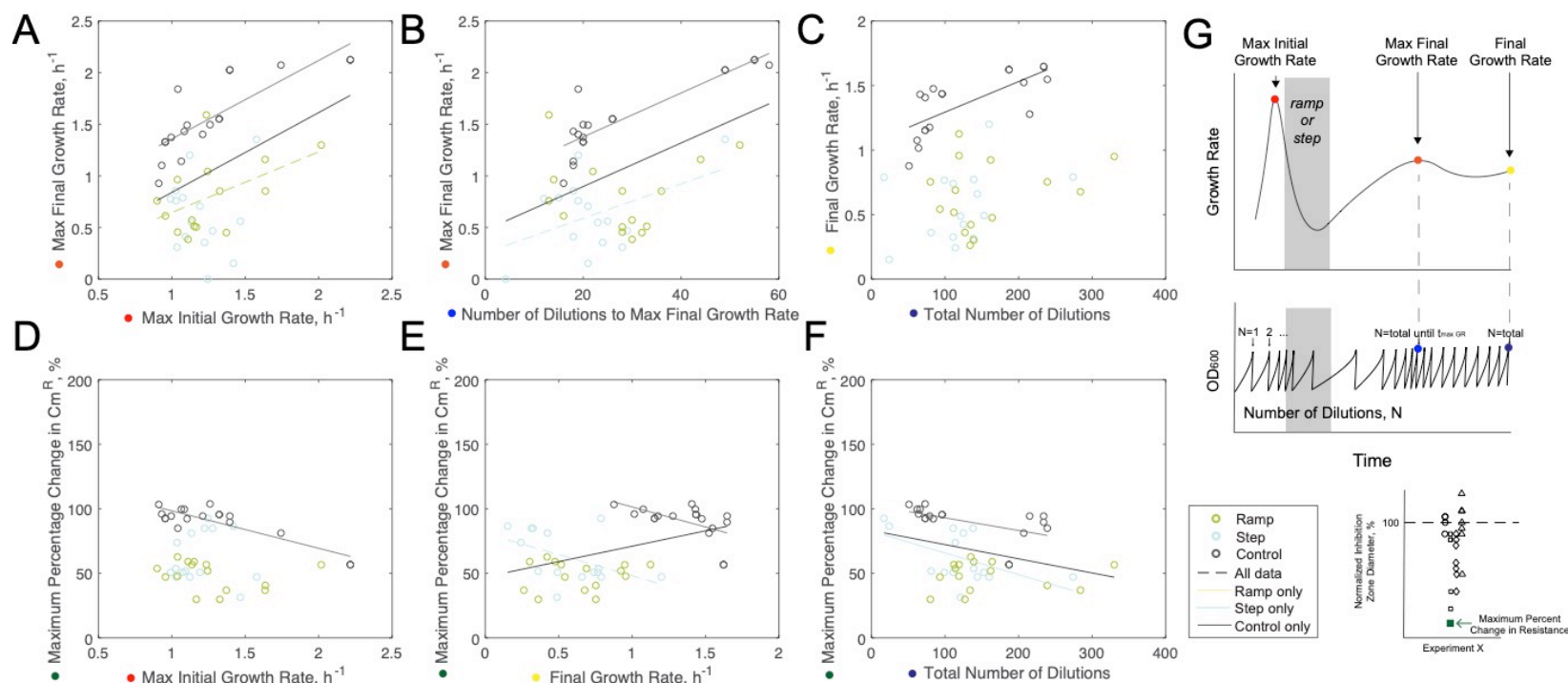


Figure 5-7. Correlations between final growth rates of cultures, initial growth rates, and number of dilution events.

(A) Maximum initial growth rate (prior to antibiotic treatment) compared to the maximum growth rate after treatment. (B) Maximum growth rate after treatment versus the number of dilutions to reach this maximum growth. (C) Final growth rate versus the final number of dilutions at the end of the experiment. (D-F) Maximum change in resistance for a culture versus the (D) maximum initial growth rate (prior to antibiotic treatment), (E) the final growth rate, and (F) the total number of dilution events. These correlations include data for all strains, with replicates: short-term ramp (yellow), step (blue), control (gray). Correlations are depicted using lines when the p value < 0.05 with colors representing which data set the correlation is from; correlations for all data are shown in black dashed lines. (G) Schematics of the parameters evaluated. There are 48 experiments represented in total: 15 experiments under short-term ramp conditions, 15 experiments under step conditions, and 18 control experiments.

In contrast, we found no statistically significant relationship between the total number of dilutions and the final growth rate for populations exposed to antibiotics (Figure 5-7D), nor between the maximum initial growth rate and the maximum percentage change in chloramphenicol resistance (Figure 5-7C). However, we did identify a slight correlation, whereby the most resistant isolates were found in populations with slower final growth rates (Figure 5-7E), which is in agreement with results in the recent literature showing correlations between susceptibility and high growth rates (321). We also asked whether the higher levels of resistance were solely correlated with the number of dilutions, as more replication events could lead to a higher number of mutations (101). We did find a correlation between resistance and the number of dilution events; however, this relationship was only significant for cells that were exposed to a step or no antibiotics (Figure 5-7F). Under these conditions, growth and resistance were inversely correlated, which may suggest that the emergence of resistance is driven by spontaneous mutations (32).

5.4. Discussion

In this work, we have highlighted how the rate of antibiotic addition—in combination with the genetic background of the strain—can bias populations towards tolerance or resistance. We found that the native regulation of efflux pump expression makes cells robust to both ramp and step introductions of stress, whereas cells overexpressing the pump but lacking upstream regulators (*acrAB*+) were more likely to be nongrowing or susceptible; this effect was also seen in cells without efflux pumps (Δ *acrB*). The regulatory network has likely adapted to achieve fast responses to the introduction of

stress. This feature may be ideal for costly machinery, such as AcrAB-TolC efflux pumps, since bacteria can regulate their responses to stress and only turn them on when necessary.

Experiments conducted with strains lacking the native regulation (*acrAB*⁺) or the efflux pumps altogether (Δ *acrB*) revealed clear differences in tolerance and resistance development that were influenced by the rate of antibiotic introduction. We found that short-term ramp introduction for *acrAB*⁺ cells led to higher levels of tolerance, resistance, and cross-resistance than the same cells exposed to a step. In addition, *acrAB*⁺ cells were also more likely to have high levels of cross-resistance under short-term ramp antibiotic introductions. Interestingly, we previously found that cells overexpressing AcrAB-TolC pumps had higher mutation rates compared to wild type cells (191). While *acrAB*⁺ cells did not appear to have an increase in resistance when compared to wild type after being treated with antibiotics, we did see a higher incidence of resistance emerging in the absence of antibiotics. Based on results from **Chapter 4** and Reference (191), we speculate that the heightened mutational rate in our *acrAB*⁺ strain increases noise in evolutionary trajectories. This is beneficial because evolved isolates are more likely to probe a wider range of mutations (**Chapter 4**). However, this could also be costly due to the accumulation of deleterious mutations in the population. In this case, the *acrAB*⁺ genotype would provide a double-edge sword when populations are attempting to optimize fitness and resistance.

Meanwhile, Δ *acrB* cells did acquire resistance, but never exhibited tolerance. While Δ *acrB* cells exposed to a ramp were more likely to acquire resistance than those exposed to a step, they were less likely to achieve as high a magnitude of resistance at more

inhibitory concentrations at 72 h. Interestingly, from whole genome sequencing in **Chapter 4**, we identified that evolved $\Delta acrB$ cells repetitively converge to a resistant genotype. This resistant genotype always had an insertion sequence in *acrS*, which is the local regulator responsible for repressing AcrEF-TolC (180). This could also explain why certain $\Delta acrB$ populations grown with a step and at inhibitory populations exhibited a bimodal resistance distribution, where isolates were either resistant (with the insertion sequence in *acrS*) or not (without the insertion sequence in *acrS*). On the other hand, less inhibitory concentrations lead to a higher frequency of resistant cells in the population, but these cells were less able to withstand high antibiotic selection pressures. As a result, the $\Delta acrB$ populations either contained only a few very resistant isolates or a greater number of less resistant isolates. This along with results from **Chapter 4** suggest that emergence of high levels of resistance evolved from wild type and *acrAB*⁺ is indeed facilitated by the AcrAB-TolC pumps themselves.

This study also highlights the importance of studying how different antibiotic treatments affect co-cultured populations. For our co-cultured *acrAB*⁺ and $\Delta acrB$ experiments, we found the most distinct differences between the two introduction rates did not necessarily reflect what we observed in the single-species population results. Clinical infections and bacterial communities are rarely, if ever, comprised of a single strain (322). Therefore, it will be interesting to assess more realistic treatments in the context of microbial communities. Overall, we found that the rate at which a bacterial population experiences stress can impact the acquisition of resistance and cross-resistance. In addition, short-term ramp perturbations in antibiotic introduction can increase both tolerance and

resistance and these effects are pronounced in *acrAB*⁺ cells.

5.5. Contributions Statement

The authors of this work were Ariel M. Langevin (A.M.L.), Imane El Meouche (I.E.M.), and Mary J. Dunlop (M.J.D.). A.M.L. and I.E.M. collected data. A.M.L. wrote custom scripts for experiments and data analysis, and performed statistical testing. A.M.L. and M.J.D. wrote the manuscript. All authors contributed to this unpublished manuscript.

5.6. Methods

5.6.1. Strains and Plasmids

We used *E. coli* strains BW25113 and BW25113 Δ *acrB*. The wild type strain BW25113 is the parent strain for the Keio collection (235). BW25113 Δ *acrB* was derived from Keio collection strain JW0451 (BW25113 Δ *acrB*::*kan*^R) (189), where we removed the kanamycin resistance marker following the pCP20 protocol from (236).

We used the plasmids pBbA5k-rfp (Δ *acrB* and wild type) and pBbA5k-*acrAB*-*sfgfp* (*acrAB*⁺) in experiments. The plasmid pBbA5k-rfp controls expression of red fluorescent protein, and is included so that all strains contain the same plasmid for consistency. The pBbA5k vector contains a medium-copy number (p15A) origin of replication, a *P*_{*lacUV5*} promoter, and a kanamycin resistance marker (238). Plasmid pBbA5k-*acrAB*-*sfgfp* is a transcriptional fusion of *acrAB* and *sfgfp* (189). Plasmids were transformed into *E. coli* BW25113 and BW25113 Δ *acrB* and then isolated on Luria Broth (LB) plates with 30 μ g/mL kanamycin for plasmid maintenance.

For the long-term ramp experiments, we used BW25113 and BW25113 $\Delta acrB$ without plasmids.

5.6.2. Bacterial Growth Conditions

For experiments from Sections 5.3.1, 5.3.3, and 5.3.4., overnight cultures were inoculated from a single colony in 10 mL LB with 30 $\mu\text{g/mL}$ kanamycin and grown in a 50 mL Erlenmeyer flask at 37°C with 200 rpm orbital shaking. After overnight growth, the optical density at 600 nm (OD_{600}) was measured, and the initial volume for each culture was set so that the initial OD_{600} for the culture in the eVOLVER turbidostat was 0.1. If the experiment was composed of a co-culture, the volumes of each of the strains were determined based on an initial OD_{600} contribution of 0.05 each; the calculated volumes for each strain were added to total an initial OD_{600} of 0.1.

5.6.3. Experimental Conditions within the eVOLVER

In the eVOLVER turbidostat, cells were grown at 37°C in LB supplemented with 30 $\mu\text{g/mL}$ kanamycin. A stir bar mixed the cultures on a medium setting, or approximately 1000 rpm (291). Cells were grown in the eVOLVER for 2-3 hours prior to the beginning of the experiment to allow for bacteria to enter exponential growth. We set the eVOLVER using an upper OD_{600} bound of 0.2 and a lower bound of 0.15 so that cultures were grown to 0.2 and then diluted back to 0.15 to maintain the turbidostat at approximately constant cell density. Samples were collected after 72 hours and used to assess tolerance and resistance within the cultures. Growth rates were calculated from OD_{600} curves, where the OD_{600} data were smoothed using a moving average across 10 data points.

Cells were subjected to a ramp, step, or no introduction of chloramphenicol, where each experiment was conducted with three biological replicates. In the ramp, the concentration of chloramphenicol increased over 6 hours. The ramp was implemented by having two media influxes, one containing 0 $\mu\text{g/mL}$ of chloramphenicol and the other 1 $\mu\text{g/mL}$. The proportion of the chloramphenicol-containing media increased across the 6-hour window until 100% of the media came from this source. The step was implemented by switching the media source from one containing 0 $\mu\text{g/mL}$ chloramphenicol to 1 $\mu\text{g/mL}$. The samples themselves were also spiked with 1 $\mu\text{g/mL}$ chloramphenicol at the same time to avoid a delay due to the time required for media cycling in the turbidostat. For the ΔacrB strain, we also ran the ramp and step experiment at a lower chloramphenicol concentration to reflect the strain's lower IC_{50} , in these cases the final concentration of chloramphenicol was 0.5 $\mu\text{g/mL}$ instead of 1 $\mu\text{g/mL}$.

For the long-term ramp experiments, the final concentrations were 5 $\mu\text{g/mL}$ or 10 $\mu\text{g/mL}$ over 72 h. These eVOLVER experiments were inoculated with a single colony for ~ 15 h before the experimental conditions changed. Samples were collected during the experiment at $t = 0, 1, 3, 6, 12, 24, 48, 72$ h and used to assess resistance of the population. Growth rates were calculated from OD_{600} curves, following Methods from **Chapter 4**.

In control experiments, we grew cells in the eVOLVER without any antibiotic treatment. As this experiment selects for fast growers, we were only able to run control experiments past 48 hours with great difficulty (i.e. dilution events were so frequent that 1 L media input bottles needed to be changed every 3 hours). We ran one experiment to completion at 72 hours and then conducted additional experiments using 24 hours as the

final time point. We confirmed that results for resistance and tolerance were similar between control samples run for 24 hours and the control that was run for 72 hours (Figure D-1, Columns 1-4). We also found that replacing the vials every 24 hours helped mitigate this seeming increase in growth rate; again at 72 hours, there were no resistant isolates observed (Figure D-1, Column 5). In a separate experiment, we also added the detergent Tween20 (Sigma Aldrich Cat. # P1379) at 0.1% (v/v) in an effort to reduce spurious OD₆₀₀ measurements caused by biofilm growth on the flask (Figure D-1, Column 6). We found that this eliminated the increasing growth rate over the 72-hour period, and still reflected the absence of resistance seen in triplicate 24 hour control experiments.

5.6.4. Measuring Co-culture Distributions

For co-cultures, samples were collected and diluted 1:10 in phosphate-buffered saline 1X (PBS) and measured with a Guava easyCyte HT sampling flow cytometer. There were 5000 counts from each read, using a threshold of 15 in the side scatter channel (SSC). The results were then sorted using a custom script to eliminate other small particles by thresholding the forward scatter channel (FSC) at 15 and setting thresholds for the red and green channels based on controls for our fluorescent proteins, RFP and sfGFP.

We additionally classified the parent strain of each isolate. Each isolate was streaked on an LB + kanamycin plate and incubated overnight at 37°C. After 24 hours, we measured whether the fluorescence of the isolate was red or green using a blue light transilluminator (IO Rodeo). For a small fraction of colonies, we were not able to determine the parent strain based on fluorescence; these samples were marked as undetermined.

5.6.5. Isolating *eVOLVER* Mutants

Using samples isolated from the end-point of the *eVOLVER* experiment, we diluted samples in PBS and plated them on LB agar. In cases where high antibiotic selection plates were used, we spun cultures down to concentrate them in advance of plating. The plates included a control for viable cells on a LB + kanamycin plate, as well as LB plates containing high doses of antibiotics: 25 µg/mL chloramphenicol, 6 µg/mL tetracycline, or 0.1 µg/mL ciprofloxacin. For plating, samples were diluted by a 10^{-5} and 10^{-6} dilution factor for LB + kanamycin; all other samples were plated at 10^0 , 10^{-2} , 10^{-4} , and 10^{-6} dilution factors. In addition, to concentrate cells we also spun down 1 mL of the culture at 5000 rpm for 7 min, resuspended the pelleted cells in 100 µL of PBS, and plated all cells. The control plates were incubated at 37°C for 24 hours and the high dose antibiotic plates were incubated at 37°C for 48 hours, allowing time for unfit mutants to grow into visible colonies. To enable accurate colony counts, we aimed for between 10-1000 colonies per plate. If not enough colonies appeared on the plate (<10), we plated again with a more concentrated sample; if too many colonies appeared on the plate (>1,000), the samples were diluted and replated (Supplementary Data).

Three colonies were isolated from each plate. These colonies were regrown in 1mL LB in a 24 well plate with kanamycin at 37°C and shaking at 200 rpm overnight.

5.6.6. Measuring Antibiotic Susceptibility

Colonies from the end-point of the *eVOLVER* experiment, in addition to colonies of the parent strains that were not subjected to growth in the *eVOLVER*, were inoculated in LB cultures with 30 µg/mL kanamycin at 37°C and 200 rpm shaking overnight. We used

10 μ L of the cultures at a 1/100 dilution in fresh LB with kanamycin. After 4 hours at 37°C and 200 rpm, we removed the culture and used cotton swabs to cover the LB and kanamycin agar with a layer of the culture (309).

Antibiotic-containing discs – chloramphenicol (30g), ampicillin (10g), tetracycline (30g), and ciprofloxacin (5g) (Thermo Fisher Scientific Cat. # CT0013B, CT0003B, CT0054B, and CT0425B, respectively) were then placed on the plate. The plate was incubated for 24 hours at 37°C. The diameter of the zone of inhibition around each disc was then measured. Based on literature and measurements of variability in replicates' inhibition zones, we concluded that cells which were within 16% of the diameter of the parent's inhibition zone were not resistant (323); 16% is two standard deviations (2σ) from the mean for all antibiotics and all strains, and should account for 95% of the variability in replicate inhibition zones, reducing false positive rates for cells that are resistant (Figure D-2A & Table D-1). The classification of each isolate depends on which plate it came from and the difference in the diameter of inhibition between the parent strain and the isolate, as well as how well the cells regrew after the eVOLVER experiments.

We also measured the dose response of the strains to different concentrations of chloramphenicol (Figure D-2B). We inoculated overnight cultures of 5 mL LB with kanamycin for each biological replicate, growing at 37°C and 200 rpm shaking. We then diluted cultures back to approximately 0.15 OD₆₀₀ in 800 μ L LB with kanamycin in a 24-well plate and added a range of chloramphenicol concentrations: 0, 0.1, 0.2, 0.5, 1.0, 2.0, 5.0, and 10 μ g/mL. We then covered the plates with an evaporation-limiting membrane (Thermo Scientific AB-0580). Plates were incubated at 37°C and 200 rpm shaking and

optical density was measured using a plate reader (BioTek Synergy H1m) at $t = 6$ h to measure toxicity during exponential growth phase.

For the long-term ramp experiments, samples were directly swabbed onto plates for a snapshot of population level resistance. These samples were only exposed to a chloramphenicol disc.

6. CONCLUSION

A deeper understanding of how complex dynamics promote or limit resistance and its evolution remains imperative. Not only will studies addressing such interactions improve our ability to select optimal antibiotic treatments in clinics, but they will also improve our ability to more accurately model both the short-term and long-term outcomes of antibiotic treatment. In this thesis, we investigated the effect of two previously understudied parameters — antibiotic introduction rates and mixed populations — on antibiotic resistance. In order to understand how antibiotic resistance and its evolution may be unknowingly promoted, we used the AcrAB-TolC efflux pump as a case study. Such efflux pumps are ubiquitous for providing multidrug resistance and are thought to not only impact antibiotic resistance, but its evolution as well.

First, we explored the effect of short-term dynamics on antibiotic resistance, more specifically how varying stress introduction rates over 6 hours impacted antibiotic resistance. In **Chapter 2**, we identified that slower stress introduction rates promoted the presence and fitness of resistant cells in the population. While this could be useful for applications in industrial biosynthesis, such patterns imply that certain antibiotic treatments (e.g. oral doses) could promote antibiotic resistance, even under antibiotic concentrations that are considered inhibitory for microbial growth. The results from this work suggest that temporal dynamics of antibiotic concentration are important factors in the emergence of antibiotic resistance.

In **Chapter 3**, we explored how mixed populations responded to antibiotic treatment. In contrast to previous studies, which demonstrated that certain

microenvironments provide a protective benefit for their neighbors (324, 325), we found that cells with AcrAB-TolC pumps harmed their neighboring cells under stressful conditions. In this case, cells with the AcrAB-TolC pumps created microenvironments with increased concentrations of extracellular antibiotics. When the microcolonies were homogenous, cells containing AcrAB-TolC pumps did not have a harmful impact on their neighbors; however, when the microcolonies were heterogenous, cells with AcrAB-TolC pumps had a deleterious effect on their neighbors who lack efflux pumps. Such results elucidated that certain pressures that more readily promote resistant phenotypes in mixed populations undergoing antibiotic treatment. Interestingly, when co-cultures were exposed to a short, 4-hour pulse of antibiotic treatment, we found that susceptible cells were actually able to recover more quickly at sub-inhibitory concentrations and non-costly resistant phenotypes were not overrepresented in the population even at very high pulse concentrations (Figure A-5). Taken together, we found that there are complex relationships in mixed populations that play a role in short-term survival to an antibiotic treatment.

Next, we explored how different factors may impact long-term outcomes antibiotic treatment, more specifically how a multi-day antibiotic treatment leads to evolution of antibiotic resistance. In **Chapter 4**, we conducted a systematic study of how antibiotic concentrations and ancestral genotypes impact the temporal evolution of antibiotic resistance. We identified that near-MIC concentrations most readily promoted the evolution of antibiotic resistance for all genotypes. Further, we found that these different genotypes were all able to achieve similar final levels of resistance. Through whole genome sequencing, we identified how each ancestral genotype evolved resistance through a suite

of unique genetic mutations. Wild type cells readily upregulated gene expression of AcrAB-TolC through insertion sequences in its local and global regulators, AcrR and MarR. Cells constitutively overexpressing AcrAB-TolC efflux pumps evolved resistance through mutations in the channels of AcrB and in the promoter region of the *acrAB* operon to tune AcrAB-TolC gene expression; these cells also acquired mutations in other genes that affect transcription, translation, localization, and degradation. These “off”-target effects could in part be due to the low expression of *mutS* with *acrAB* overexpression (191). Finally, cells without functional AcrAB-TolC efflux pumps upregulated expression of another multidrug efflux pump, AcrEF-TolC. Thus, **Chapter 4** provides a deeper understanding into how and why bacteria can robustly and rapidly gain high levels of antibiotic resistance in response to long-term antibiotic treatments.

Lastly, we explored how complex dynamics, including antibiotic introduction rates and mixed populations, influence the evolution of antibiotic resistance. In **Chapter 5**, we again identified that all genotypes were capable of robustly evolving antibiotic resistance in inhibitory conditions. The slower, short-term ramp of antibiotic introduction was most likely to promote the evolution of antibiotic resistance for all genotypes. The step antibiotic introduction rate did not prevent the evolution of antibiotic resistance entirely, but – depending on the initial population – did help to reduce the magnitude of resistance that evolved. We found variations in cross-resistance for the different starting strains, which agreed with the evolved genotypes that were reported in **Chapter 4**. We also observed that mixed populations undergoing short-term fluctuations were actually more stable and were less likely to evolve antibiotic resistance.

Additionally, in **Chapter 5**, when susceptible genotypes were exposed to more slowly changing environmental dynamics over 72 hours, we found that these populations had improved fitness and increased resistance in otherwise restrictive environments. This conclusion supports earlier work investigated in **Chapter 2**, that slowly changing stressful conditions may unnecessarily exacerbate antibiotic resistance and its evolution. We also found that mixed populations can demonstrate both selfishness, but also stability under different environmental conditions. In short, this work helps elucidate some otherwise under-explored factors of antibiotic resistance and contribute to the understanding of antibiotic resistance to enable predictive modeling in the future.

6.1. Future Directions and Outlook

In this work, we used the AcrAB-TolC efflux pumps as a case study to probe how complex environmental dynamics – such as antibiotic introduction rate and population diversity – may promote rising levels of antibiotic resistance and its evolution. Future studies may continue to explore these systems more thoroughly. For example, to confirm whether the intracellular concentration of a substrate is indeed higher due to efflux-pump containing neighbors, one could use a dye to measure the intracellular substrate concentration (Table 1-2). More complex temporal dynamics could be explored as well in order to determine how realistic antibiotic dosing treatments could affect resistance. For example, a study using antibiotic dose curves along with urine-like media in the eVOLVER could help provide insight to the best treatment methods for a urinary tract infection. Additionally, there are many antibiotic resistance mechanisms beyond efflux pumps that are threatening public health (5, 13, 14). Thus, future studies should investigate how other

antibiotic resistance mechanisms, including efflux pumps (e.g. TetA), antibiotic-inactivating enzymes (e.g. β -lactamase), or reduced permeability (e.g. OmpF), promote the evolution of antibiotic resistance as well.

Further, particular interest should be given to studying how more novel therapeutics — such as antimicrobial peptides (326), novel antibiotics (327), and combinatorial treatments with efflux pump inhibitors (328, 329) — impact the evolution of antibiotic resistance. Continued works should also probe the limitations of evolutionary experiments (97); for example, why the appearance of mutations found in this study have not been identified in clinical isolates. Finally, merging these lessons to parameterize models, such as a stochastic process (111) or population genetics framework (330), could help predict whether a treatment is destined to fail. Together, such studies will be crucial in helping to inform both how and why novel treatments might lose their efficacy before they fail in the real world.

Here, we found series of mutations which increased a strain's resistance. While we did not further investigate these mutations, it would be interesting to determine the resistance conference from each mutation, as well as to assess how the mutations could directly alter DNA binding, protein binding, and protein structures. More broadly, the increasing accessibility of DNA sequencing will enable a deeper understanding of the vast microbial diversity evolving and eliciting persistent antibiotic resistant infections (331). Similarly, the use of transcriptomics and metabolomics to evaluate transient changes, such as those enabling isolates to survive multi-day antibiotic treatments without resistance, will also expand our understanding of the unexpected loss of antibiotic efficacy (**Chapter 5 &**

Appendix E) (332, 333). Though our goal of outsmarting antibiotic resistant microbes appears more distant than predicted a decade ago; the sheer effort and perseverance of clinicians and scientists brings us closer still to a holistic understanding of antibiotic resistance and greater understanding of what we can practically do to fight back.

Appendix A: Supplementary Information for Chapter 2

	Initial OD ₇₀₀	Dataset	Strain	Mean Error (OD ₇₀₀)	Sum of Squares (OD ₇₀₀) ²	Mean Pearson Coef.	
Chloramphenicol	0.2	Full dose $t=0h$ (Figure 2-1D)	<i>sfgfp</i>	0.159±0.042	0.114	0.915±0.051	*
			<i>acrAB-sfgfp</i>	0.251±0.067	0.416	0.596±0.634	*
		Step $t=3h$ (Figure 2-3D)	<i>sfgfp</i>	0.261±0.070	0.579	0.830±0.036	
			<i>acrAB-sfgfp</i>	0.318±0.045	0.825	0.661±0.099	
		Fast ramp (Figure 2-3E)	<i>sfgfp</i>	0.113±0.029	0.108	0.905±0.097	
			<i>acrAB-sfgfp</i>	0.186±0.115	0.369	0.859±0.102	
		Slow ramp (Figure 2-3F)	<i>sfgfp</i>	0.077±0.031	0.054	0.772±0.284	
			<i>acrAB-sfgfp</i>	0.141±0.068	0.191	0.885±0.187	
		Benefit Ratio Landscape (Figure 2-4B-D)		0.551±0.227	1.013	0.789±0.293	
	0.01	Benefit Ratio Landscape (Figure 2-5A-B)		1.097±0.325	2.513	0.937±0.078	
Pinene	0.2	Step $t=3h$ (Figure A-4D)	<i>sfgfp</i>	0.321±0.074	0.646	0.461±0.131	
			<i>acrAB-sfgfp</i>	0.219±0.119	0.359	0.919±0.046	
		Fast ramp (Figure A-4E)	<i>sfgfp</i>	0.310±0.147	0.685	0.583±0.212	
			<i>acrAB-sfgfp</i>	0.331±0.212	0.881	0.787±0.117	
		Slow ramp (Figure A-4F)	<i>sfgfp</i>	0.310±0.147	0.685	0.583±0.212	
			<i>acrAB-sfgfp</i>	0.331±0.204	0.866	0.964±0.044	
		Benefit Ratio Landscape (Figure 2-6D-F)		1.226±1.058	6.746	0.617±0.144	

Table A-1. Goodness-of-fit between model and experimental data.

We define error as the absolute value of the difference between the model data and the mean of the experimental values. The error and sum of squares of the growth curve data has units of OD₇₀₀ and OD₇₀₀², respectively; the error and sum of squares are dimensionless for the benefit ratios. For this section, the statistics were taken across all experimental conditions (i.e. all concentrations of stressors): Eight different conditions for chloramphenicol and six conditions for pinene. For chloramphenicol at the lower initial inoculum level, the statistics for the benefit ratio compare four conditions.

Construct	Template	Direction	Primer (5' to 3')
pBbA5k-sfgfp	pBbA5k-rfp (334)	Forward	CACGCATGGTATGGATGAACTGTACAAA GGATCCAAACTCGAGTAAGG
		Reverse	CAGCTCTTCGCCTTTACGCATATGTATA TCTCCTTCTTAAAAGATCTTTTG
	pBbSFk-sfgfp (335)	Forward	CAAAAGATCTTTTAAGAAGGAGATATAC ATATGCGTAAAGGCCGAAGAGCTG
		Reverse	CCTTACTCGAGTTTGGATCCTTTGTACA GTTTCATCCATACCATGCGTG
pBbA5k-acrAB-sfgfp	pBbA5k-acrAB (336)	Forward	TGGTATGGATGAACTGTACAAATAATAG TGAGGATCCAAACTCGAGTA
		Reverse	CGGTACCTTTCTCCTCTTTAAAGTTAAAT GATGATCGACAGTATGGC
	pBbSFk-sfgfp (335)	Forward	GCCATACTGTCGATCATCATTTAACTTT AAAGAGGAGAAAGGTACCG
		Reverse	TACTCGAGTTTGGATCCT CACTATTATTTGTACAGTTCA TCCATACCA

Table A-2. Primers used for the construct of plasmids.

Bold indicates oligonucleotides for polymerase chain reaction amplification of inserts; normal text indicates overhangs for Gibson assembly.

Parameter	Symbol	Units	Value	Strain
Normalization term	α	1/OD ₇₀₀	10	All
Half-saturation Constant	K_s	mg/mL	2.367 ± 0.815	Single species
			4.050 ± 0.354	Multispecies
Substrate Growth Yield	γ	mL/mg	0.0587 ± 0.0038	Single species
			0.0370 ± 0.0085	Multispecies
Maximum Growth Rate	μ_{max}	OD ₇₀₀ /h	0.188	<i>rfp</i>
			0.188	<i>sfgfp</i>
			0.158	<i>acrAB-sfgfp</i>
Repression Coefficient	R_{Cm}	Dimensionless	1.567	WT
	R_{pinene}		0.0422	$\Delta acrB$
			0.0100	WT
			0.0028	$\Delta acrB$
Hill coefficient	n_{Cm}	Dimensionless	1.90	WT
	n_{pinene}		2.35	$\Delta acrB$
			6.97	WT
			3.27	$\Delta acrB$

Table A-3. Model parameters.

Parameters for the model derived from growth curve data and toxicity curves.

Data type	Strain(s)	Error (OD ₇₀₀)	Sum of Squares (OD ₇₀₀) ²	Pearson Coef.
Single species Growth Curves	<i>rfp</i>	0.248	0.061	0.991
	<i>sfgfp</i>	0.222	0.049	0.991
	<i>acrAB-sfgfp</i>	0.071	0.005	0.999
Multispecies Growth Curves	<i>rfp</i> & <i>sfgfp</i>	0.235	0.055	0.997
	<i>rfp</i> & <i>acrAB-sfgfp</i>	0.150	0.023	0.997
Toxicity Curves Chloramphenicol	WT	0.057	0.0032	0.999
	Δ <i>acrB</i>	0.057	0.0033	0.999
Toxicity Curves Pinene	WT	0.377	0.142	0.961
	Δ <i>acrB</i>	0.513	0.263	0.942

Table A-4. Statistics for model parameter selection data.

Error is defined here as the absolute value of the difference between model data and the mean of the experimental values. The data associated with these statistics can be found in Figure A-1.

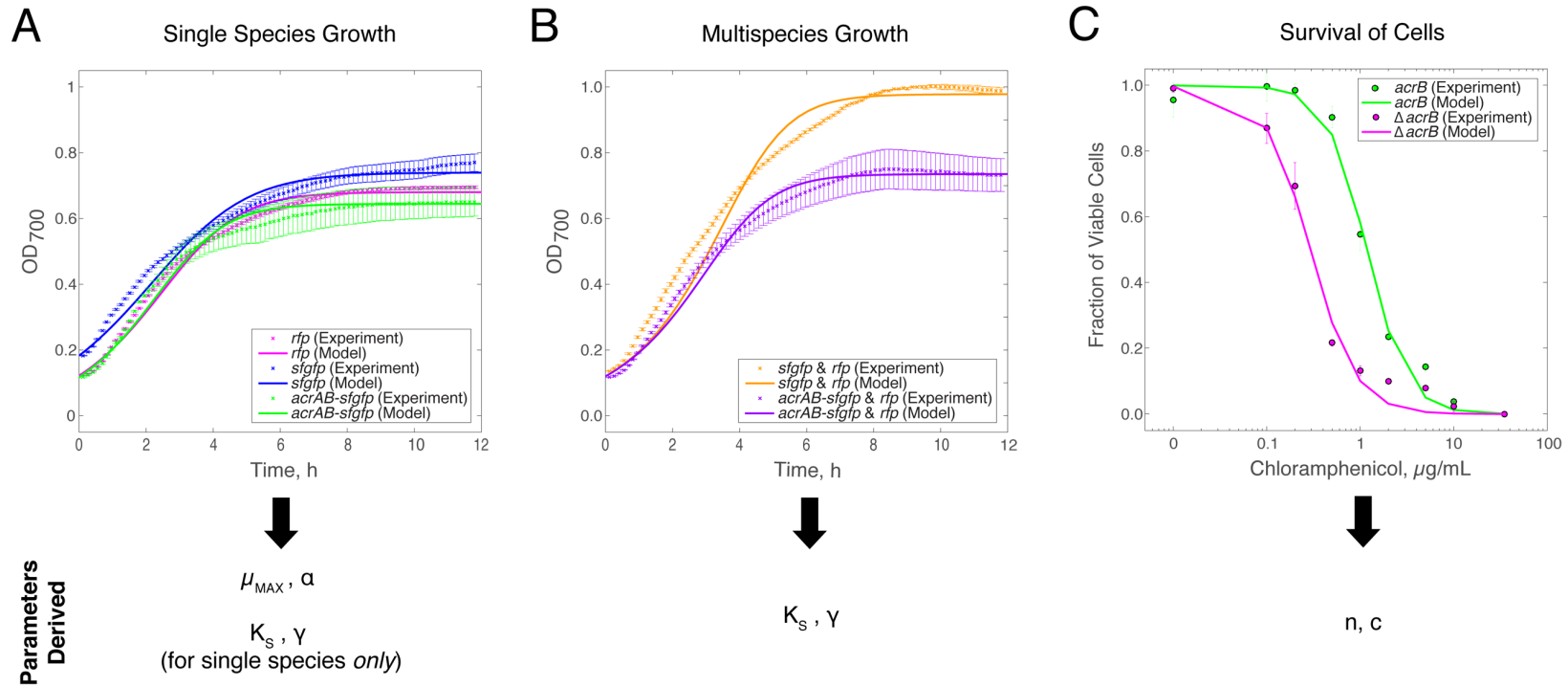


Figure A-1. Data fitting to extract model parameters.

(A) Single species growth curves determine parameters for specific strains. Growth of *rfp*, *sfgfp*, and *acrAB-sfgfp* over time are quantified by OD₇₀₀. Error bars show standard error of $n = 6$ biological replicates, except for *acrAB-sfgfp* single species growth data where $n = 2$. Single species model is fit to growth data for each strain using least-squares regression to determine parameters for the model. (B) Co-culture growth curves determine parameters for multispecies model. Growth of *rfp* co-cultured with *sfgfp* and *rfp* co-cultured with *acrAB-sfgfp* over time are quantified by OD₇₀₀. Error bars shows standard error of $n = 3$ biological replicates. Multispecies model is fit to growth curve data for co-cultured strains using least-squares regression to determine model parameters. (C) Parameters for toxicity terms are determined by killing curves. The data for toxicity of chloramphenicol (shown) and pinene (not shown) is fit with Hill functions to minimize least-squares error. Error bars show standard deviation of $n = 3$ biological replicates.

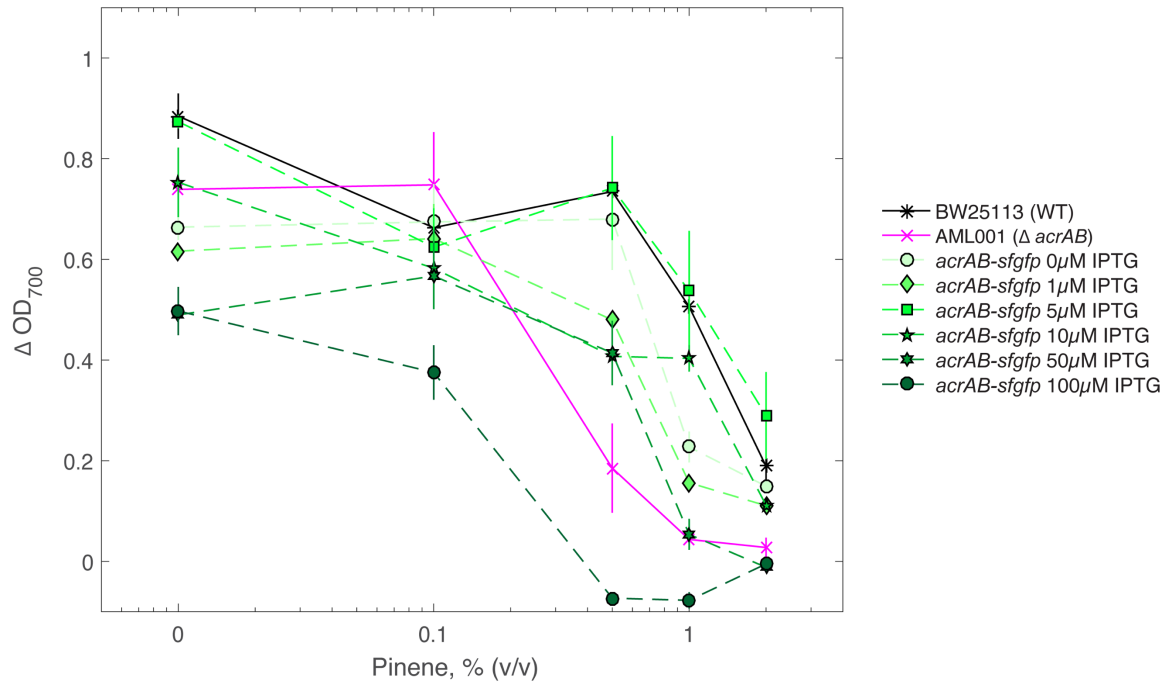


Figure A-2. Benefit and cost trade-offs of AcrAB-TolC efflux pumps in pinene.

Cell density as a function of pinene concentration. Induction of *acrAB-sfgfp* increases cell growth up to IPTG concentrations of 5 μ M, but higher concentrations reduce cell growth. Error bars in show standard error of $n = 3$ biological replicates.

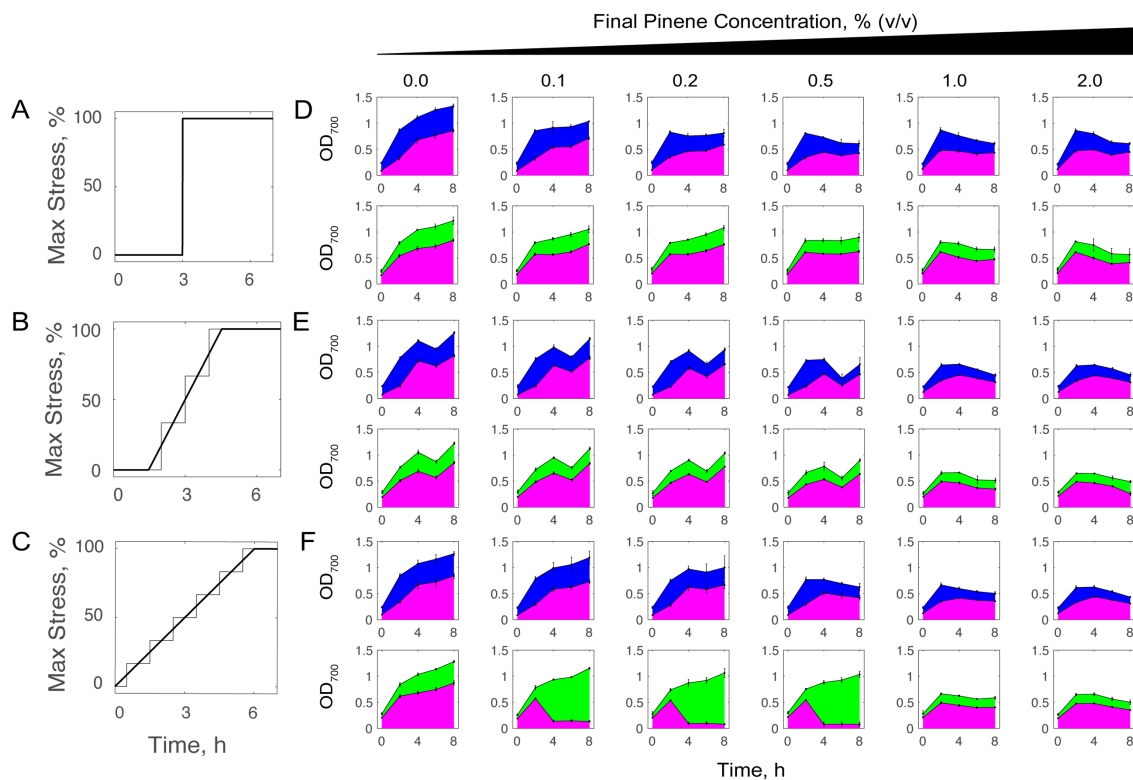


Figure A-3. Competitive growth in pinene.

(A-C) Three different rates of pinene introduction: (A) step introduction, (B) steep ramp, and (C) gradual ramp. The solid line shows the values used in the mathematical model; dashed line shows experimental treatment used to approximate the constant introduction rate. The total amounts of pinene added in (A-C) are equal. (D-F) Growth of two competing strains under different pinene treatments. As a control, top row shows competition between two strains lacking efflux pumps, *sfgfp* and *rfp*. The bottom row shows competition between a strain with the efflux pump, *acrAB-sfgfp*, and one without the efflux pump, *rfp*. Error bars show standard deviations for n = 3 biological replicates.

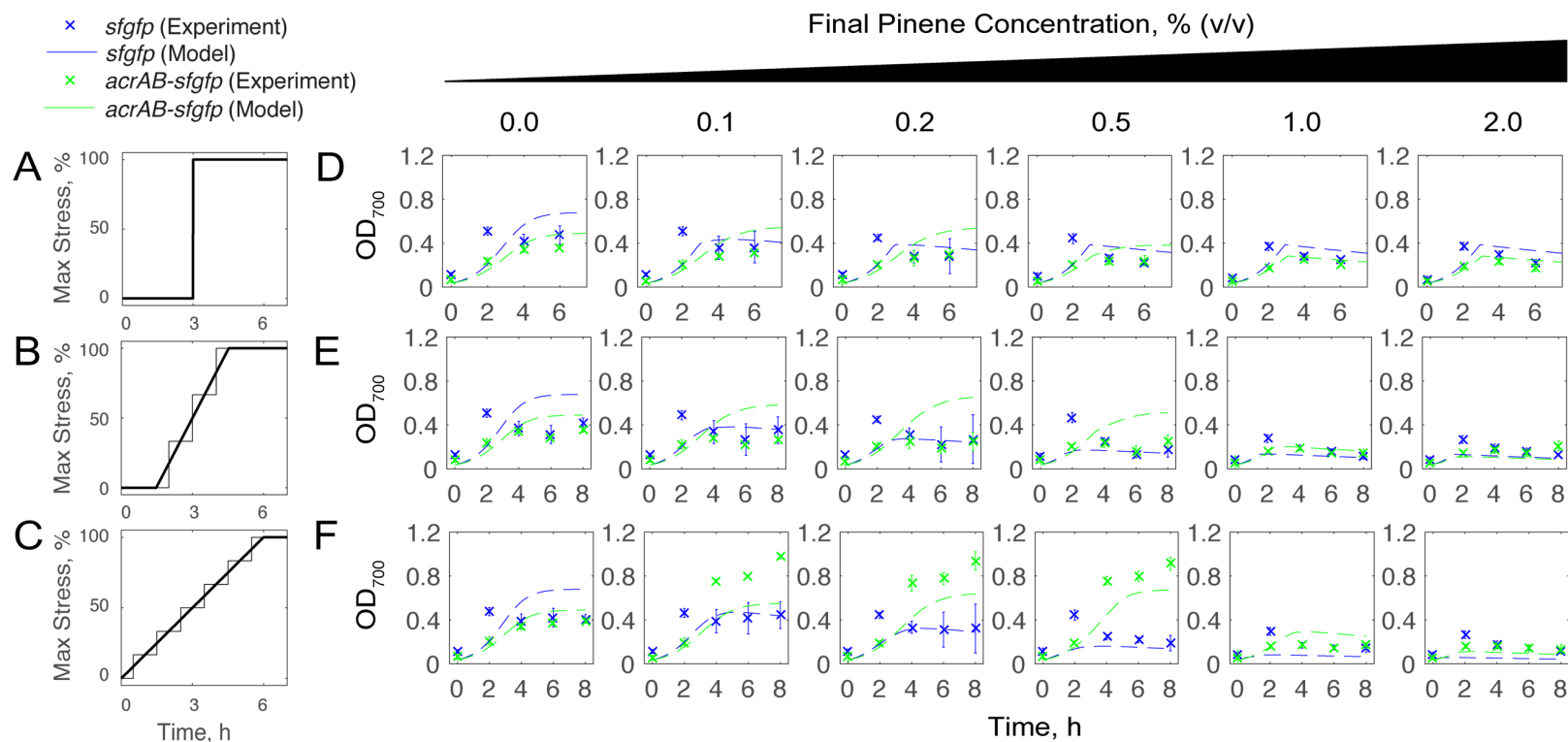


Figure A-4. Rate of pinene addition affects survival.

(A-C) Three different rates of pinene introduction: (A) step introduction, (B) steep ramp, and (C) gradual ramp. The thick solid line shows the values used in the mathematical model; thin solid line shows experimental treatment used to approximate the constant introduction rate. The cumulative antibiotic levels of pinene in (A-C) are equal. (D-F) The growth of *acrAB-sfgfp* (green) compared against growth of the control, *sfgfp*, in the competition experiments (dots) and simulations (solid lines) for different pinene introduction rates as shown in (A-C), respectively. Data points show mean and standard deviations of $n = 3$ biological replicates.

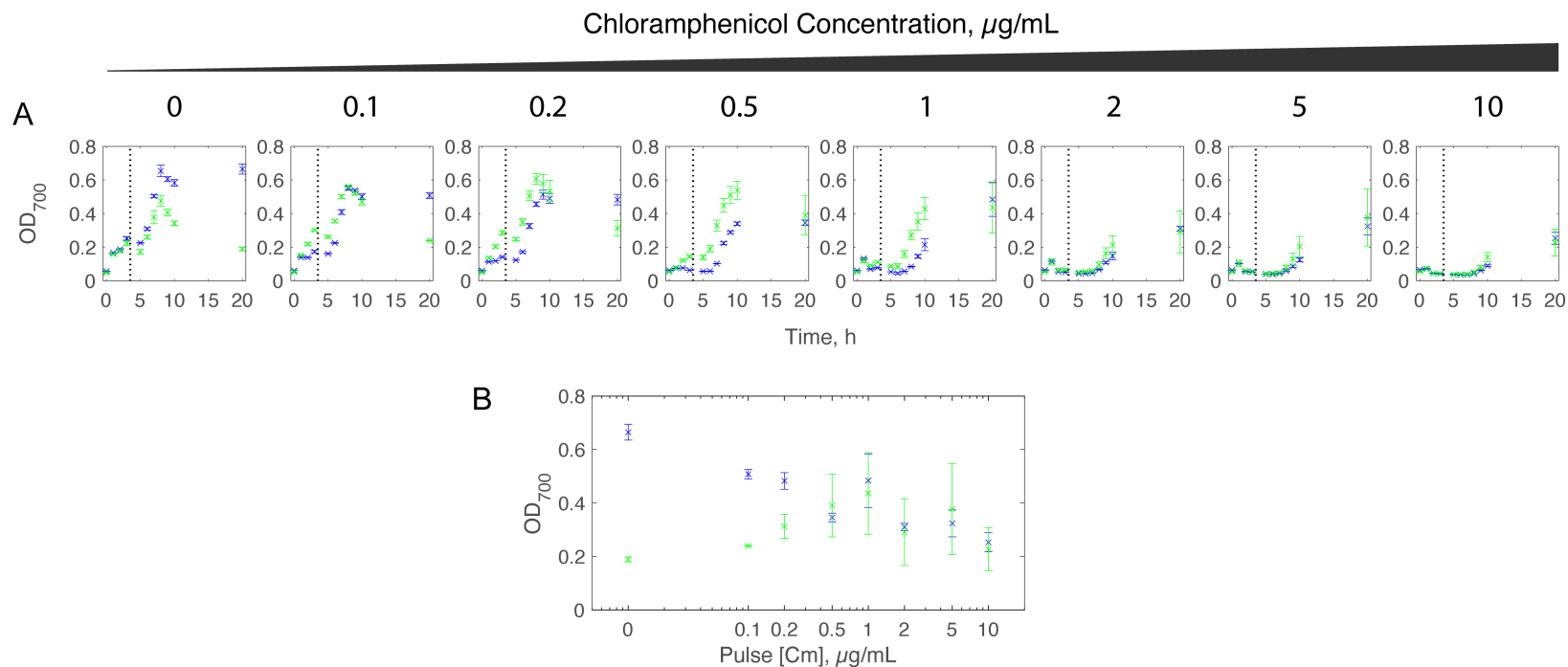


Figure A-5. Susceptible cells more readily recover from short-term pulses of antibiotics at sub-inhibitory concentrations.

(A) The growth of *acrAB-sfgfp* (green) compared against growth of the control, *sfgfp*, in the competition experiments (dots) for different t = 4 h pulses of chloramphenicol treatment. **(B)** Final OD₇₀₀ measurements t = 16 h after antibiotics were washed out. Data points show mean and standard deviations of n = 3 biological replicates.

Appendix B: Supplementary Information for Chapter 3

Parameter	Symbol	Units	Value
Initial Cell Biomass	$N(0)$	rel. cell area	1
Initial Cell Antibiotic Concentration	$C_{in}(0)$	$\mu\text{g/mL}$	0
Chloramphenicol			
Cell Doubling Time	T_d	min	60
Maximum Growth Rate	μ	rel. cell area min^{-1}	0.1106
Influx rate via Diffusion	K_{in}	min^{-1}	1
Efflux rate via Diffusion	$K_{out,\Delta acrB}$	min^{-1}	1
Efflux rate via Diffusion & Active Efflux	$K_{out,WT}$	min^{-1}	4
Repression coefficient	K_c	$\mu\text{g/mL}$	0.960
Hill coefficient	h_c	Dimensionless	1.47
Ciprofloxacin			
Cell Doubling Time	T_d	min	90
Maximum Growth Rate	μ	rel. cell area min^{-1}	0.0737
Influx rate via Diffusion	K_{in}	min^{-1}	1
Efflux rate via Diffusion	$K_{out,\Delta acrB}$	min^{-1}	1
Efflux rate via Diffusion & Active Efflux	$K_{out,WT}$	min^{-1}	3
Repression coefficient	K_c	$\mu\text{g/mL}$	0.247
Hill coefficient	h_c	Dimensionless	0.83

Table B-1. Model parameters.

Parameters for the model derived from data in Figure B-2, are calculated using from experimental doubling time, or are approximated based on the efflux efficiency (fold difference in the MIC) of different strains.

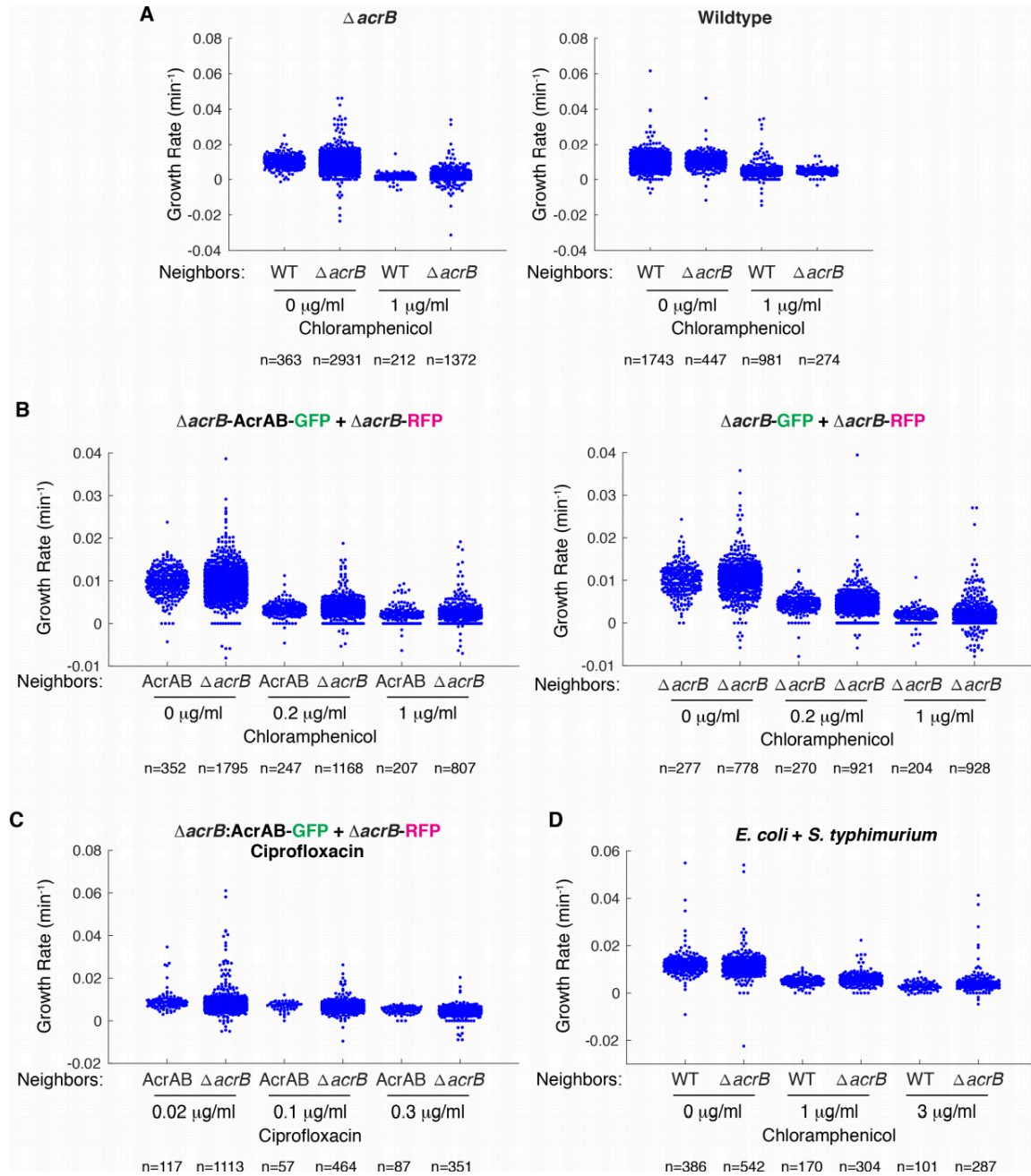


Figure B-1. Full data sets for figures including outliers and number of cells (n).

Data set corresponding to (A) Figure 3-1B-C, (B) Figure 3-2C-D, (C) Figure 3-4E, and (D) Figure 3-6. Each blue dot indicates the growth rate of a single cell. We note that in all cases, the plots shown in the main text include $\geq 97\%$ of cells. The automated image analysis process occasionally calculates artificially high or low growth rates, but this is a rare occurrence (always $< 3\%$, but more typically $< 1\%$ of cells). The full data sets can be found in Table S1 of reference (337).

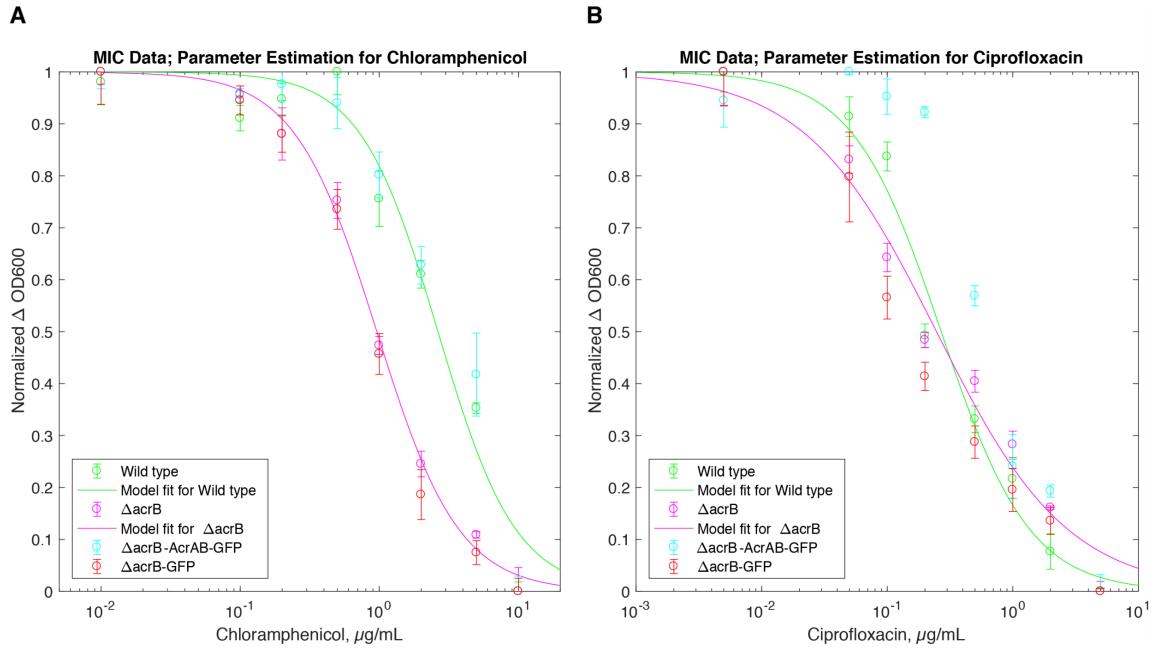


Figure B-2. Toxicity curves and data fitting for model parameters.

(A) Chloramphenicol and **(B)** ciprofloxacin experimental data for strains: wild type, ΔacrB , ΔacrB -AcrAB-GFP, and ΔacrB -GFP. Hill function fits for wild type and ΔacrB strains. Fits were conducted by minimizing least-squares error. Error bars show standard deviation of $n = 3$ biological replicates. Parameters for ΔacrB Hill function model fit are listed in Table B-1.

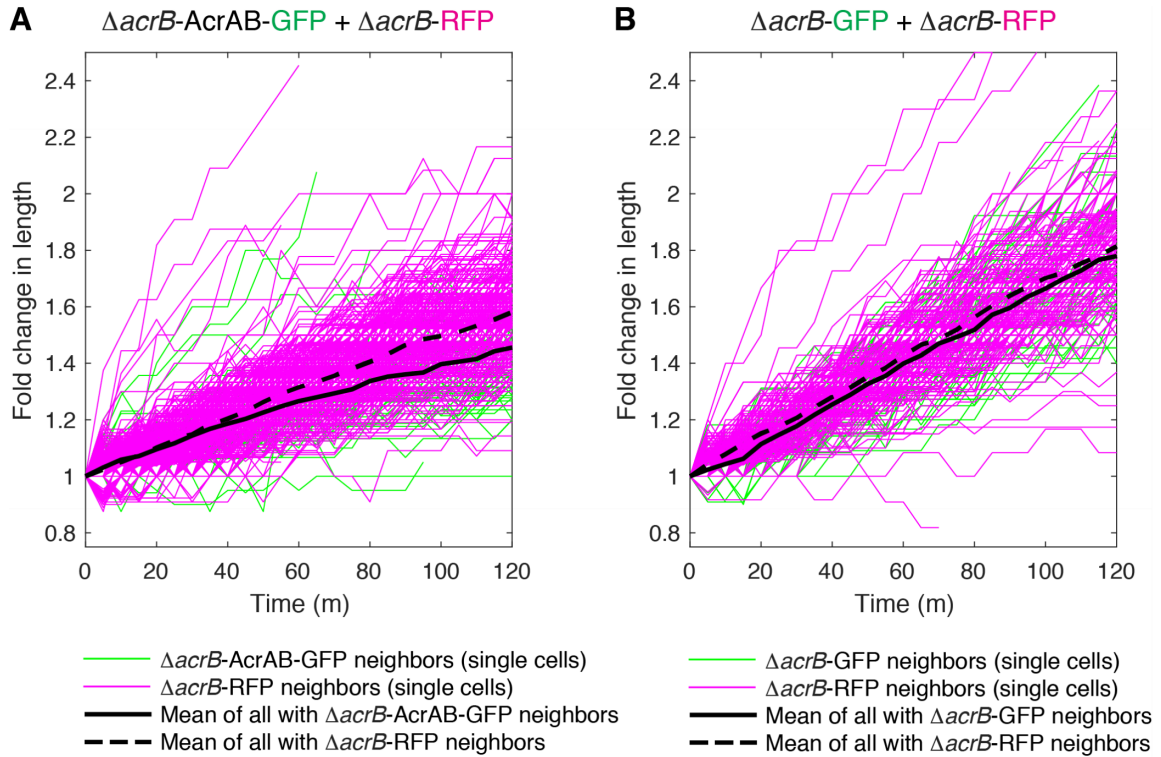


Figure B-3. Fold change in cell length over time for all individual cells.

(A) $\Delta acrB$ -RFP and AcrAB-GFP cells were mixed in ratios of 1:5 and 5:1 and grown on agarose pads with 0.2 $\mu\text{g/ml}$ chloramphenicol. Colored lines show all cell traces and black lines show the mean values, as indicated in the figure legend. A fold change of two at the final time point indicates that a cell has doubled. **(B)** $\Delta acrB$ -RFP and $\Delta acrB$ -GFP cells for conditions as described in (A).

Appendix C: Supplementary Information for Chapter 4

WT		Chloramphenicol, µg/mL								
Time 1 (h)	Time 2 (h)	0	0.2	0.5	1	2	5	10	20	
	0	1	4.35E-01	9.40E-02	7.02E-02	1.82E-02	1.33E-02	2.48E-02	2.36E-01	1.66E-01
	0	3	3.89E-01	3.17E-01	1.71E-02	1.55E-02	4.90E-03	6.18E-02	6.11E-02	7.82E-02
	0	6	3.86E-01	7.73E-02	3.90E-03	2.16E-02	2.70E-03	2.48E-02	2.56E-02	5.51E-02
	0	12	4.51E-01	6.46E-02	1.54E-02	3.21E-02	6.99E-04	4.85E-02	2.56E-02	7.00E-02
	0	24	5.07E-01	7.52E-01	1.42E-01	3.51E-02	3.59E-02	4.70E-02	2.56E-02	5.51E-02
	0	48	8.66E-01	1.81E-01	2.52E-01	6.04E-02	4.02E-02	7.70E-02	6.36E-02	5.51E-02
	0	72	3.77E-01	1.56E-01	1.92E-01	1.99E-01	7.55E-02	7.46E-02	7.94E-02	5.51E-02

AcrAB+		Chloramphenicol, µg/mL								
Time 1 (h)	Time 2 (h)	0	0.2	0.5	1	2	5	10	20	
	0	1	2.63E-01	2.12E-01	3.03E-02	7.27E-02	1.61E-02	3.43E-02	2.72E-01	5.02E-01
	0	3	1.18E-01	1.05E-01	3.74E-02	2.97E-02	1.89E-02	1.04E-01	1.85E-01	1.07E-01
	0	6	1.45E-01	2.80E-01	4.65E-02	2.08E-02	1.88E-02	3.33E-02	9.74E-02	1.04E-02
	0	12	1.77E-01	1.63E-01	3.62E-02	9.00E-03	5.54E-02	9.67E-02	9.74E-02	1.04E-02
	0	24	1.80E-01	1.18E-01	4.75E-02	8.40E-03	1.20E-02	8.73E-02	9.74E-02	1.04E-02
	0	48	4.00E-01	9.28E-02	7.78E-01	5.12E-02	2.91E-02	1.44E-01	9.74E-02	1.03E-02
	0	72	2.93E-01	1.37E-01	8.32E-01	1.75E-01	4.14E-02	2.68E-01	9.84E-02	1.04E-02

ΔacrB		Chloramphenicol, µg/mL								
Time 1 (h)	Time 2 (h)	0	0.2	0.5	1	2	5	10		
	0	1	2.75E-01	2.41E-01	3.62E-02	1.91E-01	1.15E-02	2.40E-03	1.83E-01	
	0	3	3.26E-01	1.49E-01	4.18E-02	6.45E-02	1.15E-02	4.30E-03	7.58E-02	
	0	6	3.54E-01	2.92E-02	3.25E-02	1.30E-03	1.68E-02	4.30E-03	7.58E-02	
	0	12	5.40E-01	1.63E-02	2.45E-02	1.28E-01	1.15E-02	4.30E-03	7.59E-02	
	0	24	8.36E-01	2.05E-02	3.42E-02	2.49E-01	1.15E-02	4.30E-03	7.58E-02	
	0	48	1.29E-01	3.91E-01	8.39E-02	4.06E-02	4.20E-03	4.30E-03	7.59E-02	
	0	72	5.96E-01	7.73E-01	2.63E-01	2.88E-01	7.16E-04	4.30E-03	7.58E-02	

Table C-1. *p* values for differences in growth rates for each strain.

P-values from the (paired) *t*-test for quantifying significant differences in growth rate between a given time point and the initial time point.

Direction	Primer (5' to 3')
Forward	ATGTATGTAAATCTAACGCCTGTAAATTCACGAACATATGGTGT AGGCTGGAGCTGCTTC
Reverse	CCTGGAGTCAGATTCAGGGTTATTCGTTAGTGGCAGGATTGATC CGTCGACCTGCAGTT

Table C-2. Primers for *acrR* knockout.

Bold letters denote the active priming region to amplify pKD13 from Reference (235). Primers also contain 40-nt homology regions for *acrR*.

	Chloramphenicol (µg/mL)											
	0	0.01	0.02	0.05	0.10	0.15	0.20	0.25	0.30	0.50	1	2
WT	0.389	0.355	0.919	0.919	0.900	0.567	0.494	0.832	0.474	0.714	0.275	0.107
AcrAB+	0.375	0.510	0.586	0.367	0.225	0.236	0.446	0.938	0.435	0.016	0.039	0.053
ΔacrB	0.032	0.138	0.142	0.089	0.053	0.809	0.229	0.429	0.187	0.273	0.430	0.058

Table C-3. *p* values of toxicity curves with and without Tween20.

P-values from the paired *t*-test to assess statistically significant differences in growth between samples treated with Tween20 at 0.0% and 0.2% (v/v) as shown in Figure C-7.

WT		Chloramphenicol, µg/mL									
Time 1 (h)	Time 2 (h)	0	0.2	0.5	1	2	5	10	20		
0	1	6.27E-01	4.44E-01	8.43E-02	6.82E-01	4.73E-01	1.61E-02	2.83E-01	7.80E-03		
0	3	7.62E-01	8.30E-01	5.34E-01	5.21E-01	9.80E-02	6.03E-02	3.04E-01	1.13E-02		
0	6	3.64E-01	1.33E-01	4.20E-01	3.12E-01	2.15E-01	3.51E-01	2.62E-01	3.47E-02		
0	12	9.11E-01	7.10E-01	1.62E-01	9.82E-01	3.48E-01	4.90E-01	2.94E-01	6.80E-02		
0	24	2.78E-02	6.33E-01	9.16E-01	6.00E-04	6.91E-02	3.38E-01	3.88E-01	8.41E-02		
0	48	7.97E-01	4.41E-01	8.52E-01	1.84E-01	2.87E-02	4.00E-04	4.63E-01	1.04E-01		
0	72	6.71E-01	2.40E-01	4.82E-02	5.43E-01	3.00E-02	1.10E-02	6.02E-01	1.44E-01		

AcrAB+		Chloramphenicol, µg/mL									
Time 1 (h)	Time 2 (h)	0	0.2	0.5	1	2	5	10	20		
0	1	5.02E-01	3.98E-01	2.19E-01	3.82E-01	4.05E-01	2.50E-03	9.30E-03	6.68E-02		
0	3	7.60E-02	7.66E-01	5.85E-01	8.59E-01	5.89E-02	4.04E-02	9.00E-03	3.12E-02		
0	6	8.64E-01	3.62E-02	1.44E-01	2.31E-01	3.54E-02	5.34E-02	1.60E-03	1.83E-02		
0	12	2.04E-01	9.28E-02	8.99E-01	1.40E-01	3.19E-02	4.28E-01	6.49E-02	1.82E-02		
0	24	3.95E-01	6.24E-01	5.65E-01	1.14E-01	7.36E-01	6.98E-01	7.88E-02	1.14E-02		
0	48	2.50E-01	3.33E-01	6.27E-01	1.55E-01	5.75E-01	1.41E-02	1.55E-02	1.20E-03		
0	72	5.17E-01	2.16E-02	8.37E-01	7.90E-03	1.45E-01	8.11E-02	7.00E-03	1.08E-02		

ΔacrB		Chloramphenicol, µg/mL									
Time 1 (h)	Time 2 (h)	0	0.2	0.5	1	2	5	10			
0	1	3.61E-01	2.64E-01	2.12E-01	5.50E-01	9.85E-02	4.70E-03	1.99E-02			
0	3	7.17E-01	1.51E-01	9.70E-02	9.40E-01	8.93E-02	2.26E-02	2.29E-02			
0	6	3.25E-01	7.11E-02	1.88E-01	8.83E-01	7.70E-03	2.60E-01	4.41E-02			
0	12	5.60E-01	5.00E-03	1.10E-01	5.77E-01	1.29E-01	1.48E-02	4.48E-02			
0	24	5.82E-01	3.19E-01	3.20E-02	6.78E-02	1.56E-01	2.78E-02	1.32E-01			
0	48	5.25E-01	8.00E-03	4.33E-02	1.30E-01	9.03E-01	5.47E-02	1.10E-01			
0	72	6.24E-01	6.50E-03	1.39E-01	1.51E-01	6.12E-01	1.68E-02	2.97E-01			

Table C-4. *p* values for differences in inhibition zone diameters for each strain.

P-values from the (paired) *t*-test for quantifying significant differences in resistance as measured by the diameter of inhibition zone between a given time point and the initial time point.

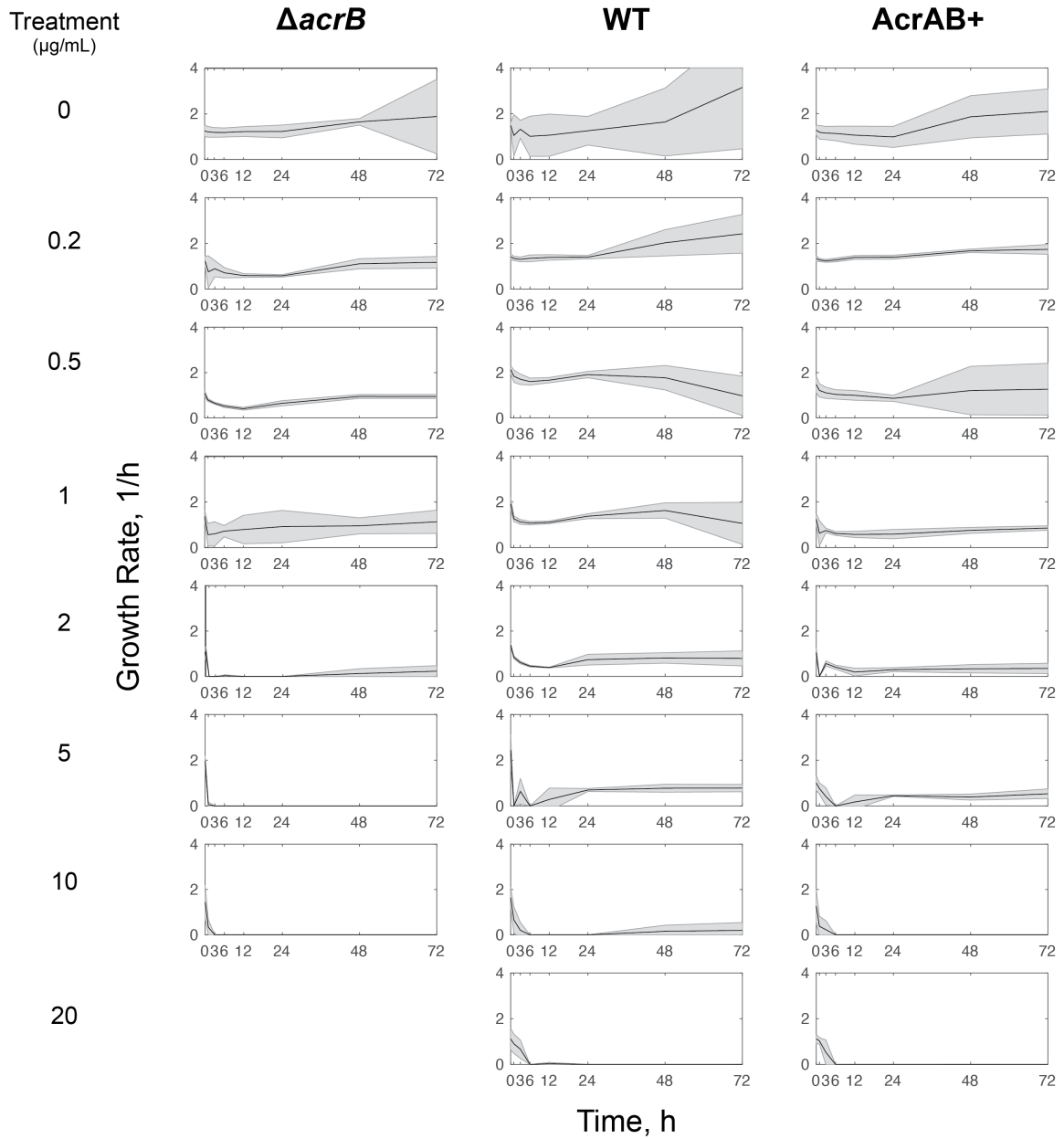


Figure C-1. Growth rates for each biological replicate and chloramphenicol treatment concentration.

Mean growth rates for $n = 3$ biological replicates. Shaded error bars show standard deviation. Cultures grown without chloramphenicol occasionally accumulated biofilms, leading to the large variations in the growth measurements for the 0 $\mu\text{g/ml}$ case.

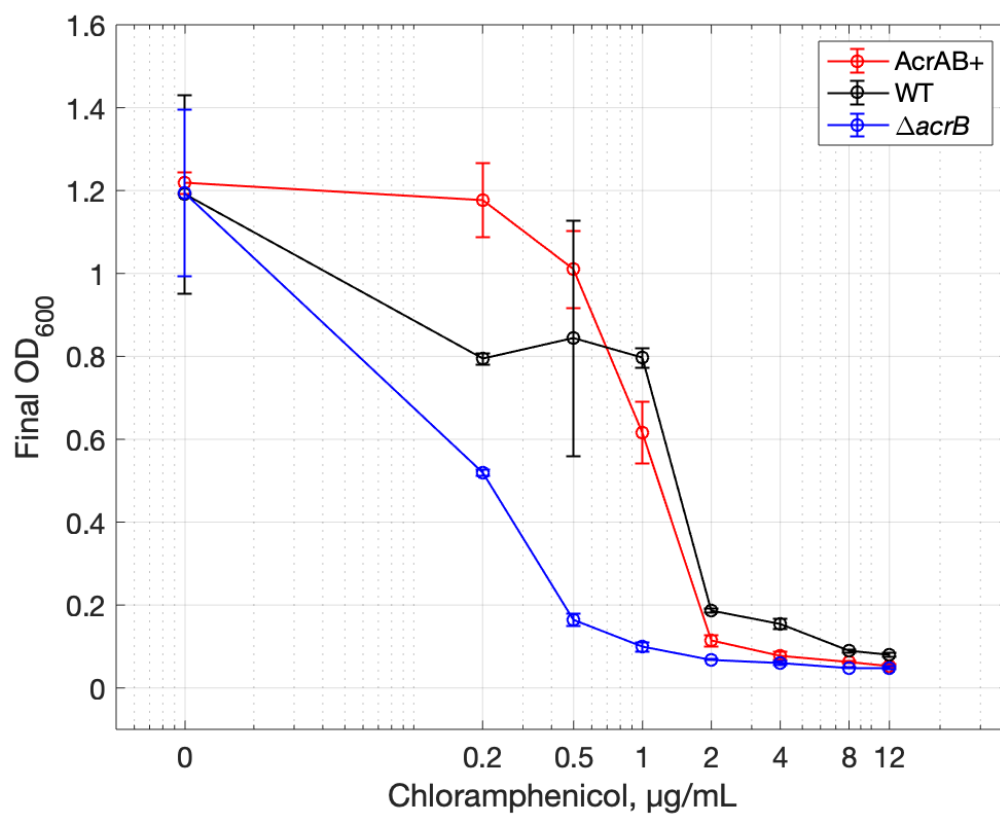


Figure C-2. Toxicity curves for each parent strain.

Final OD₆₀₀ was measured after 24 h. Data points show mean values from $n = 3$ biological replicates, error bars show standard deviation.

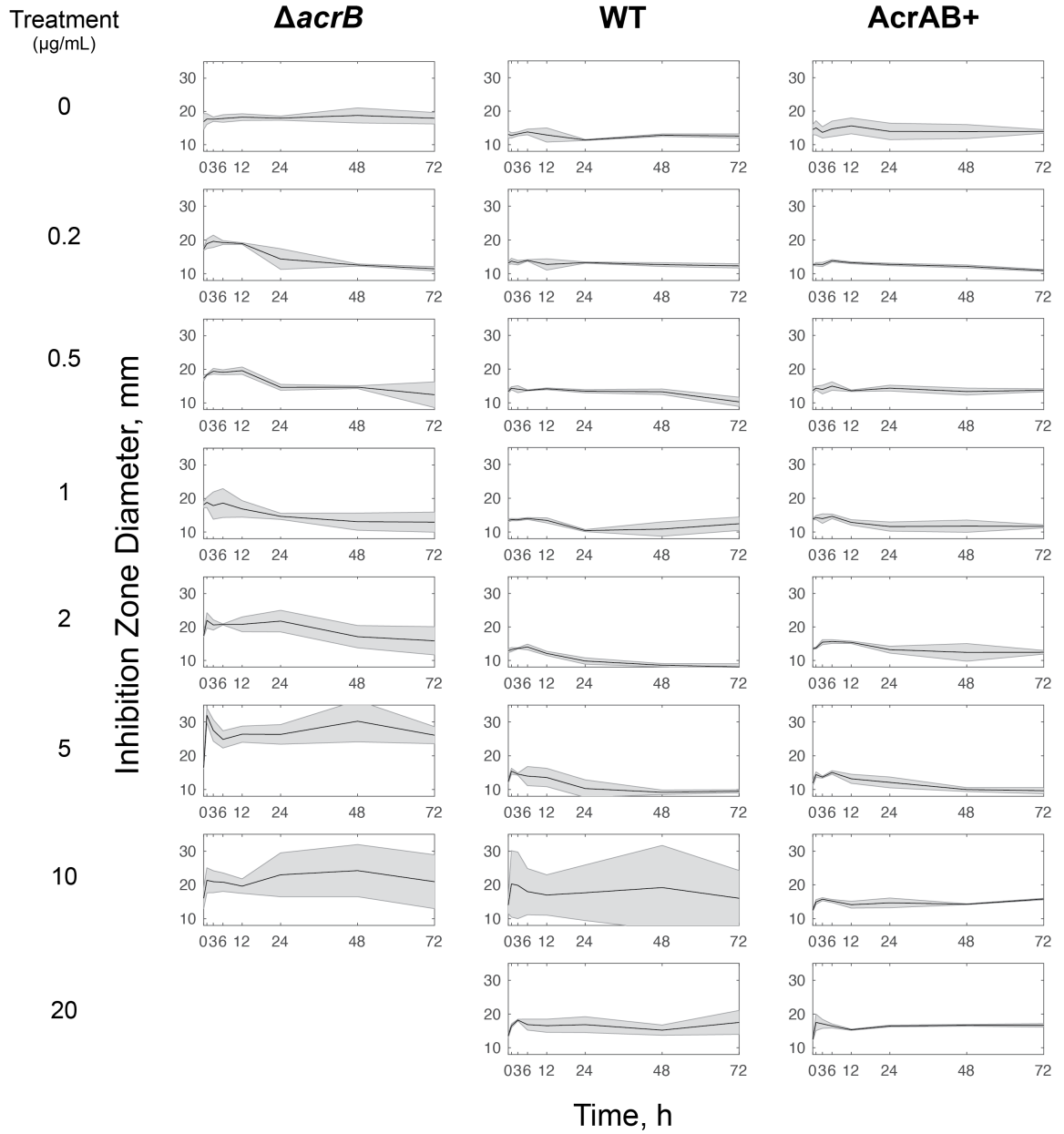


Figure C-3. Inhibition zone diameters for each biological replicate and chloramphenicol treatment concentration.

Mean diameter of inhibition zones (D_{inh}) for $n = 3$ biological replicates. Shaded error bars show standard deviation.

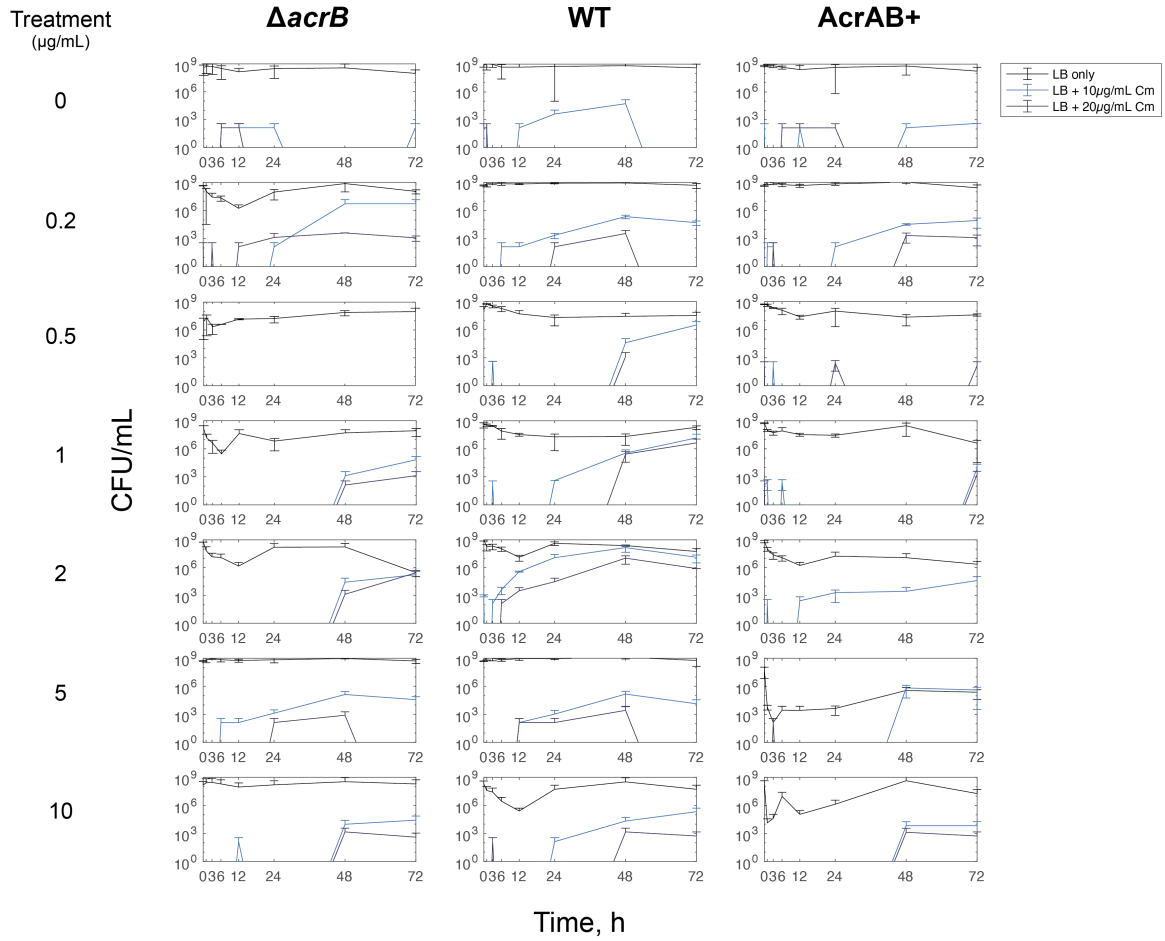


Figure C-4. Colony forming units (CFU) per mL counts for each treatment concentration.

Mean CFU/mL values from $n = 3$ biological replicates are shown, with error bars denoting standard deviation.

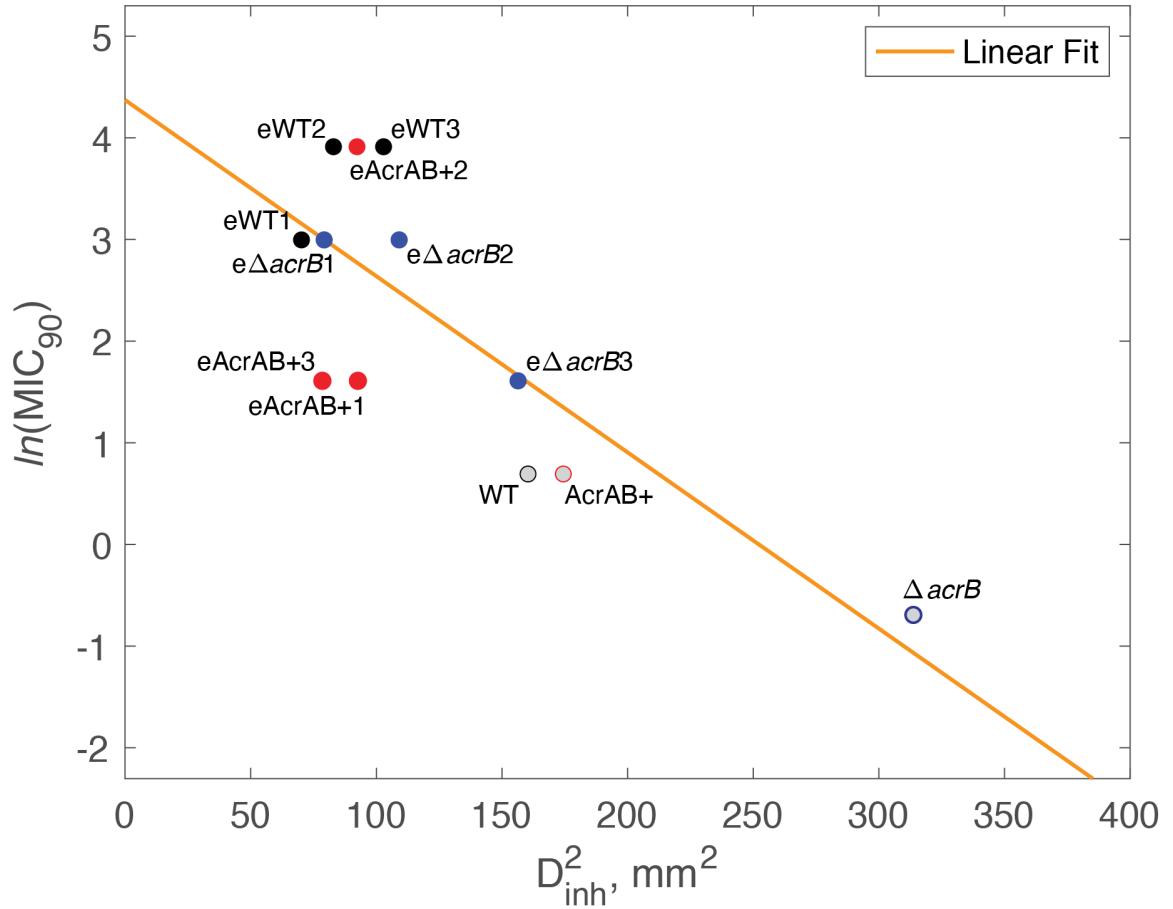


Figure C-5. Linear map between the natural log of the MIC and inhibition zone areas.

Data are from inhibition zone diameters and MIC₉₀ for each parent strains (e.g. AcrAB+) and the evolved isolates of each parent strain from three different eVOLVER experiments (e.g. eAcrAB+1, eAcrAB+2, and eAcrAB+3). MIC₉₀ is defined as the point where OD₆₀₀ is reduced to 10% of normal growth after 24 h (Figure S2). To find the linear correlation, we calculated the natural log of the MIC₉₀ and the inhibition zone areas. The parameters for this map are $Q = 30 \mu\text{g}$, $k = 57.8$, and $K = -0.971$, following the notation from Reference (310).

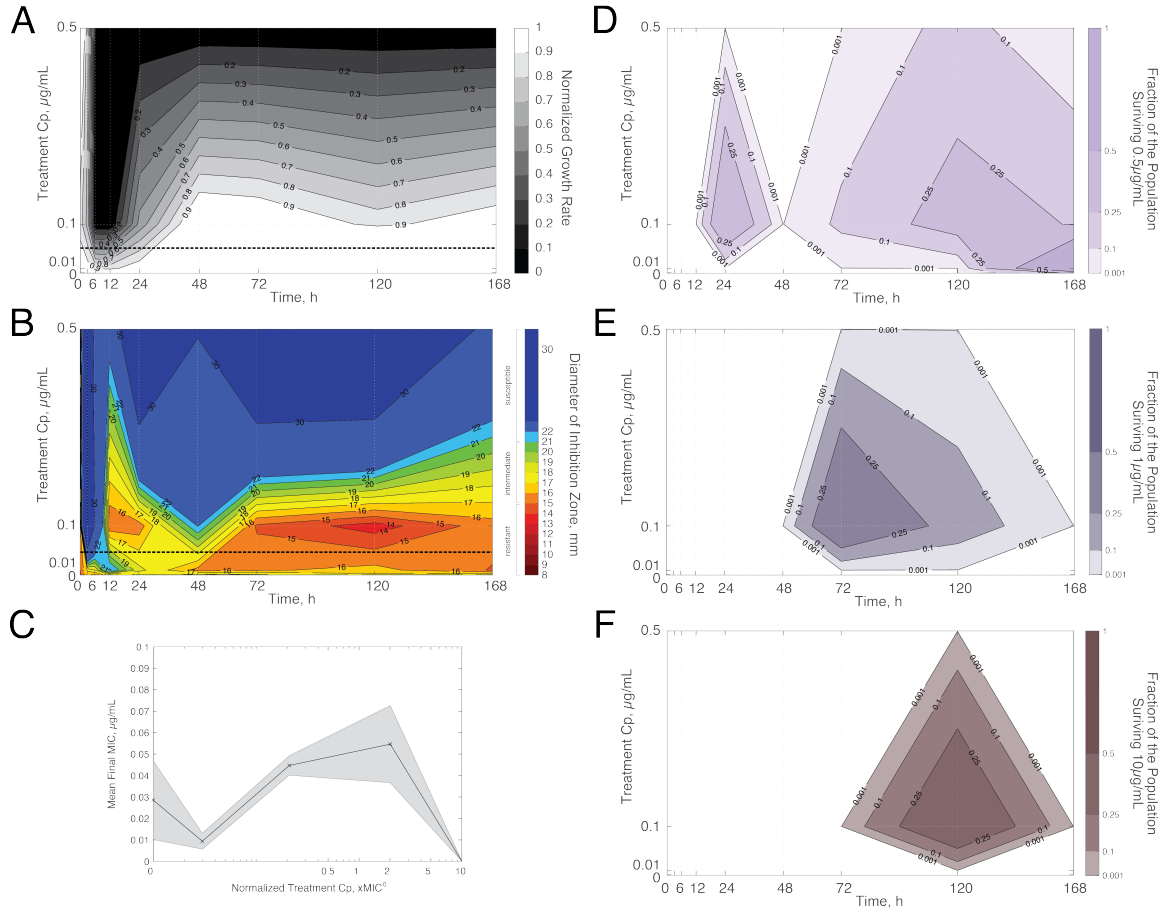


Figure C-6. Resistance and fitness of WT cells exposed to ciprofloxacin for 168 h.

(A) Average growth rate. Growth rates are normalized to growth of strains at $t = 0$ h. Lighter areas represent growth rates closer to pre-treatment values; darker areas represent reduced growth rates. $\text{MIC}^0_{\text{parent}}$ concentration is denoted with a bold dashed line (Figure C-2). (B) Average resistance. Diameter of inhibition zones were plotted for each time and treatment. Smaller inhibition zones are shown in red and correspond to resistant cells (≤ 15 mm) and larger inhibition zones are shown in blue and represent susceptible cells (≥ 21 mm); intermediate inhibition is shown with color scale from orange to green. $\text{MIC}^0_{\text{parent}}$ is denoted with a bold dashed line. (C) Average final resistance after 72 h based on treatment concentration normalized to MIC^0 . Data points show the mean of three biological replicates. Shaded error bars show standard deviation. (D-F) Mean percentage of the population, which could grow on LB plates containing (D) 0.5 $\mu\text{g/mL}$, (E) 1 $\mu\text{g/mL}$ or (F) 10 $\mu\text{g/mL}$ ciprofloxacin. Initial populations contained $\sim 10^7$ CFUs. $\text{MIC}^0_{\text{parent}}$ compared to treatment concentration is denoted with a bold dashed line.

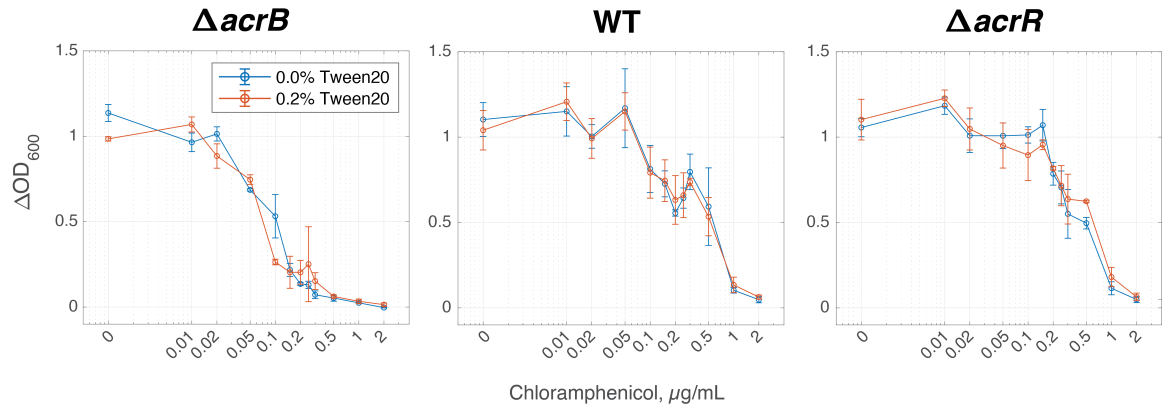


Figure C-7. Toxicity curves in the presence of Tween20.

Strains grown with and without 0.2% (v/v) Tween20. Data points show mean values from $n = 3$ biological replicates, error bars show standard deviation.

Appendix D: Supplementary Information for Chapter 5

	Cm	Amp	Tet	Cp
WT	21.2 ± 2.7	18.2 ± 1.7	21.7 ± 2.0	26.1 ± 2.2
<i>acrAB</i>⁺	27.1 ± 1.9	20.2 ± 1.3	26.7 ± 1.6	30.9 ± 1.9
<i>ΔacrB</i>	33.5 ± 3.2	24.4 ± 2.0	29.0 ± 2.1	32.3 ± 1.9

Table D-1. Inhibition zones for parent strains prior to treatment.

For the different genotypes tested, the mean diameters of the inhibition zones from the antibiotic disc susceptibility test are indicated in millimeters (mm) ± standard deviation. n = 20 biological replicates. Note that smaller numbers indicate higher resistance. Distributions are shown in Figure D-2A.

	<i>p</i> value at timepoint			
	t = 12 hours	t = 24 hours	t = 48 hours	t = 72 hours
WT	0.343	0.522	0.764	0.727
<i>acrAB</i>⁺	0.046*	0.0097*	0.295	0.724
<i>ΔacrB</i>	0.436	0.376	0.367	0.775
Co-culture	0.166	0.603	0.505	0.223

Table D-2. *p* values from two-sample t-test for growth rate difference.

Probabilities that two sets of growth rates for ramp and step are significantly different. For *p* value < 0.05, there is a 95% confidence that the growth rates for ramp and step conditions, with n = 3 biological replicates, are not similar by chance, indicated by an asterisk.

	R	p value	R	p value	R	p value	R	p value
	<i>All Combined</i>		<i>Ramp Only</i>		<i>Step Only</i>		<i>Control Only</i>	
Figure 5-7A	0.427*	2.47e-3	0.494	6.15e-2	0.029	9.20e-1	0.811*	4.41e-5
Figure 5-7B	0.485*	4.77e-4	0.0228	9.36e-1	0.450	9.25e-2	0.885*	1.06e-6
Figure 5-7C	0.205	1.62e-1	0.250	3.68e-1	0.350	2.01e-1	0.723*	6.91e-4
Figure 5-7D	-0.217	1.38e-1	-0.226	4.17e-1	0.046	8.70e-1	-0.868*	2.97e-6
Figure 5-7E	0.464*	9.02e-4	0.107	7.04e-1	-0.474	7.43e-2	-0.552*	1.75e-2
Figure 5-7F	-0.327*	2.35e-2	0.0305	9.14e-1	-0.516*	4.89e-2	-0.530*	2.36e-2

Table D-3. Pearson correlation coefficients and their *p* values.

Correlation coefficients between: (Row 1) Maximum initial growth rate (prior to antibiotic treatment) compared to the maximum growth rate after treatment. (Row 2) Maximum growth rate after treatment versus the number of dilutions to reach this maximum growth. (Row 3) Final growth rate versus the final number of dilutions at the end of the experiment. (Row 4-6) Maximum change in resistance for a culture versus the (Row 4) maximum initial growth rate (prior to antibiotic treatment), (Row 5) the final growth rate, and (Row 6) the total number of dilution events, as depicted in Figure 5-7. Pearson coefficient values denoted by an asterisk are significant with a *p* value < 0.05 and 95% confidence. Data represents the statistics for 48 experiments: 15 step experiments, 15 ramp experiments, and 18 control experiments.

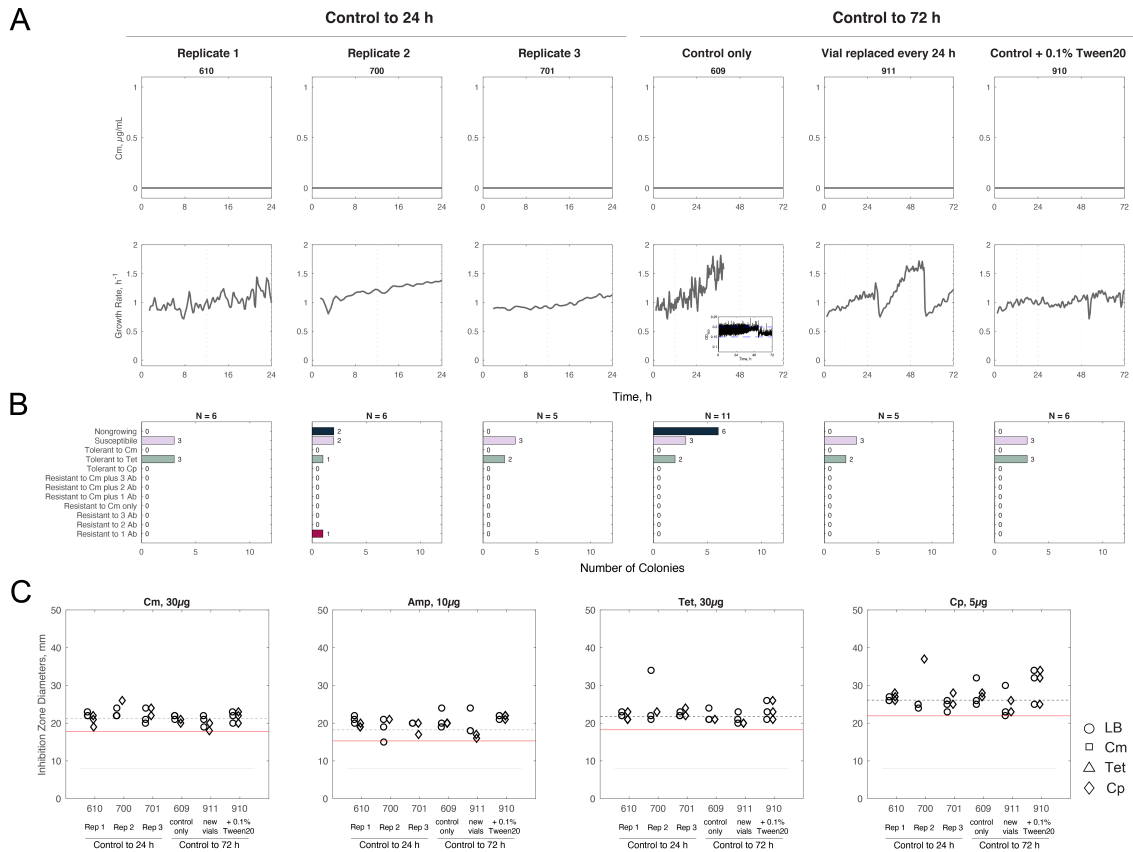


Figure D-1. Wild type control without antibiotics and the emergence of resistance and tolerance.

(A) (Top) Actual concentration of chloramphenicol over time (no antibiotic treatment) for wild type cells at 24 h (three experiments on the left) and 72 h (three experiments on the right). $n = 3$ biological replicates for 24h control and $n = 1$ biological replicate for 72 h control under 3 experimental conditions: (1) control only, (2) control with vial replaced every 24h, and (3) control with Tween20 added to media at 0.1% (v/v). (Bottom) Growth rates. We note that for the “control only” case, after approximately 40h the dilution events became so frequent that it was not possible to calculate the growth rate accurately from the slope of the OD₆₀₀ curve, though cultures continued to grow well for the full 72 h time course. (Inset) Actual OD₆₀₀ over the whole experiment. Replacing the culture vial every 24 h and adding Tween20 both addressed this problem, suggesting that biofilm formation may be an issue in the absence of antibiotics. Numbers in the plot titles refer to the experiment number. **(B)** Fates of all isolated colonies from all plates. Results were classified as: nongrowing (navy), susceptible (light pink), tolerant (light green), and resistant (burgundy). Ab, antibiotics. N represents the number of isolates from each experiment that were picked. If no colonies were found on a high antibiotic plate then no isolate could be picked. **(C)** Inhibition zone diameters for the four antibiotic disc assays. The inhibition zone diameters were normalized to the parent strain’s mean inhibition zone

(shown in black). The threshold to classify as resistant is shown in red. The symbol shape indicates which plate the colony was originally isolated from: LB only (circle), LB+Cm (square), LB+Tet (triangle), LB+Cp (diamond).

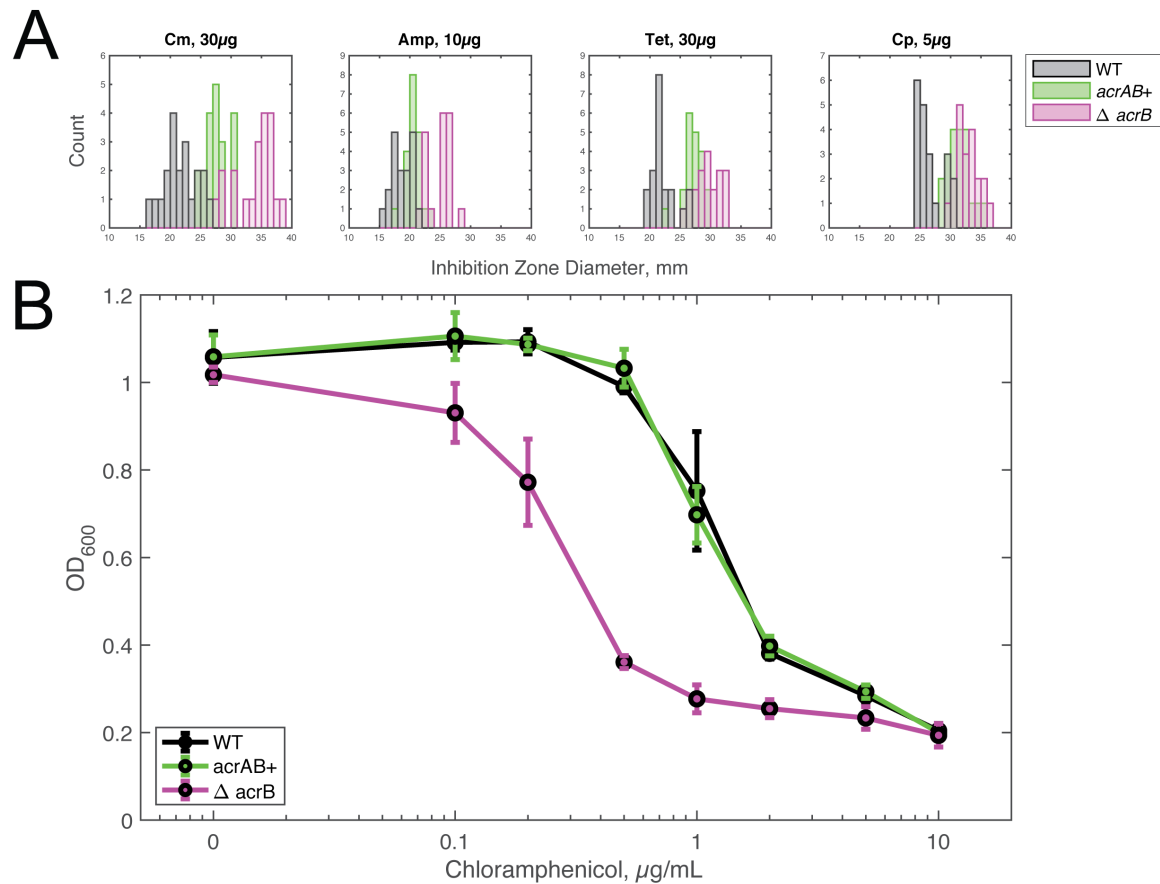


Figure D-2. *acrAB+* resistance relative to WT and Δ *acrB*.

(A) Histograms of the inhibition zones for each antibiotic for each strain. $n = 20$ biological replicates for each distribution. Cross reference with Table D-1 for the mean and standard deviations of these distributions. **(B)** Dose response curves for all three strains to chloramphenicol after 6 h, which is the time that these strains remain in exponential phase. $n = 3$ biological replicates and error bars show standard deviation.

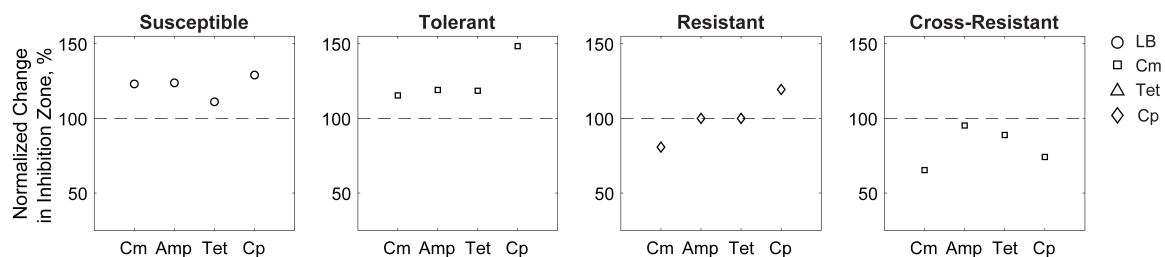


Figure D-3. Normalized inhibition zones for example isolates.

Representative classification examples (Figure 5-2B). The symbol shape indicates which plate the colony was originally isolated from: LB only (circle), LB+Cm (square), LB+Tet (triangle), LB+Cp (diamond). Susceptible cells did not grow on high antibiotic dose plates and did not have a decrease in antibiotic inhibition zone. Tolerant cells were isolated on a high dose selective plate (chloramphenicol in this specific case) but do not show increased resistance to chloramphenicol in the disc diffusion assay. Resistant isolates are classified based on a decrease in their inhibition zone diameter. Note that this example of a resistant strain here is only resistant to chloramphenicol and would be sorted into the “Resistant to Cm only” category (refer to Figure 5-2C, Figure 5-3B, and Figure 5-6B). Many strains with high resistance to chloramphenicol were often cross-resistant to other antibiotics. Cross-resistant isolates are identified as having resistance to multiple antibiotics, not chloramphenicol alone.

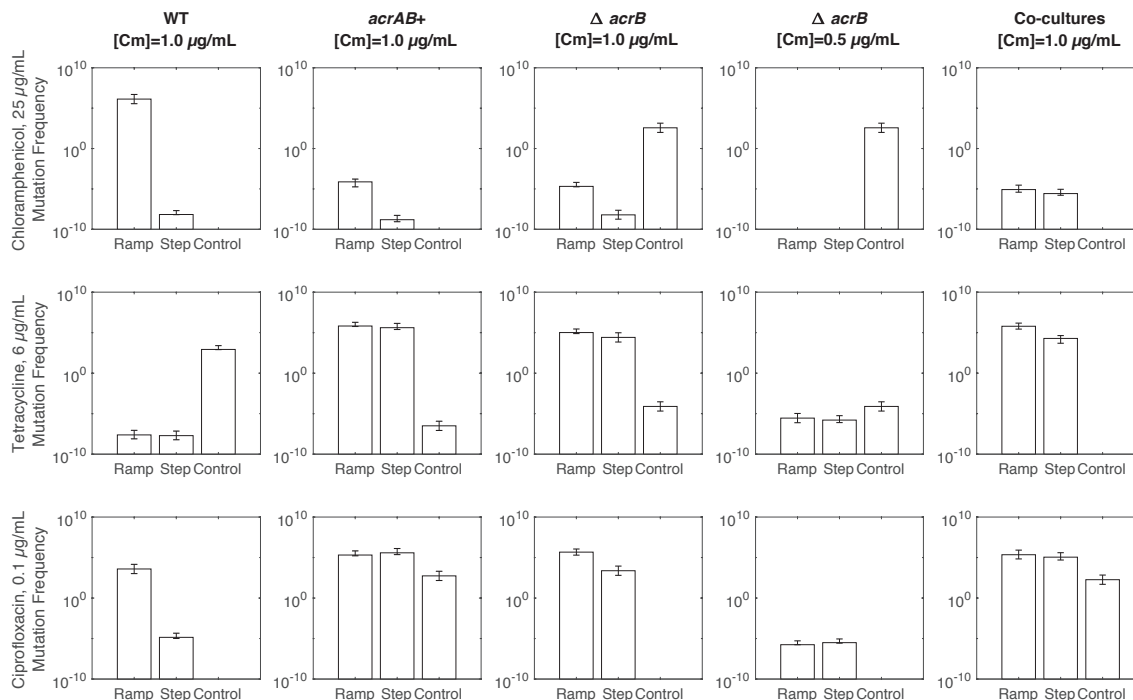


Figure D-4. Mutation frequencies at the end of the experiment.

Mutation frequencies for all strains and all experiments for the three high dose antibiotic plates for $n = 3$ biological replicates. Error bars show standard deviation. Mutation frequencies were calculated by the fraction of colony forming units per milliliter (CFU/mL) growing on high dose antibiotic plates divided by CFU/mL on LB plates containing only kanamycin for plasmid maintenance.

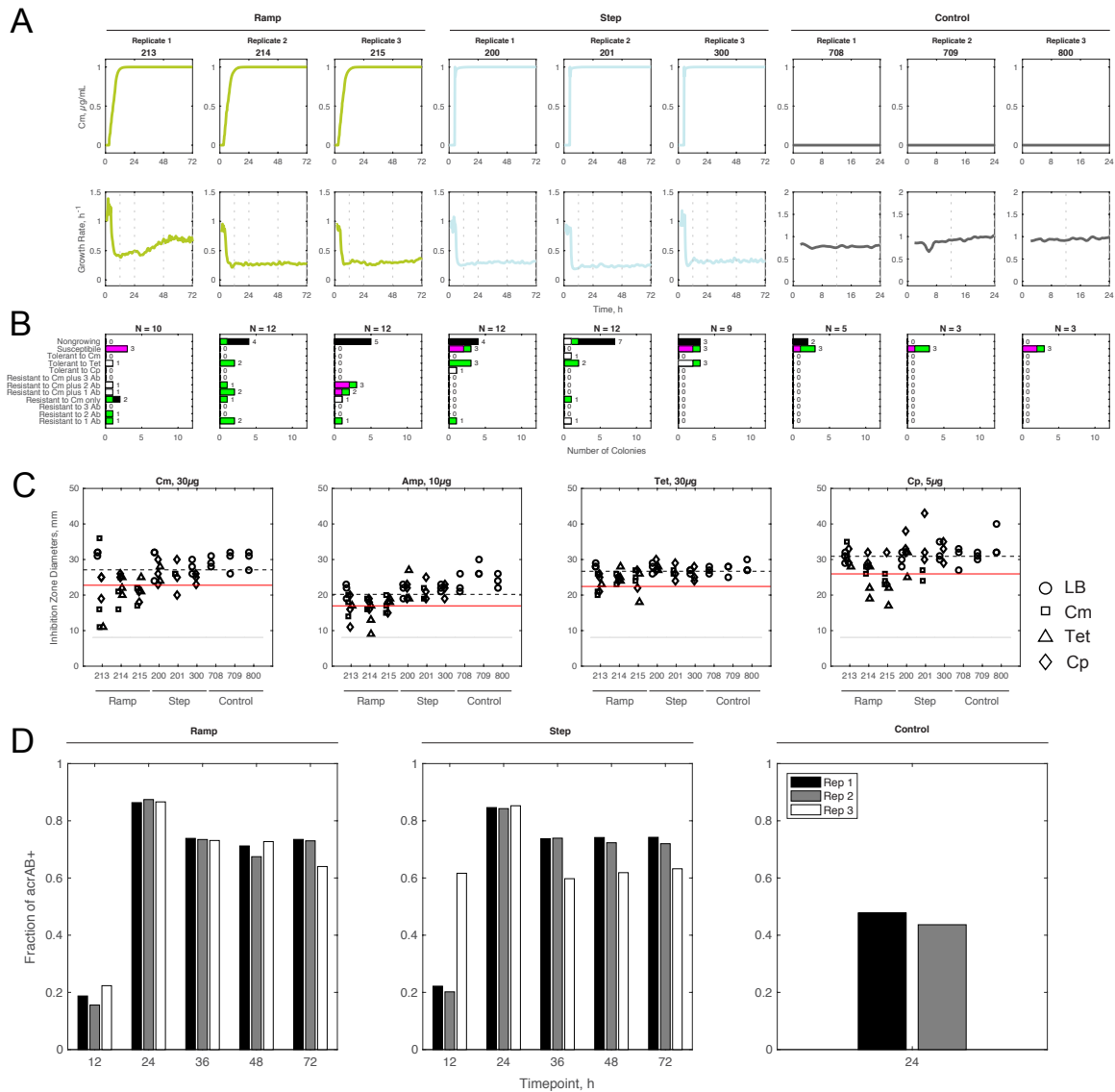


Figure D-5. All co-cultured experiments and the emergence of resistance and tolerance.

(A) (Top) Actual concentration of chloramphenicol over time along with (bottom) growth rates for co-cultured experiments. $n = 3$ biological replicates shown for each experimental condition: ramp, step, or control. Numbers in the plot titles refer to the experiment number. (B) Fates of all isolated colonies from all plates. Results were classified as: nongrowing, susceptible, tolerant, and resistant. The fate sorting shows the parent strain of the isolate: *acrAB*⁺ (green), Δ *acrB* (magenta), undetermined (white), nongrowing (black). Ab, antibiotics. N represents the number of isolates from each experiment that were picked. If no colonies were found on a high antibiotic plate then no isolate could be picked. (C) Inhibition zone diameters for the four antibiotic disc assays. The inhibition zone diameters were normalized to the parent strain's mean inhibition zone. The threshold to classify as

resistant is shown in red. The symbol shape indicates which plate the colony was originally isolated from: LB only (circle), LB+Cm (square), LB+Tet (triangle), LB+Cp (diamond). **(D)** Bar graphs depict the fraction of *acrAB*⁺ cells in the total population at different time points in the co-culture for each replicate. We were not able to reach the baseline number of counts with flow cytometry for replicate 3.

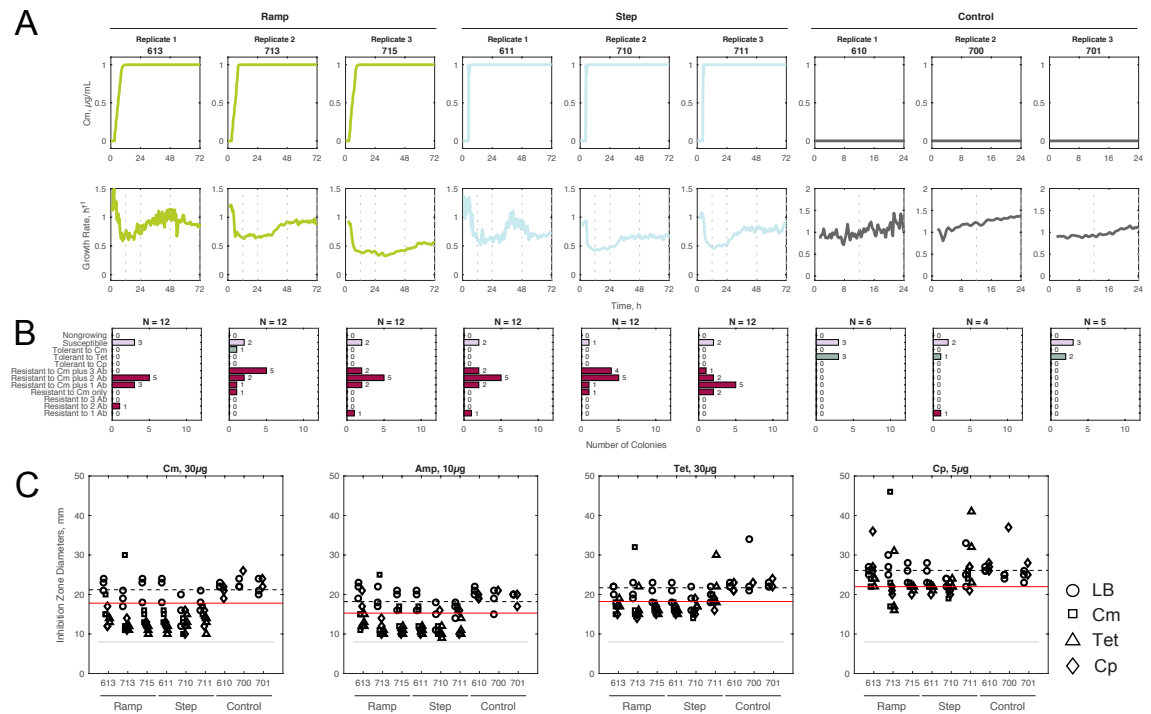


Figure D-6. All wild type experiments and the emergence of resistance and tolerance.

(A) (Top) Actual concentration of chloramphenicol over time along with (bottom) growth rates for wild type cells. Three biological replicates shown for each experimental condition: ramp, step, or control. Numbers in the plot titles refer to the experiment number. **(B)** Fates of all isolated colonies from all plates. Results were classified as: nongrowing (navy), susceptible (light pink), tolerant (light green), and resistant (burgundy). Ab, antibiotics. N represents the number of isolates from each experiment that were picked. If no colonies were found on a high antibiotic plate then no isolate could be picked. **(C)** Inhibition zone diameters for the four antibiotic disc assays. The inhibition zone diameters were normalized to the parent strain's mean inhibition zone. The threshold to classify as resistant is shown in red. The symbol shape indicates which plate the colony was originally isolated from: LB only (circle), LB+Cm (square), LB+Tet (triangle), LB+Cp (diamond).

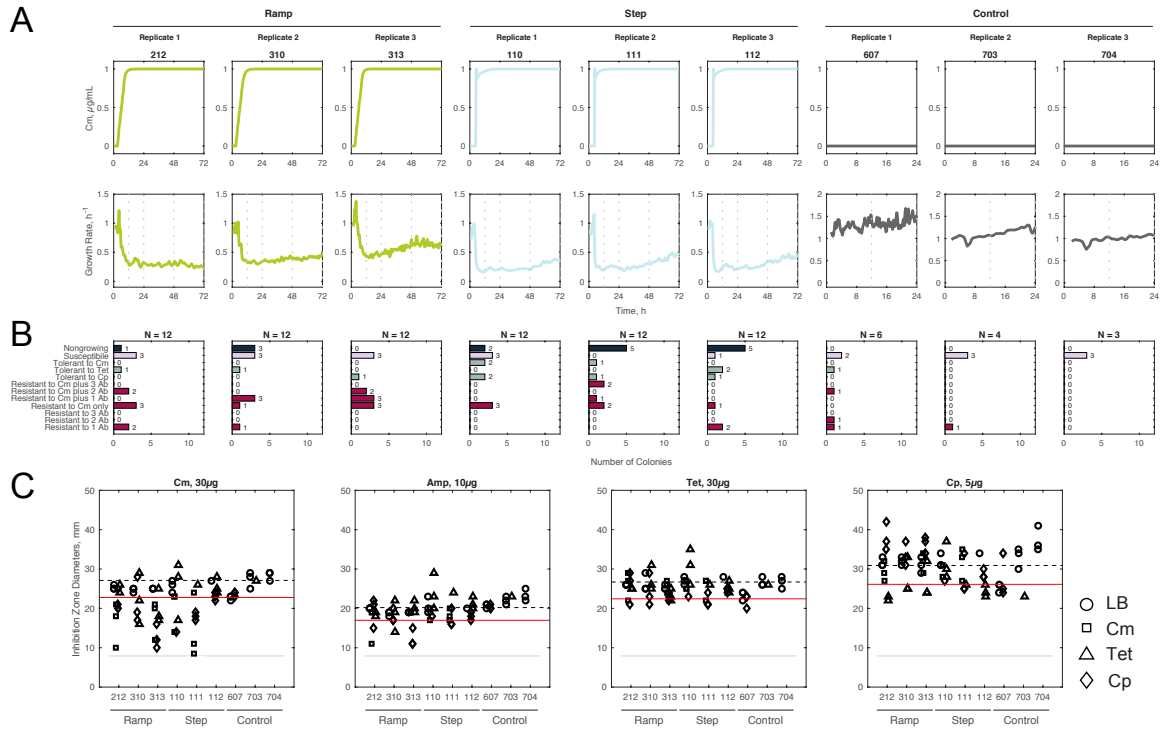


Figure D-7. All *acrAB*⁺ experiments and the emergence of resistance and tolerance.

(A) (Top) Actual concentration of chloramphenicol over time along with (bottom) growth rates for *acrAB*⁺ cells. Three biological replicates shown for each experimental condition: ramp, step, or control. Numbers in the plot titles refer to the experiment number. **(B)** Fates of all isolated colonies from all plates. Results were classified as: nongrowing (navy), susceptible (light pink), tolerant (light green), and resistant (burgundy). Ab, antibiotics. N represents the number of isolates from each experiment that were picked. If no colonies were found on a high antibiotic plate then no isolate could be picked. **(C)** Inhibition zone diameters for the four antibiotic disc assays. The inhibition zone diameters were normalized to the parent strain's mean inhibition zone. The threshold to classify as resistant is shown in red. The symbol shape indicates which plate the colony was originally isolated from: LB only (circle), LB+Cm (square), LB+Tet (triangle), LB+Cp (diamond).

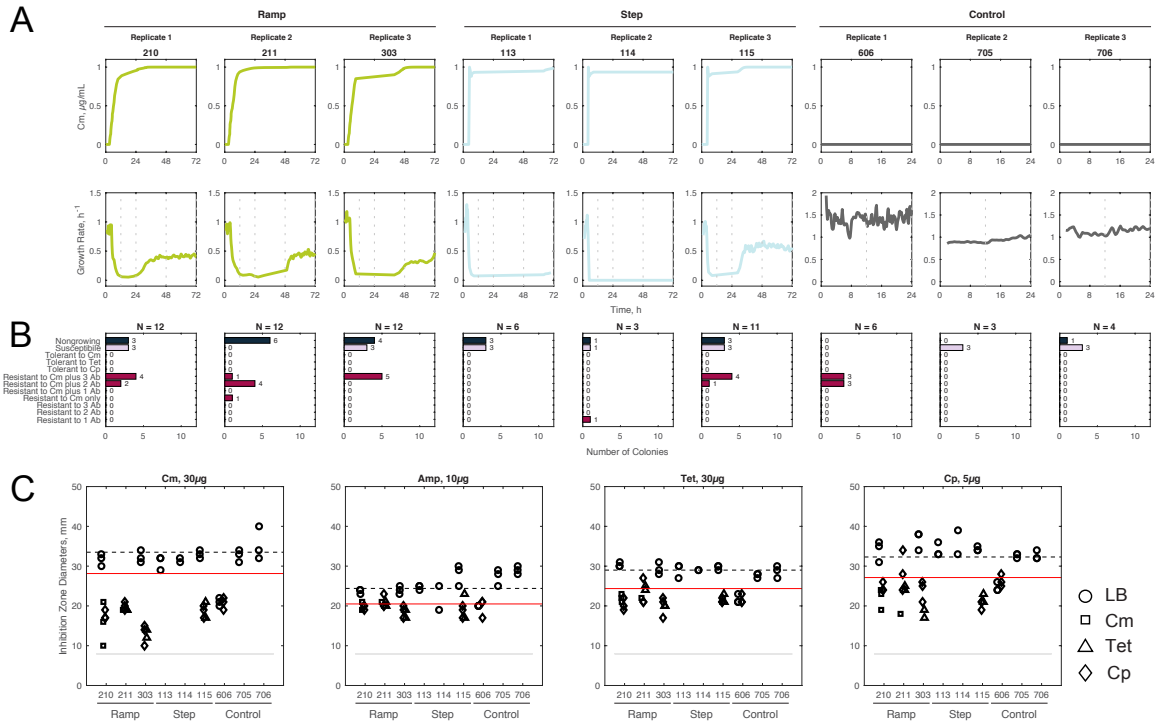


Figure D-8. All ΔacrB experiments and the emergence of resistance and tolerance at MIC_{wt} (1 $\mu\text{g/mL}$).

(A) (Top) Actual concentration of chloramphenicol over time along with (bottom) growth rates for ΔacrB cells. Three biological replicates shown for each experimental condition: ramp, step, or control. Numbers in the plot titles refer to the experiment number. **(B)** Fates of all isolated colonies from all plates. Results were classified as: nongrowing (navy), susceptible (light pink), tolerant (light green), and resistant (burgundy). Ab, antibiotics. N represents the number of isolates from each experiment that were picked. If no colonies were found on a high antibiotic plate then no isolate could be picked. **(C)** Inhibition zone diameters for the four antibiotic disc assays. The inhibition zone diameters were normalized to the parent strain's mean inhibition zone. The threshold to classify as resistant is shown in red. The symbol shape indicates which plate the colony was originally isolated from: LB only (circle), LB+Cm (square), LB+Tet (triangle), LB+Cp (diamond).

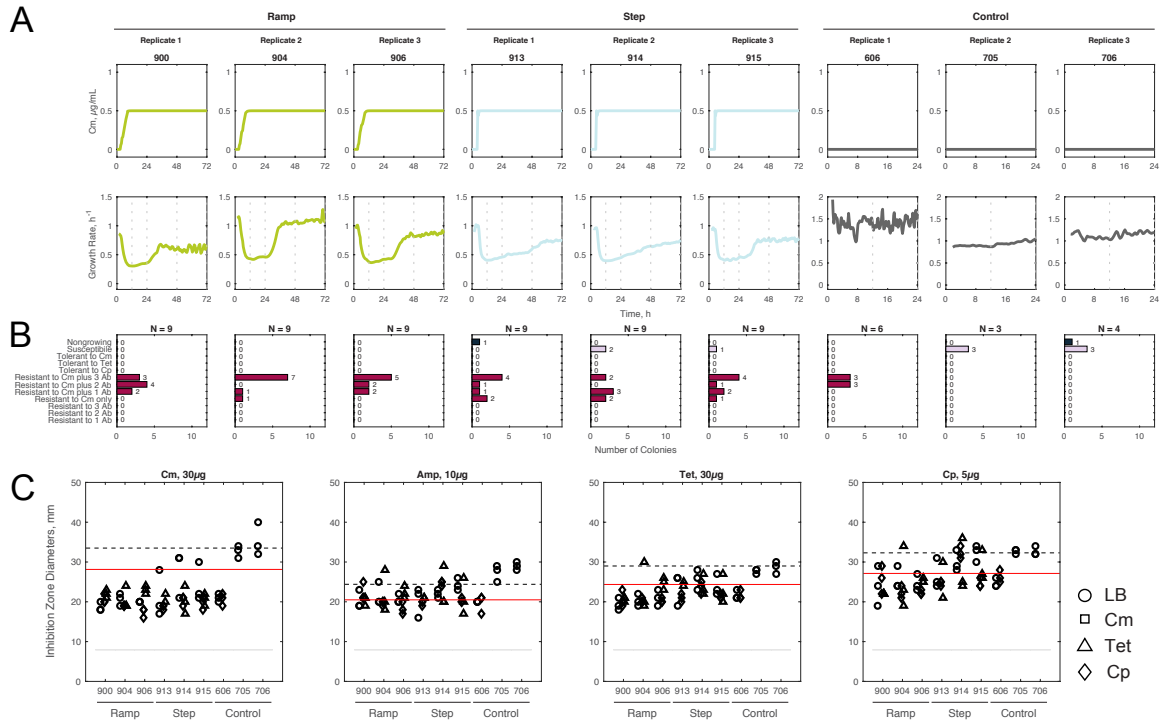


Figure D-9. All $\Delta acrB$ experiments and the emergence of resistance and tolerance at $MIC_{\Delta acrB}$ (0.5 $\mu\text{g/mL}$).

(A) (Top) Actual concentration of chloramphenicol over time along with (bottom) growth rates for $\Delta acrB$ cells. $n = 3$ biological replicates shown for each experimental condition: ramp, step, or control. Numbers in the plot titles refer to the experiment number. **(B)** Fates of all isolated colonies from all plates. Results were classified as: nongrowing (navy), susceptible (light pink), tolerant (light green), and resistant (burgundy). Ab, antibiotics. N represents the number of isolates from each experiment that were picked. If no colonies were found on a high antibiotic plate then no isolate could be picked. **(C)** Inhibition zone diameters for the four antibiotic disc assays. The inhibition zone diameters were normalized to the parent strain's mean inhibition zone. The threshold to classify as resistant is shown in red. The symbol shape indicates which plate the colony was originally isolated from: LB only (circle), LB+Cm (square), LB+Tet (triangle), LB+Cp (diamond).

Appendix E: Predicting Single Cell Fate with a c-di-GMP Biosensor

E.1. Introduction

When single cells are able to survive an antibiotic dose, antibiotic treatments fail (36). This single cell survival does not only result from genotypic changes, such as discussed in this thesis, but can also result solely from phenotypic changes, such as variations in the metabolism or gene expression of single cells (338). Earlier studies have identified that heterogeneity gene expression of a single cell provides a bet-hedging mechanism to survive antibiotic treatment; by diversifying the phenotypes in a microbial population, the population increase the likelihood that a sub-population will be able to survive (339). As a result, in recent years, there has been an increased interest in using gene expression to predict cell fates (340).

Outside of gene expression, slow growth can predict persistence in *S. enterica*, whereby slower growing cells can survive antibiotic treatment (341). Likewise, other studies have revealed a link between cell cycle proteins and antibiotic resistance in *Listeria monocytogenes* (342). This connection is assumed to be between bacterial metabolic state and an antibiotic's efficacy (338). Thus, there has been recently particular interest into whether manipulation of cell cycle or metabolism could improve antibiotic efficacy. Further, Schrader & Shapiro found that they could synthetically synchronize the cell cycles of *Caulobacter crescentus* populations (343).⁴ Outside of antibiotic resistance studies, other studies have been able to programmed the cell death of single cells at a given stage

⁴ An interesting note: ClpX – a protease that was mutated after antibiotic treatment in **Chapter 4** (Table 4-1) – plays an important role in controlling cell cycle in *C. crescentus* (351).

in their cell cycle (344).

Cyclic diguanosine monophosphate (c-di-GMP) is a small, signaling molecule that acts as a regulator of many bacterial behaviors, including cell cycle progression, biofilm formation, virulence, and motility (345, 346). Particular interest has been given to this molecule because of (1) the sheer number of regulators with c-di-GMP receptors, (2) the heterogeneity of c-di-GMP in populations, and (3) the heightened antibiotic resistance due to biofilm formation (345). Single cell c-di-GMP levels can be tracked with a biosensor (346). This biosensor uses Förster Resonance Energy Transfer (FRET) to assess how close an acceptor fluorescent protein and a donor fluorescent protein are in order to determine the conformation of the substrate binding protein, in this case PilZ, which changes conformation upon binding to c-di-GMP (346).

In this work, we study whether single cell characteristics, such as stage of cell cycle, are tied to cell fate. On a single cell level, we hypothesize that the stage in a bacterial cell cycle can hinder its ability to survive antibiotic treatment, particularly if a cell is close to division. Dually, on a population level, we hypothesize that heterogeneity can lead to a high fraction of cells surviving antibiotic resistance because of the lack of synchronization. Previously, Christen *et al.* found that c-di-GMP oscillates synchronously with a single cell's cell cycle (346). Here, we used an optimized FRET biosensor to track temporal changes in c-di-GMP. Overall, our work was an explorative direction aimed at understanding if c-di-GMP could predict cell fate and more specifically whether we would be able to manipulate the physiology of single cells to improve effectiveness of antibiotic treatments.

E.2. Results

In order to study c-di-GMP levels in *E. coli*, we optimized the biosensor from Reference (346) (see: Methods). When c-di-GMP binds to the PilZ domain of the biosensor, FRET levels are low; when there is less c-di-GMP, FRET levels are higher (Figure E-1). Using the biosensor, we were able to measure native levels of c-di-GMP. We could also measure changes to intracellular c-di-GMP levels when either extracellular c-di-GMP or zinc ions (Zn^{2+}) were added (Figure E-1). We increased intracellular c-di-GMP levels by adding extracellular c-di-GMP. We reduced intracellular c-di-GMP levels by

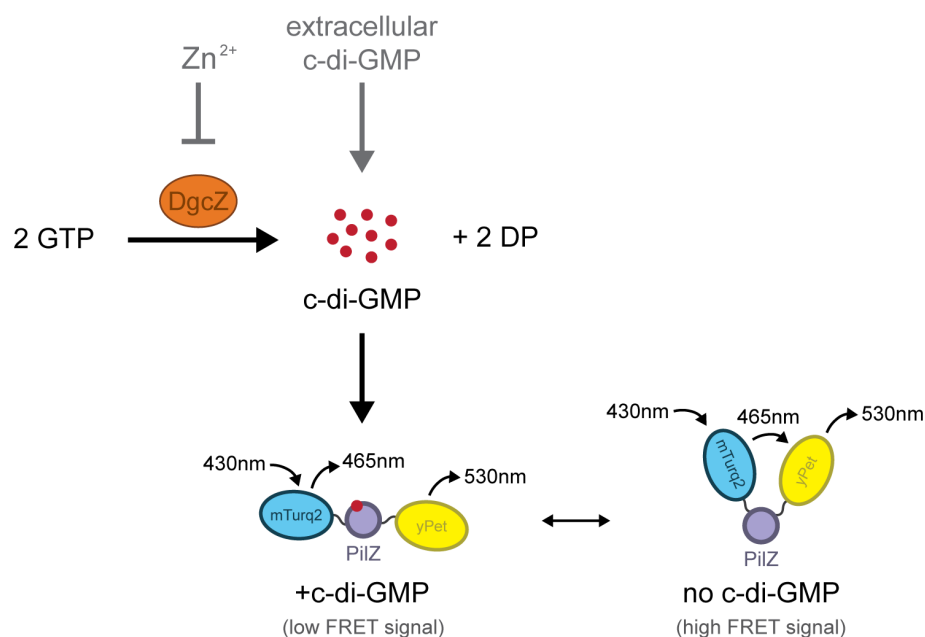


Figure E-1. Schematic of the regulation pathway of c-di-GMP and measuring c-di-GMP with the biosensor.

c-di-GMP is converted from 2 guanosine-triphosphate (GTP) molecules by a diguanylate cyclase (DgcZ); a byproduct of this reaction are 2 diphosphate molecules. DgcZ is allosterically regulated by zinc ions. c-di-GMP is measured by FRET using a biosensor, which contains a PilZ domain; PilZ changes conformation when bound to c-di-GMP.

adding Zn^{2+} , which reversibly inhibits to the enzyme responsible for producing c-di-GMP, DgcZ (Figure E-1).

Natural c-di-GMP levels were first measured (Figure E-2A-B, Column 4). As expected, when we added Zn^{2+} to the populations, we observed that the populations had higher FRET signals and lower levels of c-di-GMP (Figure E-2B, Column 1-3). The higher the concentration of Zn^{2+} the more the c-di-GMP levels shifted to the left – indicating lower intracellular c-di-GMP under the presence of higher Zn^{2+} concentrations. Likewise, when

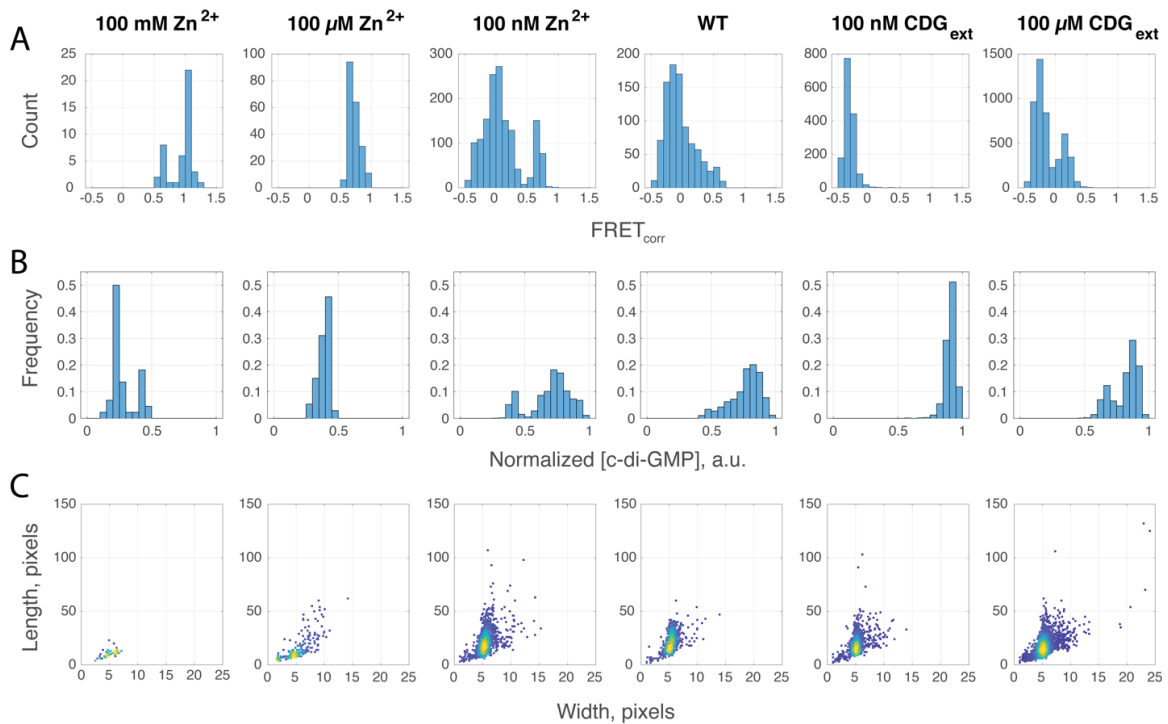


Figure E-2. Regulation of intracellular c-di-GMP concentrations shifts populations c-di-GMP and cell morphology.

(A) Histogram of corrected FRET signal (see: Methods). (B) Normalized histogram of relative c-di-GMP concentrations. (C) Morphology of cells (length by width). N = 44 - 4,500 cells. Note there are often more cells per frame for high c-di-GMP conditions.

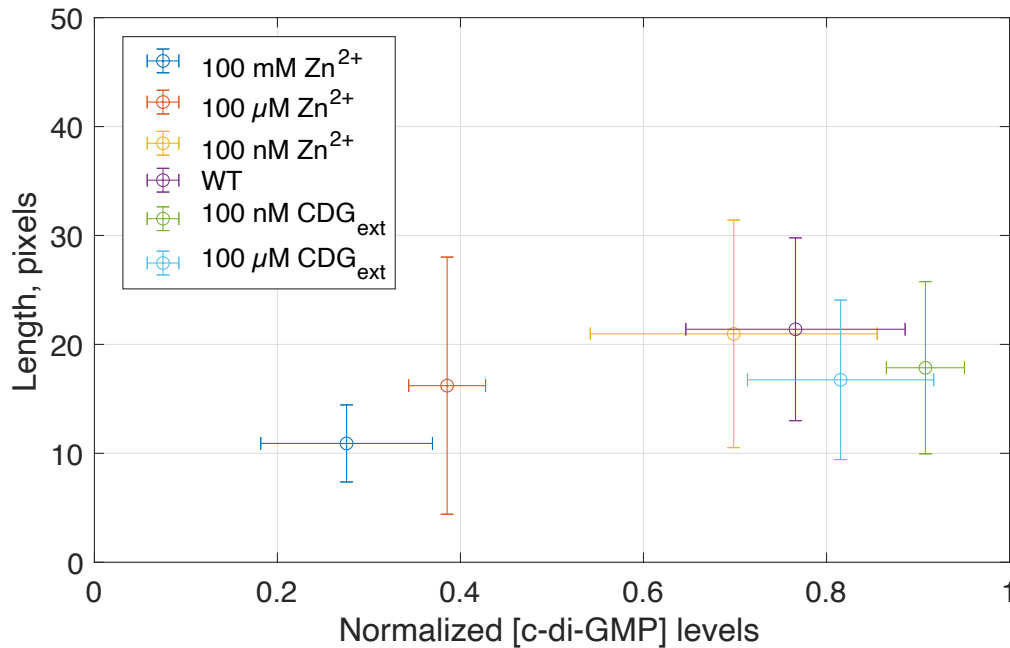


Figure E-3. Lower c-di-GMP levels reduces cell size.

Average relative c-di-GMP concentration and mean length for treated populations. Error bars are for standard deviation of $N = 44 - 4,500$ cells. Note there are often more cells per frame for high c-di-GMP conditions.

extracellular c-di-GMP is added, the histogram of c-di-GMP shifts to the further right (Figure E-2B, Column 5-6).

In analyzing these results, we also found that cells exposed to Zn^{2+} had lower c-di-GMP levels as well as shorter cells (Figure E-2C, Column 1-2 and Figure E-3). Additionally, despite collecting a similar number of frames for all conditions, there were significantly fewer cells when grown in higher Zn^{2+} concentrations. This could potentially indicate the significance of c-di-GMP for proper cell growth and function, but this more likely indicates the toxicity of Zn^{2+} , which can disrupt a number of other processes (347). However, it remains interesting that cells with low c-di-GMP were the ones surviving treatment with Zn^{2+} .

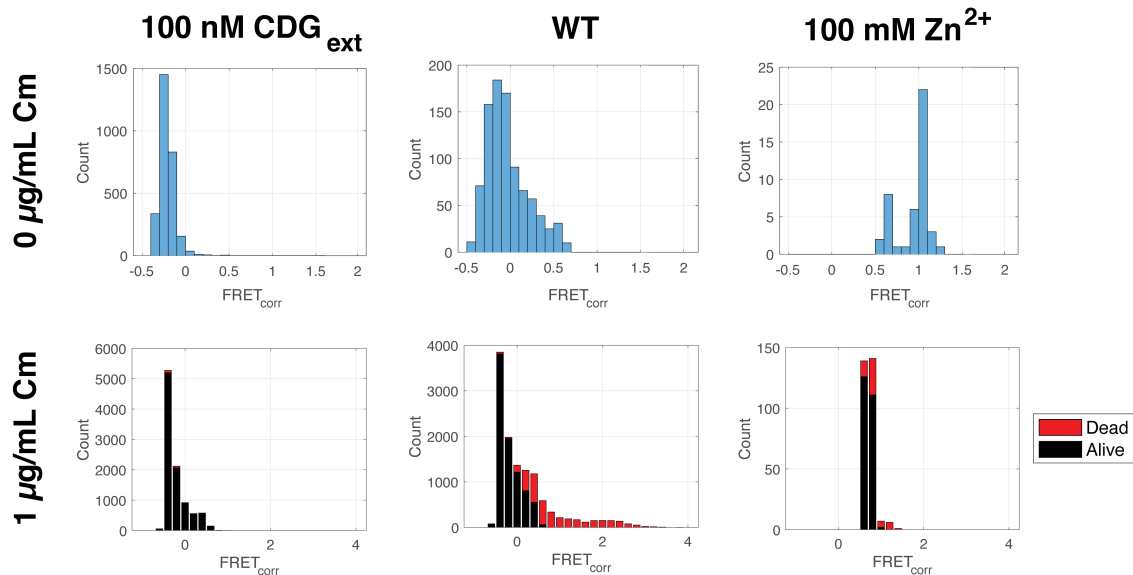


Figure E-4. Higher c-di-GMP levels are associated with increased survival.

Histogram of cells under different antibiotic stress levels (0 µg/mL or 1 µg/mL of chloramphenicol) and different c-di-GMP levels (100 nM CDG_{ext}, WT, or 100 mM Zn²⁺). We then measured using propidium iodide staining if cells were dead or alive after exposure to an antibiotic.

Lastly, we explored how the addition of antibiotics impacts cell with different c-di-GMP levels (Figure E-4). When we treated the populations with 1 µg/mL of chloramphenicol, cells with lower average c-di-GMP levels died. When populations were treated with 1 µg/mL of chloramphenicol and extracellular c-di-GMP, almost all cells lived. Interestingly, in this case, the distribution of c-di-GMP levels with and without antibiotics were qualitatively similar, which could also indicate that higher c-di-GMP may promote survival. In contrast, conditions with supplemental Zn²⁺ only had a few live cells; however, those living cells had the highest c-di-GMP levels from the distribution of the 0 µg/mL chloramphenicol condition. Thus, higher c-di-GMP levels may improve the survive of an antibiotic treatment.

We were next curious whether temporal changes in single cell c-di-GMP could predict cell fate. We first explored the temporal changes in a population's native c-di-GMP levels when a single cell grown up to a microcolony. We observed both expected oscillations in single cell c-di-GMP levels, as well as large population shifts in c-di-GMP during late exponential phase or high-density growth (Figure E-5). While other studies have been able to track oscillations in c-di-GMP to predict the where a single cell is in their cell cycle (346), we often ran into issues with photobleaching when measuring more frequently than every 7 min. The original study also worked with *B. subtilis*, which has a doubling rate of 120 min (348); whereas, the cells we studied here were *E. coli*, which can have a doubling time as fast as 20 min (349). While we were working at lower temperatures

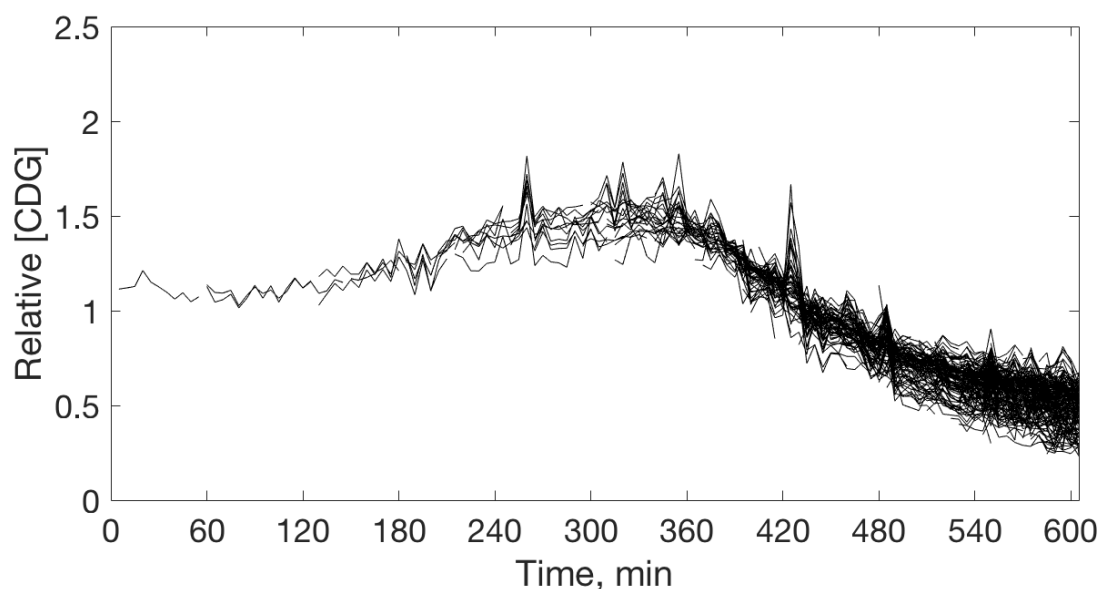


Figure E-5. Single cell oscillation of c-di-GMP from a single mother.

Relative c-di-GMP concentrations for a single mother cell and its daughter cells in a microcolony over 10 h.

and with minimal media (see: Methods), the single *E. coli* cells grew too quickly for the desired temporal resolution of the c-di-GMP oscillations. This taken together with strong population fluctuations in c-di-GMP during high density growth (between $t = 360 - 600$ min) made it challenging to use cell cycle as a predictor of single cell *E. coli* cell fate.

E.3. Discussion

In this work, we assessed a c-di-GMP biosensor as a predictor for cell cycle and cell fate. We first optimized the biosensor for higher signals by replacing the donor fluorescent protein, cyPet, with mTurq2 and by codon-optimization for *E. coli*. We found that we could regulate intracellular c-di-GMP levels by adding Zn^{2+} or extracellular c-di-GMP. Interestingly, cells exposed to high concentrations of Zn^{2+} had unique morphologies and were often slow growing, similar to persister cells (36). As such, a future direction may investigate whether there is an interplay between persistence and c-di-GMP, or whether it is possible to use c-di-GMP levels as a measure of the single cell's metabolic state.

Lastly, while we found that c-di-GMP levels might be able to predict cell fate, there was not enough temporal resolution to track and predict cell fate of single cells. Additionally, the single cell dynamics of c-di-GMP were quickly dominated by the c-di-GMP transmission cascades during biofilm formation (Figure E-5) (345). Due to these two effects, it may also be more informative to conduct this study with slower growing bacteria.

E.4. Contributions Statement

Ariel M. Langevin (A.M.L.) and Allyson Sgro (A.S.) designed experiments. Both authors optimized the biosensor. A.M.L. conducted experiments, analyzed the data, and wrote the appendix.

E.5. Methods

E.5.1. Strains and Plasmids

We used BW25113 strain of *E. coli*. The plasmid with SPY was ordered from AddGene (346). Codon-optimized versions of mTurq2 and yPet for *E. coli* were ordered from IDT as gBlocks. The pBbS8a-SPY2 plasmid was constructed using the Gibson assembly method (240). The backbone is from the BioBricks library and contains a low copy number origin of replication, pSC101, an ampicillin resistance marker, Amp^R, and an inducible arabinose promoter, P_{bad} (237). Control plasmids of pBbS8a-mTurq2 and pBbS8a-yPet were also built using Gibson assembly method (240). Plasmids were then transformed into the BW25113 host cells.

E.5.2. Growth Conditions and Time-lapse Microscopy

Cells were cultured overnight in Luria Broth (LB) medium with 100 µg/mL carbenicillin for plasmid maintenance at 200 rpm and 37°C. Cultures were refreshed by diluting 1:100 in fresh LB with 30 µg/mL kanamycin and with 100 µM arabinose to induce the biosensor. These cultures were then grown at 200 rpm and 37°C for 3 h.

E.5.3. Time-lapse Microscopy

Cells were then placed on 1.5% low-melting-point agarose pads containing 100 µM arabinose and 100 µg/mL carbenicillin. The agarose pads were made using M9 minimal media supplemented with 0.2% glycerol, 0.01% casamino acids, 0.15 µg/mL biotin, and 1.5 µM thiamine. There were experiments where: extracellular c-di-GMP was added at 0 nM, 100 nM, or 100 µM; Zn²⁺ was added at 0 nM, 100 nM, 100 µM, or 100 mM;

chloramphenicol was added at 0 or 1 $\mu\text{g/mL}$; and/or propidium iodide (PI) was added at 0 or 10 $\mu\text{g/mL}$. Images were taken with a Nikon Ti-E microscope with 100x objective lens for up to 600 min at 7 min intervals or single snaps. The microscope chamber was 32°C.

E.5.4. Data Analysis

Images were analyzed in Matlab using the SuperSegger30 image processing software to track and measure single cell characteristics and fluorescent protein levels. We used the formula from Reference (350) to measure FRET efficiency of single cells.

$$f([\text{c-di-GMP}]) = \frac{Ef_{DA}}{\gamma} = \frac{F_{ex_{\lambda D}, em_{\lambda A}}^{EPAC} - \alpha F_{ex_{\lambda A}, em_{\lambda A}}^{EPAC} - \beta F_{ex_{\lambda D}, em_{\lambda D}}^{EPAC}}{\alpha F_{ex_{\lambda A}, em_{\lambda A}}^{EPAC}} \quad \text{Eq. 18}$$

Snapshots (not shown) were used to calculate constants: α , which represents the relative acceptor fluorescence signal ($\alpha=0.9607$), and β , which represents the relative donor fluorescence signal ($\beta=0.2089$). These correction factors reduce the error due to bleedthrough and photobleaching of the accept and donor proteins. c-di-GMP levels were calculated as inversely proportional to the FRET efficiency and normalized between 0 and 1 based on maximum and minimum FRET efficiencies from all experiments.

BIBLIOGRAPHY

1. Rossolini GM, Arena F, Pecile P, Pollini S. 2014. Update on the antibiotic resistance crisis. *Current Opinion in Pharmacology* 18:56–60.
2. Aslam B, Wang W, Arshad MI, Khurshid M, Muzammil S, Rasool MH, Nisar MA, Alvi RF, Aslam MA, Qamar MU, Salamat MKF, Baloch Z. 2018. Antibiotic resistance: a rundown of a global crisis. *Infection and Drug Resistance* 11:1645–1658.
3. Nieuwlaat R, Mbuagbaw L, Mertz D, Burrows L, Bowdish DME, Moja L, Wright GD, Schünemann HJ. 2020. COVID-19 and Antimicrobial Resistance: Parallel and Interacting Health Emergencies. *Clinical Infectious Diseases* 1:ciaa773.
4. Centers for Disease Control and Prevention (CDC). 2019. Antibiotic Resistance Threats in the United States, 2019. Atlanta, GA, U.S.
5. Davies J, Davies D. 2010. Origins and Evolution of Antibiotic Resistance. *Microbiology and Molecular Biology Reviews* 74:417–433.
6. Spellberg B, Blaser M, Guidos RJ, Boucher HW, Bradley JS, Eisenstein BI, Gerding D, Lynfield R, Reller LB, Rex J, Schwartz D, Septimus E, Tenover FC, Gilbert DN. 2011. Combating antimicrobial resistance: Policy recommendations to save lives. *Clinical Infectious Diseases* 52:S397–S428.
7. Nathan C. 2004. Antibiotics at the crossroads. *Nature* 431:899–902.
8. Rather IA, Kim BC, Bajpai VK, Park YH. 2017. Self-medication and antibiotic resistance: Crisis, current challenges, and prevention. *Saudi Journal of Biological Sciences* 24:808–812.
9. Mathew AG, Cissell R, Liamthong S. 2007. Antibiotic resistance in bacteria associated with food animals: A United States perspective of livestock production. *Foodborne Pathogens and Disease* 4:115–133.
10. Abriouel H, Omar N Ben, Molinos AC, López RL, Grande MJ, Martínez-Viedma P, Ortega E, Cañamero MM, Galvez A. 2008. Comparative analysis of genetic diversity and incidence of virulence factors and antibiotic resistance among enterococcal populations from raw fruit and vegetable foods, water and soil, and clinical samples. *International Journal of Food Microbiology* 123:38–49.
11. Cerqueira F, Matamoros V, Bayona JM, Berendonk TU, Elsinga G, Hornstra LM, Piña B. 2019. Antibiotic resistance gene distribution in agricultural fields and crops. A soil-to-food analysis. *Environmental Research* 177:108608.

12. French GL. 2010. The continuing crisis in antibiotic resistance. *International Journal of Antimicrobial Agents* 36:S3–S7.
13. Boolchandani M, D’Souza AW, Dantas G. 2019. Sequencing-based methods and resources to study antimicrobial resistance. *Nature Reviews. Genetics* 20:356–370.
14. Munita JM, Arias CA. 2016. Mechanisms of Antibiotic Resistance. *Microbiology Spectrum* 4:10.1128/microbiolspec.VMBF-0016–2015.
15. Kim J, Shin B, Park C, Park W. 2017. Indole-Induced Activities of β -Lactamase and Efflux Pump Confer Ampicillin Resistance in *Pseudomonas putida* KT2440. *Frontiers in Microbiology* 8:433.
16. Hernando-Amado S, Sanz-García F, Martínez JL. 2020. Rapid and robust evolution of collateral sensitivity in *Pseudomonas aeruginosa* antibiotic-resistant mutants. *Science Advances* 6:eaba5493.
17. Brauner A, Fridman O, Gefen O, Balaban NQ. 2016. Distinguishing between resistance, tolerance and persistence to antibiotic treatment. *Nature Reviews. Microbiology* 14:320–330.
18. Gefen O, Chekol B, Strahilevitz J, Balaban NQ. 2017. TDtest: easy detection of bacterial tolerance and persistence in clinical isolates by a modified disk-diffusion assay. *Scientific Reports* 7:41284.
19. MacLean RC, San Millan A. 2019. The evolution of antibiotic resistance. *Science* 365:1082–1083.
20. Yelin I, Kishony R. 2018. Antibiotic Resistance. *Cell* 172:1136–1136.e1.
21. Redondo-Salvo S, Fernández-López R, Ruiz R, Vielva L, de Toro M, Rocha EPC, Garcillán-Barcia MP, de la Cruz F. 2020. Pathways for horizontal gene transfer in bacteria revealed by a global map of their plasmids. *Nature Communications* 11:1–13.
22. Lerminiaux NA, Cameron ADS. 2019. Horizontal transfer of antibiotic resistance genes in clinical environments. *Canadian Journal of Microbiology* 65:34–44.
23. Alekshun MN, Levy SB. 2007. Molecular Mechanisms of Antibacterial Multidrug Resistance. *Cell* 128:1037–1050.
24. Li B, Qiu Y, Song Y, Lin H, Yin H. 2019. Dissecting horizontal and vertical gene transfer of antibiotic resistance plasmid in bacterial community using microfluidics. *Environment International* 131:105007.
25. Durrant M, Li MM, Siranosian B, Bhatt AS. 2019. Mobile genetic element insertions

drive antibiotic resistance across pathogens. *bioRxiv* 527788.

26. Vandecraen J, Chandler M, Aertsen A, Van Houdt R. 2017. The impact of insertion sequences on bacterial genome plasticity and adaptability. *Critical Reviews in Microbiology* 43:709–730.
27. Raeside C, Gaffé J, Deatherage DE, Tenaillon O, Briska AM, Ptashkin RN, Cruveiller S, Médigue C, Lenski RE, Barrick JE, Schneider D. 2014. Large chromosomal rearrangements during a long-term evolution experiment with *Escherichia coli*. *mBio* 5:e01377-14.
28. Nicoloff H, Perreten V, Levy SB. 2007. Increased genome instability in *Escherichia coli* ion mutants: Relation to emergence of multiple-antibiotic-resistant (Mar) mutants caused by insertion sequence elements and large tandem genomic amplifications. *Antimicrobial Agents and Chemotherapy* 51:1293–1303.
29. Andersson DI, Hughes D. 2009. Gene Amplification and Adaptive Evolution in Bacteria. *Annual Review of Genetics* 43:167–195.
30. Nicoloff H, Perreten V, McMurphy LM, Levy SB. 2006. Role for tandem duplication and lon protease in AcrAB-TolC-dependent multiple antibiotic resistance (Mar) in an *Escherichia coli* mutant without mutations in *marRAB* or *acrRAB*. *Journal of Bacteriology* 188:4413–4423.
31. Reams AB, Roth JR. 2015. Mechanisms of gene duplication and amplification. *Cold Spring Harbor Perspectives in Biology* 7:a016592.
32. Balaban NQ, Helaine S, Lewis K, Ackermann M, Aldridge B, Andersson DI, Brynildsen MP, Bumann D, Camilli A, Collins JJ, Dehio C, Fortune S, Ghigo J-M, Hardt W-D, Harms A, Heinemann M, Hung DT, Jenal U, Levin BR, Michiels J, Storz G, Tan M-W, Tenson T, Van Melderen L, Zinkernagel A. 2019. Definitions and guidelines for research on antibiotic persistence. *Nature Reviews Microbiology* 17:441–448.
33. Dalhoff A, Ambrose PG, Mouton JW. 2009. A Long Journey from Minimum Inhibitory Concentration Testing to Clinically Predictive Breakpoints: Deterministic and Probabilistic Approaches in Deriving Breakpoints. *Infection* 37:296–305.
34. 1971. Antibiotic Sensitivity Testing. *British Medical Journal* 2:416.
35. Lázár V, Kishony R. 2019. Transient antibiotic resistance calls for attention. *Nature Microbiology* 4:1606–1607.
36. Balaban NQ, Merrin J, Chait R, Kowalik L, Leibler S. 2004. Bacterial persistence as a phenotypic switch. *Science* 305:1622–1625.

37. El Meouche I, Siu Y, Dunlop MJ. 2016. Stochastic expression of a multiple antibiotic resistance activator confers transient resistance in single cells. *Scientific Reports* 6:19538.
38. Masterton RG. 2000. Surveillance studies: How can they help the management of infection? *Journal of Antimicrobial Chemotherapy* 46:53–58.
39. World Health Organization (WHO). 2018. High levels of antibiotic resistance found worldwide, new data shows. Bangkok, Thailand.
40. Hanberger H, Diekema D, Fluit A, Jones R, Struelens M, Spencer R, Wolff M. 2001. Surveillance of antibiotic resistance in European ICUs. *Journal of Hospital Infection* 48:161–176.
41. Grundmann H, Klugman KP, Walsh T, Ramon-Pardo P, Sigauque B, Khan W, Laxminarayan R, Heddini A, Stelling J. 2011. A framework for global surveillance of antibiotic resistance. *Drug Resistance Updates* 14:79–87.
42. Hsu LY, Tan TY, Tam VH, Kwa A, Fisher DA, Koh TH, Krishnan P, Chiew YF, Jureen R, Tee N. 2010. Surveillance and correlation of antibiotic prescription and resistance of gram-negative bacteria in Singaporean hospitals. *Antimicrobial Agents and Chemotherapy* 54:1173–1178.
43. Bax R, Bywater R, Cornaglia G, Goossens H, Hunter P, Isham V, Jarlier V, Jones R, Phillips I, Sahm D, Senn S, Struelens M, Taylor D, White A. 2001. Surveillance of antimicrobial resistance - What, how and whither? *Clinical Microbiology and Infection* 7:316–325.
44. Walsh C. 2000. Molecular mechanisms that confer antibacterial drug resistance. *Nature* 406:775–781.
45. Shallcross LJ. 2014. Editorials: Antibiotic overuse: A key driver of antimicrobial resistance. *British Journal of General Practice* 64:604–605.
46. Alumran A, Hurst C, Hou X-Y. 2012. Antibiotics Overuse in Children with Upper Respiratory Tract Infections in Saudi Arabia: Risk Factors and Potential Interventions. *Clinical Medicine and Diagnostics* 1:8–16.
47. Mo WY, Chen Z, Leung HM, Oi A, Leung W. 2017. Application of veterinary antibiotics in China's aquaculture industry and their potential human health risks. *Environmental Science and Pollution Research (international edition)* 24:8978–8989.
48. Martin MJ, Thottathil SE, Newman TB. 2015. Antibiotics overuse in animal agriculture: A call to action for health care providers. *American Journal of Public*

Health 105:2409–2410.

49. Bengtsson-Palme J, Milakovic M, Švecová H, Ganjto M, Jonsson V, Grabic R, Udikovic-Kolic N. 2019. Industrial wastewater treatment plant enriches antibiotic resistance genes and alters the structure of microbial communities. *Water Research* 162:437–445.
50. Gilbert DN, Guidos RJ, Boucher HW, Talbot GH, Spellberg B, Edwards JE, Michael Scheld W, Bradley JS, Bartlett As JG. 2010. The 10 X 20 initiative: Pursuing a global commitment to develop 10 new antibacterial drugs by 2020. *Clinical Infectious Diseases* 50:1081–1083.
51. Wen Z, Shang Y, Xu G, Pu Z, Lin Z, Bai B, Chen Z, Zheng J, Deng Q, Yu Z. 2020. Mechanism of Eravacycline Resistance in Clinical *Enterococcus faecalis* Isolates From China. *Frontiers in Microbiology* 11:916.
52. Bai B, Lin Z, Pu Z, Xu G, Zhang F, Chen Z, Sun X, Zheng J, Li P, Deng Q, Yu Z. 2019. In vitro Activity and Heteroresistance of Omadacycline Against Clinical *Staphylococcus aureus* Isolates From China Reveal the Impact of Omadacycline Susceptibility by Branched-Chain Amino Acid Transport System II Carrier Protein, Na/Pi Cotransporter Family Protein, and Fibronectin-Binding Protein. *Frontiers in Microbiology* 10:2546.
53. Long SW, Olsen RJ, Mehta SC, Palzkill T, Cernoch PL, Perez KK, Musick WL, Rosato AE, Musser JM. 2014. PBP2a mutations causing high-level ceftaroline resistance in clinical methicillin-resistant *Staphylococcus aureus* isolates. *Antimicrobial Agents and Chemotherapy* 58:6668–6674.
54. Steele JM, Seabury RW, Hale CM, Mogle BT. 2018. Unsuccessful treatment of methicillin-resistant *Staphylococcus aureus* endocarditis with dalbavancin. *Journal of Clinical Pharmacy and Therapeutics* 43:101–103.
55. Shen T, Penewit K, Waalkes A, Xu L, Salipante S, Nath A, Werth B. 2019. Identification of a novel tedizolid resistance mutation in *rpoB* of methicillin-resistant *Staphylococcus aureus*. *bioRxiv* 827501.
56. Talbot GH, Jezek A, Murray BE, Jones RN, Ebright RH, Nau GJ, Rodvold KA, Newland JG, Boucher HW. 2019. The infectious diseases society of America's 10 × '20 initiative (10 new systemic antibacterial agents US food and drug administration approved by 2020): Is 20 × '20 a possibility? *Clinical Infectious Diseases* 69:1–11.
57. Cohen DT, Zhang C, Fadzen CM, Mijalis AJ, Hie L, Johnson KD, Shriver Z, Plante O, Miller SJ, Buchwald SL, Pentelute BL. 2019. A chemoselective strategy for late-stage functionalization of complex small molecules with polypeptides and proteins.

Nature Chemistry 11:78–85.

58. Lackraj T, Birstonas S, Kacori M, Foster DB. 2020. Dps protects enterohemorrhagic *Escherichia coli* against acid-induced antimicrobial peptide killing. *Journal of Bacteriology* 202:e00114-20.
59. Wright GD. 2016. Antibiotic Adjuvants: Rescuing Antibiotics from Resistance. *Trends in Microbiology* 24:862–871.
60. Van Loon HJ, Vriens MR, Fluit AC, Troelstra A, Van Der Werken C, Verhoef J, Bonten MJM. 2005. Antibiotic rotation and development of Gram-negative antibiotic resistance. *American Journal of Respiratory and Critical Care Medicine* 171:480–487.
61. Yeh PJ, Hegreness MJ, Aiden AP, Kishony R. 2009. Drug interactions and the evolution of antibiotic resistance. *Nature Reviews. Microbiology* 7:460–466.
62. Neu HC. 1991. Synergy and antagonism of combinations with quinolones. *European Journal of Clinical Microbiology & Infectious Diseases* 10:255–261.
63. Yilancioglu K, Cokol M. 2019. Design of high-order antibiotic combinations against *M. tuberculosis* by ranking and exclusion. *Scientific Reports* 9:1–11.
64. Liu J, Gefen O, Ronin I, Bar-Meir M, Balaban NQ. 2020. Effect of tolerance on the evolution of antibiotic resistance under drug combinations. *Science* 367:200–204.
65. Grossman TH, Starosta AL, Fyfe C, O'Brien W, Rothstein DM, Mikolajka A, Wilson DN, Sutcliffe JA. 2012. Target- and resistance-based mechanistic studies with TP-434, a novel fluorocycline antibiotic. *Antimicrobial Agents and Chemotherapy* 56:2559–2564.
66. Honeyman L, Ismail M, Nelson ML, Bhatia B, Bowser TE, Chen J, Mechiche R, Ohemeng K, Verma AK, Cannon EP, Macone A, Tanaka SK, Levy S. 2015. Structure-activity relationship of the aminomethylcyclines and the discovery of omadacycline. *Antimicrobial Agents and Chemotherapy* 59:7044–7053.
67. Pfaller MA, Huband MD, Rhomberg PR, Flamm RK. 2017. Surveillance of omadacycline activity against clinical isolates from a global collection (North America, Europe, Latin America, Asia-Western Pacific), 2010-2011. *Antimicrobial Agents and Chemotherapy* 61:e00018-17.
68. Carpenter CF, Chambers HF. 2004. Daptomycin: Another novel agent for treating infections due to drug-resistant gram-positive pathogens. *Clinical Infectious Diseases* 38:994–1000.

69. Montera CI, Stock F, Murray PR. 2008. Mechanisms of resistance to daptomycin in *Enterococcus faecium*. *Antimicrobial Agents and Chemotherapy* 52:1167–1170.
70. Gaynes R, Monnet D. 1997. The contribution of antibiotic use on the frequency of antibiotic resistance in hospitals. *CIBA Foundation Symposia* 207:47–60.
71. Giamarellou H, Antoniadou A. 1997. The effect of monitoring of antibiotic use on decreasing antibiotic resistance in the hospital. *CIBA Foundation Symposia* 207:76–92.
72. Werth BJ, Jain R, Hahn A, Cummings L, Weaver T, Waalkes A, Sengupta D, Salipante SJ, Rakita RM, Butler-Wu SM. 2018. Emergence of dalbavancin non-susceptible, vancomycin-intermediate *Staphylococcus aureus* (VISA) after treatment of MRSA central line-associated bloodstream infection with a dalbavancin- and vancomycin-containing regimen. *Clinical Microbiology and Infection* 24:429.e1–429.e5.
73. Zeng W, Xu W, Xu Y, Liao W, Zhao Y, Zheng X, Xu C, Zhou T, Cao J. 2020. The prevalence and mechanism of triclosan resistance in *Escherichia coli* isolates from urine samples in Wenzhou, China. *Antimicrobial Resistance & Infection Control* 9:161.
74. Pérez-Parra S, Peña-Monje A, Recio JL, García-García F. 2017. Comparative activity of tedizolid against clinical isolates of linezolid-resistant coagulase-negative staphylococci and methicillin-resistant *Staphylococcus aureus*. *Enfermedades infecciosas y microbiología clinica (English ed)* 35:323–324.
75. Gravey F, Cattoir V, Ethuin F, Fabre L, Beyrouthy R, Bonnet R, Le Hello S, Guérin F. 2020. *ramR* deletion in an *Enterobacter hormaechei* isolate as a consequence of therapeutic failure to key antibiotics in a long-term hospitalized patient. *Antimicrobial Agents and Chemotherapy* 64:e00962-20.
76. Lipsitch M, Bergstrom CT, Levin BR. 2000. The epidemiology of antibiotic resistance in hospitals: Paradoxes and prescriptions. *Proceedings of the National Academy of Sciences of the United States of America* 97:1938–1943.
77. Austin DJ, Anderson RM. 1999. Studies of antibiotic resistance within the patient, hospitals and the community using simple mathematical models. *Philosophical Transactions of the Royal Society of London Series B: Biological Sciences* 354:721–738.
78. Andersson DI, Hughes D. 2011. Persistence of antibiotic resistance in bacterial populations. *FEMS Microbiology Reviews* 35:901–911.
79. Andersson DI, Levin BR. 1999. The biological cost of antibiotic resistance. *Current*

Opinion in Microbiology 2:489–493.

80. Fleming-Dutra KE, Hersh AL, Shapiro DJ, Bartoces M, Enns EA, File TM, Finkelstein JA, Gerber JS, Hyun DY, Linder JA, Lynfield R, Margolis DJ, May LS, Merenstein D, Metlay JP, Newland JG, Piccirillo JF, Roberts RM, Sanchez G V., Suda KJ, Thomas A, Woo TM, Zetts RM, Hicks LA. 2016. Prevalence of inappropriate antibiotic prescriptions among us ambulatory care visits, 2010-2011. *JAMA: The Journal of the American Medical Association* 315:1864–1873.
81. Peniston JH, Barfield M, Gonzalez A, Holt RD. 2020. Environmental fluctuations can promote evolutionary rescue in high-extinction-risk scenarios. *Proceedings of the Royal Society B: Biological Sciences* 287:20201144.
82. Alexander HK, MacLean RC. 2020. Stochastic bacterial population dynamics restrict the establishment of antibiotic resistance from single cells. *Proceedings of the National Academy of Sciences of the United States of America* 117:19455–19464.
83. Li J, Xie S, Ahmed S, Wang F, Gu Y, Zhang C, Chai X, Wu Y, Cai J, Cheng G. 2017. Antimicrobial activity and resistance: Influencing factors. *Frontiers in Pharmacology* 8:364.
84. Stone LK, Baym M, Lieberman TD, Chait R, Clardy J, Kishony R. 2016. Compounds that select against the tetracycline-resistance efflux pump. *Nature Chemical Biology* 12:902–904.
85. Baym M, Stone LK, Kishony R. 2016. Multidrug evolutionary strategies to reverse antibiotic resistance. *Science* 351:aad3292.
86. Esiobu N, Armenta L, Ike J. 2002. Antibiotic resistance in soil and water environments. *International Journal of Environmental Health Research* 12:133–144.
87. Wistrand-Yuen E, Knopp M, Hjort K, Koskiniemi S, Berg OG, Andersson DI. 2018. Evolution of high-level resistance during low-level antibiotic exposure. *Nature Communications* 9:1599.
88. Russ D, Glaser F, Shaer Tamar E, Yelin I, Baym M, Kelsic ED, Zampaloni C, Haldimann A, Kishony R. 2020. Escape mutations circumvent a tradeoff between resistance to a beta-lactam and resistance to a beta-lactamase inhibitor. *Nature Communications* 11:1–9.
89. Stanton IC, Murray AK, Zhang L, Snape J, Gaze WH. 2020. Evolution of antibiotic resistance at low antibiotic concentrations including selection below the minimal selective concentration. *Communications Biology* 3:1–11.

90. Sandegren L. 2014. Selection of antibiotic resistance at very low antibiotic concentrations. *Upsala Journal of Medical Sciences* 119:103–107.
91. Zhang Y, Gu AZ, He M, Li D, Chen J. 2017. Subinhibitory Concentrations of Disinfectants Promote the Horizontal Transfer of Multidrug Resistance Genes within and across Genera. *Environmental Science and Technology* 51:570–580.
92. Santos-Lopez A, Marshall CW, Scribner MR, Snyder DJ, Cooper VS. 2019. Evolutionary pathways to antibiotic resistance are dependent upon environmental structure and bacterial lifestyle. *eLife* 8:e47612.
93. Drenkard E, Ausubel FM. 2002. *Pseudomonas* biofilm formation and antibiotic resistance are linked to phenotypic variation. *Nature* 416:740–743.
94. Stewart PS. 2002. Mechanisms of antibiotic resistance in bacterial biofilms. *International Journal of Medical Microbiology* 292:107–113.
95. Stewart PS. 1994. Biofilm accumulation model that predicts antibiotic resistance of *Pseudomonas aeruginosa* biofilms. *Antimicrobial Agents and Chemotherapy* 38:1052–1058.
96. Brooun A, Liu S, Lewis K. 2000. A dose-response study of antibiotic resistance in *Pseudomonas aeruginosa* biofilms. *Antimicrobial Agents and Chemotherapy* 44:640–646.
97. Van Den Bergh B, Michiels JE, Wenseleers T, Windels EM, Boer P Vanden, Kestemont D, De Meester L, Verstrepen KJ, Verstraeten N, Fauvart M, Michiels J. 2016. Frequency of antibiotic application drives rapid evolutionary adaptation of *Escherichia coli* persistence. *Nature Microbiology* 1:16020.
98. Jiao Y, Baym M, Veres A, Kishony R. 2016. Population diversity jeopardizes the efficacy of antibiotic cycling. *bioRxiv* 082107.
99. Mancuso CP, Lee H, Abreu CI, Gore J, Khalil AS. 2020. Environmental fluctuations reshape an unexpected diversity-disturbance relationship in a microbial community. *bioRxiv* 2020.07.28.225987.
100. Lenski RE, Rose MR, Simpson SC, Tadler SC. 1991. Long-term experimental evolution in *Escherichia coli*. I. Adaptation and divergence during 2000 generations. *American Naturalist* 138:1315–1341.
101. Lenski RE, Travisano M. 1994. Dynamics of adaptation and diversification: a 10,000-generation experiment with bacterial populations. *Proceedings of the National Academy of Sciences of the United States of America* 91:6808–6814.

102. Toprak E, Veres A, Yildiz S, Pedraza JM, Chait R, Paulsson J, Kishony R. 2013. Building a morbidostat: An automated continuous-culture device for studying bacterial drug resistance under dynamically sustained drug inhibition. *Nature Protocols* 8:555–567.
103. Toprak E, Veres A, Michel J-B, Chait R, Hartl DL, Kishony R. 2011. Evolutionary paths to antibiotic resistance under dynamically sustained drug selection. *Nature Genetics* 44:101.
104. Barrick JE, Yu DS, Yoon SH, Jeong H, Oh TK, Schneider D, Lenski RE, Kim JF. 2009. Genome evolution and adaptation in a long-term experiment with *Escherichia coli*. *Nature* 461:1243–1247.
105. Alon Cudkowicz N, Schuldiner S. 2019. Deletion of the major *Escherichia coli* multidrug transporter AcrB reveals transporter plasticity and redundancy in bacterial cells. *PLoS One* 14:e0218828.
106. Baym M, Lieberman TD, Kelsic ED, Chait R, Gross R, Yelin I, Kishony R. 2016. Spatiotemporal microbial evolution on antibiotic landscapes. *Science* 353:1147–1151.
107. Marchant J. 2018. When antibiotics turn toxic. *Nature* 555:431–433.
108. Knopp M, Andersson DI. 2015. Amelioration of the Fitness Costs of Antibiotic Resistance Due To Reduced Outer Membrane Permeability by Upregulation of Alternative Porins. *Molecular Biology and Evolution* 32:3252–63.
109. Martínez JL, Baquero F, Andersson DI, Martinez JL, Baquero F, Andersson DI. 2007. Predicting antibiotic resistance. *Nature Reviews. Microbiology* 5:958–965.
110. Lopatkin AJ, Collins JJ. 2020. Predictive biology: modelling, understanding and harnessing microbial complexity. *Nature Reviews. Microbiology* 18:507–520.
111. Marrec L, Bitbol A-FF. 2018. Quantifying the impact of a periodic presence of antimicrobial on resistance evolution in a homogeneous microbial population of fixed size. *Journal of Theoretical Biology* 457:190–198.
112. Chevereau G, Dravecká M, Batur T, Guvenek A, Ayhan DH, Toprak E, Bollenbach T. 2015. Quantifying the Determinants of Evolutionary Dynamics Leading to Drug Resistance. *PLoS Biology* 13:e1002299.
113. Furusawa C, Horinouchi T, Maeda T. 2018. Toward prediction and control of antibiotic-resistance evolution. *Current Opinion in Biotechnology* 54:45–49.
114. Knopp M, Andersson DI. 2018. Predictable phenotypes of antibiotic resistance

mutations. mBio 9:e00770-18.

115. Chen X, Yin H, Li G, Wang W, Wong PK, Zhao H, An T. 2019. Antibiotic-resistance gene transfer in antibiotic-resistance bacteria under different light irradiation: Implications from oxidative stress and gene expression. *Water Research* 149:282–291.
116. Björkman J, Nagaev I, Berg OG, Hughes D, Andersson DI. 2000. Effects of environment on compensatory mutations to ameliorate costs of antibiotic resistance. *Science* 287:1479–1482.
117. Smith S V., Gould IM. 2004. Optimization of antibiotic dosing schedules in the light of increasing antibiotic resistance. *Expert Review of Anti-Infective Therapy* 2:227–234.
118. Strauss SK, Schirman D, Jona G, Brooks AN, Kunjapur AM, Nguyen Ba AN, Flint A, Solt A, Mershin A, Dixit A, Yona AH, Csörgő B, Busby BP, Hennig BP, Pál C, Schraivogel D, Schultz D, Wernick DG, Agashe D, Levi D, Zabezhinsky D, Russ D, Sass E, Tamar E, Herz E, Levy ED, Church GM, Yelin I, Nachman I, Gerst JE, Georgeson JM, Adamala KP, Steinmetz LM, Rübsam M, Ralser M, Klutstein M, Desai MM, Walunjkar N, Yin N, Hefetz NA, Jakimo N, Snitser O, Adini O, Kumar P, Smith RSH, Zean R, Hazan R, Rak R, Kishony R, Johnson S, Nouriel S, Vonesch SC, Foster S, Dagan T, Wein T, Karydis T, Wannier TM, Stiles T, Olin-Sandoval V, Mueller WF, Bar-On YM, Dahan O, Pilpel Y. 2019. Evolthon: A community endeavor to evolve lab evolution. *PLoS Biology* 17(3):e3000182.
119. Hughes D, Andersson DI. 2017. Evolutionary Trajectories to Antibiotic Resistance. *Annual Review of Microbiology* 71:579–596.
120. Hallinen KM, Karslake J, Wood KB. 2020. Delayed antibiotic exposure induces population collapse in enterococcal communities with drug-resistant subpopulations. *eLife* 9:e52813.
121. Maeda T, Iwasawa J, Kotani H, Sakata N, Kawada M, Horinouchi T, Sakai A, Tanabe K, Furusawa C. 2020. High-throughput laboratory evolution and evolutionary constraints in *Escherichia coli*. *bioRxiv* 2020.02.19.956177.
122. Webber MA, Piddock LJV. 2003. The importance of efflux pumps in bacterial antibiotic resistance. *Journal of Antimicrobial Chemotherapy* 51:9–11.
123. Nikaido H. 1998. Antibiotic Resistance Caused by Gram-Negative Multidrug Efflux Pumps. *Clinical Infectious Diseases* 27:S32–S41.
124. Levy SB. 2002. Active efflux, a common mechanism for biocide and antibiotic resistance. *Journal of Applied Microbiology* 92:65S-71S.

125. Fernando DM, Kumar A. 2013. Resistance-Nodulation-Division multidrug efflux pumps in Gram-negative bacteria: Role in virulence. *Antibiotics* 2:163–181.
126. Nikaido H. 1998. Multiple antibiotic resistance and efflux. *Current Opinion in Microbiology* 1:516–523.
127. Van Bambeke F, Michot JM, Tulkens PM. 2003. Antibiotic efflux pumps in eukaryotic cells: Occurrence and impact on antibiotic cellular pharmacokinetics, pharmacodynamics and toxicodynamics. *Journal of Antimicrobial Chemotherapy* 51:1067–1077.
128. Van Bambeke F, Balzi E, Tulkens PM. 2000. Antibiotic efflux pumps. *Biochemical Pharmacology* 60:457–470.
129. Martinez JL, Sánchez MB, Martínez-Solano L, Hernandez A, Garmendia L, Fajardo A, Alvarez-Ortega C. 2009. Functional role of bacterial multidrug efflux pumps in microbial natural ecosystems. *FEMS Microbiology Reviews* 33:430–449.
130. Poole K. 2008. Bacterial Multidrug Efflux Pumps Serve Other Functions. *Microbe* 3:179–185.
131. Paulsen IT, Park JH, Choi PS, Saier MH. 2006. A family of Gram-negative bacterial outer membrane factors that function in the export of proteins, carbohydrates, drugs and heavy metals from Gram-negative bacteria. *FEMS Microbiology Letters* 156:1–8.
132. Thanassi DG, Cheng LW, Nikaido H. 1997. Active efflux of bile salts by *Escherichia coli*. *Journal of Bacteriology* 179:2512–2518.
133. Nakamura H, Hachiya N, Tojo T. 1978. Second acriflavine sensitivity mutation, *acrB*, in *Escherichia coli* K-12. *Journal of Bacteriology* 134:1184–7.
134. Sulavik MC, Houseweart C, Cramer C, Jiwani N, Murgolo N, Greene J, Didomenico B, Shaw KJ, Miller GH, Hare R, Shimer G. 2001. Antibiotic susceptibility profiles of *Escherichia coli* strains lacking multidrug efflux pump genes. *Antimicrobial Agents and Chemotherapy* 45:1126–1136.
135. Lister IM, Raftery C, Mecsas J, Levy SB. 2012. *Yersinia pestis* AcrAB-TolC in antibiotic resistance and virulence. *Antimicrobial Agents and Chemotherapy* 56:1120–1123.
136. Ricci V, Tzakas P, Buckley A, Coldham NC, Piddock LJV. 2006. Ciprofloxacin-resistant *Salmonella enterica* serovar typhimurium strains are difficult to select in the absence of AcrB and TolC. *Antimicrobial Agents and Chemotherapy* 50:38–42.

137. Morona R, Manning PA, Reeves P. 1983. Identification and characterization of the TolC protein, an outer membrane protein from *Escherichia coli*. *Journal of Bacteriology* 153:693–699.
138. Ma D, Cook DN, Alberti M, Pon NG, Nikaido H, Hearst JE. 1993. Molecular cloning and characterization of *acrA* and *acrE* genes of *Escherichia coli*. *Journal of Bacteriology* 175:6299–6313.
139. Eicher T, Seeger MA, Anselmi C, Zhou W, Brandstätter L, Verrey F, Diederichs K, Faraldo-Gómez JD, Pos KM. 2014. Coupling of remote alternating-access transport mechanisms for protons and substrates in the multidrug efflux pump AcrB. *eLife* 3:e03145.
140. Sun J, Deng Z, Yan A. 2014. Bacterial multidrug efflux pumps: Mechanisms, physiology and pharmacological exploitations. *Biochemical and Biophysical Research Communications* 453:254–267.
141. Muller RT, Pos KM. 2015. The assembly and disassembly of the AcrAB-TolC three-component multidrug efflux pump. *Biological Chemistry* 396:1083–1089.
142. Shi X, Chen M, Yu Z, Bell JM, Wang H, Forrester I, Villarreal H, Jakana J, Du D, Luisi BF, Ludtke SJ, Wang Z. 2019. *In situ* structure and assembly of the multidrug efflux pump AcrAB-TolC. *Nature Communications* 10:1–6.
143. Bavro VN, Pietras Z, Furnham N, Pérez-Cano L, Fernández-Recio J, Pei XY, Misra R, Luisi B. 2008. Assembly and Channel Opening in a Bacterial Drug Efflux Machine. *Molecular Cell* 30:114–121.
144. Wang Z, Fan G, Hryc CF, Blaza JN, Serysheva II, Schmid MF, Chiu W, Luisi BF, Du D. 2017. An allosteric transport mechanism for the AcrAB-TolC multidrug efflux pump. *eLife* 6:e24905.
145. Zwama M, Yamasaki S, Nakashima R, Sakurai K, Nishino K, Yamaguchi A. 2018. Multiple entry pathways within the efflux transporter AcrB contribute to multidrug recognition. *Nature Communications* 9:1–9.
146. Nakashima R, Sakurai K, Yamasaki S, Nishino K, Yamaguchi A. 2011. Structures of the multidrug exporter AcrB reveal a proximal multisite drug-binding pocket. *Nature* 480:565–569.
147. Yu EW, Aires JR, Nikaido H. 2003. AcrB multidrug efflux pump of *Escherichia coli*: Composite substrate-binding cavity of exceptional flexibility generates its extremely wide substrate specificity. *Journal of Bacteriology* 185:5657–5664.
148. Zakharov SD, Eroukova VY, Rokitskaya TI, Zhalnina M V., Sharma O, Loll PJ,

- Zgurskaya HI, Antonenko YN, Cramer WA. 2004. Colicin occlusion of OmpF and TolC channels: Outer membrane translocons for colicin import. *Biophysical Journal* 87:3901–3911.
149. German GJ, Misra R. 2001. The TolC protein of *Escherichia coli* serves as a cell-surface receptor for the newly characterized TLS bacteriophage. *Journal of Molecular Biology* 308:579–585.
 150. Tringe SG, von Mering C, Kobayashi A, Salamov AA, Chen K, Chang HW, Podar M, Short JM, Mathur EJ, Detter JC, Bork P, Hugenholtz P, Rubin EM. 2005. Comparative Metagenomics of Microbial Communities. *Science* 308:554–557.
 151. Kobayashi N, Nishino K, Yamaguchi A. 2001. Novel macrolide-specific ABC-type efflux transporter in *Escherichia coli*. *Journal of Bacteriology* 183:5639–5644.
 152. Nishino K, Yamaguchi A. 2002. EvgA of the two-component signal transduction system modulates production of the YhiUV multidrug transporter in *Escherichia coli*. *Journal of Bacteriology* 184:2319–2323.
 153. Borges-Walmsley MI, Walmsley AR. 2001. The structure and function of drug pumps. *Trends in Microbiology* 9:71–79.
 154. Nagakubo S, Nishino K, Hirata T, Yamaguchi A. 2002. The putative response regulator BaeR stimulates multidrug resistance of *Escherichia coli* via a novel multidrug exporter system, MdtABC. *Journal of Bacteriology* 184:4161–4167.
 155. Koronakis V, Eswaran J, Hughes C. 2004. Structure and Function of TolC: The Bacterial Exit Duct for Proteins and Drugs. *Annual Review of Biochemistry* 73:467–489.
 156. Piddock LJV. 2006. Multidrug-resistance efflux pumps - Not just for resistance. *Nature Reviews. Microbiology* 4:629–636.
 157. Ruiz C, Levy SB. 2014. Regulation of *acrAB* expression by cellular metabolites in *Escherichia coli*. *Journal of Antimicrobial Chemotherapy* 69:390–399.
 158. Zgurskaya HI, Krishnamoorthy G, Ntrel A, Lu S. 2011. Mechanism and function of the outer membrane channel TolC in multidrug resistance and physiology of enterobacteria. *Frontiers in Microbiology* 2:189.
 159. Luhe AL, Gerken H, Tan L, Wu J, Zhao H. 2012. Alcohol tolerance of *Escherichia coli* *acrR* and *marR* regulatory mutants. *Journal of Molecular Catalysis B: Enzymatic* 76:89–93.
 160. Zhu M, Dai X. 2018. High Salt Cross-Protects *Escherichia coli* from Antibiotic

Treatment through Increasing Efflux Pump Expression. *mSphere* 3:e00095-18.

161. Martin RG, Gillette WK, Rhee S, Rosner JL. 1999. Structural requirements for marbox function in transcriptional activation of mar/sox/rob regulon promoters in *Escherichia coli*: Sequence, orientation and spatial relationship to the core promoter. *Molecular Microbiology* 34:431–441.
162. Blanco P, Hernando-Amado S, Reales-Calderon J, Corona F, Lira F, Alcalde-Rico M, Bernardini A, Sanchez M, Martinez J. 2016. Bacterial Multidrug Efflux Pumps: Much More Than Antibiotic Resistance Determinants. *Microorganisms* 4:14.
163. Watanabe R, Doukyu N. 2012. Contributions of mutations in *acrR* and *marR* genes to organic solvent tolerance in *Escherichia coli*. *Applied Microbiology and Biotechnology Express* 2:1–11.
164. Barbosa TM, Levy SB. 2000. Differential Expression of over 60 Chromosomal Genes in *Escherichia coli* by Constitutive Expression of MarA. *Journal of Bacteriology* 182:3467–3474.
165. Alekshun MN, Levy SB. 1999. The mar regulon: multiple resistance to antibiotics and other toxic chemicals. *Trends in Microbiology* 7:410–3.
166. Chubiz LM, Rao C V. 2011. Role of the mar-sox-rob regulon in regulating outer membrane porin expression. *Journal of Bacteriology* 193:2252–2260.
167. Hidalgo E, Leautaud V, Demple B. 1998. The redox-regulated SoxR protein acts from a single DNA site as a repressor and an allosteric activator. *EMBO Journal* 17:2629–2636.
168. Rosenberg EY, Bertenthal D, Nilles ML, Bertrand KP, Nikaido H. 2003. Bile salts and fatty acids induce the expression of *Escherichia coli* AcrAB multidrug efflux pump through their interaction with Rob regulatory protein. *Molecular Microbiology* 48:1609–1619.
169. Warner DM, Levy SB. 2010. Different effects of transcriptional regulators MarA, SoxS and Rob on susceptibility of *Escherichia coli* to cationic antimicrobial peptides (CAMPs): Rob-dependent CAMP induction of the *marRAB* operon. *Microbiology* 156:570–578.
170. Martin RG, Rosner JL. 2004. Transcriptional and translational regulation of the *marRAB* multiple antibiotic resistance operon in *Escherichia coli*. *Molecular Microbiology* 53:183–191.
171. Martin RG, Jair KW, Wolf RE, Rosner JL. 1996. Autoactivation of the *marRAB* multiple antibiotic resistance operon by the *marA* transcriptional activator in

- Escherichia coli*. Journal of Bacteriology 178:2216–2223.
172. Deochand DK, Grove A. 2017. MarR family transcription factors: dynamic variations on a common scaffold. Critical Reviews in Biochemistry and Molecular Biology 52:595–613.
 173. Saridakis V, Shahinas D, Xu X, Christendat D. 2008. Structural Insight on the Mechanism of Regulation of the MarR Family of Proteins: High-Resolution Crystal Structure of a Transcriptional Repressor from *Methanobacterium thermoautotrophicum*. Journal of Molecular Biology 377:655–667.
 174. Ma D, Alberti M, Lynch C, Nikaido H, Hearst JE. 1996. The local repressor AcrR plays a modulating role in the regulation of *acrAB* genes of *Escherichia coli* by global stress signals. Molecular Microbiology 19:101–112.
 175. Subhadra B, Kim J, Kim DH, Woo K, Oh MH, Choi CH. 2018. Local repressor AcrR regulates AcrAB efflux pump required for biofilm formation and virulence in *Acinetobacter nosocomialis*. Frontiers in Cellular and Infection Microbiology 8:270.
 176. Kim YJ, Young Im S, Lee JO, Kim O Bin. 2016. Potential swimming motility variation by AcrR in *Escherichia coli*. Journal of Microbiology and Biotechnology 26:1824–1828.
 177. Padilla E, Llobet E, Doménech-Sánchez A, Martínez-Martínez L, Bengoechea JA, Albertí S. 2010. *Klebsiella pneumoniae* AcrAB efflux pump contributes to antimicrobial resistance and virulence. Antimicrobial Agents and Chemotherapy 54:177–183.
 178. Su CC, Rutherford DJ, Yu EW. 2007. Characterization of the multidrug efflux regulator AcrR from *Escherichia coli*. Biochemical and Biophysical Research Communications 361:85–90.
 179. Gu R, Li M, Su CC, Long F, Routh MD, Yang F, McDermott G, Yu EW. 2008. Conformational change of the AcrR regulator reveals a possible mechanism of induction. Acta Crystallographica Section F: Structural Biology and Crystallization Communications 64:584–588.
 180. Hirakawa H, Takumi-Kobayashi A, Theisen U, Hirata T, Nishino K, Yamaguchi A. 2008. AcrS/EnvR represses expression of the *acrAB* multidrug efflux genes in *Escherichia coli*. Journal of Bacteriology 190:6276–6279.
 181. Lomovskaya O, Lewis K, Matin A. 1995. EmrR is a negative regulator of the *Escherichia coli* multidrug resistance pump *emrAB*. Journal of Bacteriology 177:2328–2334.

182. Monsieurs P, De Keersmaecker S, Navarre WW, Bader MW, De Smet F, McClelland M, Fang FC, De Moor B, Vanderleyden J, Marchal K. 2005. Comparison of the PhoPQ regulon in *Escherichia coli* and *Salmonella typhimurium*. *Journal of Molecular Evolution* 60:462–474.
183. Rodionov DA, Rodionov DA, Gelf MS, A A, Rakhmaninova RB. 2001. Comparative approach to analysis of regulation in complete genomes: multidrug resistance systems in gamma-proteobacteria. *Journal of Molecular Microbiology and Biotechnology* 3:319–24.
184. Swick MC, Morgan-Linnell SK, Carlson KM, Zechiedrich L. 2011. Expression of Multidrug Efflux Pump Genes *acrAB-tolC*, *mdfA*, and *norE* in *Escherichia coli* Clinical Isolates as a Function of Fluoroquinolone and Multidrug Resistance. *Antimicrobial Agents and Chemotherapy* 55:921–924.
185. Baucheron S, Tyler S, Boyd D, Mulvey MR, Chaslus-Dancla E, Cloeckaert A. 2004. AcrAB-TolC directs efflux-mediated multidrug resistance in *Salmonella enterica* serovar typhimurium DT104. *Antimicrobial Agents and Chemotherapy* 48:3729–3735.
186. de Cristóbal RE, Vincent PA, Salomón RA. 2006. Multidrug resistance pump AcrAB-TolC is required for high-level, Tet(A)-mediated tetracycline resistance in *Escherichia coli*. *Journal of Antimicrobial Chemotherapy* 58:31–36.
187. Karve SM, Daniel S, Chavhan YD, Anand A, Kharola SS, Dey S. 2015. *Escherichia coli* populations in unpredictably fluctuating environments evolve to face novel stresses through enhanced efflux activity. *Journal of Evolutionary Biology* 28:1131–1143.
188. Kiem S, Schentag JJ. 2008. Interpretation of antibiotic concentration ratios measured in epithelial lining fluid. *Antimicrobial Agents and Chemotherapy* 52:24–36.
189. Langevin AM, Dunlop MJ. 2018. Stress introduction rate alters the benefit of AcrAB-TolC efflux pumps. *Journal of Bacteriology* 200:e00525-17.
190. Zhu Y, Zhou C, Wang Y, Li C. 2020. Transporter Engineering for Microbial Manufacturing. *Biotechnology Journal* 15:e1900494.
191. El Meouche I, Dunlop MJ. 2018. Heterogeneity in efflux pump expression predisposes antibiotic-resistant cells to mutation. *Science* 362:686–690.
192. Papkou A, Hedge J, Kapel N, Young B, MacLean RC. 2020. Efflux pump activity potentiates the evolution of antibiotic resistance across *S. aureus* isolates. *Nature Communications* 11:1–15.

193. Levison ME, Levison JH. 2009. Pharmacokinetics and Pharmacodynamics of Antibacterial Agents. *Infectious Disease Clinics of North America* 23:791–815.
194. Buchetics M, Dragosits M, Maurer M, Rebnegger C, Porro D, Sauer M, Gasser B, Mattanovich D. 2011. Reverse engineering of protein secretion by uncoupling of cell cycle phases from growth. *Biotechnology and Bioengineering* 108:2403–2412.
195. Mao J, Blanchard AE, Lu T. 2014. Slow and Steady Wins the Race: A Bacterial Exploitative Competition Strategy in Fluctuating Environments 4:240–248.
196. Xue B, Leibler S. 2016. Evolutionary learning of adaptation to varying environments through a transgenerational feedback. *Proceedings of the National Academy of Sciences of the United States of America* 113:11266–11271.
197. Leibler S, Kussell E. 2010. Individual histories and selection in heterogeneous populations. *Proceedings of the National Academy of Sciences of the United States of America* 107:13183–13188.
198. Yurtsev EA, Conwill A, Gore J. 2016. Oscillatory dynamics in a bacterial cross-protection mutualism. *Proceedings of the National Academy of Sciences of the United States of America* 113:6236–6241.
199. Kussell E, Leibler S. 2005. Phenotypic diversity, population growth, and information in fluctuating environments. *Science* 309:2075–2078.
200. Young JW, Locke JCW, Altinok A, Rosenfeld N, Bacarian T, Swain PS. 2012. Measuring single-cell gene expression dynamics in bacteria using fluorescence time-lapse microscopy. *Nature Protocols* 7:80–88.
201. Levin-Reisman I, Ronin I, Gefen O, Braniss I, Shores N, Balaban NQ. 2017. Antibiotic tolerance facilitates the evolution of resistance. *Science* 355:826–830.
202. Parmar KM, Hathi ZJ, Dafale NA. 2017. Control of Multidrug-Resistant Gene Flow in the Environment Through Bacteriophage Intervention. *Applied Biochemistry and Biotechnology* 181:1007–1029.
203. Lennen RM, Politz MG, Kruziki MA, Pfleger BF. 2013. Identification of Transport Proteins Involved in Free Fatty Acid Efflux in *Escherichia coli*. *Journal of Bacteriology* 195:135–144.
204. Melnyk AH, Wong A, Kassen R. 2015. The fitness costs of antibiotic resistance mutations. *Evolutionary Applications* 8:273–283.
205. Elkins CA, Nikaido H. 2002. Substrate Specificity of the RND-Type Multidrug Efflux Pumps AcrB and AcrD of *Escherichia coli* Is Determined Predominately by

Two Large Periplasmic Loops. *Journal of Bacteriology* 184:6490–6498.

206. Blair JMA, Piddock LJ V. 2009. Structure, function and inhibition of RND efflux pumps in Gram-negative bacteria: an update. *Current Opinion in Microbiology* 12:512–519.
207. Du D, Wang Z, James NR, Voss JE, Klimont E, Ohene-Agyei T, Venter H, Chiu W, Luisi BF. 2014. Structure of the AcrAB-TolC multidrug efflux pump. *Nature* 509:512–515.
208. Lee A, Mao W, Warren MS, Mistry A, Hoshino K, Okumura R, Ishida H, Lomovskaya O. 2000. Interplay between Efflux Pumps May Provide Either Additive or Multiplicative Effects on Drug Resistance. *Journal of Bacteriology* 182:3142–3150.
209. Piddock LJ V. 2006. Clinically Relevant Chromosomally Encoded Multidrug Resistance Efflux Pumps in Bacteria. *Clinical Microbiology Reviews* 19:382–402.
210. Krishna R, Mayer LD. 2000. Multidrug resistance (MDR) in cancer: Mechanisms, reversal using modulators of MDR and the role of MDR modulators in influencing the pharmacokinetics of anticancer drugs. *European Journal of Pharmaceutical Sciences* 11:265–283.
211. Soto SM. 2013. Role of efflux pumps in the antibiotic resistance of bacteria embedded in a biofilm. *Virulence* 4:223–229.
212. Turner WJ, Dunlop MJ. 2015. Trade-Offs in Improving Biofuel Tolerance Using Combinations of Efflux Pumps. *ACS Synthetic Biology* 4:1056–1063.
213. Dunlop MJ, Dossani ZY, Szmidt HL, Chu HC, Lee TS, Keasling JD, Hadi MZ, Mukhopadhyay A. 2011. Engineering microbial biofuel tolerance and export using efflux pumps. *Molecular Systems Biology* 7:487.
214. Fisher MA, Boyarskiy S, Yamada MR, Kong N, Bauer S, Tullman-Ercek D. 2014. Enhancing Tolerance to Short-Chain Alcohols by Engineering the *Escherichia coli* AcrB Efflux Pump to Secrete the Non-native Substrate n-Butanol. *ACS Synthetic Biology* 3:30–40.
215. Harrison M, Dunlop M. 2012. Synthetic Feedback Loop Model for Increasing Microbial Biofuel Production Using a Biosensor. *Frontiers in Microbiology* 3:360.
216. Schlecht HP, Bruno C. 2017. Chloramphenicol - Infectious Diseases. Merck Manuals.
217. Cabeen MT, Jacobs-Wagner C. 2005. Bacterial cell shape. *Nature Reviews*.

Microbiology 3:601–610.

218. Jardetzky O. 1963. Studies on the Mechanism of Action of Chloramphenicol: I. The Conformation of Chloramphenicol in Solution. *Journal of Biological Chemistry* 238:2498–2508.
219. Okusu H, Ma D, Nikaido H. 1996. AcrAB efflux pump plays a major role in the antibiotic resistance phenotype of *Escherichia coli* multiple-antibiotic-resistance (Mar) mutants. *Journal of Bacteriology* 178:306–308.
220. Tomala K, Korona R. 2013. Evaluating the Fitness Cost of Protein Expression in *Saccharomyces cerevisiae*. *Genome Biology and Evolution* 5:2051–2060.
221. Smith DR, Chapman MR. 2010. Economical Evolution: Microbes Reduce the Synthetic Cost of Extracellular Proteins. *mBio* 1.
222. Li X-Z, Plésiat P, Nikaido H. 2015. The Challenge of Efflux-Mediated Antibiotic Resistance in Gram-Negative Bacteria. *Clinical Microbiology Reviews* 28:337–418.
223. Olivares Pacheco J, Alvarez-Ortega C, Alcalde Rico M, Martínez JL. 2017. Metabolic Compensation of Fitness Costs Is a General Outcome for Antibiotic-Resistant *Pseudomonas aeruginosa* Mutants Overexpressing Efflux Pumps. *mBio* 8:e00500-17.
224. Maleki D, Honarmand Jahromy S, Zare Karizi S, Eslami P. 2017. The Prevalence of *acrA* and *acrB* Genes Among Multiple-Drug Resistant Uropathogenic *Escherichia coli* Isolated From Patients With UTI in Milad Hospital, Tehran. *Avicenna Journal of Clinical Microbiology and Infection*, 2016th-09–05 ed. 4:e39785.
225. Monod J. 1949. The Growth of Bacterial Cultures. *Annual Review of Microbiology* 3:371–394.
226. Fujikawa H, Sakha MZ. 2014. Prediction of Microbial Growth in Mixed Culture with a Competition Model. *Biocontrol Science* 19:89–92.
227. Van Impe JF, Poschet F, Geeraerd AH, Vereecken KM. 2005. Towards a novel class of predictive microbial growth models. *International Journal of Food Microbiology* 100:97–105.
228. Dekel E, Alon U. 2005. Optimality and evolutionary tuning of the expression level of a protein. *Nature* 436:588–592.
229. Sarria S, Wong B, Martín HG, Keasling JD, Peralta-Yahya P. 2014. Microbial Synthesis of Pinene. *ACS Synthetic Biology* 3:466–475.

230. Nikaido H, Takatsuka Y. 2009. Mechanisms of RND Multidrug Efflux Pumps. *Biochimica et Biophysica Acta* 1794:769–781.
231. Rendi R, Ochoa S. 1962. Effect of Chloramphenicol on Protein Synthesis in Cell-free Preparations of *Escherichia coli*. *Journal of Biological Chemistry* 237:3711–3713.
232. Wang J-F, Xiong Z-Q, Li S-Y, Wang Y. 2013. Enhancing isoprenoid production through systematically assembling and modulating efflux pumps in *Escherichia coli*. *Applied Microbiology and Biotechnology* 97:8057–8067.
233. Mingardon F, Clement C, Hirano K, Nhan M, Luning EG, Chanal A, Mukhopadhyay A. 2015. Improving olefin tolerance and production in *E. coli* using native and evolved AcrB. *Biotechnology and Bioengineering* 112:879–888.
234. Young JW, Locke JCW, Elowitz MB. 2013. Rate of environmental change determines stress response specificity. *Proceedings of the National Academy of Sciences of the United States of America* 110:4140–4145.
235. Baba T, Ara T, Hasegawa M, Takai Y, Okumura Y, Baba M, Datsenko KA, Tomita M, Wanner BL, Mori H. 2006. Construction of *Escherichia coli* K-12 in-frame, single-gene knockout mutants: the Keio collection. *Molecular Systems Biology* 2:2006.0008.
236. Sharan SK, Thomason LC, Kuznetsov SG, Court DL. 2009. Recombineering: a homologous recombination-based method of genetic engineering. *Nature Protocols* 4:206–223.
237. Anderson JC, Dueber JE, Leguia M, Wu GC, Goler JA, Arkin AP, Keasling JD. 2010. BglBricks: A flexible standard for biological part assembly. *Journal of Biological Engineering* 4:1.
238. Lee TS, Krupa RA, Zhang F, Hajimorad M, Holtz WJ, Prasad N, Lee SK, Keasling JD. 2011. BglBrick vectors and datasheets: A synthetic biology platform for gene expression. *Journal of Biological Engineering* 5:12.
239. Rossi NA, Dunlop MJ. 2017. Customized Regulation of Diverse Stress Response Genes by the Multiple Antibiotic Resistance Activator MarA. *PLoS Computational Biology* 13:e1005310.
240. Gibson DG, Young L, Chuang RY, Venter JC, Hutchison CA, Smith HO. 2009. Enzymatic assembly of DNA molecules up to several hundred kilobases. *Nature Methods* 6:343–345.
241. Hecht A, Endy D, Salit M, Munson MS. 2016. When Wavelengths Collide: Bias in

- Cell Abundance Measurements Due to Expressed Fluorescent Proteins. *ACS Synthetic Biology* 5:1024–1027.
242. Griffiths MJ, Garcin C, van Hille RP, Harrison STL. 2011. Interference by pigment in the estimation of microalgal biomass concentration by optical density. *Journal of Microbiological Methods* 85:119–123.
 243. Pedelacq J-D, Cabantous S, Tran T, Terwilliger TC, Waldo GS. 2006. Engineering and characterization of a superfolder green fluorescent protein. *Nature Biotechnology* 24:79–88.
 244. Shaner NC, Campbell RE, Steinbach PA, Giepmans BNG, Palmer AE, Tsien RY. 2004. Improved monomeric red, orange and yellow fluorescent proteins derived from *Discosoma* sp. red fluorescent protein. *Nature Biotechnology* 22:1567–1572.
 245. Baranyi J, Roberts TA, McClure P. 1993. A non-autonomous differential equation to model bacterial growth. *Food Microbiology* 10:43–59.
 246. Nazzaro F, Fratianni F, De Martino L, Coppola R, De Feo V. 2013. Effect of Essential Oils on Pathogenic Bacteria. *Pharmaceuticals* 6:1451–1474.
 247. Mukaka MM. 2012. A guide to appropriate use of Correlation coefficient in medical research. *Malawi Medical Journal : The Journal of Medical Association of Malawi* 24:69–71.
 248. Bos J, Zhang Q, Vyawahare S, Rogers E, Rosenberg SM, Austin RH. 2015. Emergence of antibiotic resistance from multinucleated bacterial filaments. *Proceedings of the National Academy of Sciences of the United States of America* 112:178–183.
 249. Zhang Q, Lambert G, Liao D, Kim H, Robin K, Tung CK, Pourmand N, Austin RH. 2011. Acceleration of emergence of bacterial antibiotic resistance in connected microenvironments. *Science* 333:1764–1767.
 250. Sorg RA, Lin L, van Doorn GS, Sorg M, Olson J, Nizet V, Veening JW. 2016. Collective Resistance in Microbial Communities by Intracellular Antibiotic Deactivation. *PLoS Biology* 14:1–19.
 251. Udekwi KI, Parrish N, Ankomah P, Baquero F, Levin BR. 2009. Functional relationship between bacterial cell density and the efficacy of antibiotics. *Journal of Antimicrobial Chemotherapy* 63:745–757.
 252. Brook I. 1989. Inoculum effect. *Reviews of Infectious Diseases* 11:361–368.
 253. Meredith HR, Srimani JK, Lee AJ, Lopatkin AJ, You L. 2015. Collective antibiotic

- tolerance: mechanisms, dynamics and intervention. *Nature Chemical Biology* 11:182.
254. Evans KC, Benomar S, Camuy-Vélez LA, Nasser EB, Wang X, Neuenswander B, Chandler JR. 2018. Quorum-sensing control of antibiotic resistance stabilizes cooperation in *Chromobacterium violaceum*. *ISME Journal* 12:1263–1272.
 255. Tanouchi Y, Lee AJ, Meredith H, You L. 2013. Programmed cell death in bacteria and implications for antibiotic therapy. *Trends in Microbiology* 21:265–270.
 256. Li X-Z, Nikaido H. 2016. Efflux-Mediated Antimicrobial Resistance in Bacteria, p. 219–259. *In* *Efflux-Mediated Antimicrobial Resistance in Bacteria*, 1st ed. Springer International Publishing.
 257. Siu Y, Fenno J, Lindle JM, Dunlop MJ. 2018. Design and Selection of a Synthetic Feedback Loop for Optimizing Biofuel Tolerance. *ACS Synthetic Biology* 7:16–23.
 258. Nikaido H, Pagès JM. 2012. Broad-specificity efflux pumps and their role in multidrug resistance of Gram-negative bacteria. *FEMS Microbiology Reviews*.
 259. Venter H, Mowla R, Ohene-Agyei T, Ma S. 2015. RND-type drug efflux pumps from Gram-negative bacteria: Molecular mechanism and inhibition. *Frontiers in Microbiology* 6:1–11.
 260. Bergmiller T, Andersson AMC, Tomasek K, Balleza E, Kiviet DJ, Hauschild R, Tkačik G, Guet CC. 2017. Biased partitioning of the multidrug efflux pump AcrAB-TolC underlies long-lived phenotypic heterogeneity. *Science* 356:311–315.
 261. Pu Y, Zhao Z, Li Y, Zou J, Ma Q, Zhao Y, Ke Y, Zhu Y, Chen H, Baker MAB, Ge H, Sun Y, Xie XS, Bai F. 2016. Enhanced Efflux Activity Facilitates Drug Tolerance in Dormant Bacterial Cells. *Molecular Cell* 62:284–294.
 262. Wang R, Kalchayanand N, Schmidt JW, Harhay DM. 2013. Mixed biofilm formation by Shiga toxin-producing *Escherichia coli* and *Salmonella enterica* serovar typhimurium enhanced bacterial resistance to sanitization due to extracellular polymeric substances. *Journal of Food Protection* 76:1513–1522.
 263. McClelland M, Sanderson KE, Spieth J, Clifton SW, Latreille P, Courtney L, Porwollik S, Ali J, Dante M, Du F, Hou S, Layman D, Leonard S, Nguyen C, Scott K, Holmes A, Grewal N, Mulvaney E, Ryan E, Sun H, Florea L, Miller W, Stoneking T, Nhan M, Waterston R, Wilson RK. 2001. Complete genome sequence of *Salmonella enterica* serovar Typhimurium LT2. *Nature* 413:852–856.
 264. Susman L, Kohram M, Vashistha H, Nechleba JT, Salman H, Brenner N. 2018. Individuality and slow dynamics in bacterial growth homeostasis. *Proceedings of*

- the National Academy of Sciences of the United States of America 115:E5679–E5687.
265. Flake GW. 1998. *The computational beauty of nature*, 1st ed. The MIT Press, Cambridge, MA.
 266. Bonabeau E. 2002. Agent-based modeling: Methods and techniques for simulating human systems. *Proceedings of the National Academy of Sciences of the United States of America* 99:7280–7287.
 267. Scott SR, Din MO, Bittihn P, Xiong L, Tsimring LS, Hasty J. 2017. A stabilized microbial ecosystem of self-limiting bacteria using synthetic quorum-regulated lysis. *Nature Microbiology* 2:17083–17083.
 268. Srimani JK, Huang S, Lopatkin AJ, You L. 2017. Drug detoxification dynamics explain the postantibiotic effect. *Molecular Systems Biology* 13:948.
 269. Smith PA, Koehler MFT, Girgis HS, Yan D, Chen Y, Chen Y, Crawford JJ, Durk MR, Higuchi RI, Kang J, Murray J, Paraselli P, Park S, Phung W, Quinn JG, Roberts TC, Rougé L, Schwarz JB, Skippington E, Wai J, Xu M, Yu Z, Zhang H, Tan MW, Heise CE. 2018. Optimized arylomycins are a new class of Gram-negative antibiotics. *Nature* 561:189–194.
 270. Sousa MC. 2019. New antibiotics target the outer membrane of bacteria. *Nature* 576:389–390.
 271. Imai Y, Meyer KJ, Inishi A, Favre-Godal Q, Green R, Manuse S, Caboni M, Mori M, Niles S, Ghiglieri M, Honrao C, Ma X, Guo JJ, Makriyannis A, Linares-Otoya L, Böhringer N, Wuisan ZG, Kaur H, Wu R, Mateus A, Typas A, Savitski MM, Espinoza JL, O'Rourke A, Nelson KE, Hiller S, Noinaj N, Schäberle TF, D'Onofrio A, Lewis K. 2019. A new antibiotic selectively kills Gram-negative pathogens. *Nature* 576:459–464.
 272. Hart EM, Mitchell AM, Konovalova A, Grabowicz M, Sheng J, Han X, Rodriguez-Rivera FP, Schwaid AG, Malinverni JC, Balibar CJ, Bodea S, Si Q, Wang H, Homsher MF, Painter RE, Ogawa AK, Sutterlin H, Roemer T, Black TA, Rothman DM, Walker SS, Silhavy TJ. 2019. A small-molecule inhibitor of BamA impervious to efflux and the outer membrane permeability barrier. *Proceedings of the National Academy of Sciences of the United States of America* 116:21748–21757.
 273. Luther A, Urfer M, Zahn M, Müller M, Wang SY, Mondal M, Vitale A, Hartmann JB, Sharpe T, Monte F Lo, Kocherla H, Cline E, Pessi G, Rath P, Modaresi SM, Chiquet P, Stiegeler S, Verbree C, Remus T, Schmitt M, Kolopp C, Westwood MA, Desjonquères N, Brabet E, Hell S, LePoupon K, Vermeulen A, Jaisson R, Rithié V, Upert G, Lederer A, Zbinden P, Wach A, Moehle K, Zerbe K, Locher HH,

- Bernardini F, Dale GE, Eberl L, Wollscheid B, Hiller S, Robinson JA, Obrecht D. 2019. Chimeric peptidomimetic antibiotics against Gram-negative bacteria. *Nature* 576:452–458.
274. Newton J, Fenton K. 2015. Health Matter – tackling antimicrobial resistance. Public Health England.
 275. Ventola CL. 2015. The Antibiotic Resistance Crisis: Part 1: Causes and Threats. *Pharmacy and Therapeutics* 40:277–283.
 276. Yoshida M, Reyes SG, Tsuda S, Horinouchi T, Furusawa C, Cronin L. 2017. Time-programmable drug dosing allows the manipulation, suppression and reversal of antibiotic drug resistance *in vitro*. *Nature Communications* 8:1–11.
 277. Kohanski MA, DePristo MA, Collins JJ. 2010. Sublethal Antibiotic Treatment Leads to Multidrug Resistance via Radical-Induced Mutagenesis. *Molecular Cell* 37:311–320.
 278. Andersson DI, Hughes D. 2012. Evolution of antibiotic resistance at non-lethal drug concentrations. *Drug Resistance Updates* 15:162–172.
 279. Jahn LJ, Munck C, Ellabaan MMH, Sommer MOA. 2017. Adaptive Laboratory Evolution of Antibiotic Resistance Using Different Selection Regimes Lead to Similar Phenotypes and Genotypes. *Frontiers in Microbiology* 8:816.
 280. Reding C, Catalán P, Jansen G, Bergmiller T, Rosenstiel P, Schulenburg H, Gudelj I, Beardmore R. 2019. Hotspot Dosages of Most Rapid Antibiotic Resistance Evolution. *bioRxiv* 866269.
 281. Delcour AH. 2009. Outer Membrane Permeability and Antibiotic Resistance. *Biochimica et Biophysica Acta* 1794:808–816.
 282. Blair JMA, Webber MA, Baylay AJ, Ogbolu DO, Piddock LJ V. 2015. Molecular mechanisms of antibiotic resistance. *Nature Reviews. Microbiology* 13:42–51.
 283. Kobyłka J, Kuth MS, Müller RT, Geertsma ER, Pos KM. 2020. AcrB: a mean, keen, drug efflux machine. *Annals of the New York Academy of Sciences* 1459:38–68.
 284. Webber MA, Talukder A, Piddock LJ V. 2005. Contribution of mutation at amino acid 45 of AcrR to *acrB* expression and ciprofloxacin resistance in clinical and veterinary *Escherichia coli* isolates. *Antimicrobial Agents and Chemotherapy* 49:4390–4392.
 285. Olliver A, Vallé M, Chaslus-Dancla E, Cloeckaert A. 2004. Role of an *acrR* mutation in multidrug resistance of *in vitro*-selected fluoroquinolone-resistant

- mutants of *Salmonella enterica* serovar Typhimurium. FEMS Microbiology Letters 238:267–272.
286. Wang H, Dzink-Fox JL, Chen M, Levy SB. 2001. Genetic characterization of highly fluoroquinolone-resistant clinical *Escherichia coli* strains from China: Role of *acrR* mutations. Antimicrobial Agents and Chemotherapy 45:1515–1521.
 287. Singh R, Swick MC, Ledesma KR, Yang Z, Hu M, Zechiedrich L, Tama VH. 2012. Temporal interplay between efflux pumps and target mutations in development of antibiotic resistance in *Escherichia coli*. Antimicrobial Agents and Chemotherapy 56:1680–1685.
 288. Lukačišinová M, Fernando B, Bollenbach T. 2020. Highly parallel lab evolution reveals that epistasis can curb the evolution of antibiotic resistance. Nature Communications 11:3105.
 289. Sood S. 2016. Chloramphenicol - A Potent Armament Against Multi-Drug Resistant (MDR) Gram Negative Bacilli? Journal of Clinical and Diagnostic Research 10:DC01–DC03.
 290. Nitzan O, Kennes Y, Colodner R, Saliba W, Edelstein I H, Raz R, Chazan B. 2015. Chloramphenicol use and susceptibility patterns in Israel: a national survey. The Israel Medical Association Journal 17:27–31.
 291. Wong BG, Mancuso CP, Kiriakov S, Bashor CJ, Khalil AS. 2018. Precise, automated control of conditions for high-throughput growth of yeast and bacteria with eVOLVER. Nature Biotechnology 36:614.
 292. Chetri S, Bhowmik D, Paul D, Pandey P, Chanda DD, Chakravarty A, Bora D, Bhattacharjee A. 2019. AcrAB-TolC efflux pump system plays a role in carbapenem non-susceptibility in *Escherichia coli*. BMC Microbiology 19:210.
 293. Clinical and Laboratory Standards Institute. 2013. M100-S23 Performance Standards for Antimicrobial Susceptibility Testing; Twenty-Third Informational Supplement, 33rd ed. Wayne, PA.
 294. Andersson DI, Balaban NQ, Baquero F, Courvalin P, Glaser P, Gophna U, Kishony R, Molin S, Tønjum T. 2020. Antibiotic resistance: turning evolutionary principles into clinical reality. FEMS Microbiology Reviews 44:171–188.
 295. McMurtry LM, Levy SB. 2013. Amino acid residues involved in inactivation of the *Escherichia coli* multidrug resistance repressor MarR by salicylate, 2,4-dinitrophenol, and plumbagin. FEMS Microbiology Letters 349(1):16–24.
 296. Linkevicius M, Sandegren L, Andersson DI. 2013. Mechanisms and fitness costs of

- tigecycline resistance in *Escherichia coli*. *Journal of Antimicrobial Chemotherapy* 68:2809–2819.
297. Lu J, Jin M, Nguyen SH, Mao L, Li J, Coin LJM, Yuan Z, Guo J. 2018. Non-antibiotic antimicrobial triclosan induces multiple antibiotic resistance through genetic mutation. *Environment International* 118:257–265.
 298. Ching C, Zaman MH. 2020. Development and selection of low-level multi-drug resistance over an extended range of sub-inhibitory ciprofloxacin concentrations in *Escherichia coli*. *Scientific Reports* 10:1–9.
 299. Hickman RA, Munck C, Sommer MOA. 2017. Time-Resolved Tracking of Mutations Reveals Diverse Allele Dynamics during *Escherichia coli* Antimicrobial Adaptive Evolution to Single Drugs and Drug Pairs. *Frontiers in Microbiology* 8:893.
 300. Grenier F, Matteau D, Baby V, Rodrigue S. 2014. Complete genome sequence of *Escherichia coli* BW25113. *Genome Announcements* 2(5):e01038-14.
 301. Kinana AD, Vargiu A V., Nikaido H. 2013. Some ligands enhance the efflux of other ligands by the *Escherichia coli* multidrug pump AcrB. *Biochemistry* 52:8342–8351.
 302. Hoeksema M, Jonker MJ, Brul S, Ter Kuile BH. 2019. Effects of a previously selected antibiotic resistance on mutations acquired during development of a second resistance in *Escherichia coli*. *BMC Genomics* 20:284.
 303. Ray MJ, Tallman GB, Bearden DT, Elman MR, McGregor JC. 2019. Antibiotic prescribing without documented indication in ambulatory care clinics: national cross sectional study. *BMJ: British Medical Journal (Clinical research edition)* 367:l6461.
 304. Falagas ME, Makris GC, Dimopoulos G, Matthaiou DK. 2008. Heteroresistance: a concern of increasing clinical significance? *Clinical Microbiology and Infection* 14:101–104.
 305. Hennessy TW, Petersen KM, Bruden D, Parkinson AJ, Hurlburt D, Getty M, Schwartz B, Butler JC. 2002. Changes in Antibiotic-Prescribing Practices and Carriage of Penicillin-Resistant *Streptococcus pneumoniae*: A Controlled Intervention Trial in Rural Alaska. *Clinical Infectious Diseases* 34:1543–1550.
 306. Čižman M. 2003. The use and resistance to antibiotics in the community. *International Journal of Antimicrobial Agents* 21(4):297–307.
 307. Datta S, Costantino N, Court DL. 2006. A set of recombineering plasmids for gram-negative bacteria. *Gene* 379:109–115.

308. Datsenko KA, Wanner BL. 2000. One-step inactivation of chromosomal genes in *Escherichia coli* K-12 using PCR products. *Proceedings of the National Academy of Sciences of the United States of America* 97:6640–6645.
309. Andrews JM. 2001. BSAC standardized disc susceptibility testing method. *Journal of Antimicrobial Chemotherapy* 48:43–57.
310. Kronvall G. 1982. Analysis of a single reference strain for determination of gentamicin regression line constants and inhibition zone diameter breakpoints in quality control of disk diffusion antibiotic susceptibility testing. *Journal of Clinical Microbiology* 16:784–793.
311. Deatherage DE, Barrick JE. 2014. Identification of mutations in laboratory-evolved microbes from next-generation sequencing data using *breseq*. *Methods in Molecular Biology* 1151:165–188.
312. Feugeas J-P, Tourret J, Launay A, Bouvet O, Hoede C, Denamur E, Tenailon O. 2016. Links between Transcription, Environmental Adaptation and Gene Variability in *Escherichia coli*: Correlations between Gene Expression and Gene Variability Reflect Growth Efficiencies. *Molecular Biology and Evolution* 33:2515–2529.
313. Maisnier-Patin S, Andersson DI. 2004. Adaptation to the deleterious effects of antimicrobial drug resistance mutations by compensatory evolution. *Research in Microbiology* 155:360–369.
314. Schulz zur Wiesch P, Engelstädter J, Bonhoeffer S. 2010. Compensation of Fitness Costs and Reversibility of Antibiotic Resistance Mutations. *Antimicrobial Agents and Chemotherapy* 54:2085–2095.
315. Chalmers G, Kozak GK, Hillyer E, Reid-Smith RJ, Boerlin P. 2010. Low minimum inhibitory concentrations associated with the tetracycline-resistance gene *tet(C)* in *Escherichia coli*. *Canadian Journal of Veterinary Research* 74:145–8.
316. Goswami M, Subramanian M, Kumar R, Jass J, Jawali N. 2016. Involvement of Antibiotic Efflux Machinery in Glutathione-Mediated Decreased Ciprofloxacin Activity in *Escherichia coli*. *Antimicrobial Agents and Chemotherapy* 60:4369–74.
317. Chandrasekar V, Knabel SJ, Anantheswaran RC. 2015. Modeling development of inhibition zones in an agar diffusion bioassay. *Food Science & Nutrition* 3:394–403.
318. Kohanski MA, Dwyer DJ, Collins JJ. 2010. How antibiotics kill bacteria: from targets to networks. *Nature Reviews. Microbiology* 8:423–35.
319. Fernández L, Hancock REW. 2012. Adaptive and Mutational Resistance: Role of Porins and Efflux Pumps in Drug Resistance. *Clinical Microbiology Reviews*

25:661–681.

320. Maneewannakul K, Levy SB. 1996. Identification of *mar* mutants among quinolone-resistant clinical isolates of *Escherichia coli*. *Antimicrobial Agents and Chemotherapy* 40:1695–8.
321. Lee AJ, Wang S, Meredith HR, Zhuang B, Dai Z, You L. 2018. Robust, linear correlations between growth rates and β -lactam-mediated lysis rates. *Proceedings of the National Academy of Sciences of the United States of America* 115:4069–4074.
322. Stubbendieck RM, Vargas-Bautista C, Straight PD. 2016. Bacterial Communities: Interactions to Scale. *Frontiers in Microbiology* 7:1234.
323. Barry AL, Fay GD, Atchison FW. 1972. Quality Control of Antimicrobial Disc Susceptibility Testing with a Rapid Method Compared to the Standard Methods. *Antimicrobial Agents and Chemotherapy* 2:419–422.
324. Drescher K, Nadell CD, Stone HA, Wingreen NS, Bassler BL. 2014. Solutions to the public goods dilemma in bacterial biofilms. *Current Biology* 24:50–55.
325. Nadell CD, Bassler BL, Levin SA. 2008. Observing bacteria through the lens of social evolution. *Journal of Biology* 7:1–4.
326. León-Buitimea A, Garza-Cárdenas CR, Garza-Cervantes JA, Lerma-Escalera JA, Morones-Ramírez JR. 2020. The Demand for New Antibiotics: Antimicrobial Peptides, Nanoparticles, and Combinatorial Therapies as Future Strategies in Antibacterial Agent Design. *Frontiers in Microbiology* 11:1669.
327. Martínez JL, Baquero F, Andersson DI. 2011. Beyond serial passages: New methods for predicting the emergence of resistance to novel antibiotics. *Current Opinion in Pharmacology* 11:439–445.
328. Opperman TJ, Nguyen ST. 2015. Recent advances toward a molecular mechanism of efflux pump inhibition. *Frontiers in Microbiology* 6:421.
329. Marshall RL, Lloyd GS, Lawler AJ, Element SJ, Kaur J, Ciusa ML, Ricci V, Tschumi A, Kühne H, Alderwick LJ, Piddock LJV. 2020. New multidrug efflux inhibitors for gram-negative bacteria. *mBio* 11:1–19.
330. Levin BR, Perrot V, Walker N. 2000. Compensatory Mutations, Antibiotic Resistance and the Population Genetics of Adaptive Evolution in Bacteria. *Genetics* 154:985–97.
331. Levy SF, Blundell JR, Venkataram S, Petrov DA, Fisher DS, Sherlock G. 2015.

- Quantitative evolutionary dynamics using high-resolution lineage tracking. *Nature* 519:181–186.
332. Qin H, Wai-Sing Lo N, Fong-Chuen Loo J, Lin X, Kay-Yuen Yim A, Kwok-Wing Tsui S, Chi-Kong Lau T, Ip M, Chan T-F. 2018. Comparative transcriptomics of multidrug-resistant *Acinetobacter baumannii* in response to antibiotic treatments. *Scientific Reports* 8:3515.
 333. Yang JH, Bening SC, Collins JJ. 2017. Antibiotic efficacy — context matters. *Current Opinion in Microbiology* 39:73–80.
 334. Heibisch E, Knebel J, Landsberg J, Frey E, Leisner M. 2013. High Variation of Fluorescence Protein Maturation Times in Closely Related *Escherichia coli* Strains. *PLoS One* 8:e75991.
 335. Khmelinskii A, Keller PJ, Bartosik A, Meurer M, Barry JD, Mardin BR, Kaufmann A, Trautmann S, Wachsmuth M, Pereira G, Huber W, Schiebel E, Knop M. 2012. Tandem fluorescent protein timers for in vivo analysis of protein dynamics. *Nature Biotechnology* 30:708–714.
 336. Megerle JA, Fritz G, Gerland U, Jung K, Rädler JO. 2008. Timing and Dynamics of Single Cell Gene Expression in the Arabinose Utilization System. *Biophysical Journal* 95:2103–2115.
 337. Wen X, Langevin AM, Dunlop MJ. 2018. Antibiotic export by efflux pumps affects growth of neighboring bacteria. *Scientific Reports* 8:15120.
 338. Stokes JM, Lopatkin AJ, Lobritz MA, Collins JJ. 2019. Bacterial Metabolism and Antibiotic Efficacy. *Cell Metabolism* 30:251–259.
 339. Dhar N, McKinney JD. 2007. Microbial phenotypic heterogeneity and antibiotic tolerance. *Current Opinion in Microbiology* 10:30–38.
 340. Rossi NA, El Meouche I, Dunlop MJ. 2019. Forecasting cell fate during antibiotic exposure using stochastic gene expression. *Communications Biology* 2:1–7.
 341. Pontes MH, Groisman EA. 2019. Slow growth determines nonheritable antibiotic resistance in *Salmonella enterica*. *Science Signaling* 12:3938.
 342. Rismondo J, Halbedel S, Gründling A. 2019. Cell shape and antibiotic resistance are maintained by the activity of multiple *ftsW* and *rodA* enzymes in *Listeria monocytogenes*. *mBio* 10:1448–1467.
 343. Schrader JM, Shapiro L. 2015. Synchronization of *Caulobacter crescentus* for investigation of the bacterial cell cycle. *JoVE: Journal of Visualized Experiments*

98:e52633.

344. Lee H, Lee DG. 2019. Programmed Cell Death in Bacterial Community: Mechanisms of Action, Causes and Consequences. *Journal of Microbiology and Biotechnology* 29:1014–1021.
345. Valentini M, Filloux A. 2016. Biofilms and Cyclic di-GMP (c-di-GMP) signaling: Lessons from *Pseudomonas aeruginosa* and other bacteria. *Journal of Biological Chemistry* 291:12547–12555.
346. Christen M, Kulasekara HD, Christen B, Kulasekara BR, Hoffman LR, Miller SI. 2010. Asymmetrical distribution of the second messenger c-di-GMP upon bacterial cell division. *Science* 328:1295–7.
347. Yeo J, Dippel AB, Wang XC, Hammond MC. 2018. In Vivo Biochemistry: Single-Cell Dynamics of Cyclic Di-GMP in *Escherichia coli* in Response to Zinc Overload. *Biochemistry* 57:108–116.
348. Burdett IDJ, Kirkwood TBL, Whalley JB. 1986. Growth kinetics of individual *Bacillus subtilis* cells and correlation with nucleoid extension. *Journal of Bacteriology* 167:219–230.
349. Liang ST, Ehrenberg M, Dennis P, Bremer H. 1999. Decay of *rpIN* and *lacZ* mRNA in *Escherichia coli*. *Journal of Molecular Biology* 288:521–538.
350. Sgro AE, Schwab DJ, Noorbakhsh J, Mestler T, Mehta P, Gregor T. 2015. From intracellular signaling to population oscillations: bridging size- and time-scales in collective behavior. *Molecular Systems Biology* 11:779.
351. Jenal U, Fuchs T. 1998. An essential protease involved in bacterial cell-cycle control. *EMBO Journal* 17:5658–5669.
352. Reading E, Ahdash Z, Fais C, Ricci V, Wang-Kan X, Grimsey E, Stone JW, Mallocci G, Lau AM, Findlay H, Konijnenberg A, Booth PJ, Ruggerone P, Vargiu AV, Piddock LJV, Politis A. 2020. Perturbed structural dynamics underlie inhibition and altered specificity of the multidrug efflux pump AcrB. *bioRxiv* 2020.04.27.063511.
353. Nikaido H. 1996. Multidrug efflux pumps of gram-negative bacteria. *Journal of Bacteriology* 178:5853–5859.

CURRICULUM VITAE

